Università degli Studi di Milano-Bicocca
Dipartimento di Informatica, Sistemistica e Comunicazione
Dottorato di Ricerca in Informatica – XXVIII Cycle

Complex Heterogeneous Crowding Phenomena: Multi-Agent Modeling, Simulation, Empirical Evidences and the Case of Elderly Pedestrians

Luca Crociani
Ph.D. Thesis

Thesis supervisor: Prof. Dr. Giuseppe Vizzari
Thesis tutor: Prof. Dr. Stefania Bandini

Alla mia famiglia.
Ai miei amici.
Ai miei professori e colleghi, in Italia, Germania e Giappone.
A tutte le persone che mi sono state vicine e che mi hanno aiutato in questo periodo.
E specialmente a te, Nonno.

To my family.
To my friends.
To my professors and colleagues, in Italy, Germany and Japan.
To all the persons who have been close to me and who helped me in this period.
And especially to you, Grandpa.

Contents

1 Introduction **1**
1.1 Modeling and Simulation of Pedestrian Dynamics 3
1.2 Considering the Heterogeneity of the Crowd 4
1.3 Contributions and Overview of the Thesis 6
1.4 Selection of Relevant Publications 6
1.5 Other Publications 7

2 State Of The Art **11**
2.1 Macroscopic Modeling 16
2.2 Mesoscopic Models 21
2.3 Microscopic Models 26
2.3.1 Operational Level Representation 27
2.3.2 Models Dealing with Tactical Level 36
2.4 Considering Heterogeneity and Differences in the Simulated Population 39
2.5 Validation of the Models: The Available Knowledge on the Modeled Dynamics 41
2.5.1 The Pedestrian Fundamental Diagram 42
2.5.2 Analysis of Space Utilization 45
2.5.3 Validation of The Tactical Level: Assumptions and Possibilities . 47

3 A Discrete Model for the Operational and Tactical Levels of Pedestrian Behavior **49**
3.1 The Discrete Representation of the Environment 50
3.1.1 The Path Fields 53
3.1.2 The Obstacle Field 55
3.1.3 The Proxemics Field 56
3.1.4 The Density Field 56
3.2 Different Levels of Knowledge: an Abstract Representation of the Environment to Encompass Tactical Level Decisions 58
3.3 Time and Update Strategy 62
3.4 The Architecture of the Agent 64
3.4.1 The Body of the Agent 65
3.4.2 Adaptation Mechanism for Group Cohesion Preservation 73
3.4.3 Considering Slower Pedestrians: An Innovative Approach for the Management of Heterogeneous Speeds in Discrete Environments 76
3.4.4 Modeling Classes of Pedestrians and Regions 80
3.4.5 A Tactical Level Component for Dynamical Path Planning 83

4 Validation And Experiments **99**
4.1 Properties of the Operational Level and Validation 99
4.1.1 Fundamental Diagram for uni-directional and bi-directional Flow 100
4.1.2 Evaluating the Effects of a Rotation of the Environment 103
4.1.3 Evaluation of the Cohesion Mechanism for Pedestrian Groups . . 108
4.2 Tests on Tactical Level 111
4.2.1 Modeling Different Classes of Agents and Environments 111
4.2.2 Simulation of an Evacuation Scenario 113
4.3 A Preliminar Analyis of the Computational Times 116

5 Coupling Mesoscopic and Microscopic Simulations: A Multiscale Model for Detailed Simulations of Urban Areas **121**
5.1 An Optimized Model for Fast Pedestrian Simulations 123
5.1.1 Environment Representation and Floor Fields 123
5.1.2 Method for the Local Density estimation 124
5.1.3 Rules of the Dynamics: Definition and Implementation for 2-dimensional Environments 126
5.1.4 Model Properties & Validation 130
5.2 Iterative Route Assignment Strategy 132
5.2.1 Plans Creation 133
5.2.2 Plans Selection 134
5.2.3 Plans Termination 135
5.3 Results on Experimental Scenarios 135
5.3.1 Paradoxes in Transportation Networks 135
5.3.2 Effects of Bi-directional Flows on the System 140
5.3.3 Simulation of a Large Scenario 143
5.3.4 Computational Times Analysis 145

6 Conclusions and Future Research Directions **147**

A An In-vivo Observation to Understand the Behavior of Pedestrian Groups **151**
A.1 Level of Density and Service 152
A.2 Flow Composition 153
A.3 Trajectories and Walking Speed 153
A.4 Group Proxemics Dispersion 154

List of Figures

1.1 The three levels of behaviour, taken by Schadschneider et al. [2009]. . . . 2

1.2 The possible applications of the pedestrian and crowd simulations models. The two bottom pictures are taken respectively from Wagoum et al. [2012a] and Leal-Taixé et al. [2011]. 5

2.1 The Analysis–Synthesis framework for the research on pedestrian dynamics. The synthesis is dedicated to modeling and simulation while analysis to data gathering and knowledge improvement, but they are completely correlated and follow the same main goal of understanding and predicting the complex system. 11

2.2 Classification of the literature on modeling and simulation of pedestrian dynamics. Three major approaches can be recognized, from numerical simulations which consider only the aggregated flow until the microscopic modeling of individual behaviors. 13

2.3 The three levels of individual behavior, stated in Hoogendoorn and Bovy [2004] and also reported in Schadschneider et al. [2009]. 15

2.4 Two examples of potential fields typically used in continuous model. In both cases the targets are the openings on the right of the scenario. The pictures have been taken from Twarogowska et al. [2014] and Kretz et al. [2014]. 18

2.5 The speed–density and flow–density relations achieved with the two explained formulations. The purple line denotes the linear function, while the non-linear one is plotted with the green line. 20

2.6 Reproduction of the Braess paradox with a second order model [Twarogowska et al., 2014] (pictures taken from the paper). The evacuation times in case of a room with the exit surrounded by obstacles are significantly smaller than in the other case, where the formation of a circular area of high densities (so-called *clogging effect*) generates circulation delays and higher evacuation times. 21

2.7 An example network representation (b) of a portion of the Milan street map (b), taken from Google Maps®. Each edge of the graph contains 1-dimensional queues that will host the simulated individuals, either vehicles or pedestrians. The uni-dimensionality of the queues implies that a normal street of two lanes, one per direction, will configure two different queues between the two nodes. 24

2.8 (a) Graphical description of the social forces acting on the highlighted pedestrian. (b) Lane formation effects emerged with the simulation of a bi-directional flow (taken from Helbing and Molnar [1995]). 29

2.9 A qualitative comparison between observations and simulations of the work of Moussaïd et al. [2010]. The lane pattern is the mostly observed at low densities, while at moderate densities the groups tend to compress themselves composing a v-like pattern. 31

2.10 Calibration of the model of Blue and Adler [2001], by simulating a long corridor of 10 lanes of cells and with different configuration of p_exchg. The picture is taken from the paper: here the authors used the term *Volume* to denote *Flow*. 34

2.11 (a) Graphical examples of a static floor field, generated from an exit centered in (x=16,y=0). (b) The situation of two dynamic ones, together with the current position of two populations of pedestrians moving in opposite directions. The self-organization of flows in separated lanes is clearly visible. 35

2.12 Qualitative comparison of the four strategies for the management of the tactical level defined in Wagoum et al. [2012b] (picture taken from the paper). 38

2.13 (a) Traveling options available at the website tfl.gov.uk: they already consider necessities derived by having walking impairments. (b) Example of groups composed by an elderly person and a caretaker. The two persons will practically cover the same trajectory. 41

2.14 A qualitative representation of the pedestrian fundamental diagram (a) and a plot containing multiple data-sets and definitions from the literature (taken from Zhang et al. [2012]), in the form density(ρ) – flow (J_s). 43

2.15 A set of pedestrians positions and their associated Voronoi cells (taken from Steffen and Seyfried [2010]). 44

2.16 Comparison of the fundamental diagram for uni and bi-directional pedestrian flow, in the form density–speed (a) and density–flow (b), achieved with the experiments of Zhang et al. [2012]. The experiments configuration is shown in (c). The pictures have been taken from the paper. 45

2.17 Analysis of the space utilization in stars from Burghardt et al. [2013]. From left to right each image shows densities, velocities and flows over the space. The three configurations of the flow (S1 – S3 – S6) are ordered in a decreasing way and have been achieved by regulating the width of the entrance door to the stairway. 46

2.18 The scenario configuration of the experiment that will be performed in Tokyo. 48

3.1 Overview of the agents architecture facing the modeling problem. 50

3.2 An example scenario annotated with the spatial markers of the model. The scenario is a toy representation of a university building, with a few lessons rooms containing waiting areas (modeled with intermediate targets). . . . 52
3.3 (a) Graphical representation of the first three floor fields of the model (the red cells are obstacles, while the blue object is a final destination). (b) Difference between the manhattan and chessboard metric with $\sqrt{2}$ over corners. . . . 54
3.4 An example scenario with 3 regions divided by 3 openings. . . . 56
3.5 An example representation of the density field values during the simulation (for simplicity, the values of $Area(Q_{(i,j),r})$ are omitted). The radius chosen in this case is 0.8 m, understandable by the illustrated red circles. 58
3.6 The cognitive model proposed by Paris et al. [2006] (a) and the one proposed by Shao and Terzopoulos [2007] (b). . . . 59
3.7 (a) A sample annotated scenario representing an apartment composed of 5 rooms. The cognitive map associated to this environment is shown in (c). The procedure for the computation of the graph iteratively adds nodes and edges with the field diffusion from the openings objects (b). (d) The cognitive map integrated with the mapping to the path fields of openings, that will be used by the agents. . . . 61
3.8 The conflict detection activity: the intention of movement of agents are collected in a additional data structure that links the chosen destinations to the agents. Multiple choices of the same destination cell are saved in a dedicated list, in order to maintain the computational time of this task very limited. . . . 63
3.9 A graphical representation of the proposed hybrid architecture of the agent. The tactical level component generates the set of destinations that the body will have to reach, under the influence of the floor fields. . . . 65
3.10 A typical situation that can arise with bi-directional flow (here lighter pedestrians try to go to the right and vice-versa for the darker ones), even by employing mechanisms stimulating the well-known lane formation. To face this problem, this model allows a temporary double occupation of cells. . . . 70
3.11 Graphical representation of a group composed of nine members and the area of the convex polygon that contains all the group members . . . 75
3.12 Graphical representation of $Balance(k)$, for $k = 1$ and $\delta = 2.5$ . . . 76
3.13 Space covered by the agent, per step, in a scenario where only diagonal movements are possible, shown on the left. . . . 79
3.14 Space covered by the agent in the second set of tests. Blue dots are obtained with the *sub-urn* method, while red ones without. The green line describes 1.31 m/sec. . . . 81

3.15 A schema depicting an example representation of a staircase, that will change the speed of the pedestrian according to the parameter *slope*. . . 82
3.16 The life-cycle of the agent. 83
3.17 The basic method for the route choice, producing the path with the minimum number of crossed nodes between the agent position (in yellow) and destination (in green). The route #1 will be the output, without considering the possibility offered by the route #2 in terms of distance. . 85
3.18 From the left: the example scenario of the university buiding, also shown at the beginning of the Chapter and the respective cognitive map. 85
3.19 The cognitive map with the integration of the distance between markers, inside each region. For simplicity the data are represented with a tabular version but, given the symmetry of the relation, more optimized data-structures can be easily defined (e.g. dictionary). 86
3.20 A concave region can imply the plausibility of a path crossing it twice, but its identification is not elementary. 88
3.21 The correct paths for this environment. Inside r_2 the choice between the two openings is also determined by the congestion. 89
3.22 Application of the Paths Tree computation algorithm in an example scenario. 94
3.23 Examples of surroundings of different sizes, for two configurations of the environment. 95
3.24 The final life-cycle of the agent: the core component of the dynamical route choice procedure is the wayfinding, which is now performed with the Paths Tree. The last decision node linking at it manages the activation of the procedure, with respect to the perceived congestion. 98

4.1 The corridors used for the fundamental diagram tests. 101
4.2 Comparison with the fundamental diagrams from simulations and data-sets from the literature. 102
4.3 Example of emergence of the lane formation effect with the simulation of bi-directional flow. In these simulations both large and stable lanes (on the top) and more dynamic ones (on the bottom) have been arisen. . 103
4.4 Fundamental diagrams achieved with the simulation of bi-directional flow in the corridor. The empirical data-sets are taken from Older [1968] and Weidmann [1993]. 104
4.5 The corridors used for the environment rotation experiments. 105
4.6 Achieved fundamental diagrams comparing the flow generated with the two corridors, in case of uni-directional and bi-directional flow. 106
4.7 Comparison of density diagrams for the T-junction scenario in the case of 0 and 45 rotation. 107
4.8 Fundamental diagram achieved with the staircase scenario. 108

4.9 From the left: an overview of the Vittorio Emanuele II gallery, the streaming of passerby within the walkway and a snapshot of the recorded video images with the superimposed grid for the data analysis. A completely similar grid will be used for the simulation scenario, with pedestrian flows directed either to north or south sides. 109
4.10 The qualitative test scenario (a), representing an entrance to a building with a small stair and a ramp for people with mobility impairments. In (b) a "merge" between the paths tree dedicated to *normal* agents and for the *region selective* agents is shown. The dashed branch, passing through the stairs region, appears only in the normal agents tree. This approach automatically lets the *region selective* agent (blue colored) choose the ramp instead of the stairs (c – d). 112
4.11 The environment (a) and respective paths tree (b) used for the second experiment. The traveling times written in the paths tree nodes refer only to the normal agent class. 115
4.12 A diagram showing the evolution of the number of pedestrians still in the scenario in time (a) and a graph showing the evolution of travel time for pedestrians entering the simulation environment at a given time (b). 116
4.13 The test scenario respectively with a high and low sensitivity of the agents for the plan re-computation. A few, but important, differences can be identified and explain the impact of the low sensitivity on the congestion areas: in this case the route adaptation is performed a bit after, leading to higher congestion in the employed exits. 117
4.14 Times for the computation of a single step achieved with the simulation of the operational level. 118
4.15 The benchmark scenario (a) used for the analysis of the computational times of the tactical level and the respective results (b). 119

5.1 The proposed approach for the multi-scale simulation system, employing mesoscopic simulations with MATSim and microscopic simulations with the discrete model proposed in this Chapter. 122
5.2 Example of a scenario with different paths leading to the exit. The need to stop the floor field diffusion of the intermediate target $B2$ in the cell of A is evident: by diffusing it over the whole space, pedestrians travelling from $B1$ to $B2$ would travel as well through A cells. 125
5.3 The density field working principle: at the beginning of the time-step, pedestrians signal their presence by adding 1 in the nearby cells (here the radius is 2 cells). 126
5.4 The jam (a) and counter-flow (b) rules. In (a), the cell that became empty remains blocked. In (b) two counter-flow pedestrians (the light pedestrian follows the dark color and vice-versa) swap their positions. . 128

5.5 Activity diagram illustrating the algorithm for the swapping rule of the CA. Pedestrians check the direction of the others in front by the floor field (FF) and are allowed to choose movements in positions occupied by counterflow pedestrians. At the end of the step, the Pedestrian Synchronizer swaps only those pedestrians, where movement choices match. 129

5.6 Fundamental diagrams for uni-directional (a) and bi-directional (b) flows. Black dots are measurements from the simulations, while gray circles are the empirical data from Zhang et al. [2011, 2012]. Average flow per simulated density is indicated by the solid curve. 131

5.7 Illustration of the route assignment search strategy. 132

5.8 Graph representations of the network explained by Braess [1968] (a) and Daganzo [1998] (b). Labels of edges represent their cost. 136

5.9 (a) Implementation of the Braess (the corridor at the center is the additional link) and (b) Daganzo (with bottleneck width of 1.2 m) experiments. The environment borders and blue objects represent the nodes of the underlying network. 137

5.10 Average travel times of agents within the simulations of the Braess (a) and Daganzo (b) paradox scenarios. 138

5.11 Iterative system optimum search for the scenario of the Braess (a) and Daganzo (b) paradox. 139

5.12 A frame taken from the footage of the experiments performed by Plaue et al. [2012] and the CA environment layout for both 90- and 180-degree intersection experiments. 141

5.13 Time series of density and speed of 180-degree intersection experiment compared with CA simulation. 142

5.14 Time series of density and speed of 90-degree intersection experiment compared with CA simulation. 143

5.15 Simulation of the large scenario: the top row refers to the base setting, while the bottom one shows the dynamics with the introduction of counter-flow. All screenshots are taken at the same simulation time, around 5:30min. 144

5.16 Computing time analysis: (a) computing time of route computation and CA simulation over iteration number, achieved with the simulation of the large scenario; (b) computational times per single time-step over the number of agents. 146

A.1 From the left: an overview of the Vittorio Emanuele II gallery, the streaming of passerby within the walkway and a snapshot of the recorded video images with the superimposed grid for data analysis 152

A.2 A diagram showing most frequent positions, normalized with respect to the centroid and the movement direction, assumed by members of couples (a), triples (b) and groups of four members (c). 156

List of Tables

4.1 Assignment of the calibration parameters regarding the operational level model. 100
4.2 Average groups dispersion achieved by the simulations (standard deviation inside breaks). 109
4.3 Average speeds of groups. 110
4.4 Average traveled distance of groups. 110

5.1 Assignment of the parameters of the new CA model. 127

1
Introduction

The usage of computer simulations generating plausible, realistic or effective (according to different criteria) trajectories of moving entities in synthetic environments, maybe replicating existing or planned ones, represent a goal of different areas in computer science, from robotics to complex systems studies. With this category of works, we are referring to models able to make decisions about the movements of entities *located* in an environment by considering, on the one hand, their local interactions with physical objects and with other entities (e.g. to adjust their trajectory and avoid collisions). On the other hand, these models have also to consider the way these entities are using perceived information about the overall state of the system, aiming to re-schedule, or also to change, their actual *plan* of activities.

The overall design a model for the simulation of the movement behavior of some entities, in fact, represents a task that can be decomposed into three levels, considering the three well-known behavioral levels from the transportation field[1]. These levels, shown in Figure 1.1, consider different activities and objectives of the simulated entities:

- the **strategical** level describes to the generation of the main objective of the day;
- the **tactical** level is related to the generation and scheduling of all activities necessary to reach the final goal, building the individual *plan*;
- the **operational** level, finally, is the lowest one and refers to the physical execution of each activity of the plan (i.e. movement of the entity in the space).

Depending on their aims, models in the literature can be more focused on one level than the others. In traffic or pedestrian simulation models the strategic level is often substituted with actual data about human activities[2], whereas in robotics, the goals are generally set by the creators of the artificial entities. Tactical and operational levels, instead, have been highly debated in the literature, with different levels of detail.

[1]In the field of pedestrian dynamics, this scheme has been firstly proposed by Hoogendoorn and Bovy [2004] and it is also reported by Schadschneider et al. [2009]. However, similar schemes can be found in the preceding literature of vehicular traffic [Michon, 1985].

[2]From questionnaires or field studies characterizing the mobility of people at urban level or within more circumscribed contexts.

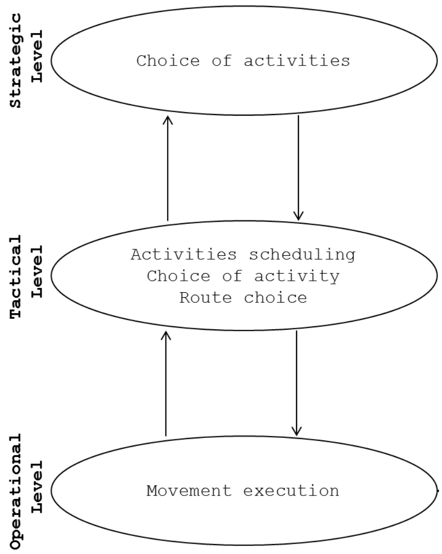

Figure 1.1: *The three levels of behaviour, taken by Schadschneider et al. [2009].*

The reproduction of the physical properties of the system has been the main aim of this branch of the modeling and simulation line of research and it has been extended and applied for a wide set of purposes. Designing algorithms to simulate the raw movement well in the space have been highly discussed in the field of robotics, in order to find effective methods to let robots avoid obstacles in the environment. First approaches were described by the usage of so-called *potential fields*, which are implementation of distances driving the simulated entities towards the destination, possibly letting them to avoid obstacles. The first work taking this perspective has been presented in Khatib [1986]. Problems generated by this approach have been discussed in Koren and Borenstein [1991], while a variation of this algorithm able to overcome these issues has been proposed in Borenstein and Koren [1989].

The simulation of microscopic behavior and interactions has been widely investigated also in the field of computational biology, to simulate the behavior of cells or other micro-organism in biological environments[Walker et al., 2004, Emonet et al., 2005]. It is necessary to state that the models in this field are slightly different from the ones described before, since the studied entities do not actually make decisions about movement, but they essentially follow rules given by the environment in which they are situated. Particularly interesting approaches have been defined with the aim to simulate the behavior of micro-organisms that will used to construct synthetic biology circuits or devices, in order to test the architectures and the expected calculations [Goni-Moreno and Amos, 2014].

A significant effort has been spent for the production of models related to traffic engineering, investigating the capacity of the transportation network and its critical points where the congestion is emerging and causing significant delays. The research of this field firstly focused only on the simulation of vehicular traffic, starting from the simple consideration of a uni-directional environment, for the simulation of a single lane [Gipps, 1981, Nagel and Schreckenberg, 1992], and then considering also multiple lanes and overcoming behavior [Nagel et al., 1998].

The study of pedestrian dynamics is considered significantly more complex than the vehicular traffic, given the much less constrained movement and variables (think to crowded situations with multi-directional flows), and so the interest on this field has arrived later. Nonetheless, starting from the nineties, the production of models for this purpose has rapidly grown up due to the importance of their application and to the significant advancements in computational resources and capacity. This branch of the modeling and simulation field constitutes a consolidated approach as well and the contributions provided by this Thesis will be mainly located in this branch. The motivations of this choice will be part of the discussion of the next Section.

1.1 Modeling and Simulation of Pedestrian Dynamics

Starting from 2000, many studies from the *United Nations* have emphasized that urbanization is currently one of the most significant tendencies of the world population [Wor, 2011]: among the provided analysis, it has been forecast that from 2025 the 58% of the global population will live in cities and urban agglomerate.

The analysis and prediction of possible outcomes of crowded situations, therefore, is gaining more and more importance for the global society, with the aim to avoid crowd disasters as, for example, it recently happened at the *Love Parade* in Duisburg or also the crowd stampede recently happened at the *Makkah Pilgrimage*, both dramatically causing a relevant number of injuries and deaths. For the planning of new transportation infrastructures and areas that will host crowded events it is very important to consider a dynamic analysis that passes through the simulation of the pedestrian flows, but this is not the only application of these simulations. In this context, pedestrian dynamics models can find several applications:

- as off-line decision support systems, for designers of buildings which will undergo crowded situations (e.g. train or subway stations) or organizers of large events (e.g. an exposition), in order to improve the safety and the walkability of the environment;
- as on-line simulation systems that can support evacuation situations [Wagoum et al., 2012a, Georgoudas et al., 2010];
- to improve the results of tracking algorithms in the field of computer vision (e.g. Leal-Taixé et al. [2011]), where the problem of *occlusion* of pedestrians, occurring in dense situations or in camera with a non-zenithal perspective, negatively impacts on the results.

This applications are graphically summarized in Figure 1.2. Regarding the first one, the usage of computer models to simulate the pedestrian dynamics can help designers to perform a deep and dynamical analysis of their projects, allowing them to populate and simulate environments by configuring the so-called *what-if* scenarios. By analyzing the evolution of local densities and flows among the environment, providing also estimations of origin-destination traveling times, these tests support the improving of the overall security and perceived comfort for the future users of the environments. Given the importance of this kind of analysis, several off-the-shelf simulators have been already developed and can be currently found on the market[3]. These tools provide simulation frameworks whereby it is possible to configure sufficiently heterogeneous populations of pedestrians (e.g. with different walking speeds) and, in some cases, even to simulate the presence of groups of people (modelled with an attractive force among members, although this feature is generally not systematically documented and evaluated). However, although some significant results have been achieved, the overall issue of simulating large, heterogeneous crowds of pedestrians still presents open challenges, since the crowd is a complex system and all of these mathematical/computational models can be improved for obtaining more microscopic and realistic simulations, according to the empirical knowledge about the system which is continuously growing.

The realization of on-line simulation systems for the assistance of evacuation does not necessarily imply the usage of a different models. The main issue of this application, in fact, is related to the computing times of the simulator, that has to be significantly faster than real-time even with the simulation of a large crowds with tens of thousands of pedestrians. This objective has two outcomes: (i) the design of a very efficient simulation model that naturally scales the computational times with the number of simulated pedestrians; (ii) the usage of novel technologies for a massively parallel implementation of the computational model, implying the usage of super-computers that allows a very fast execution of the simulator. The approaches that will be proposed in this Thesis will not be precisely aimed to the development of such on-line simulation system, counting instead on the realization of an off-line system. On the other hand, the modeling approach that will be taken, composing a discrete representation of the environment, represent an intrinsically efficient methodology, therefore the implementation of such faster than real-time system could be a future direction of this research work.

1.2 Considering the Heterogeneity of the Crowd

The title of this Thesis should have already suggested to the reader that part of the methodologies that will be proposed are aimed to the consideration of the crowd as a system composed of non-homogeneous entities. This finds quite elementary reasons by

[3]see `http://www.evacmod.net/?q=node/5` for a significant although not necessarily comprehensive list of simulation platforms.

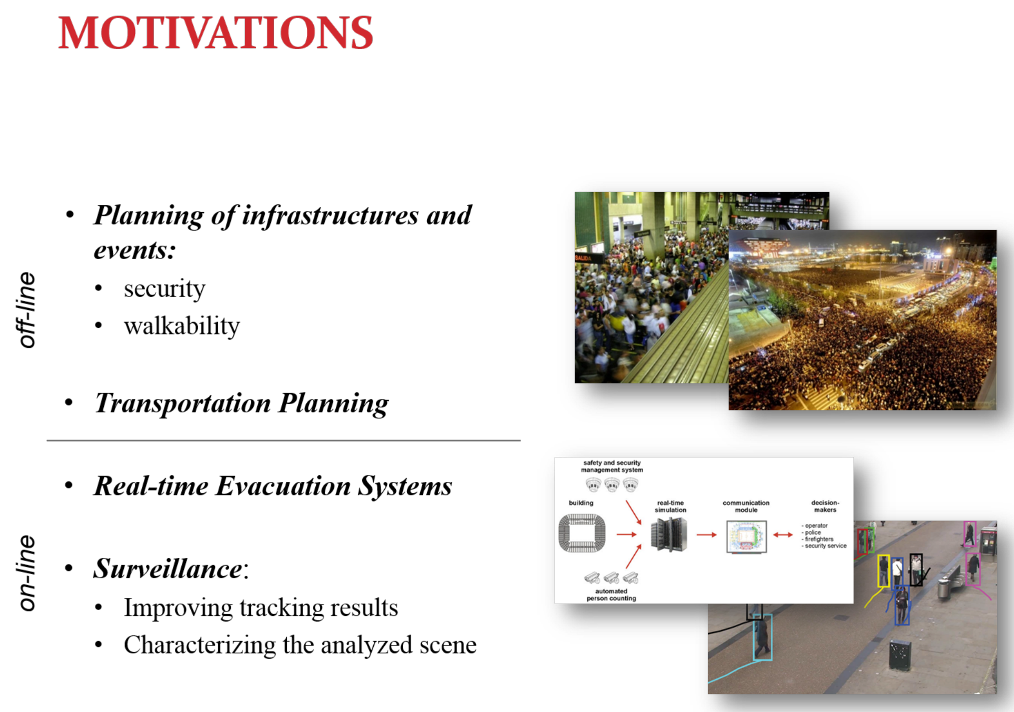

Figure 1.2: *The possible applications of the pedestrian and crowd simulations models. The two bottom pictures are taken respectively from Wagoum et al. [2012a] and Leal-Taixé et al. [2011].*

thinking to the reproduction of different element of the environment that systematically imply a different behavior: as an example, just consider the walking speed on stairs or escalators. On the other hand, additional motivations can be found by considering the differences in the walking behavior of pedestrians regarding their age, that has been found to be significant (see, e.g., Willis et al. [2004]).

The consideration of this category of pedestrians gains importance by taking into account two other arising tendencies of the global society, which are the decreasing of the fertility rate and the increasing of life expectancy. Together, they are leading to the well-known phenomenon of the *Ageing Society* [Wor, 2002], which represents one of the main challenges of the more economically developed countries. The concept of *Age-Friendly city*, defined by the World Health Organization [Age, 2007], describes a framework for the development of cities which encourages the *active ageing* of their citizens, allowing them to maintain an active and productive status in the society, that delays the moment in which they will become a cost. Mobility naturally represents a key feature of this framework, being significant with respect either to transportation and accessibility of facilities.

1.3 Contributions and Overview of the Thesis

The discussion of the Thesis work will be organized as the following.

Chapter 2 will propose a thoroughly discussion of the state of the art of modeling and simulation of pedestrian dynamics, identifying different classes and approaches of modeling, in order to let the reader understand the contributions brought by the proposed models. An additional discussion of the validation problem will conclude the Chapter, describing the instrument generally used for this task.

Chapter 3 will discuss the first main contribution of the Thesis, which is an innovative microscopic model, based on the discrete modeling approach, dealing with operational and tactical level of behavior and considering heterogeneity in the simulated population.

Chapter 4 will present an analysis of the model properties, showing the validation tests regarding the operational layer and some experimental scenarios showing the functioning and properties of the tactical level component.

Chapter 5 will propose another discrete model, more simple in the behavioral rules, that is suitable for an integration with a mesoscopic simulation system that employs an iterative algorithm to deal with the route choice and tactical level of behavior. This work moves towards the realization of a multi-scale model allowing the simulation of heterogeneous modes of transportation at a more macroscopic level and considering microscopical details in purely pedestrian environments.

Chapter 6 will conclude the Thesis discussion, by providing also possible extension of the current state of the research.

1.4 Selection of Relevant Publications

The works and methodologies that will be proposed and discussed in this elaborate have already produced publications in International Journals or in the proceedings of International Conferences. The following list summarizes the *major* contributions of the overall Thesis.

- Models and algorithms for the operational level:
  - A discrete model considering groups:

    Vizzari, G., Manenti, L., **Crociani, L.**: Adaptive pedestrian behaviour for the preservation of group cohesion. Complex Adaptive Systems Modeling **1** (2013) 1–29.
  - An approach to deal with heterogeneous velocities in discrete environments:

    Bandini, S., **Crociani, L.**, Vizzari, G.: Heterogeneous speed profiles in discrete models for pedestrian simulation. Poster at the 93rd Transportation Research Board annual meeting, Washington, January 2014 - Committee number AHB45 - TRB Committee on Traffic Flow Theory and Characteristics arXiv preprint arXiv:1401.8132 (2014).

- The consideration of elderlies on the simulations:

  Bandini, S., **Crociani, L.**, Vizzari, G.: Pedestrian Simulation: Considering Elderlies in the Models and in the Simulation Results. Ambient Assisted Living (2015).

- Approaches for tactical level:
  - A hybrid agent architecture to encompass operational and tactical level of behavior:

    Crociani, L., Invernizzi, A., Vizzari, G.: A Hybrid Agent Architecture for Enabling Tactical Level Decisions in Floor Field Approaches. Transportation Research Procedia (2014) 618–623.
  - Modeling adaptive hybrid agents to allow dynamical decisions at tactical level

    Crociani, L., Piazzoni, A., Vizzari, G., Bandini, S.: Adaptive Tactical Decisions in Pedestrian Simulation: A Hybrid Agent Approach In: AI*IA 2015: Advances in Artificial Intelligence. Lecture Notes in Computer Science, Vol. 9336 (2015) 58–71.

- Towards multi-scale modeling of pedestrian and vehicular traffic:

  Crociani, L., Lämmel, G.: Multi-destination Pedestrian Flows in Equilibrium: a Cellular Automaton Based Approach. Computer Aided Civil and Infrastructure Engineering (CACAIE). (In Press)

1.5 Other Publications

Additional publications of the proposed approaches and, also, of other works not necessarily included in this Thesis is listed in the following:

Journal Papers:

- Bandini, S., Crociani, L., Vizzari, G.: An Approach for Managing Heterogeneous Speed Profiles in Cellular Automata Pedestrian Models. Journal of Cellular Automata. (In Press)
- Crociani, L., Piazzoni, A., Vizzari, G., Bandini, S.: When Reactive Agents Are Not Enough: Tactical Level Decisions in Pedestrian Simulation. Intelligenza Artificiale. IOS Press. (In Press)

Conference Papers:

- Boukas, E., Crociani, L., Manzoni, S., Vizzari, G., Gasteratos, A., Sirakoulis, G.C.: An intelligent tool for the automated evaluation of pedestrian simulation. In: Artificial Intelligence: Methods and Applications. Lecture Notes in Computer Science, Vol. 8445 (2014) 136–149.
- Bandini, S., Crociani, L., Vizzari, G.: Modeling heterogeneous speed profiles in discrete models for pedestrian simulation. In: Proceedings of the 2014 international conference on Autonomous agents and multi-agent systems, International Foundation for Autonomous Agents and Multiagent Systems (2014) 1541–1542.
- Bandini, S., Crociani, L., Gorrini, A., Vizzari, G.: Empirical investigation on pedestrian dynamics in presence of groups: a real world case study. In: Proceedings of the 2014 international conference on Autonomous agents and multi-agent systems, International Foundation for Autonomous Agents and Multiagent Systems (2014) 1545–1546.
- Crociani, L., Vizzari, G.: An Integrated Model for the Simulation of Pedestrian Crossings. In: 11th International Conference on Cellular Automata for Research and Industry. Lecture Notes in Computer Science, Vol. 8751 (2014) 670–679.
- Crociani, L., Manenti, L., Vizzari, G.: Makksim: Mas-based crowd simulations for designers decision support. In: Advances on Practical Applications of Agents and Multi-Agent Systems. Lecture Notes in Computer Science, Vol. 7879 (2013) 25–36.
- Crociani, L., Manenti, L., Vizzari, G.: Pedestrians and crowd simulations with makksim – A demonstration. In: Advances on Practical Applications of Agents and Multi-Agent Systems. Lecture Notes in Computer Science, Vol. 7879 (2013) 267–270.
- Crociani, L., Vizzari, G., Bandini, S.: Towards the introduction of parallelism in the makksim pedestrian simulator. In: Parallel Computing Technologies. Lecture Notes in Computer Science, Vol. 7979 (2013) 310–315.
- Bandini, S., Crociani, L., Vizzari, G.: Social interactions in crowds of pedestrians: An adaptive model for group cohesion. In: AI*IA 2013: Advances in Artificial Intelligence. Lecture Notes in Computer Science, Vol. 8249 (2013) 288–299.
- Bandini, S., Crociani, L., Vizzari, G.: Heterogeneous Pedestrian Walking Speed in Discrete Simulation Models. In: Traffic and Granular Flow 2013. Springer International Publishing (2013) 273–279.

Workshop Papers:

- Crociani, L., Piazzoni, A., Vizzari, G.: Adaptive Hybrid Agents for Tactical Decisions in Pedestrian Environments. Workshop from Objects to Agents 2015 (WOA 2015).

- Crociani, L., Gorrini, A., Vizzari, G.: Pedestrian dynamics in presence of groups: an agent-based model applied to a real world case study. Eighth International Workshop on Agents in Traffic and Transportation (2014). Held at the 13th Int. Conf. on Autonomous Agents and Multiagent Systems (AAMAS 2014).
- Bandini, S., Crociani, L., Vizzari, G.: Agent Based Pedestrian Simulation: Considering Elderlies in the Simulated Population. Artificial Intelligence for Ambient Assisted Living (2014).
- Bandini, S., Crociani, L., Vizzari, G.: Towards a more comprehensive estimation of social costs in pedestrian facilities. The challenge of Ageing Society: technological roles and opportunities for Artificial Intelligence (2013).
- Khan, S.D., Crociani, L., Vizzari, G.: Integrated analysis and synthesis of pedestrian dynamics: First results in a real world case study. Workshop from Objects to Agents 2013 (WOA 2013).

2
State Of The Art

Research on pedestrian dynamics has significantly grown in the last years, due to the increasing needs of analyzing the safety of environments that have to host large crowds. Public spaces and pedestrian environments, in fact, need to be analyzed to understand the evolution of flows, identifying critical points and improving the safety on one side, and to find ways to optimize and improve the performances on the other (e.g. travel times, level of services, social costs).

The research in this area can be classified according to the framework introduced by Bandini et al. [2014] and shown in Figure 2.1, general for the investigation of complex systems. The design of the simulator, that includes all assumptions made by the modelers, characterizes the *synthesis* side and will lead to the production of simulated data. The *analysis* phase is fundamental for the acquisition of new knowledge and

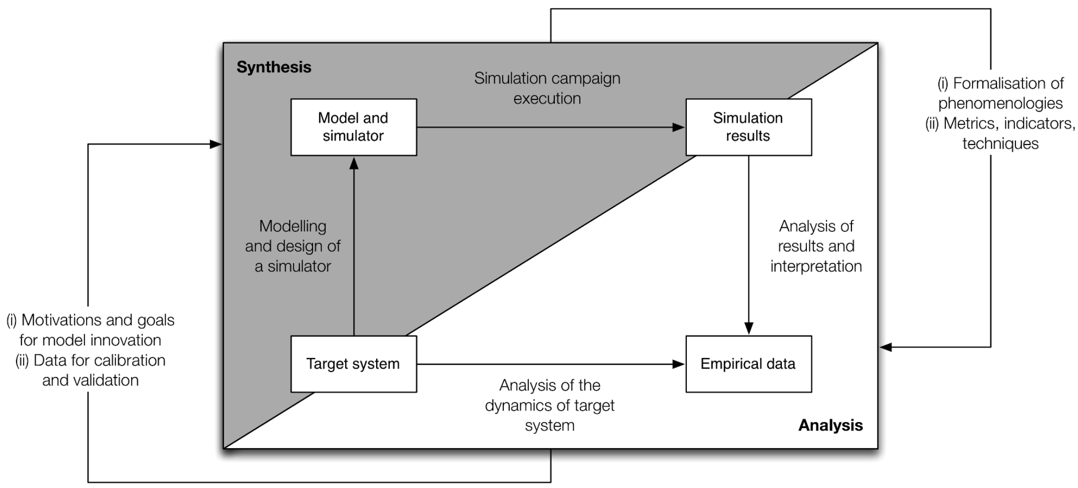

Figure 2.1: *The Analysis–Synthesis framework for the research on pedestrian dynamics. The synthesis is dedicated to modeling and simulation while analysis to data gathering and knowledge improvement, but they are completely correlated and follow the same main goal of understanding and predicting the complex system.*

empirical data, that will be used to validate the simulation results.

Much effort has been spent on the analysis of the pedestrian dynamics, principally providing empirical data about the physical motion by means of *in-vivo* observations of the real-world. The quality of these observations is more appreciable since they are unobtrusive and records the real dynamics, without applying any influence. On the other hand, the high number of variables influencing the behavior of the observed pedestrians leads to difficulties in thoroughly understanding the dynamic phenomena implied by the movement of crowds of pedestrians and the correlation among these phenomena. Several researches in this perspective can be found in the literature, from seminal and now dated works (e.g. Older [1968], Fruin [1971]), to more recent ones (e.g. Willis et al. [2004], Helbing et al. [2007], Schultz et al. [2010], Bandini et al. [2014]) dedicated to understand the influence of specific variables, like groups [Bandini et al., 2014] or even panic [Helbing et al., 2007]. In order to achieve a higher degree of control on the situation and to obtain a more systematic understanding of the correlation among variables, another branch of the research has developed, dedicated to *in-vitro* experiments in controlled conditions and environmental settings where the dynamics is easier to analyze [Zhang et al., 2011, 2012, Liu et al., 2014]. For the overall analysis side, the work-flow of data and trajectories collection for this purpose has been significantly improved with the new technologies proposed for automatic tracking and extraction of empirical data (e.g., Liu et al. [2009], Boltes et al. [2011], Boltes and Seyfried [2013]), proposing also new techniques for the automatic recognition of groups of pedestrians (e.g. Solera et al. [2013]).

On the other hand, works on the synthesis side have produced a relevant number of simulation models, that can lead to new inferences and suggestions about the studied dynamics (e.g. identifying an increasing of flow by positioning an obstacle in presence of bottlenecks, as in Yanagisawa et al. [2009]) or to simulation systems usable to analyze the evolution of pedestrian flows and giving information to improve the safety of environments [Wagoum et al., 2012a, Georgoudas et al., 2010]. Since this thesis is focused on the synthesis side, the literature chapter here presented will be focused on this topic.

The literature of pedestrian simulation can be structured and classified, as shown in the Figure 2.2, among three principal perspectives: macroscopic, mesoscopic and microscopic modeling approach. This classification comes from the vehicular traffic simulation but it can be as well applied to the pedestrian literature.

Generally, the criterion used to categorize a model among these classes is related to the consideration of individuals in the simulation. A model that simulates each individual pedestrian is considered as microscopic, independently from the level of details of the behavioral model. A macroscopic model, instead, threats the problem from a higher perspective, simulating the crowd as a whole entity where pedestrians are represented only by the concept of density. The mesoscopic approach is something in between the two perspectives, since the entities are aggregated into groups, in order

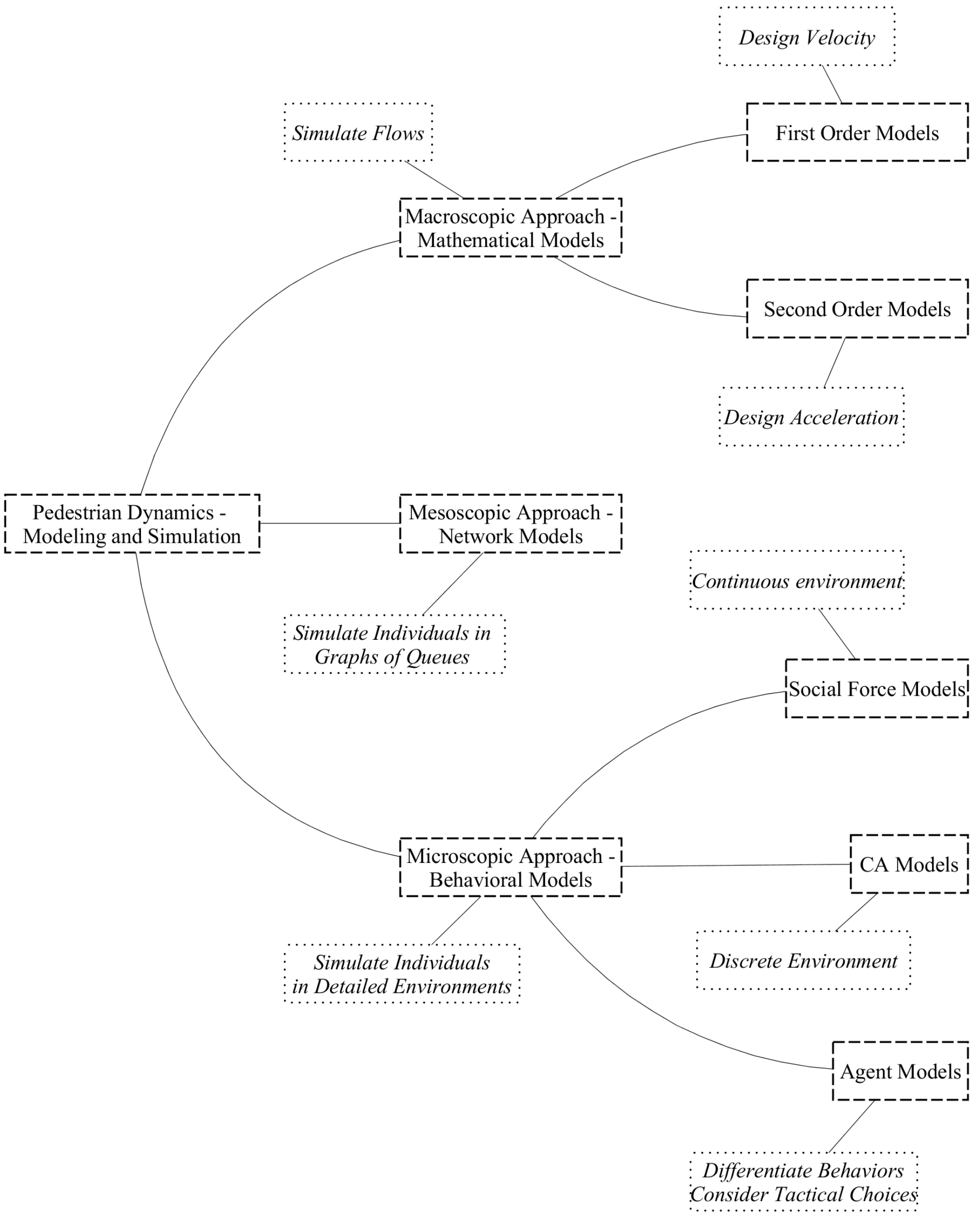

Figure 2.2: *Classification of the literature on modeling and simulation of pedestrian dynamics. Three major approaches can be recognized, from numerical simulations which consider only the aggregated flow until the microscopic modeling of individual behaviors.*

to abstract their behavior without too much loss on the precision of the simulations.

Nonetheless, it must be noted that this is not the only criterion that can be applied to categorize models. The literature discussion that will be proposed in this Chapter will present a slightly different categorization by using another perspective, which follows the logic applied for the realization of the works described afterwards (in particular the one presented in Chapter 5). In this proposal the criterion is related to the granularity of the individual behavior in the model, ranging from the not consideration of individuals of the macroscopic models to a detailed representation of microscopic ones. The middle class refers to models which share the characteristic of these two classes, by considering individuals (or also groups of them) but representing their behaviors in a more abstract way, with lower fidelity.

The modeling categories and their peculiarities are finally described in the following:

- Macroscopic models propose mathematical frameworks based on *partial differential equations* systems, which describe the evolution of flows in planar environments. Individuals and their interactions are not considered and this makes these models more suitable for the simulation of high densities situations. The main characteristic of this approach, in fact, is that it deals with *fractions* of pedestrians: only the local density is considered, thus the crowd is modeled as a fluid where each person is decomposed in a continuum. These models are relatively simple (only a few parameters describe the dynamics) and computationally efficient with respect to the simulated population, since the simulation times grow only with the size of the simulated space. Inside the macroscopic class it is possible to recognize another classification among first order models, that describe the velocity of pedestrian and models of second order which consider their acceleration.
- Mesoscopic models describe the dynamics of traffic, including both the vehicular and the pedestrian one, in very large environments like cities. The proportions of the simulated space implies a loss of its details and leads to a network representation where each city road will describe one edge between nodes describing roads intersections. The simulation of each edge is managed with a queue model, based on the assumption that a certain relationship exists between density of the area and velocity of entities moving through it (i.e. the fundamental diagram, explained in Section 2.5.1). Each queue of the network hosts the individuals in a 1-dimensional environment and generates the out-flow by mainly considering its characteristics (e.g. width of the link, free flow speed, etc.). The individual behavior and interactions are, thus, also represented in an abstract manner.
- Microscopic modeling is a *bottom-up* approach that aims at reproducing the aggregated phenomena and statistics of the system by means of the interactions among pedestrians, which are designed with the individual behaviors – the main modeling objective of the class. Regarding the approach to the representation of the individual, three sub-classes can be identified: force-based models design pedestrians as particles moved by attractive and repulsive forces, composing a system of *ordinary differential* equations; cellular automata (CA) models imple-

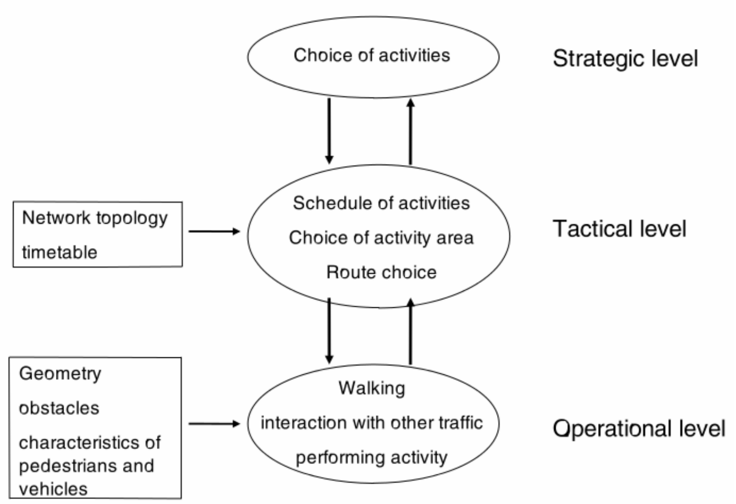

Figure 2.3: *The three levels of individual behavior, stated in Hoogendoorn and Bovy [2004] and also reported in Schadschneider et al. [2009].*

ments pedestrians as states of cells, moved with ad hoc rules or with probabilities influenced by potential fields; agent–based models are the most expressive class and describe pedestrians as individual agents, with its own characteristics and preferences. The framework of the agent–based systems, in addition, allows the introduction of reasoning mechanisms for the consideration of decisions at higher levels of pedestrian behavior.

An important difference between the macroscopic approach and the meso and microscopic ones is that, while the first one limits the modeling perspective on the variation of aggregated quantities like densities and flows, the lower two both aims at representing the dynamics by means of the collection of individuals behaviors, singularly modeled. Naturally, modeling the individual behavior is a complex task and needs to be clarified. As stated by Hoogendoorn and Bovy [2004], in order to accomplish this task a modeler has to consider three levels of behavior, shown in Figure 2.3. It must be noted that this logical scheme actually comes from the literature of vehicular traffic modeling: to give an example, it has been already provided in the work by Michon [1985] and also applied by Timpf et al. [1992].

In particular, at the strategic level the person formulates his/her abstract plan and the final objective of the journey, motivating the overall decision to move. To give an example, let us think to a person that in the morning has to go to work. At the tactical level, the plan is decomposed into a scheduled set of activities to be executed and, in particular, the route choice activity is here performed. This means that decisions regarding the roads to drive through, in case of traffic dynamics, or the paths along the pedestrian environments are taken at this level. Coming back to the example, it can be stated that the person is going to take the 8:00 AM train from the station, then take a bus, then walk to the working place. At the operational level, each activity is physically executed, i.e., the person will perform the movement from his/her position to each intermediate destination, until the final target is reached.

The literature of modeling and simulation will be now discussed in the following sections of this chapter, classified along the three modeling perspectives. Together with the description of the microscopic modeling approach, a brief discussion on the approaches and possibilities dedicated to the consideration of heterogeneity in the simulated population, with particular references to the fragile users and aged people, will be provided.

The problem of the models validation will be tackled in Section 2.5, with a summary description of the empirical data used for this purpose. The section will describe how the current knowledge on the physical pedestrian movement can be employed to ensure the reliability of a simulation model at the walking behavior level. For the validation of procedures that enhance the simulated behavior at tactical level – considering changes of the individual plans by considering dynamical elements such as congestion –, possible directions to overcome the lack of human knowledge will be proposed.

2.1 Macroscopic Modeling

The *macroscopic* models, defined also as continuum models [Duives et al., 2013], belong to a modeling class essentially characterized by a mathematical approach, that simulates the dynamics with a partial differential equations system, either of first or second order. This approach, therefore, describes a numerical simulation framework where the flows of persons are simulated in bi-dimensional planar spaces, generally denoted as $\Omega \subset \mathbb{R}^2$. The presence of walls and other obstacles in the environment, that will affect the flow dynamics, is modeled with additional subsets of Ω.

The element that characterizes the scope of modeling of this class is the missing consideration of individual pedestrians in the simulation, since the aim is to directly reproduce the crowd flows.

Earliest approaches belonging to this class were described by finding analogies between the dynamics of a crowd and a kinetic gas (Henderson [1971]) or a fluid (Helbing [1992]). Henderson [1971] pointed out that the Maxwell–Boltzmann statistic is suitable to describe the dynamics of a crowd in a particular state. In his pioneering work, he described the crowd as a fluid, recognizing two phases of the complex system: a *gaseous* phase where the crowd is "loosely packed" and a *liquid* phase where this is "densely packed". The Maxwell–Boltzmann theory is used only for the gaseous phase, pointing out that the real world measurements about distributions of velocities and densities are well-fitted, except for a significant deviation from the frequency mode. This is attributed to the composition of the observed crowd, inhomogeneous by considering the gender, concluding that the error would decrease by observing homogeneous crowds. The analogy between gas-kinetic theory and crowd dynamics was extended by Helbing [1992], who introduced the concept of individual by describing its type of motion, or intended velocity. He described the role of the *temperature* and *pressure* parameters of this kinetic to achieve in this model collective effects of pedestrian dynamics, like jams (different distributions of densities), lane formation or propagation of waves. He also pointed out the limits that characterize this approach in simulating low densities situations, which must be properly managed as well.

Later approaches, that will be now analyzed more in details, moved towards the reproduction of the dynamics with methods taken from continuum mechanics (e.g. Hughes [2002]). These models avoid analogies with other systems and design the crowd flows employing two main elements: the density and velocity of pedestrians. These works belongs to the class of *first order* models, since the function directly puts the two dimensions into relationship. The dynamics of movement is achieved by directly describing the differential equations that model the variation of local densities in the space (i.e. the flow) along the time window of the simulation. The mechanisms that lead to the changes in densities are firstly constrained by a mass conservation principle, that for more clarity is provided with the following formulation:

$$\begin{cases} \partial_t \rho + \mathrm{div}_{\mathbf{x}}(\rho \overrightarrow{v}) = e - d \\ \rho(0, \mathbf{x}) = \rho_0(\mathbf{x}) \end{cases}$$

With $\mathbf{x} \in \Omega$ and $t > 0$ identifying the time instant. The conservation principle, thus, ensures that the local densities are preserved unless there is a flow towards or from the considered point. A variation of the total simulated mass in the considered area can be only given by entrances, positively, or destinations, negatively. In this formulation the incoming flow from entrances is defined with the function $e(t, \mathbf{x})$, while out-flow through the exits is described by $d(t, \mathbf{x})$.

To model the direction of movement of the flows from each position of the space, potential fields that represents continuous gradients spread from the simulated destination areas are generally associated to the environment. These gradients contain information about the minimal distance – or also time – a pedestrian has to cover to reach the target from an arbitrary position $\mathbf{x} \in \Omega$. A mathematical formulation of the potential $\phi : \Omega \to \mathbb{R}$ is given by the *Eikonial* equation:

$$\begin{cases} |\nabla_{\mathbf{x}} \phi| = C(t, \mathbf{x}, \rho) & \text{for } \mathbf{x} \in \Omega \\ \phi(t, \mathbf{x}) = 0 & \text{for } \mathbf{x} \in \Gamma_{destination} \end{cases}$$

Here $\Gamma_{destination} \subset \Omega$ represents the area of the destination of the simulated flows. The function $C(t, \mathbf{x}, \rho) \geq 0$ implements the cost function that will design the diffusion

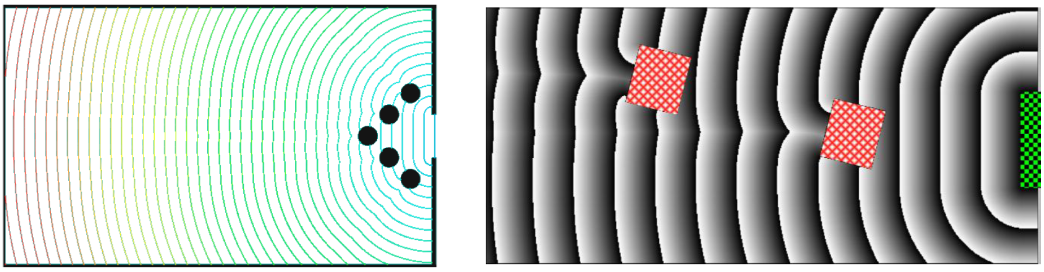

(a) (b)

Figure 2.4: *Two examples of potential fields typically used in continuous model. In both cases the targets are the openings on the right of the scenario. The pictures have been taken from Twarogowska et al. [2014] and Kretz et al. [2014].*

of the field, the so-called *running cost*. This can also employ factors like hazards (e.g. smoke) or regions implying a different velocity of the pedestrians (e.g. ramps). Two simple graphical examples of potential fields are depicted in Fig. 2.4. As it is possible to note by the picture, the positive feature of the potential is that the values are spread as a wave from the target position, diffused along the space by taking into consideration the shapes of obstacles and walls. The values inside the potential field, thus, will not represent the raw Euclidean distance.

The last element needed to compose the dynamics of the flows is the function describing the *velocity* that pedestrians can assume in each position of the planar space. This function is particularly important since represents the core element of the model, generating the overall movement in the simulation scenario. By taking into consideration the representation of the velocity function, two main classes of macroscopic models can be recognized: *first order* models design the velocity as directly dependent on the local density; *second order* models deal, instead, with acceleration – basic element of momentum equations. A simple linear formulation of the first order for the speed - density relation, typically used in this scope (e.g. Hughes [2002], Hoogendoorn et al. [2013]), is:

$$V(\rho) = v_{max}\left(1 - \frac{\rho}{\rho_{max}}\right)$$

v_{max} and ρ_{max} are calibration parameters and respectively describe the maximum velocity and density considered for the simulations. In order to obtain a plausible representation of the pedestrian dynamics, fitting the data-sets about the fundamental diagram, a setting for the two parameters is described by $v_{max} = 1.5$ m/s and $\rho_{max} = 5.5$ ped/m^2. A plot of the function with these parameters is depicted in Figure 2.5(a) by the purple line. Figure 2.5(b) shows the analogous relation flow–density achieved with $Q(\rho) = V(\rho) \cdot \rho$. It is possible to note that the simple linear function generates a flow with maximum value of around 2 ped/ms that fits with the maximum pedestrian flow observed in the real world. The critical density value that generates the maximum flow, on the other hand, is too high and not realistic: 2.75 ped/m^2, while in the real world this is typically observed between 1.5 and 1.8 ped/m^2. In addition, the maximum density considered is not comparable with the reality, where local densities reaching even 10 ped/m^2 are observable[1].

Despite these limitations, this simple function has been applied in the relevant literature of this type. A significant work is the mathematical model from Hughes [2002], where equations and concepts from continuum mechanics have been applied to realize a macroscopic model of pedestrian flows. In particular, flows of different types of pedestrians are modeled by means of local density and velocity parameters, composing a first order model, where the dynamics is generate by means also of the equations of mass conservation. Different potentials are used to direct different classes of pedestrians towards different targets. A limitation on the applicability of this model has been presented by Twarogowska et al. [2014], that exemplified the fact that it was not possible to reproduce a significant difference among flows simulated in different evacuation scenarios, generated by adding obstacles around the exit.

In the work of Hoogendoorn et al. [2013], a mathematical model extending the kinetic wave model [Lighthill and Whitham, 1955] has been presented, using a linear formulation of the speed-density relation. The peculiarity of this paper is the usage of an iterative approach for the simulation model, with the aim to find the flows optimum in planar and continuous environments. The algorithm to the research of the optimum uses an optimal path calculation that at each iteration varies with the resulting local densities achieved at previous iteration, so that the pedestrian travel times are minimized. The paper shows two simple applications of the mathematical model, describing evacuations with uni-directional flows where choices and flow distributions between intermediate targets and openings in the environment affect the total travel times.

The limitations explained before about the usage of a linear function, for the speed-density relation, are overcome with a non-linear formulation. An example is given by the following formula:

$$V(\rho) = v_{max} \cdot e^{\left(-\frac{\rho}{\rho_{max}}\right)^{\rho}}$$

Figure 2.5 graphically explains the differences in the speed–density and flow–density relations with the two formulations, by configuring $v_{max} = 1.5$ m/s and $\rho_{max} = 5.5$ ped/m^2. The improvement is sensibly perceivable, especially by looking at the flow diagram.

Second order models (e.g. Twarogowska et al. [2014]) design the evolution of the dynamics by means of the conservation of mass and a momentum balance equation,

[1] A more detailed explanation about the knowledge on the pedestrian fundamental diagram will be provided in Section 2.5.

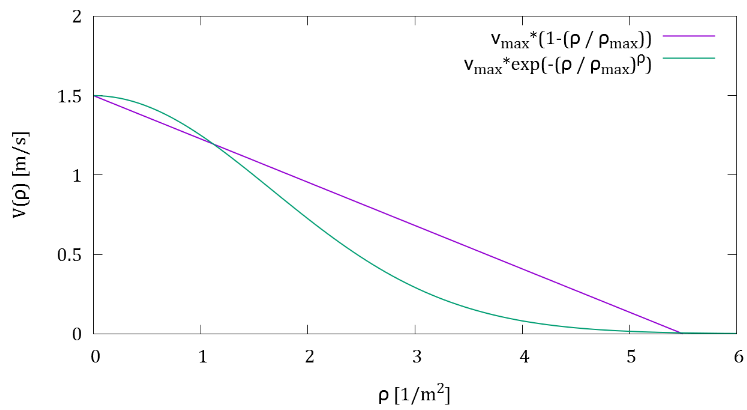

(a)

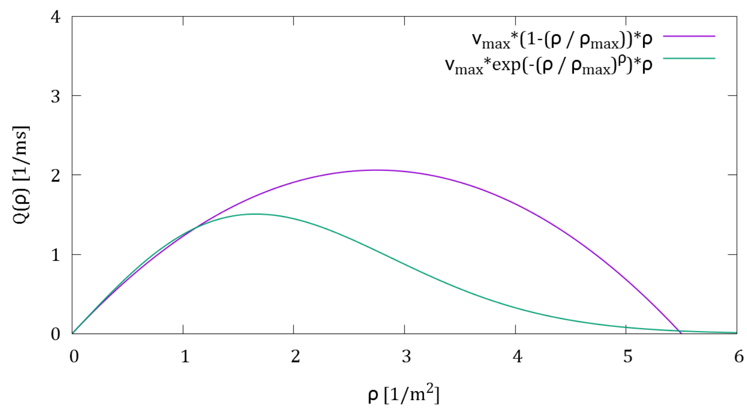

(b)

Figure 2.5: *The speed–density and flow–density relations achieved with the two explained formulations. The purple line denotes the linear function, while the non-linear one is plotted with the green line.*

which describes the changes in the acceleration of pedestrians in the space. A typically applied formulation of the second order (e.g. Jiang et al. [2010]) is:

$$\partial_t(\rho\overrightarrow{v}) + \mathrm{div}_{\mathbf{x}}(\rho\overrightarrow{v}\otimes\overrightarrow{v}) + \nabla_{\mathbf{x}}P(\rho) = \frac{1}{\tau}(\rho V(\rho)\overrightarrow{v} - \rho\overrightarrow{v})$$

where $P(\rho) > 0$ models the internal pressure, τ the response time and $V(\rho) = v_{max}e^{-\left(\frac{\rho}{\rho_{max}}\right)^{\rho}}$ is the variation of the velocity among density. The paper of Twarogowska et al. [2014] shows that the usage of their second order model leads to a differentiation of the evacuation times from a room where obstacles of different shapes have

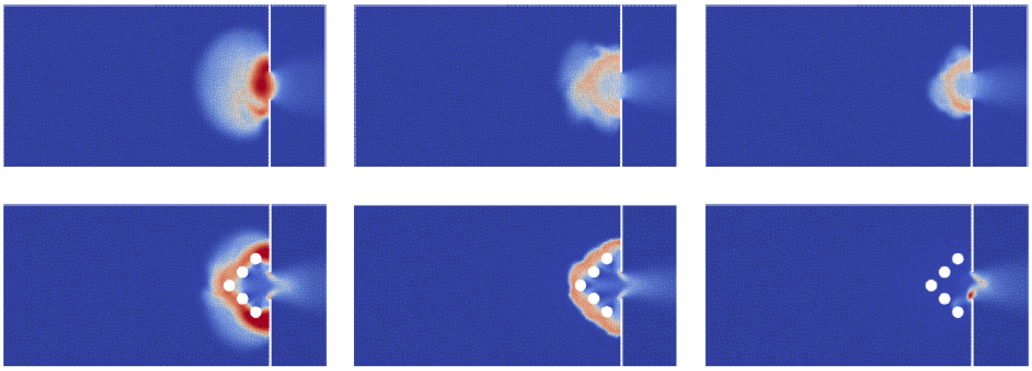

Figure 2.6: *Reproduction of the Braess paradox with a second order model [Twarogowska et al., 2014] (pictures taken from the paper). The evacuation times in case of a room with the exit surrounded by obstacles are significantly smaller than in the other case, where the formation of a circular area of high densities (so-called* clogging effect*) generates circulation delays and higher evacuation times.*

been placed (see Figure 2.6). In particular, they show that the *Braess* paradox [Braess et al., 2005] is achievable with the model, in the sense that by surrounding the exit with a set of columns of the same width, the clogging effect of the flow decreases and the evacuation times are successfully improved.

To conclude this discussion on the macroscopic modeling perspective, this can be described as an efficient approach for the simulation of high densities situations: the crowd is modeled as whole system of flows composed by homogeneous particles, where the dynamics is generated by only a few parameters and the number of particles does not affect the computational times of the simulation. On the other hand, this methodology is not much suitable for the simulation of low densities and in case of counter-flows, where the interactions and characteristics among the individual pedestrians can significantly affect the resulting dynamics. In addition, the approach for modeling leads to quite abstract formulas and laws which not always have a direct meaning or have similarities with observed phenomena. More detailed effects like the presence of pedestrian groups in the crowd, therefore, are hard to be described and constitute limitations of this modeling perspective for the simulation of complex situations.

2.2 Mesoscopic Models

As it has been introduced at the beginning of this Chapter, in the literature the term "mesoscopic" generally refers to models whose entities describe groups of pedestrians (or vehicles), thus they constitute an intermediate point between the simulation of all individuals in microscopic models and the macroscopic simulation of a unique complex entity.

Following this perspective, the work by Navarro et al. [2013] proposed an approach that switches from a detailed microscopic behavioral model to a mesoscopic one, for sake of computational efficiency. The work is an improvement to the dynamic level of detail switching previously proposed in Navarro et al. [2011], where the change of perspective was between the microscopic model and a macroscopic one, linking thus individuals to a unique flow entity instead of intermediate groups. Both approaches proposes a formal definition of the agent-based system, where functions to determine the *affinity* between couples of agents are firstly defined, analyzing the distance from both a physical and a psychological perspective[2]. These functions are used to perform the *macroscopic* [Navarro et al., 2011] or *mesoscopic* [Navarro et al., 2013] aggregation, with an additional utility function. In Navarro et al. [2013], the authors show that the mesoscopic aggregation is able to save as well computational times, suffering much less the loss of precision that arisen with the switch to the macroscopic model. The formal agent model has been applied to different scenarios of crowd simulation, by using the platform SE-Star [Navarro et al., 2015] that implements the microscopic behavioral model of pedestrians.

As previously stated, in this manuscript the axes used for the models classification analyzes the granularity of the individual behavioral models, thus with this perspective the mesoscopic modeling class also contains models characterized by the concept of individual, instead of modeling the crowd as a whole system of flows, but by only giving a few details on the interactions among them. Many models using this point of view are also denoted as *network* models, due to the representation of the environment as a graph where the edges represent 1-dimensional environments (implementing, e.g., a city street), crossing in presence of the nodes. The individuals of the system can only be located inside the links, that can be customized with the width and speed limit that will precisely describe the local flow. This modeling perspective has been widely applied for the vehicular traffic simulation, where the large dimensions of the environment that has to be simulated is suitable for an efficient network representation and the interactions among individuals are more easy to abstract, due to the constrained space that can be effectively designed as a set of 1-dimensional queues. Nonetheless, several applications for the pedestrian modeling can be found in the literature (see, e.g., Forcael et al. [2014]), designed to simulated evacuation of metropolitan cities.

The modeling approach is a "crossing point" between the macroscopic and microscopic ones, since the environment is modeled with lower details – from a higher perspective – than in microscopic models, but the consideration of individuals describes a lower perspective than the macroscopic one. In these models the agents take decisions

[2]In the proposed implementation this distance is set to 0 if the agents pursue the same target, 1 otherwise.

about their route (i.e. tactical level decisions), but the actuation of their decision at the operational level is managed by queues that regulate the movement according to pre-defined speed-density relationships. In this way, the lack of a more precise spatial representation is compensated by a mechanism causing the actual travel time to consider the plausible effects of potential conflicts in movement at the operational level.

In order to clarify the environment representation and the mechanisms that lead to the simulation of the dynamics of the system, a graphical outline of the mesoscopic modeling framework is depicted in Figure 2.7.

Regarding the literature of this modeling class, the work proposed by Forcael et al. [2014] describes a network model for the simulation and optimization of evacuation routes in large metropolitan areas, assuming only evacuation by walk. The search of the optimal route is performed with an *ant colony optimization* strategy, a bio-inspired optimization algorithm that imitates the ants behavior. The procedure is briefly summarized by the following:

- the ants randomly chooses their initial path in the environment;
- once an ant finds a food source, it will use its traveled path to come back to the nest, by leaving a trace of pheromone that will influence the movement of other ants;
- since the pheromone trail is evaporating, the ants that found a shortest path towards the food source will leave a trail with more pheromone, that will be probably more chosen. This will let the ants to converge to the usage of shortest paths towards the food sources.

The environment is modeled with a graph representation whose links describes roads of the city. The model contains 4 variables to allow the calibration, including two parameters for the management of the pheromone, i.e., the quantity of the pheromones left by the ants and the evaporation coefficient. The other two parameters are related to a qualitative description of environmental features. The first one characterize the status of the roads: from a good condition describing a wide road, until a poor condition describing a hazardous way (e.g. close to gas pipelines). The latter parameter is used for a fuzzy description of the slope of city roads, distinguishing steep roads, streets with moderate slopes and streets with negative slopes in the direction of the movement. The model validation has been performed with data gathered in the field by means of two drills, executed in the coastal town of Penco, in Chile. These real world experiments employed a representative, yet small sample of participants. In addition, elements such as the effect of density in travel times of links are not considered in the calculation of the optimal route, limiting in this way the applicability and reliability of the model.

A few more words have to be spent regarding an open-source simulation system

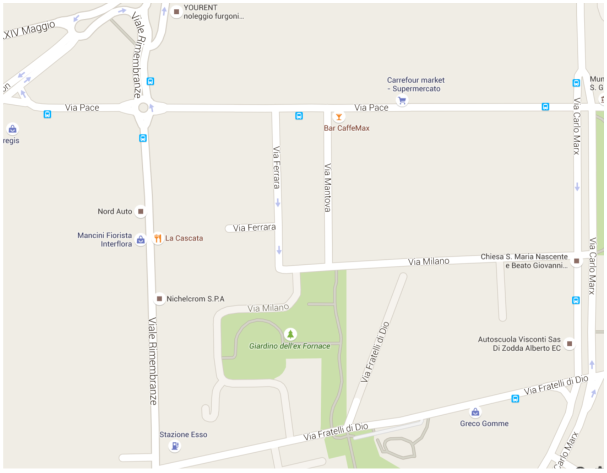

(a)

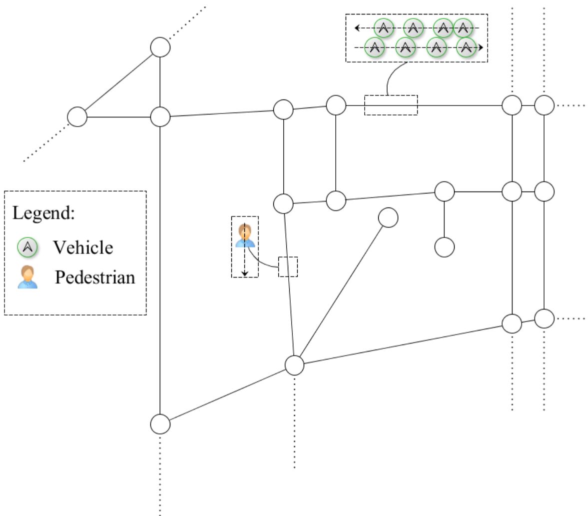

(b)

Figure 2.7: *An example network representation (b) of a portion of the Milan street map (b), taken from Google Maps®. Each edge of the graph contains 1-dimensional queues that will host the simulated individuals, either vehicles or pedestrians. The uni-dimensionality of the queues implies that a normal street of two lanes, one per direction, will configure two different queues between the two nodes.*

based on the mesoscopic perspective, that is, the *MATSim* simulator[3]. This software, in fact, has been integrated with a simulation model that will be presented in Chapter 5 of

[3] http://matsim.org/

this Dissertation, with the aim of allowing to increase the details of the simulation in several parts of the metropolitan environment.

The MATSim simulator allows to model and analyze the evolution of vehicular and pedestrian traffic in metropolitan areas, by means of a queue model. The queues composing the environment network logically implement the road lanes of the city, as linked 1-dimensional environments. The simulation of the dynamics inside each queue is based on the Gawron queue model [Gawron, 1998], that simulates the out-coming flow from each links by means of their customization parameters, shown with the following:

- the length l of the link;
- the free-flow traveling speed ν_{ff} inside the link;
- the number of lanes n of the link;
- the flow capacity $\hat{q}$ of the link, limiting the out-coming flow from l.

This means that an arbitrary agent a will stay inside the link at least l/ν_{ff} seconds, but the eventual occupation of the link from additional agents will imply an additional permanence to a according to $\hat{q}$. An additional delay is given by the storage capacity of each link $c = \frac{l \cdot n}{l_{veh}}$, where l_{veh} is the length of the simulated vehicles, that limits the upstream flow from other links. The total delay accumulates on the following agents. By varying these parameters, a link of the graph can be configured to reproduce pedestrian flow, as in the work of Lämmel et al. [2009] where MATSim is used to simulate possible evacuations scenarios for the city of Padang, in Indonesia.

The queue model avoids details in the environment and in the interactions among the simulated entities, but on the other hand it is still able to provide a reliable simulation of traffic flows, in a significantly efficient way. The importance of the efficiency in spite of level of detail is given by the iterative approach of MATSim, that implements an algorithm for the iterative search of a *Nash equilibrium* or the *system optimum* among the flows configurations for the traffic network. In the field of game theory, the Nash equilibrium defines a state of a game where the interested entities cannot improve their gain by unilaterally changing their own strategy or plan. The system optimum instead denotes the state where the configuration of the individual plans is optimal and provides the maximum average gain, or the minimum average travel time in this context. Naturally, the system optimum implies to some entities to "sacrifice" their own profit to increase the value of the average gain for the whole population. This definitions make the Nash equilibrium state more plausible and appropriate, since in the everyday life persons are more aimed to increase their own profit. In MATSim, the convergence to one of the two different states is configured with the *cost function*, that describes the way each individual will perceive the travel times at each iteration: a simple collection of the experienced travel times let the system to move towards a Nash equilibrium, while an additional perception of information about the delays caused to the following individuals, due to eventual congestion, will lead to the system optimum.

Independently from the convergence approach, at the first iteration of the simulation campaign the routes of the agents are calculated basing on the shortest path towards their destinations in the map, by means of well-known routing algorithm such as A* or the Dijkstra algorithm. Initially, in fact, the environment network contains only information about the traveling times in a *free flow* situation, statically calculated from the scenario configuration. With this initial setting, several congested areas will probably arise in the simulated network, causing delays in the travel times of the agents. At the end of each iteration, thus, each agent collects their experienced travel time inside the links it traveled through in the previous iteration and uses this information to compute the next route.

2.3 Microscopic Models

Microscopic modeling of pedestrian dynamics has emerged in the 90s, where the growing availability of computing power made a fully detailed simulation of the motion possible. Microscopic modeling has, in fact, the aim to reproduce the aggregate behavior of a crowd by means of a set of simple rules that manages the behavior of the individuals.

As it has been introduced at the beginning of this Chapter, according to Hoogendoorn and Bovy [2004] and Schadschneider et al. [2009], in order to model the individual behavior of pedestrians one has to consider 3 different levels of behavior. The three levels describe the action of decomposition of the goal of the journey, by forming a set of activities that describe individual paths. Each path represents an atomic action that is physically performed with the walking activity, according to the behavioral rules of the individuals. To improve the readability, the three levels of behavior are reported and exemplified below:

- **Strategic level**: at the highest level the person formulates his/her abstract plan and final objective, motivating the overall decision to move (e.g. "I am going to the University today to follow my courses and meet my friend Paul");
- **Tactical level**: the set of activities to complete the plan is computed and scheduled (e.g. "I am going to take the 8:00 AM train from station XYZ then walk to the Department, then meet Paul at the cafeteria after courses, then ..."");
- **Operational level**: each activity is physically executed, i.e., the person perform the movement from his/her position to the current destination (e.g. precise walking trajectory and timing, such as a sequence of occupied cells and related turn in a discrete spatial representation and simulation).

The consistent, yet not complete, knowledge on the fundamental diagram[Zhang et al., 2011, 2012] (given its importance in this context, this will be explained with full details in the validation discussion of this chapter) permitted a validation of the physics simulated at the operational level, in terms of quantitative aggregated data. This let the recent literature on microscopic modeling to be more focused on the reproduction of the pure physical movement at the operational level. The configuration of the two highest levels – strategic and tactical – has typically been left to the end user side, aiming thus at providing models for the simulation of pedestrian flows with static sources and sinks.

A few recent works, on the other hand, have been proposed to dynamically manage the tactical level, and this low number is principally due to the difficulties for the evaluation and validation of these approaches. Despite this limit, the author retains that the literature of pedestrian dynamics is sufficiently mature to start exploring procedures that take into account this higher level. The tactical level, in fact, is very relevant for producing reliable simulations, especially by thinking to evacuation scenarios where the strong aim to minimize the traveling times can lead to repeated change of the path. The relevance of the strategic level, instead, is limited in purely pedestrian scenarios and has not been considered in microscopic modeling, considering also the work here discussed. The following sections will now analyze the state of art of the operational and tactical level of microscopic modeling.

2.3.1 Operational Level Representation

The literature dealing with the simulation of the "raw" movement of pedestrian behavior is quite ample and many different modeling approaches can be identified. Several minor differences, in fact, can be recognized among the modeling styles, such as deterministic vs non-deterministic models, but they describe more peculiarities than categories of models. An effective classification of the literature can be achieved by analyzing the way the space is represented. Models providing the movement in a continuous environment typically simulate the dynamics with an approach based on Newtonian forces, representing thus pedestrians as particles moved by attractive or repulsive forces. A discrete environment, instead, provides less details in the space and trajectories of pedestrians, but overall it offers a more optimized way to define the mechanisms of the simulations, usually realized with probabilistic functions of movement. The two approaches, thus, do not differ only in the way they represent the walkable space, but also in the design of the behavioral rules that will guide the simulated pedestrians.

Models with a Continuous Environment

The models based in a continuous environment are also typically called *force–based* or *particle–based* models, since they essentially extend the idea of the well-known social force model by Helbing and Molnar [1995]. In these works, each pedestrian is represented as a Newtonian particle and the motion of the crowd is simulated by means of attractive or repulsive forces, as shown in Fig. 2.8(a). In the social force model, Helbing and Molnar firstly introduced four kinds of forces acting on each particle and, thus, on each pedestrian:

1. the force that attracts pedestrians towards their destination, modeled as a polygon;
2. a repulsive force acting among all pedestrians, which wants to describe the natural tendency of people to maintain a certain distance between each other;
3. a repulsive force acting between pedestrians and obstacles, to let them assume more comfortable trajectories;
4. a force that attracts pedestrians, to model pedestrians walking closer like groups of friends.

The basic movement of each particle is, indeed, achieved with the sum of the four forces acting on it. Repulsive forces will have a negative value and all forces from or towards one object are emitted in the closest point of its polygon to the pedestrian (see repulsive forces emitted by walls in Fig. 2.8(a)). Another interesting particular of the social force model is that it is assumed that the presence of the persons and obstacles in front of the pedestrian will have a strongest effect than the elements on the back. This models a basic perception component of the pedestrians, which can be realized by multiplying with a factor c, with $0 < c < 1$, the forces directed to the bottom half of the shape of the pedestrian.

Given the sum of all forces at a time-step t on a pedestrian a denoted as $\overrightarrow{F}_a(t)$, the force that will accelerate a is in the end calculated as:

$$\frac{d\overrightarrow{w}}{dt} = \overrightarrow{F}_a(t) + fluctuations$$

The factor $fluctuations$ represents a random perturbation and has the aim to provide non-determinism in the simulations. The non-determinism is, in fact, an important observable feature of any complex system of the real world, since there is no possibility to identify all the variables acting on systems and their components. The social force model threw solid basis for microscopic modeling in continuous environment, given its ability to reproduce well-known effects of pedestrian dynamics, by means of a small set of simple rules. Even if a quantitative validation has not been discussed in their paper, the authors have qualitatively shown the emergence of *lane formation* in case of bi-directional flows, as reported in Fig.2.8(b), or also *oscillations at bottlenecks*, which are the fluctuations of the direction of flow in case of bottleneck crossed by two opposite pedestrian streams.

Due to these positive peculiarities, the approach provided by the social force model has been widely extended for different applications or improvements. A different

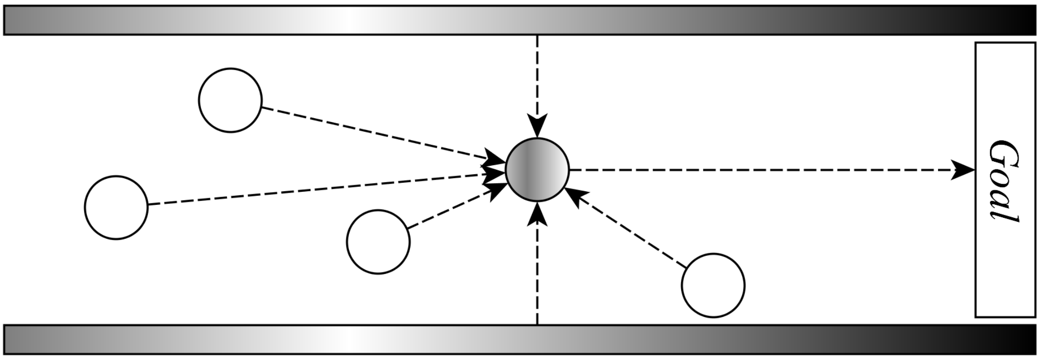

(a)

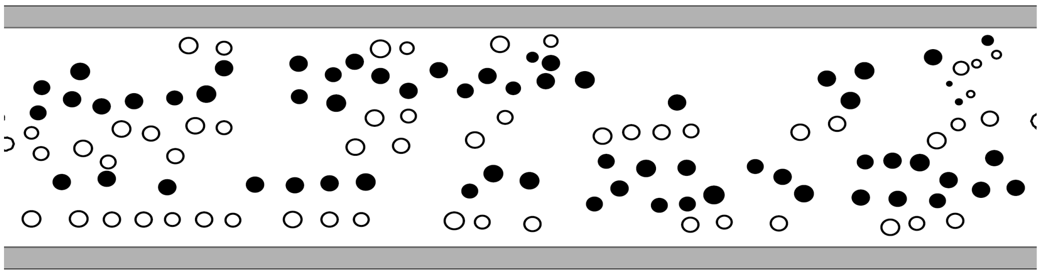

(b)

Figure 2.8: *(a) Graphical description of the social forces acting on the highlighted pedestrian. (b) Lane formation effects emerged with the simulation of a bi-directional flow (taken from Helbing and Molnar [1995]).*

enunciation of the repulsive force acting between pedestrians has been formulated by Yu et al. [2005] in the so-called *centrifugal force model*. The name describes the consideration of both distances and relative velocities as parameters of the repulsive force, describing a similarity with the enunciation of centrifugal force in mechanics. The positive peculiarity of this model is that by depending on the relative velocities of pedestrians, a repulsive force has effects only if the distance between the two pedestrians is going to decrease, i.e., the person in front has a lower speed than the one in the back.

An important extension of this work is the one provided by Chraibi et al. [2010]. In the proposed model, the definition of the repulsive force is slightly changed from the one of Yu et al. [2005], since it includes the consideration of the *desired speed* of pedestrians. With this modification, the centrifugal force model has been improved in terms of simplicity and computational efficiency, since it allowed to avoid any overlap between the shape of pedestrians, without using a centralized collisions detector that was previously needed in the model of Yu et al. [2005]. Another peculiarity of the work of Chraibi et al. [2010] is the definition of a dynamical ellipse to represent the pedestrians, which varies its long side a according to the instantaneous velocity v_i and a calibration parameter τ_a:

$$a = a_{min} + \tau_a v_i$$

The usage of a dynamical shape to represent pedestrians finds its motivations in describing both the space occupation and the space needed of a walking person, assumed to vary from a_{min} when the person is not moving to $a_{min} + \tau_a v_{max}$ when the person is moving at his/her maximum walking speed.

A different perspective on modeling pedestrian dynamics in a continuous environment has been recently provided by von Sivers and Köster [2014]. In this work, in fact, the authors disregarded the usage of forces to model the motion, designing an *utility-based* model in favor of a more realistic definition of the model rules, aiming at directly simulating the strides of pedestrians. In the proposed mathematical model, each pedestrian search at every step his/her next position in a disk centered in the current position, according to an utility function that describes the behavioral rules described above (distance between persons and obstacles and proximity to the goal). With the optimization in the disk, the pedestrians are able to change the length of their strides and in this way the space utilization and local densities simulated by the model are slightly improved.

Another branch of pedestrian dynamics simulation, which is debated also with continuous environment models, is represented by the consideration of groups behavior in the crowd model. The models described above, in fact, neglected this aspect, by not considering at all the behavior of persons walking together or, as for the social force model, by introducing yet not exploring a model component dedicated to this aspect. Studies which emphasized that the crowd is mainly composed by groups date back to late 70s with the work of Aveni [1977], but the interest in the group dynamics by modelers arisen only recently. More detailed observations have highlighted the differences in walking behavior among individual pedestrians and persons walking in group [Willis et al., 2004, Costa, 2010, Moussaïd et al., 2010] and moved the research interests. Other analysis have also shown that, regarding the crowd composition, groups are typically the most frequent element. In Bandini et al. [2014] the observed individual pedestrians were about 16%. In addition, Bandini et al. [2014] observed that couples were the most recurring type of groups (about 44%), followed by groups of 4 (23%) and triples (18%).

Models dealing and investigating the group component in this literature branch are mostly force-based and extend or modify the attractive force between pedestrians already introduced by the social force model. The work of Moussaïd et al. [2010] introduced a perception mechanism for the pedestrians in groups and focused on their space utilization. The work mainly aimed to reproduce the so-called *lane pattern* of groups, as shown in Fig. 2.9, since it is the most observed in the real world. A

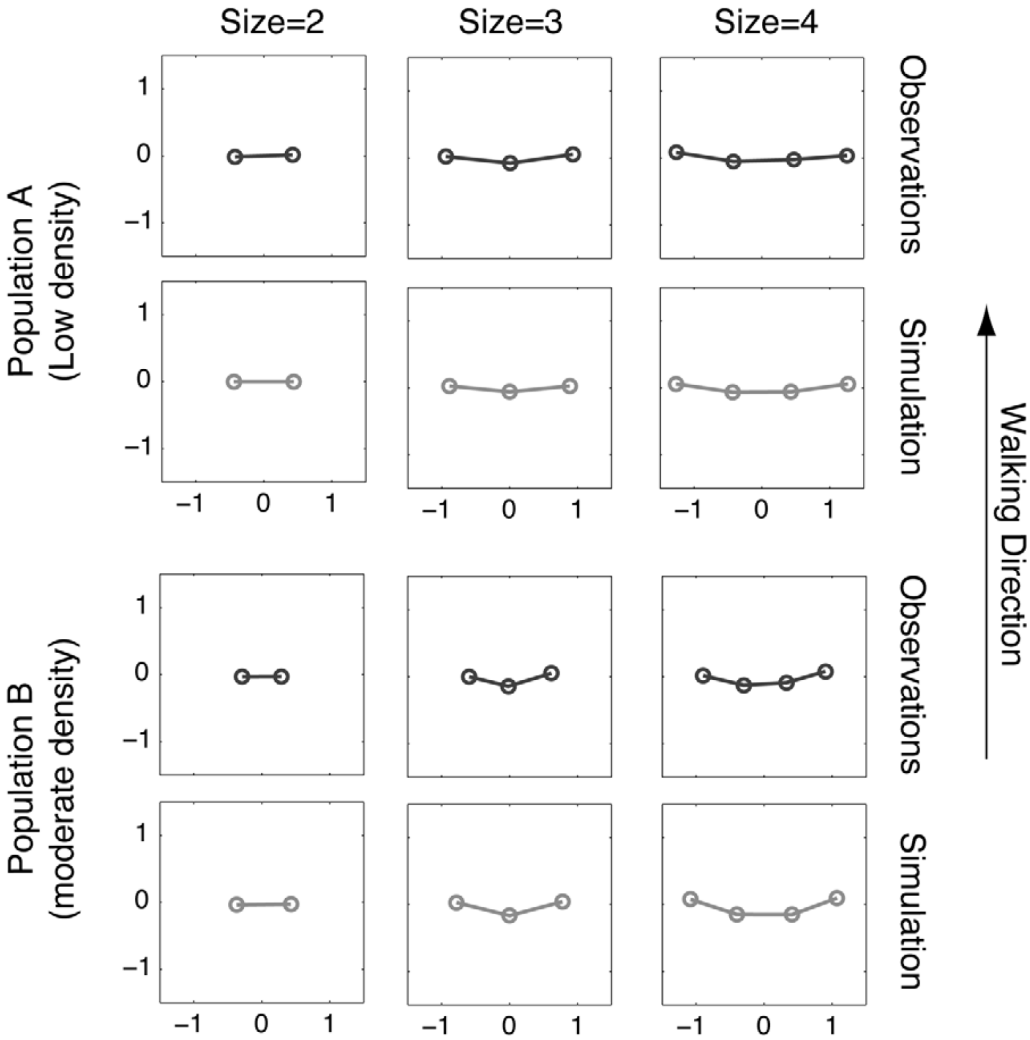

Figure 2.9: *A qualitative comparison between observations and simulations of the work of Moussaïd et al. [2010]. The lane pattern is the mostly observed at low densities, while at moderate densities the groups tend to compress themselves composing a v-like pattern.*

more exploratory work is the one provided by Qiu and Hu [2010], where so-called *structured* groups are modeled with an additional force acting between members of different groups, in order to model large groups like team supporters at a stadium. The main criticism of the work of Qiu and Hu [2010] is the difficulties that arise with the calibration, since the forces acting on structured groups are managed with matrices where the strength of the force is described for all couples of involved pedestrians, leading the model to lose on the simplicity side.

Models with a Discrete Environment

Cellular automata based models represent a less precise paradigm to reproduce details of the environment and individual trajectories, but they have been even more explored in the literature able, given the simplicity of this approach and its capability to fit as well the aggregated data of pedestrian dynamics. What is more, cellular automata represent a more efficient modeling approach than the continuous environment model, intrinsically suitable for parallel implementations.

Before the application of the cellular automata approach for pedestrian dynamics, this has been applied to vehicular traffic simulation, which initially gained more interest. An important work that threw the basis of this branch of simulation has been the model of Nagel and Schreckenberg [1992]. In this work, the authors introduced a very simple cellular automata model for the simulation of single lane vehicular traffic, which yields the basic properties of the traffic flow dynamics. The model reproduces the cars motion by means of four simple rules, executed at each time-step with the following order:

1. Acceleration: each car increases its velocity v by 1 until v_{max}, if the car ahead is farther than $v + 1$;
2. Slowing down: if a car is at position i and the car ahead is located at $i + j, j \leq v$, the following car decreases its speed v until $j - 1$;
3. Randomization: every car decreases its velocity v of 1 with probability p;
4. Car motion: each car moves forward of v cells.

Beyond its simplicity, this small set of rules is appreciable both on a qualitative and quantitative side. Well-known effects like the emergence of jams out-of-nowhere and the back propagation of density waves are observable in the simulations. Regarding the quantitative results, the model provides a triangular fundamental diagram that can be calibrated with the parameters v_{max} and p and that represents the typically observed shape for data of traffic and pedestrian flow (see Sec. 2.5).

Thanks to this features, the model of Nagel and Schreckenberg [1992] has become a basis of the traffic dynamics simulation and has been widely extended. Rickert et al. [1996] extended this work into a two-lane model that introduces rules for overtaking. Nagel et al. [1998] give a more general approach to simulate two-lane streets, evaluating different rules for managing the overtaking by considering differences in country laws (they implemented USA and European driving and overtaking rules). An extension to bi-directional flows of cars, modeling two lanes with different direction of movement and with rules granting a safe overtaking with the temporary occupation of the other lane has been given by Simon and Gutowitz [1998]. Moussa [2008] proposed an advancement that avoids passing vehicles from getting stuck with oncoming traffic.

When the interests on pedestrian dynamics has begun to rise, first approaches on the cellular automata side have aimed at describing the motion with extensions of the models for vehicular traffic, by preserving the modeling style hardly based on a set of rules. Among the first “adaptations” of vehicular traffic cellular automata to pedestrian dynamics, Blue and Adler [1998] proposed a model where pedestrians have been designed to walk on a multi-lane ring road, differing by their desired speed and moving along the same direction. The pedestrians were capable of performing lane-changes to overtake slower or jammed pedestrians. As for the vehicular traffic models, different speeds have been modeled by allowing more movement per time-step to the pedestrians. The lane changing movement is designed as a side-step, configuring thus the classical Von Neumann neighborhood for pedestrian movement.

A bi-directional cellular automata model for pedestrian flow in channels of arbitrary width is given by Fukui and Ishibashi [1999]. Conflicts between oncoming pedestrians are solved by simply using the side-stepping. In this way, this model displayed lane formation behavior for low densities, but when densities exceed a certain threshold a rapid and permanent state transition from free flow to total jam is observed. This freezing effect of the simulation is quite unrealistic, since it is well-known that in case of bi-directional flow the emergence of lanes maintain the flow quite stable even until relatively high densities [Zhang et al., 2012].

The implausible rapid state transition from free flow to total jam has been avoided in the work of Blue and Adler [2001], which manage bi-directional flows more realistically by granting to pedestrians moving in opposite directions to swap their positions under dense situations. This mechanism is managed and calibrated with a probability p_exchg that the position exchange is executed. As shown in Fig. 2.10, by acting on the parameter the model can be calibrated to reproduce a realistic fundamental diagram for bi-directional flow. Blue and Adler proposed a generalization of this model to manage multi-directional flows in Blue and Adler [2000].

A criticism of the approach above described that can come to mind is that it allows only to simulate bi-directional or multi-directional flows of pedestrians in elementary portions of the environment. The presence of obstacles, in fact, has not been contemplated and in this way the simulation of even a simple environment can be not feasible: it is true that the space can be subdivided in a set of linked rectangular grids, but this is maybe a too complicated task (also considering that at that time continuous space models were already able to manage arbitrary environments).

A change of perspective that gave more importance to the cellular automata approach has been provided by Burstedde et al. [2001] with the well-known *floor field* model. This work generalizes the rules for the pedestrian movement to let them independent from the environment and flows configuration. The main peculiarity of the floor field model is the implementation of a bio-inspired mechanism, describing the chemotaxis in populations of ants. As explained in the previous section, in fact, these insects find the shortest path towards sources of food by releasing pheromones in the air. In the floor field model, the analogy between pedestrians and ants is realized by means of a dynamical grid, called dynamic floor field and denoted as τ_d, where at each

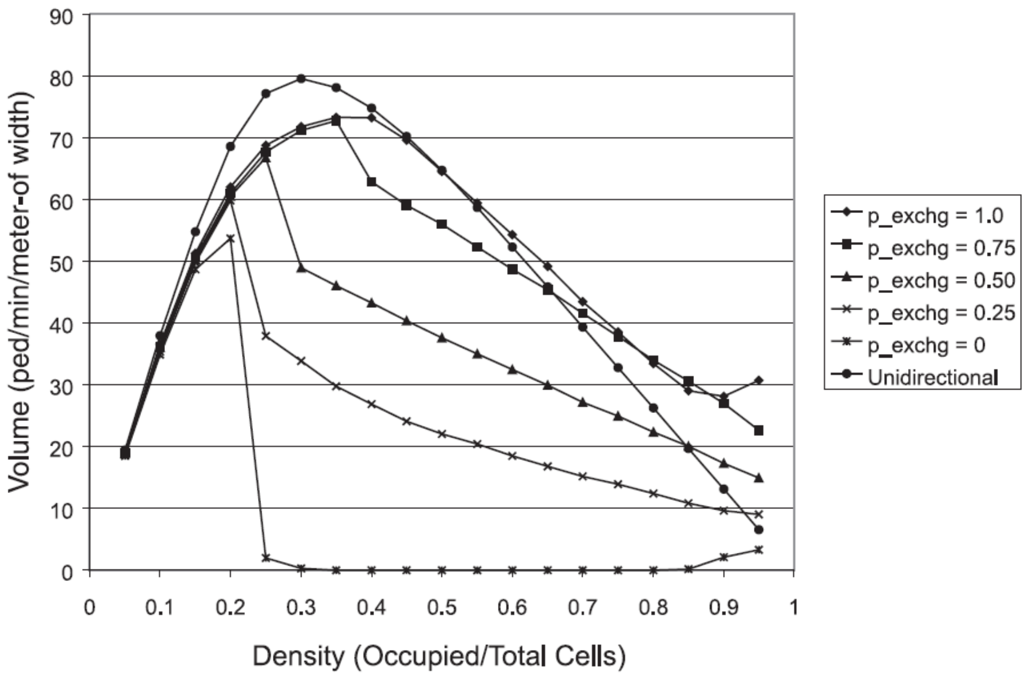

Figure 2.10: *Calibration of the model of Blue and Adler [2001], by simulating a long corridor of 10 lanes of cells and with different configuration of* p_exchg. *The picture is taken from the paper: here the authors used the term* Volume *to denote* Flow.

step the pedestrians who succeeded to move spread a gradient from their position, representing the pheromone. Burstedde et al. [2001], of course, did not intend to model the movement of pedestrians towards a destination as a population of ants, yet they want to adapt the interaction mechanism of these insects to model the following behavior of persons that mainly lead to the emergence of lanes in situation of bi-directional flow. Technically, in the dynamic floor field the spread is performed according to two parameters:

- the *diffusion* D, describing how much pheromone is left by each pedestrian;
- the *decay* δ, which defines the life duration of the pheromone traces during the simulation.

In order to drive pedestrian towards their target, the concept of *static floor field* (defined as τ_s) has been introduced, denoting a grid where another gradient is spread a-priori of the simulation. This potential is computed from the cells of one target and provides information about the discrete distance between each cell and the target. The static and dynamic floor fields are graphically exemplified in Fig. 2.11. Instead of using a set of rules, the movement of pedestrian in this model is realized with a probability

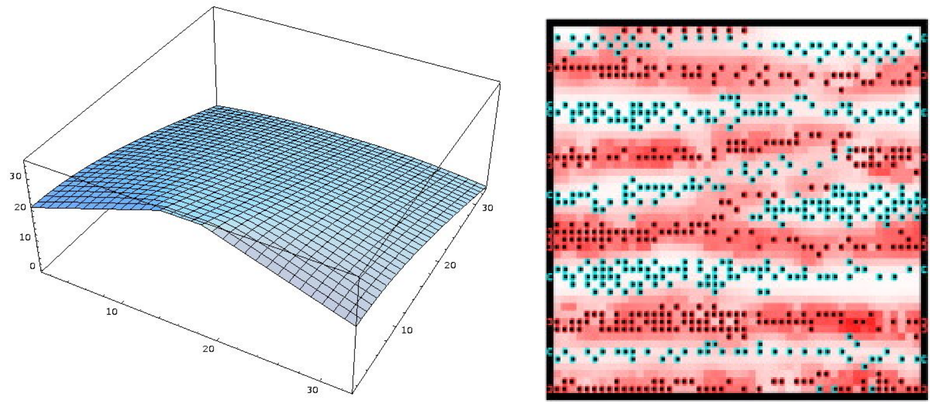

(a) (b)

Figure 2.11: *(a) Graphical examples of a static floor field, generated from an exit centered in (x=16,y=0). (b) The situation of two dynamic ones, together with the current position of two populations of pedestrians moving in opposite directions. The self-organization of flows in separated lanes is clearly visible.*

function, applied at each time-step to all pedestrians. By denoting (i, j) as a neighbor position of a pedestrian and $(0, 0)$ as his/her position, the movement probability has been defined as the following:

$$p_{ij} = Ne^{(\beta J_s \Delta_s(i,j))+(\beta J_d \Delta_d(i,j))} d_{ij}(1 - \eta_{ij})$$

Where $\Delta_s(i, j)$ and $\Delta_d(i, j)$ are defined as $\tau_{s||d}(i, j) - \tau_{s||d}(0, 0)$. The meaning of N is to normalize the probability and to provide $\sum_{ij} p_{ij} = 1$. J_s and J_d are the calibration parameters for the static and dynamic floor fields. β is a sort of temperature parameter and its increasing enhance the differences between the probability values, leading the simulations to be more deterministic. η_{ij} denotes the presence of pedestrians in the position (i, j) (being 1 if the cell is occupied) and avoids any movement in already occupied cells. d_{ij}, finally, is a correction factor that prevents the pedestrians to be confused by the pheromones they just have left.

The floor field model has, therefore, given a general discrete approach for modeling the pedestrian behavior and, for this reason, it has been widely investigated and extended by works in the literature (note that also the work presented in this Thesis is an extension). To give some important examples, Kirchner et al. [2003b] extended the model by introducing a parameter called *friction* in the conflict management, which describe the probability that a conflict (i.e., a choice of the same cell between more pedestrians at one time-step) is solved with the non-movement of all the pedestrians involved, building an analogy with hesitation of pedestrians. The friction parameter improved quantitatively the results in terms of the fundamental diagram. Kirchner et al.

[2004] discussed methods to deal with different speeds, since the basic floor field model implements only one desired speed for all the population of pedestrians. This work additionally investigated the usage of a finer grid discretization (the works presented above generally modeled the space as a grid of cells of 40×40 cm^2 size) that aims to decrease the error in the reproduction of the environment and space utilization of pedestrians. On the other hand, a finer discretization can negatively affect the efficiency of the model. Another interesting work in the direction of fine grain discretization of the space have been provided by Was et al. [2012]. The authors modeled the environment with a grid of cells of 25×25 cm^2, representing the shape of a pedestrian as an ellipse centered in one cell and that occupies also part of the surrounding cells. The provided modeling approach is less abstract than the floor field model, since the rules managing the probability of movement takes into consideration the concept of proxemics and social distances formulated in the field of sociology by Hall [1966].

The consideration of groups as a significant component of the pedestrian flow has been investigated also in the discrete approach. The work of Sarmady et al. [2009] designed a cellular automata building a *least effort* algorithm to deal with the behavior of individual persons and pedestrians in groups. To manage the group behavior by maintaining low the computational costs of the model, they assumed a leader-follower group structure, where the leader is attracted more by the target and followers have high probabilities to move closer to the leader, in order to maintain the group compact. A more recent work dealing with pedestrian groups has been provided by Seitz et al. [2014], who distinguished as well the role of group leader even if in a dynamical way. In this model, in fact, the leader of the group is assumed to be the closest person to the group target, thus during the simulation all the group members are able to become leader. Other differences appear in the environment structure, which is represented with an hexagonal grid, which solves the difference in movement length between diagonal and linear moves, derived by the standard square cells grid, but also give more constrains to the movement of particles. In addition, in order to better reproduce the cohesion of the group members, the model assumes a velocities of pedestrians that varies with the distance between the person and the group center of gravity, called the *centroid*.

2.3.2 Models Dealing with Tactical Level

The tactical level has gained interest only recently in the literature of pedestrian dynamics modeling and simulation, despite its relevance for the simulation of a realistic behavior. By thinking to situations like evacuations, in fact, consider that the rushing situation leads on a first hand to jamming and to not linear increases of travel times. The consequence of this is that highly congested exits can be at some point considered as not anymore usable by some persons, who will then change their current route. Decisions dynamically undertaken at the tactical level are, therefore, very important for the overall realism of the simulations.

In the field of computer graphics and gaming, high-level path planning algorithms have been investigated and proposed by means of graph-based methods (e.g. Geraerts and Overmars [2007], Geraerts [2010]). These algorithms aimed more at reproducing visually realistic trajectories of agents in 3-dimensional environment and thus the aims do not intersect the ones of this field. For this purpose these models will not be discussed in this Thesis.

On the pedestrian dynamics side, a relevant recent work has been proposed by Wagoum et al. [2012b]. The presented work deals with tactical level decisions during evacuation and uses the generalized centrifugal force model [Chraibi et al., 2010] for the management of the physics of motion. The tactical choices of pedestrians are taken on a graph representation of the environment, where the nodes for the decisions describe doors or other bottlenecks where jams can arise. Dealing with evacuation, the pedestrians are designed to have the common objective to reach the exit in the shortest possible time. To do this, during the simulation they dynamically calculate the *quickest* path towards the exit, which is the way that implies the shortest time to reach the final destination. With the aim of minimizing the time, thus, the simulated pedestrians do not only have to consider the shortest path, but also alternative ways which allow to pass through a smaller congestion. This idea will be considered and extended in the tactical level model presented in the next Chapter.

In order to define a proper strategy to minimize the traveling time of pedestrians, the authors defined four special quantities:

- the re-routing time t_r for a pedestrian, defining the time-steps when the pedestrian path re-calculation is activated;
- the jamming queue $Q(\overrightarrow{n}_i)$, composed by all the pedestrians p in the nearby of a node $\overrightarrow{n}_i$ with velocity $\overrightarrow{v}_p(t) \leq \overrightarrow{v}_{min}$ ($\overrightarrow{v}_{min}$ is the velocity threshold that defines pedestrians in a jam);
- the reference pedestrian p_j, belonging to a jamming queue, for a pedestrian p_i that evaluates the route. p_j is the closest visible pedestrian to p_i in the considered queue;
- the visibility range $\nu(p)$, which limits the set of visible nodes from the position of a pedestrian p.

By means of these four quantities, the traveling time for a pedestrian p_i ($\overrightarrow{x}_i$ is its position and $\overrightarrow{v}_i$ its velocity) towards a node $\overrightarrow{n}_j$ is calculated as the following:

$$t(\overrightarrow{x}_i, \overrightarrow{n}_j) = \begin{cases} \dfrac{||\overrightarrow{x}_i - \overrightarrow{x}_r||}{||\overrightarrow{v}_i||} + \dfrac{||\overrightarrow{x}_j - \overrightarrow{n}_j||}{||\overrightarrow{v}_{ra}||}, & \text{if reference pedestrian } p_r \text{ is found} \\ \\ \dfrac{||\overrightarrow{x}_i - \overrightarrow{n}_j||}{||\overrightarrow{v}_i||}, & \text{otherwise} \end{cases}$$

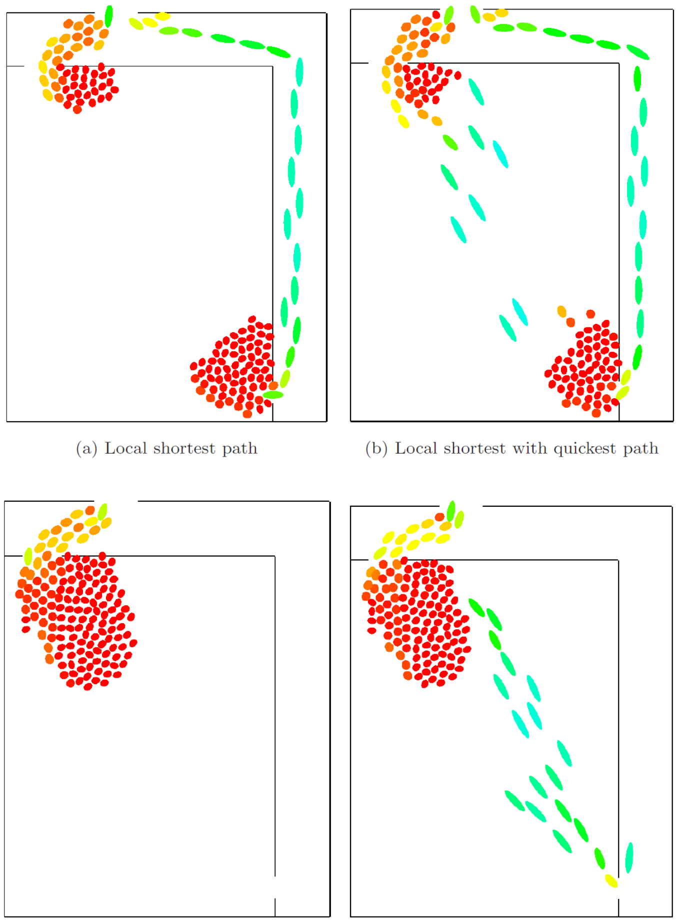

(a) Local shortest path
(b) Local shortest with quickest path
(c) Global shortest path
(d) Global shortest with quickest path

Figure 2.12: *Qualitative comparison of the four strategies for the management of the tactical level defined in Wagoum et al. [2012b] (picture taken from the paper).*

with $\overrightarrow{v}_{ra}$ the velocity of the reference pedestrian p_r averaged over a period of time that defines the observation time of the pedestrians.

This model allows the pedestrians to dynamically decide the route to minimize their traveling time, by avoiding congestion. This approach is tested on the basis of four strategies for the route choice management, given by the combination of applying the shortest or quickest path, either with a local (with the aim to faster go out from the current room) or global (with the aim to faster reach the destination) strategy. The global route is computed on the graph representation of the environment by using the well-known Floyd–Warshall routing algorithm, with the cost of each route described by the traveling time calculated as above. For more clearence, the qualitative comparison of the four strategies is reported in Figure 2.12.

A different approach for the management of the tactical level has been proposed by Kretz et al. [2014]. In this work, the simulation system *VisWalk*[4] is used for the operational level. This off-the-shelf system is declared to be an implementation of the social force model by Helbing and Molnar [1995]. The extension for the management of the tactical level illustrates an iterative algorithm that, at the end of each iteration, re-computes the routes of the agents basing on the traveling times experienced in the simulation. In particular, the algorithm selects and changes a number γ of routes of the pedestrians with maximum mean traveling time, by assigning them the route with minimum traveling time of the iteration. The quantity γ is calculated as:

$$\gamma = \left(\frac{tMax - tMin}{tMax + tMin}\right)^{\delta}$$

with $tMax$ and $tMin$ the maximum and minimum average traveling time of the iteration. δ is the calibration parameter of the algorithm. The approach is thus different from the previously presented one, since during the simulation the pedestrians routes are static. In some way, this approach could be seen as similar to the one by Hoogendoorn et al. [2013] but, in that work, the tactical decisions are embedded in the variations of the potential field at each iteration: the individuals are not really considered since the model is macroscopic!

Another interesting feature of this work is that the intermediate targets considered for the route choice are automatically generated on the basis of the environment and obstacle configuration: before the beginning of the simulation, the potential field used for driving pedestrian is analyzed and intermediate targets are generated in correspondence of significant local variation of the potential, generated by obstacles. The procedure is then re-computed with the potential field spread from the new intermediate targets, generating other targets until the environment has been completely analyzed.

2.4 Considering Heterogeneity and Differences in the Simulated Population

In the microscopic modeling approach the crowd is typically modeled as an homogeneous mass: the pedestrians are equally modeled or the differences among them are not analyzed nor emphasized. The arising of problems on a global scale, such as the so-called *ageing society* [Wor, 2002], which has been described in the introduction Chapter, led to the production of a few interesting models that are particularly tailored on the analysis of the impact of population heterogeneity.

An interesting work is the one proposed by Shafabakhsh et al. [2013], which is focused on the analysis of the effects of increasing the presence of elderly people in

[4] http://vision-traffic.ptvgroup.com/en-us/products/ptv-viswalk/

the pedestrian flow. The authors have only considered the operational level for the simulations, by using – and calibrating against real world data – the free pedestrian simulation software *Micro-PedSim*[5]. The model underlying the simulation system is an extension of the social force model. By means of the simulations of three walkways of different widths, the authors pointed out that a linear increase of the presence of aged pedestrians would lead to a non-linear decrease of the average walking speed in crowded scenarios.

Another work focused on the impact of the presence of aged pedestrians in the mobility and space utilization has been proposed by Shimura et al. [2014]. Using the discrete environment approach, the authors proposes a cellular automata model specifically tailored to simulate the movement of normal pedestrians walking at standard speed and slower aged pedestrians. In order to provide a qualitative validation of the proposed cellular automata, a controlled experiment has been carried out with a set of 25 students, which has been divided in two groups with the aim to describe the two different walking speeds of pedestrians. The experiment represented a uni-directional flow in a small corridor, with different configurations of the initial positions of the two pedestrian groups. The aim of the investigation has been to analyze the behavior of normal pedestrians in overtaking the slower ones, initially located in the front of the pedestrian flow, and the usage of the space after this "moving bottleneck". By comparing the analysis with the simulation results, the authors have shown a good agreement of the simulations with the behavior observed in the footage of the experiments.

A peculiarity of these two briefly explained works is that they both provide a good framework that considers the presence of fragile users of the environments, yet they are focused on the reproduction of the pure walking. Particular aspects of the behavior which have also been highlighted by Bandini et al. [2015] are still neglected in this literature. By thinking to the element of groups, an aged person would be probably walking with a caretaker and this would compose a slightly different form of group. The two persons, in fact, will walk strictly together and their path will be practically the same (some examples are shown in Figure 2.13(b)). On the tactical level side, instead, another aspect that should be considered is that structural elements of the environment like stairs might influence the route choice of an elderly person much more than other phenomena like the congestion. As it is shown in Figure 2.13(a), these peculiarities have been already considered for the route planner of the *Transport For London* website, even including the walking speed. For these reasons, these aspects will be taken into consideration and will be subject of part of the works presented in the next Chapter.

[5]http://people.revoledu.com/kardi/research/pedestrian/MicroPedSim/download.htm

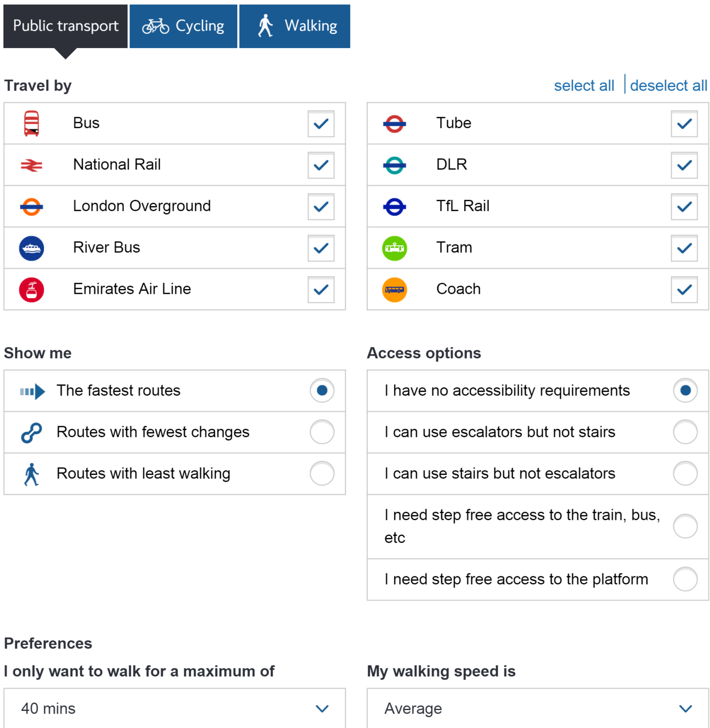

(a)

(b)

Figure 2.13: *(a) Traveling options available at the website* `tfl.gov.uk`*: they already consider necessities derived by having walking impairments. (b) Example of groups composed by an elderly person and a caretaker. The two persons will practically cover the same trajectory.*

2.5 Validation of the Models: The Available Knowledge on the Modeled Dynamics

In the previous Sections, a brief yet sufficiently wide description of the literature on the simulation has been provided, therefore it should now be clear what are the objectives, the potentials and the criticisms of the state-of-the-art modeling approaches. Before closing this Chapter, however, it must be still clarified which are the instruments and the currently available knowledge to perform the validation and, therefore, to scientifically certify the reliability of the simulations provided by a model.

As also for the modeling and simulation side, the main aims of the investigations have been focused on the pure physical aspects of the dynamics. By means of experiments and observations of real-world scenarios, aggregated data of the fundamental diagram have been, in fact, the main subject of this line of research and will be explained in the following section.

2.5.1 The Pedestrian Fundamental Diagram

The fundamental diagram describes the analogous and reciprocal relations between *density*, *flow* and *speed* of the investigated entity. The different forms of the relation are analogous since they respect the equation:

$$J = \rho \cdot \nu$$

with the standard notation defining J as the flow, ρ as the density and ν as the velocity. This instrument has been initially introduced in the field of vehicular transportation but, with the rising of the interest on pedestrian traffic and also the qualitative analogies of the fundamental diagrams of the two forms of motion, it has been studied and applied also in this context.

The fundamental diagram of both pedestrian and vehicular dynamics, in fact, can be *qualitatively* described by the curve shown in Figure 2.14(a). By increasing the density, the flow J_s is increasing until the reach of the environment capacity, represented in the picture with the dashed blue line. After this point, also called the *critical density*, the scenario gets congested and the output flow starts to decrease. Naturally, this is only an initial and qualitative description of the phenomenon, since the position of the critical density and its image on the diagram must still be clarified. In addition, the representation here provided shows a perfect symmetry between the *free-flow* state, the left part of the fundamental diagram, and the *congested* state, but in the reality the relation is not symmetric at all. Despite this critics, this qualitative curve rises up a very important point of the research on the simulation of pedestrian dynamics: the application of a pedestrian dynamics model helps to recognize the critical areas of an environment and, if possible, to design solutions that are able to maintain the local densities below the critical level.

In order to understand the trend of the fundamental diagram of pedestrians in a more quantitative way, a lot of studies have been performed and in various situations. Figure 2.14(b) illustrates some data-sets that can be found in the literature. A commonly recognized feature is that normally the reachable densities do not overcome 6 persons/m^2: the data set from Helbing et al. [2007] actually reaches the value of 10

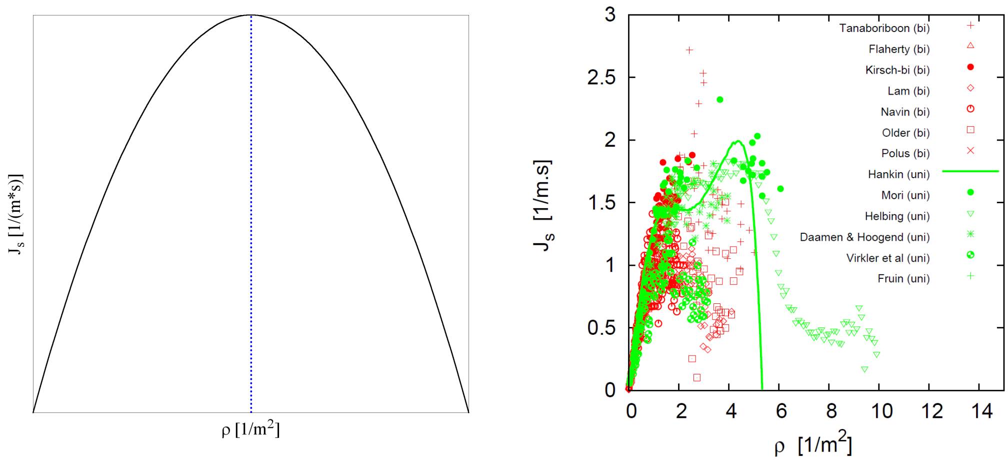

(a) (b)

Figure 2.14: *A qualitative representation of the pedestrian fundamental diagram (a) and a plot containing multiple data-sets and definitions from the literature (taken from Zhang et al. [2012]), in the form density(ρ) – flow (J_s).*

persons/m^2, but it has been achieved with the observation of a part of the Makkah pilgrimage, which is a very particular and overcrowded situation. It is quite clear that the fundamental diagram can vary significantly depending, first of all, on the pedestrian flow configuration. The specific flow in case of uni-directional motion (e.g. Helbing et al. [2007]) is generally higher than in the bi-directional case (e.g. Older [1968]). Other differences have been also recognized among cultures: the work of Chattaraj et al. [2009] emphasizes differences between the uni-directional flow of German and Indian people, observed with the same experimental procedure. In addition, also the method for the calculation of local densities and the corresponding flow or speed can lead to systematic differences in the results. Earlier data-sets (e.g. the one of Predtechenskii and Milinski [1978]), in fact, have been achieved with a completely manual tracking method. The procedure consists in watching the recorded footage or set of photographs and: (i) counting the number of people inside the observed area for achieving the density value; (ii) calculating the traveling time between the two lines in the scene.

A more recent and advanced investigation on the fundamental diagram of uni-directional and bi-directional flow has been carried out in Zhang et al. [2011] and Zhang et al. [2012]. In these works, a set of controlled experiments have been performed in elementary portions of environment, such as straight corridors and a so-called t-junction composed by two merging corridors with a 90-degrees intersection. The analysis illustrated in Zhang et al. [2011] firstly compared methods for the calculation of the pedestrians local density, emphasizing the stability of the *Voronoi* method. This

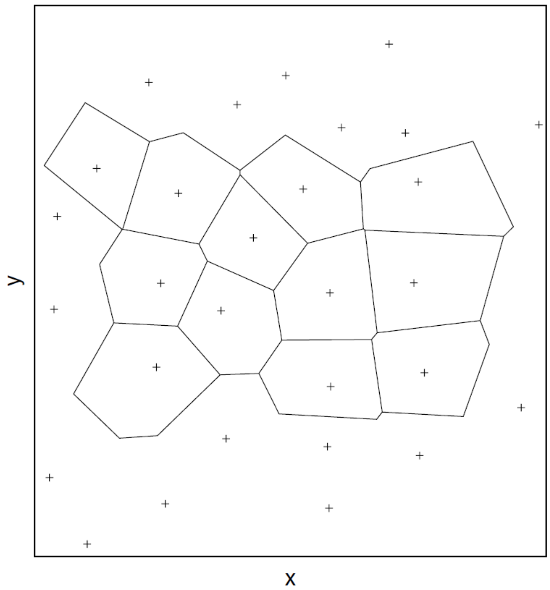

Figure 2.15: *A set of pedestrians positions and their associated Voronoi cells (taken from Steffen and Seyfried [2010]).*

method has been firstly proposed in Steffen and Seyfried [2010] and designs the density calculation by measuring the area of the Voronoi cells computed with the positions of pedestrians. In particular, a Voronoi polygon associated to a pedestrian p' is computed with the set of edges (i) that are perpendicular to edges (p', p_n), p_n is a neighbor pedestrian to p' and (ii) that forms a closed polygon. A graphical example is shown in Figure 2.15. The Voronoi method on one hand gives a mathematical description of the available space of each pedestrian and, on the other, it has the positive peculiarity to provide a continuous and stable value of density inside an arbitrary observed area.

The work of Zhang et al. [2012] particularly pointed out the differences between uni-directional and bi-directional flow. The authors performed a set of experiments in corridors of different widths and with different flow configuration, regulated by two bottlenecks placed before the extremes of the corridor, as shown in Figure 2.16(c). The achieved fundamental diagrams are reported in Figure 2.16(a) and (b). By looking at the results, it is visible that the critical density value is lower in the case of bi-directional flow, while on the other hand it remains stable at higher values, reaching an even better flow value at about 3 persons/m^2. The trend of the data-set, however, is not complete since for the bi-directional experiments the maximum local density reached has been around 3.5 persons/m^2, while was about 4 for the uni-directional case. In addition, it must be noted that, in order to reach densities higher than 3 persons/m^2 in the uni-directional case, the authors configured a bottleneck at the end of the observed corridor (this also explains the clear separation of results from 2.5 and 4 persons/m^2).

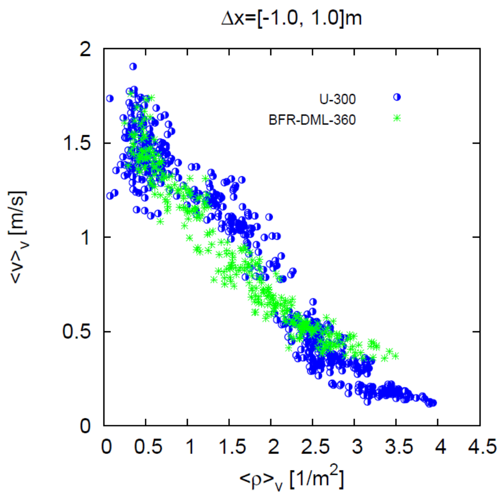

(a) Density-velocity

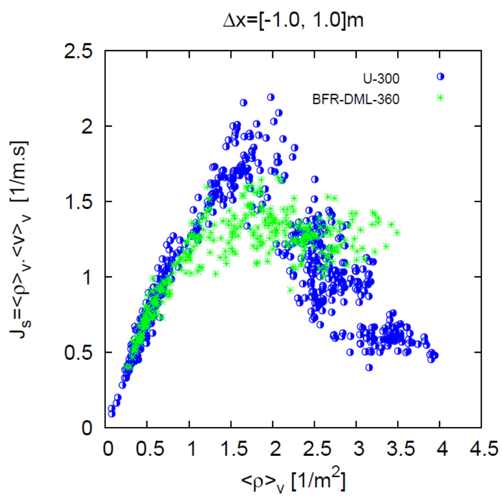

(b) Density-specific flow

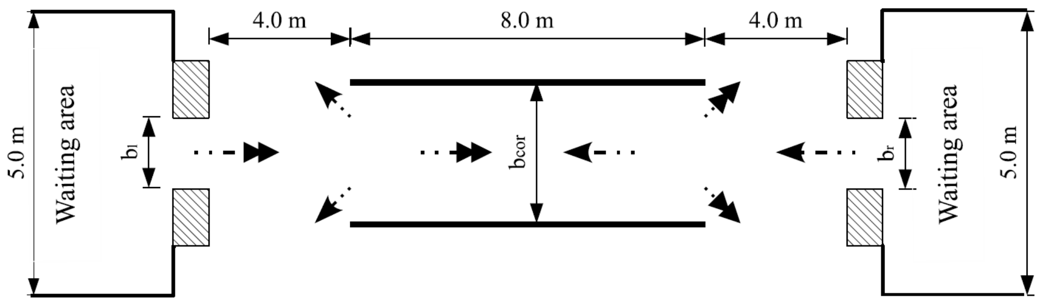

(c) Scenario configuration

Figure 2.16: *Comparison of the fundamental diagram for uni and bi-directional pedestrian flow, in the form density–speed (a) and density–flow (b), achieved with the experiments of Zhang et al. [2012]. The experiments configuration is shown in (c). The pictures have been taken from the paper.*

2.5.2 Analysis of Space Utilization

The fundamental diagram helps to understand if the model is able to reproduce reliable output flows along the simulated environment, quantitatively analyzing if it is too constrained, predicting higher traveling times than they would be in the reality, or otherwise too fast, predicting faster pedestrians than observed. Additional knowledge is, therefore, needed to understand if the rules of movement of the model are realistic: if the simulated pedestrians are covering the space as it would be possibly used in the real-world and, also, if it is not generating unrealistic congestion.

For these purposes, heat maps aggregating the usage of the space by pedestrians

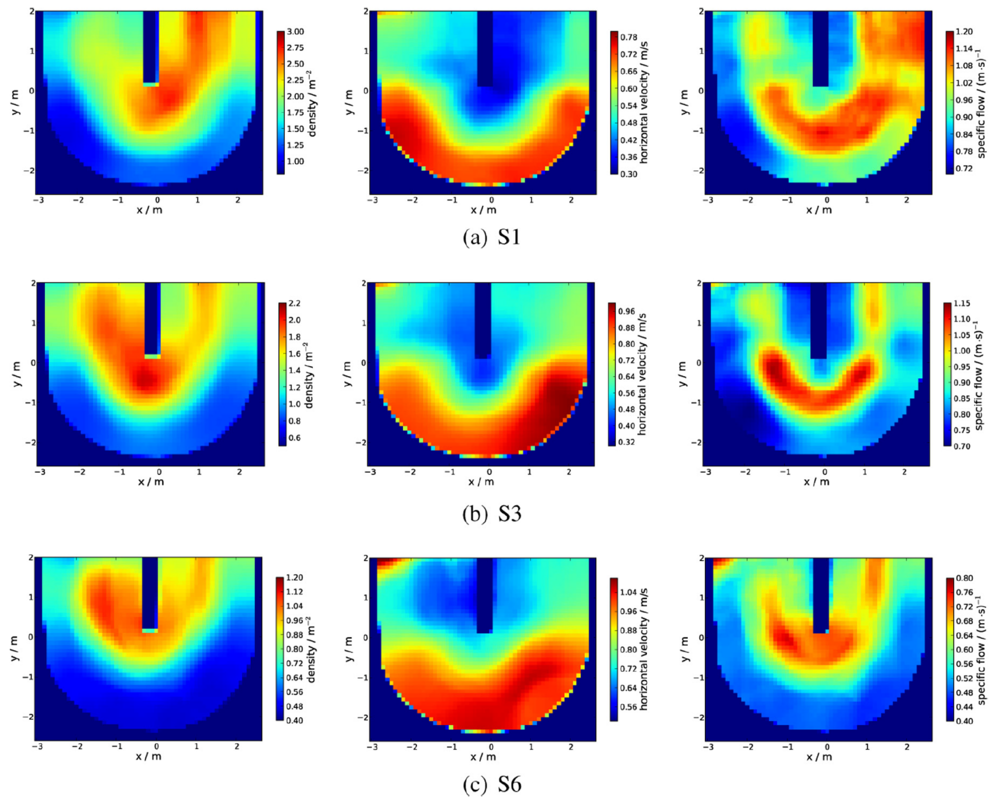

Figure 2.17: *Analysis of the space utilization in stars from Burghardt et al. [2013]. From left to right each image shows densities, velocities and flows over the space. The three configurations of the flow (S1 – S3 – S6) are ordered in a decreasing way and have been achieved by regulating the width of the entrance door to the stairway.*

and their local densities over time represent a more qualitative yet very important instrument. Significant results have been carried out with the works in Burghardt et al. [2013] and Boltes et al. [2011], which report heat maps aggregating the position of the observed pedestrians over time. These data provides information about their densities and velocities along the space and let to understand which are the less used parts or, also, what could be the evolution of congestion in the environment. Figure 2.17 reports the space analysis of Burghardt et al. [2013] and exemplifies the output information. The experiments executed for that work had the aim to analyze and achieve a fundamental diagram for the movement on stairs and they have been performed in the stairways of the ESPRIT Arena of Düsseldorf (Germany). For the space utilization analysis, an external stairway composed of two small stairs linked with a U-turn shape have been observed. The three rows of the figure differentiate results over three runs of the experiment, configured with three different arrival flows to the upper part of the stairs, in the top-right of each image. All flows in the scenarios, thus, were configured with downwards direction in the stairs. By looking at the results, the pictures show that the increase of the inflow to the stairways translates the area with higher density from the lower to the upper staircase, generating more congestion and conflicts at the turning point at the center of the image.

2.5.3 Validation of The Tactical Level: Assumptions and Possibilities

Despite the tactical level has been already explored with some works on the modeling side, the knowledge on the analysis side is still very poor to allow some kind of validation.

To face this problem and move towards a validation of the tactical level model that will be presented in the next Chapter, a controlled experiment is planned to be performed in collaboration with the group of Prof. Nishinari of the Research Center for Advanced Science and Technology (RCAST) of the University of Tokyo. Unfortunately, due to the available time, the results of the experiment will not be available in time to appear in this Thesis, but the procedure will be explained as well to give an overall idea of its objectives.

The tactical level model proposed in the next Chapter introduces an adaptability of pedestrians route choice, during the simulation, depending on the perceived traveling times towards their final destination. This implies that a growing congestion in an intermediate point of the scenario will increase the traveling time in a non-linear way, leading the agents to adapt their route at some point, depending on the existence and the peculiarities of the alternatives. This phenomena is naturally very complex and a clear understanding needs a significant research work, in order to disentangle question marks about when, how and what type of alternative ways we are really considering during an evacuation or in a normal situation. With the aim to reach a base-line knowledge of the adaptability of route choice, an evacuation of an elementary environment providing two possible routes will be tested and observed in the planned experiment. The setting is graphically explained in Figure 2.18.

As it is possible to realize from the image, the environment configuration implies a straight shortest route (Path_A) towards the destination and an alternative one (Path_B) whose length can be regulated by the length of the middle wall. The two routes implies to pass through an opening which is smaller than the entrance to the scenario, therefore they are both bottlenecks. The hypothesis is, thus, that most of the people will choose the shortest route and a growing congestion will arise in front of its opening. This will increase the adoption of the Path_B during the experiment time.

The video analysis will be performed with the pedestrian tracking tool *PeTrack*[6], whose technical details can be found in Boltes and Seyfried [2013]. To allow an automatic extraction of the trajectories by the software, the participants to the experiments

[6] www.fz-juelich.de/ias/jsc/EN/Research/ModellingSimulation/CivilSecurityTraffic/PedestrianDynamics/Activities/petrack/petrackNode.html

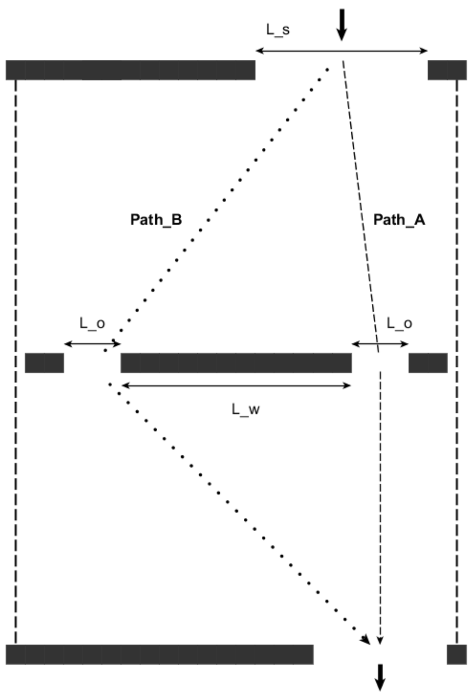

Figure 2.18: *The scenario configuration of the experiment that will be performed in Tokyo.*

will be asked to wear colored caps. The trajectories will be aggregated among the possible choices, described by a direct choice of a route of the two or a choice which has been changed during the experiment. The final object of the study will be, thus, the analysis of the impact of the arising congestion in the choice between the two paths, understanding if the choice of Path_B will grow linearly from the beginning or if there will be some state transitions.

3

A Discrete Model for the Operational and Tactical Levels of Pedestrian Behavior

The literature review provided in the previous Chapter has provided ideas on what are the needs and the requirements for the realization of a microscopic model of pedestrian dynamics. In particular, it should be now clear that a microscopic model must represent decisions at different level, differentiating between decisions that compose a high-level route, chosen according to particular necessities and beliefs, and the physical movement describing the actuation of this route. Summarizing, the following components of the behavior must be – and will be – taken into consideration for the model design:

- reproduce the walking behavior in the environment, both at low and high densities and considering arbitrary configuration of obstacles;
- represent social relationships and pedestrian groups;
- consider differences in the simulated population, by allowing the possibility to differentiate velocities;
- consider the composition of a high-level route at tactical level;
- population heterogeneity must be considered also at this level, taking into account the necessities of users of the environment that might not be able to employ particular routes (e.g. containing stairs).

Despite this problem statement is informal, it already provides suggestions on the necessities to provide reasoning in different forms and at different levels. The movement must be reproduced in a detailed environment, but the composition of the route requires a consideration of a more abstract representation that involves other information. This requirements led to the usage of the agent-based approach for the modeling, in particular with the definition of a *hybrid* agent architecture whose concept is illustrated in Figure 3.1.

This concept designs a single pedestrian as an agent that, as shown in the Figure, is composed of two main elements. The *body* reproduces the walking motion in the environment from sources to destinations, considering the elements which influence

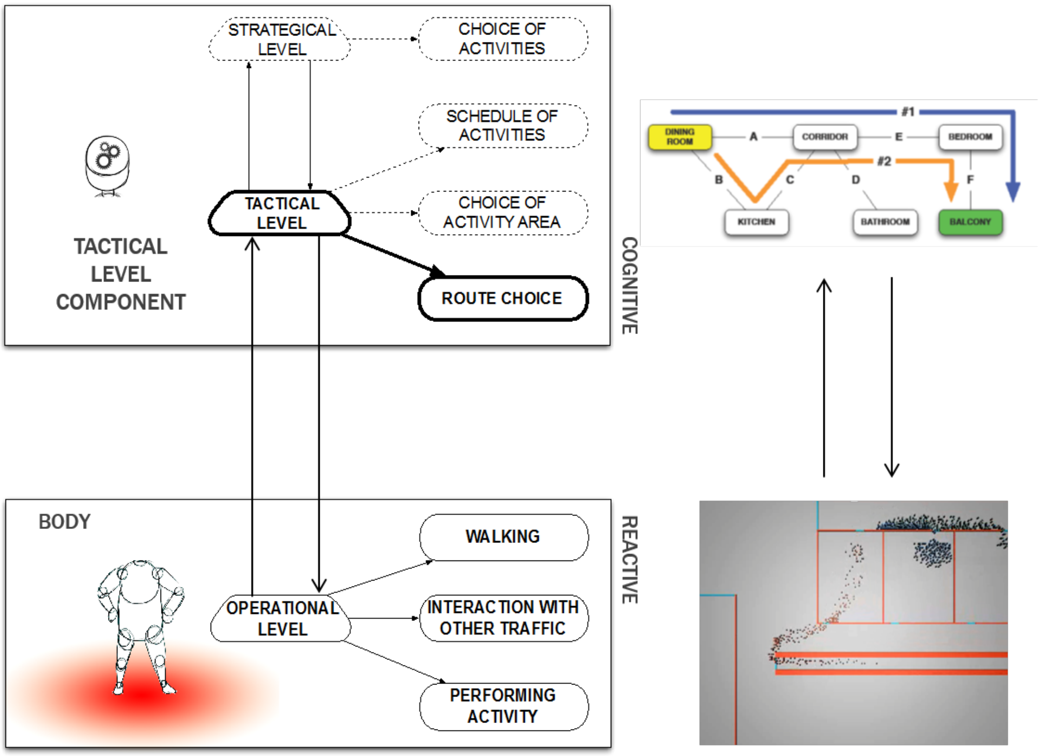

Figure 3.1: *Overview of the agents architecture facing the modeling problem.*

the operational level and that have been described in the previous Chapter. The *tactical level component* is dedicated to the reasoning on the graph-like representation of the space, where the route computation will be performed according to the peculiarities of the environment *regions* and of the agent itself.

In this Chapter, the discrete approach to the definition of the environment will be firstly discussed, concerning both the physical structure and the high-level knowledge. The configuration of the time discretization and the update strategy will follow the discussion. Finally, the behavior of the agents will be described, firstly considering the component for the operational level to then arrive at the proposed approach for the management of the route choice activity.

3.1 The Discrete Representation of the Environment

At the physical layer the model is discrete and the environment is modeled with a rectangular grid of 40 cm sided square cells. The size is chosen considering the average area occupied by a pedestrian [Weidmann, 1993], and also respecting the maximum densities usually observed in real scenarios (see Section 2.5.1). The cells have a state that informs the agents about the possibilities for movement: each one can be vacant or occupied by obstacles or pedestrians. In particular, the state indicates if the cell is occupied by one or two pedestrians:

$$State(c) = s : s \in FREE, OBSTACLE, ONE\_PED, TWO\_PEDS$$

The last case is allowed only in a controlled way to simulate overcrowded situations, where the pedestrian density reaches values above the 6.25 ped/m^2 limit of the cell configuration.

The information related to the simulation scenario is represented with *spatial markers* introduced by the user at design-time. These objects define special sets of cells describing the generation points of agents in the scenario, their possible destinations – either intermediate or final – and all non-walkable areas as walls or other zones where pedestrians cannot enter (e.g. the railways of a train station). In particular, this set of markers has been introduced to allow the movement at the operational level and the reasoning at the tactical level:

- *start areas* , places were pedestrians are generated: they contain information for pedestrian generation both related to the type of pedestrians and to the frequency of generation. In particular, a start area can generate different kinds of pedestrians according to two approaches: (i) *frequency-based generation*, in which pedestrians are generated during all the simulation according to a frequency distribution; (ii) *en-bloc generation*, in which a set of pedestrians is generated at once in the start area when the simulation starts;
- *intermediate destinations* , areas where the pedestrians might need to pass through, such as a ticket machine. An intermediate destination can also imply a particular behavior, such as waiting;
- *openings* , sets of cells that divide, together with the obstacles, the environment into regions;
- *regions* , objects that describe the type of the region where they are located: with them it is possible to design stairs, ramps and other portion of the space that imply a particular behavior of pedestrians;
- *final destinations* , the ultimate targets of pedestrians;
- *obstacles* , non-walkable cells defining obstacles and non-accessible areas.

To improve the understanding, an example scenario with a complete annotation of markers is depicted in Figure 3.2. The user annotation of the space allows the definition of virtual grids of the environment, as containers of information for the agents and their movement. This model adopts the floor field approach firstly proposed by Burstedde et al. [2001] and explained in the previous Chapter. The approach

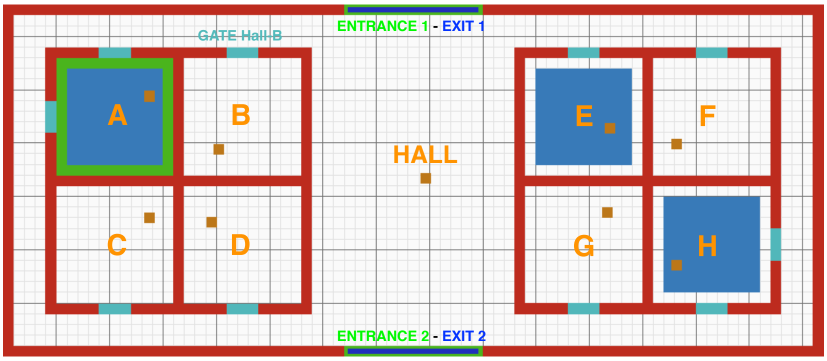

Figure 3.2: *An example scenario annotated with the spatial markers of the model. The scenario is a toy representation of a university building, with a few lessons rooms containing waiting areas (modeled with intermediate targets).*

illustrates the generation of a set of superimposed grids, similar to the grid of the environment, that will host particular gradients used for the movement towards a destination, either intermediate or final, or for other interactions among pedestrians or between pedestrians and static obstacles of the environment. The goal of these grids is to support long range interactions by representing the state of the environment (namely, the presence of pedestrians and their capability to be perceived from nearby cells) in terms of field modifications. In this way, a local perception for pedestrians actually simply consists in gathering the necessary information in the relevant cells of the floor field grids. In other works, the concept of perception and the relative implementation is more thoroughly investigated, starting from the definition of the *field of view* mechanism in humans: in the work of Paris and Donikian [2009] the pedestrian perception from a cognitive point of view is illustrated, while a more physical approach is examined in Shao and Terzopoulos [2007]. Nonetheless, in CA based approaches such a precise perception model is rarely employed, since it would significantly and negatively impact on the computational side, but still the achieved results are often extremely interesting. For this reason, it has been decided to employ a simple perception model and evaluate its adequacy.

A floor field can be static, created at the beginning and not changed during the simulation, or dynamic, initially containing zero values which are then updated during the simulation time. In the proposed model, four floor fields are defined:

- the *path field*, indicating the distance to a destination point (final and intermediate destinations or openings) and acting as a potential field that drives pedestrians towards it;
- the *obstacle field*, containing a gradient spread out from the positions of obstacles and used to allow the pedestrians to assume smooth trajectories in the obstacles

surroundings;

- the *proxemics field*, where a gradient from each pedestrian is spread out at each time-step of the simulation;
- the *density field*, another dynamic field that is used to estimate the local pedestrian density in a discrete way. Its main purpose is the calculation of statistics of the simulation, such as the *cumulative mean density*, but as it will be explained later the density values are also used for a particular function of the *overlapping* mechanism in the agents behavioral model.

The first three floor fields are graphically exemplified in Figure 3.3(a). The first two types of floor fields are generated from static objects, therefore they will not be changed during the simulation as it will happen with the proxemics field. The floor fields introduced in the model will be now analyzed with full details.

3.1.1 The Path Fields

The values spread over the static floor fields can be performed by using different existing methodologies, as discussed by Kretz et al. [2006]. This is a particularly important point, since the way of diffusion of the gradient will systematically influence the space utilization of the simulated pedestrians. In this model, the *chessboard metric* with the $\sqrt{2}$ variation over corners [Kretz et al., 2006] is used to produce the spreading of the information in the path and obstacle fields. This choice allows the agents, whose movements at each step are localized in the Moore neighborhood structure, to travel the shortest path over the discrete grid and towards the destination. For more clearness, the improvement of the chosen metric is illustrated in Figure 3.3(b). It is visible how the usage of the Manhattan metric – which adds 1 to the value of each cell of the Von Neumann neighborhood – generates an artifact in the space utilization with the generation of triangular jamming areas around bottlenecks. The diffusion with the $\sqrt{2}$ variation significantly improves the result.

The overall procedure for the computation of the path field is described in Algorithm 1. The algorithm is the same for a field computation spread either from the cell of an intermediate target, of a final destination or of an opening object.

A detail of the procedure that needs further discussion is related to the check performed at line 16. The outcome of this check is that the field diffusion will stop in correspondence of the cell of an opening object, in addition to the cells of obstacles. The diffusion is thus limited to the region/s where the object is located (for the case of openings the spread will be performed in the two linked regions). This technical detail has two particular meanings. First of all, with the modeling a realistic scenario, a modeler will probably have to design a relevant number of targets, therefore there will be numerous path fields. By constraining the field diffusion, a relevant gain in terms of time and space complexity of this aspect will be provided. The second meaning resides,

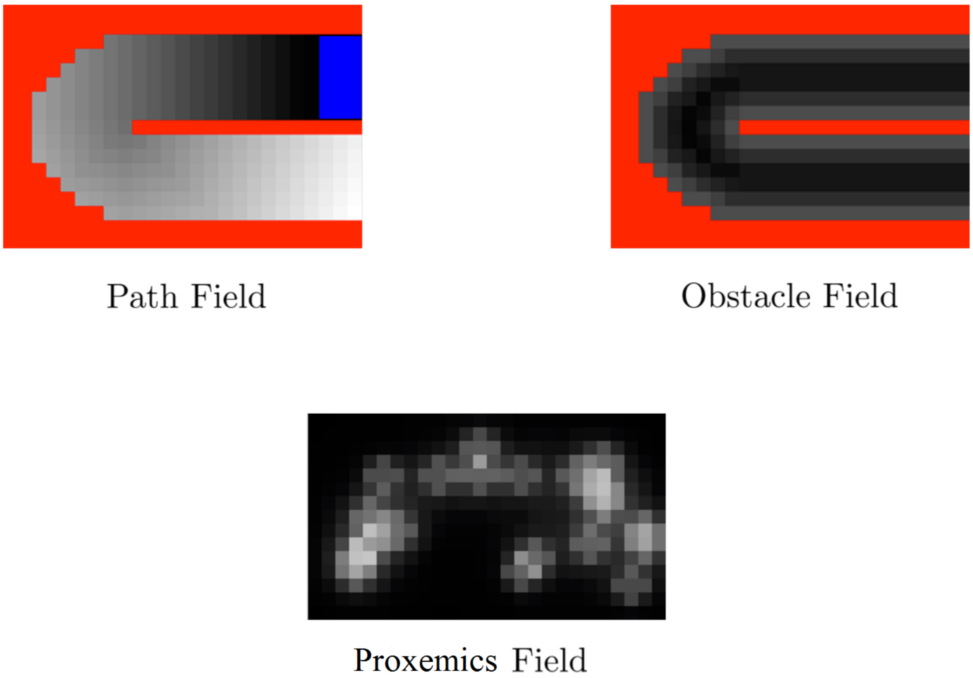

(a)

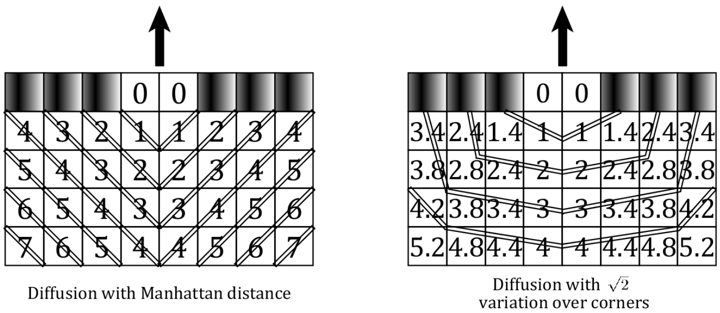

(b)

Figure 3.3: *(a) Graphical representation of the first three floor fields of the model (the red cells are obstacles, while the blue object is a final destination). (b) Difference between the manhattan and chessboard metric with* $\sqrt{2}$ *over corners.*

instead, in the overall simulated behavior. Figure 3.4 illustrates an example scenario with several possible paths towards the exit. With the aim to let the agent able to walk through these paths, it is mandatory to stop the field diffusion of the opening B2 in the linked regions: the spread of the values over the all environment would let the agent arrived in B1 and wanting to continue to B2 (as described by the arrow) to pass as well

Algorithm 1 The path field diffusion

Input: the set of cells *destination* (the object from where the spread begins)
Output: the path field associated to *destination*

```
L ← Cells(destination)
L.set_all_values(0)
while L ≠ ∅ do
    temp ← L[0]
    delete(L[0])
    N ← neighbors(temp)
    N ← filter_obstacles(N)
    for n ∈ N do
        if n ∈ VonNeumannNeighbors(temp) then
            newValue ← temp.value + 1
        else
            newValue ← temp.value + sqrt(2)
        end if
        if n.value = Null ∨ n.value > newValue then
            n.value ← newValue
            if get_marker(n).type ≠ 'opening' then    ▷ this limits the field diffusion
                L.enqueue(n)
            end if
        end if
    end for
end while
```

through A, following the shortest path.

3.1.2 The Obstacle Field

The obstacle field is overall similar to the path field, except from the procedure of diffusion that illustrates some differences. First of all, the algorithm do not expect a stop of the diffusion as above described since the field is unique for the all environment. Moreover, at the end of the diffusion the values inside the grid are inverted as:

$$ObstacleField(c) = Max(ObstacleField) - ObstacleField(c)$$

In this way the grid will contain higher values next to the obstacles, decreasing with the increase of the distance.

Finally, the spreading has a limit described by a distance radius ρ_{obs}, that for the presented tests has been fixed to 3 cells. This is also visible in Figure 3.3(a).

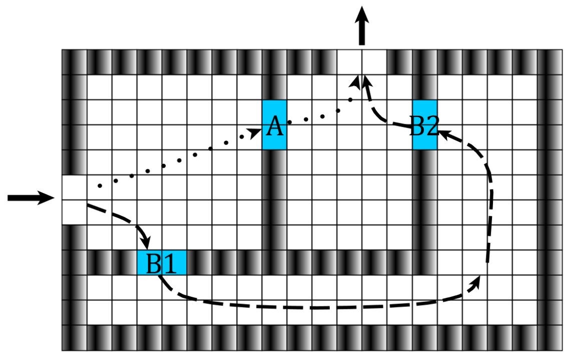

Figure 3.4: *An example scenario with 3 regions divided by 3 openings.*

3.1.3 The Proxemics Field

The aim of the proxemics field is to provide information to the agents in order to let them be able to avoid congested areas with the movements at local level. As above introduced, this grid is dynamic and, starting from a grid of 0 values, it is modified according to the following mechanism:

- if a pedestrian is generated in a cell, a unitary value 1 is added to the grid in correspondence of the cell. A gradient is then diffused to neighbor cells in a range given by a radius $r = 2$ m (equal to five cells from c, considering the proposed scale of discretization), but the value added decreases with the inverse of the square of the distance between the neighbor cell and p, as $v = \frac{1}{d^2}$;
- when a pedestrian p moves in a cell with coordinates (i, j), the proxemic field is modified by adding 1 to the cell in which he/she is moving, and subtracting 1 from his/her old position. The modification is applied also to neighbor cells with the diffusion explained in the previous point.

Hence, the pedestrians cause a modification to the proxemics field by adding a value $v = \frac{1}{d^2}$ to cells whose distance d from their current position is below a given threshold r, fixed at 2 m in the presented tests. The unitary value 1 in the position of the agent simply finds motivation in $\lim_{r \to 0^+} \frac{1}{d^2} = \infty$.

The way the values of the three floor fields will be employed for the realization of the pedestrian movement will be described in Section 3.4.1.

3.1.4 The Density Field

The method proposed for the calculation of the local density follows the logic of the diffusion from the pedestrians position explained for the proxemics field. Differently, this method calculates the discrete *number density* of pedestrians in a circular area of fixed radius $r \in \mathbb{R}$ centered on each cell of the environment. A few preliminary definitions represents the core of the method:

- Let $E_{(i,j)}$ the number of pedestrians in the cell (i, j). Given the configuration of the model, each cell can be occupied by maximum 2 pedestrians, therefore $E_{(i,j)} \in \{0, 1, 2\}$;
- Let $c_{(x,y)}$ be the cell of the environment identified by coordinates (x, y);
- Let $Q_{r,(a,b)}$ be the discrete area containing the disc of radius r and centered in $c_{(a,b)}$:

$$Q_{(a,b),r} = \left\{c_{(x,y)} : (x-a)^2 + (y-b)^2 \leq r^2\right\}$$

.

Given the status of the simulation at an arbitrary time-step, each value of the field $DensityField_{(i,j)}$ is calculated as the following:

$$DensityField_{(i,j)} = \sum_{(x,y)} \frac{\nu_{(i,j),(x,y)}}{Area(Q_{(i,j),r})}$$

First of all, the function $\nu_{(i,j),(x,y)}$ indicates the number of agents in the cell $c_{(x,y)}$ contained in $Q_{(i,j),r}$:

$$\nu_{(i,j),(x,y)} = \begin{cases} E_{(x,y)} & \text{if } c_{(x,y)} \in Q_{(i,j),r} \\ 0 & \text{otherwise} \end{cases}$$

The function $Area$, instead, calculates the area of the input region $Q_{(i,j),r}$ and is straightforward for a normal situation in which only walkable cell are contained. On the other hand, the presence of obstacles must be clarified: a raw usage of the area of the discretized disc would imply that eventual obstacles in the environment would negatively impact on the local density, decreasing its value. Therefore, $Area(Q_{(i,j),r})$ must be defined in order to only consider walkable cells in the surrounding of $c_{(i,j)}$:

$$Area(Q_{(i,j),r}) = \sum_{c_{(x,y)}} Area(c_{(x,y)}) : c_{(x,y)} \in Q_{(i,j),r} \wedge State(c_{(x,y)}) \neq OBSTACLE$$

$$Area(c_{(x,y)}) = CellSide^2$$

This implies that the values of $Area(Q_{(i,j),r})$ are different from cell to cell, thus to not impact the computational times these values must be pre-computed together with the density field. For a better understanding, the working principle of the density grid is exemplified in Figure 3.5.

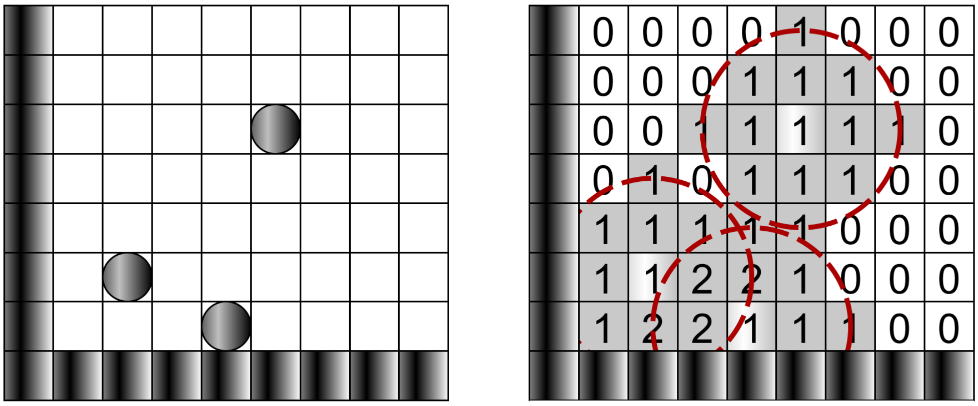

Figure 3.5: *An example representation of the density field values during the simulation (for simplicity, the values of $Area(Q_{(i,j),r})$ are omitted). The radius chosen in this case is 0.8 m, understandable by the illustrated red circles.*

3.2 Different Levels of Knowledge: an Abstract Representation of the Environment to Encompass Tactical Level Decisions

The instruments for the annotation defined for the environment representation allow the design of simulation scenarios where flows of pedestrians can be generated either simply from start areas to final targets or also considering many *intermediate destinations* in the journey, with the composition of more articulated movement plans for the pedestrians. Coming back to the scheme of the three levels of behavior of pedestrians provided in Chapter 2, the proposed annotation tools are already sufficient for the simulation of the pure movement towards a destination at the operational level and a raw reproduction of the tactical level by manual scripting from the user of the simulator[1]. On the other hand, this research aims at avoiding this exhausting work of the user, by providing a model encompassing also the tactical level. This will allow the agents to autonomously compute their plan, calculating a high level path through the settings that considers possible intermediate destinations.

The construction of such a plan requires the possibility to explore and process a much simpler data structure, in particular an abstract map in terms of a graph-like common-sense and cognitively logical representation of the environment [Bandini et al., 2007]. The way the humans build these logical maps is object of study mainly for psychology and neurosciences, although methods for representation of them are studied and applied also in architecture and geography.

[1]Note that this is the actual work-flow of most of the off-the-shelf simulator systems used for pedestrian flow analysis.

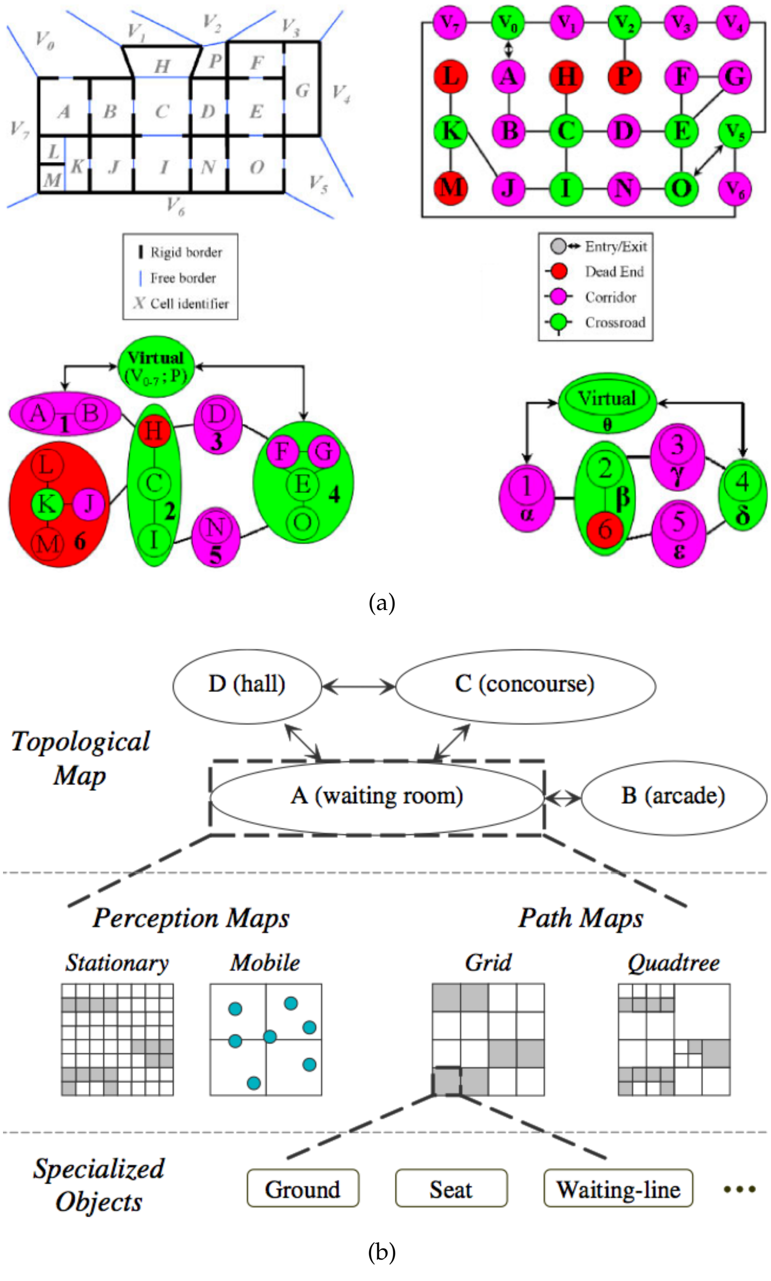

Figure 3.6: *The cognitive model proposed by Paris et al. [2006] (a) and the one proposed by Shao and Terzopoulos [2007] (b).*

Baroni [1998] reported some contributions from these sciences about these mental maps, called *cognitive maps*. One of the relevant theories cited in her book is about gender differentiation of perspective: male tend to have a *survey* perspective, i.e.

as they're watching the environment from the top as in viewing a map, opposite to female's route perspective, in which landmarks gain importance. Although it is just a stylized fact, it is admitted that there are tendency in gender to have different perspective. a.M. Galea and Kimura [1993] confirm the previous theory saying that women have a more photographic memory, i.e. they are more attracted by landmarks and are able to remember an high number of them, while men have a more generic point of view on the entire environment allowing them to better understand distances. They also try to give an explication saying it is related to a prehistoric reason: women staying near the village had to remember more references, while men were employed with hunt so they had to remember the entire route to come back home.

A concept that seems to be collectively admitted is about hierarchical structure of these maps: Taylor and Tversky [1992] talk about organization of landmarks in a sort of tree. A landmark can help remember a small region of the space that, in turn, can help remember a bigger region.

Taking into account these contributions (or part of them), some agent-based models have been developed in the field computer sciences. The work by Paris et al. [2006] and Shao and Terzopoulos [2007] are particularly important. Both implementations use hierarchical graphs to represent the environment, but they differ regarding means of different layers. The one by Paris et al. [2006] (see Figure 3.6(a)) uses a three-layered *Informed Hierarchical Topological Graph* (IHT-graph) as cognitive map, in which elements represent regions (and sub-regions) of the environment without storing geometrical information, and each level is a merge/dilatation of the upper/lower adjacent level. Instead the one by Shao and Terzopoulos [2007] (see Figure 3.6(b)) is more heterogeneous, at the higher level there are regions linked together in order to have a topological representation of the environment, for each of them at a lower level there are perception maps and path maps to represent it physically, then there is a more lower level in which there are specifications for objects and zone of the relative portion of the world.

For what concerns this model, a simple and complete representation of the *cognitive map* of agents is automatically derived by the annotated scenario. This employs the path fields diffusion from the opening objects with an algorithm that for more clearance is graphically explained in Figure 3.7. As it can be understood by Figure 3.7(c), the abstraction of the environment into the cognitive map illustrates a mapping of regions to the nodes of the graph, while openings will be represented as edges with unitary weight. Each node contains information on the name and type of region that is linked, achieved with the region marker. In addition, eventual intermediate targets positioned by the user inside the region will be mapped as parameter, together with the path field spread out from these objects. Hence these intermediate destinations are essentially included in the sub-area they are part of. Each edge contains, instead, only the reference to the path field diffused from the opening, as shown 3.7(d). Openings that connect the same pair of regions (i.e. multiple doors between two rooms) will be represented as

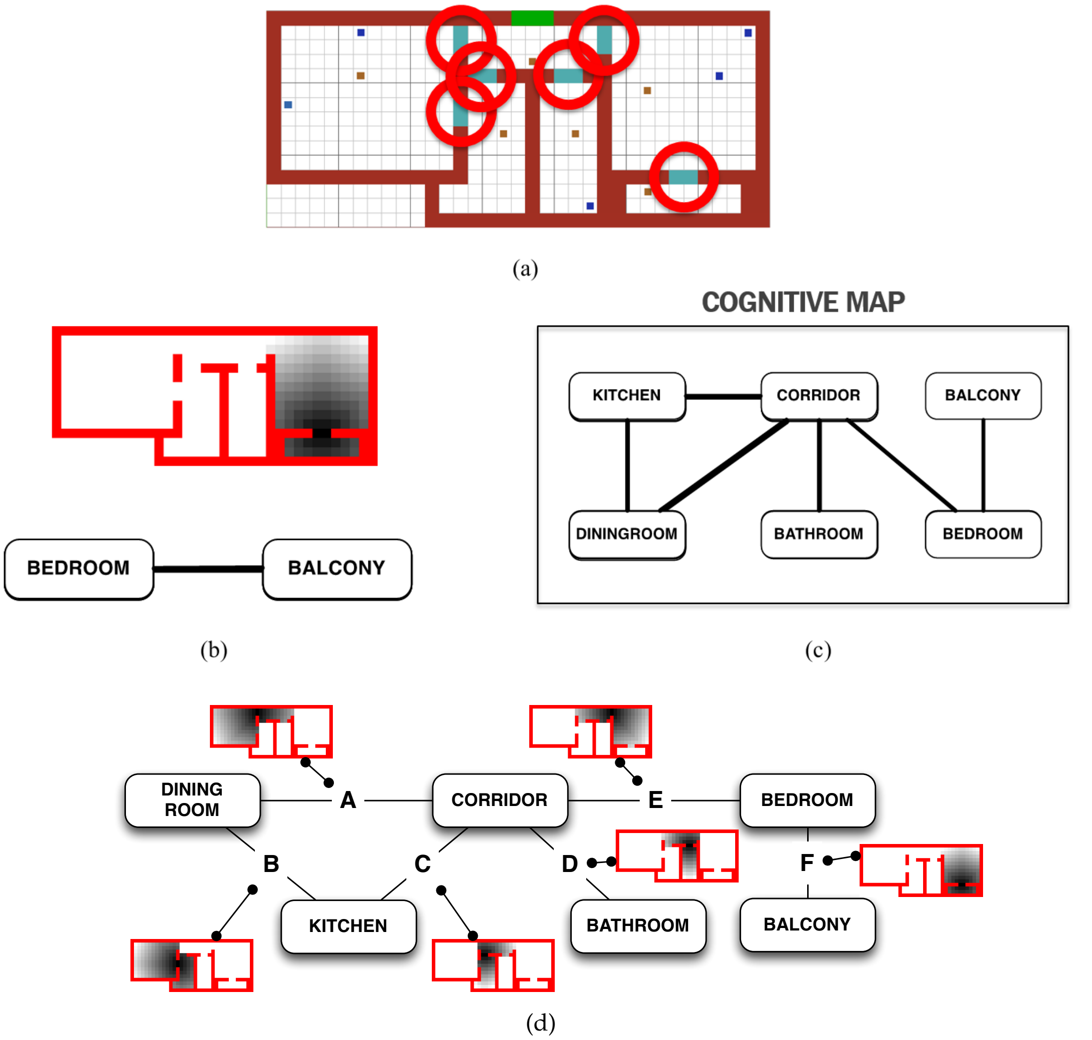

Figure 3.7: *(a) A sample annotated scenario representing an apartment composed of 5 rooms. The cognitive map associated to this environment is shown in (c). The procedure for the computation of the graph iteratively adds nodes and edges with the field diffusion from the openings objects (b). (d) The cognitive map integrated with the mapping to the path fields of openings, that will be used by the agents.*

different edges.

Moreover, the final destinations are represented with annotated edges leading to a special node that is not associated to any sub-area designed by the user. This node will describe, in fact, the area "outside" of the simulated world. As it will be discussed in Section 3.4.5, this structure is particularly suited for simple path planning algorithms that can be employed in the agent's tactical level.

3.3 Time and Update Strategy

Time is also discrete in the model. In order to allow a maximum desired pedestrian velocity of 1.6 m/s, in accordance with the empirical observations (see Section 2.5.1), the duration of a single time-step is assumed to be 0.25 s: in discrete models like the one here proposed, the velocity of the entities is generated by the ratio $\frac{cell\ side}{turn\ duration}$. It must be noted that, given the usage of a square cells grid for the space representation, this rule is only respected with the linear movements in the Von Neumann neighborhood. Since the agents of this model are allowed to move in the Moore neighborhood, diagonal movements are thus generating an instantaneous velocity of $\frac{0.4\cdot\sqrt{2}}{0.25}$ m/s. However, as it will explained in Section 3.4.3, this modeling artifact has been successfully tackled with an innovative extension dedicated to the reproduction of different speeds in discrete environments.

The assumption and usage of a discrete time implies to take decisions regarding the update strategy for the agents, i.e., the order in which they will choose and execute the movement at each time-step. In the current literature, the following update strategies have been proposed [Klüpfel, 2003]:

- *sequential* update, in which the pedestrians are updated one after the other and always in the same order. This order depends on the one of their generation;
- *shuffled sequential update*, for which the pedestrians are updated one after the other, but with an order that is re-computed every time-step;
- *frozen shuffled sequential update*, which is a slight modification of the shuffled sequential one. This approach designs a shuffling of the order only at the beginning of the simulation, providing thus each pedestrian with a priority factor (differently from the other ones, this approach is more recent and has been proposed by Appert-Rolland et al. [2011]);
- *parallel* update, in which the pedestrians choose the movement to perform at the same time, generating conflicts which must be solved with additional rules.

In cellular automata models for crowd simulation, parallel update is generally preferred [Schadschneider et al., 2009], since the sequential update schemes generates an artificial synchronization of the simulated particles. Blue and Adler [1999], in fact, point out that "*with sequential updates the order of each move becomes unrealistically important, since as each entity moves, the next entity re-positions in relation to the previous entity. Thus, the first entity would act the position of all entities over the whole lattice*". In addition, Kirchner et al. [2003a] state also that the simulations are more realistic if a *friction* mechanism is introduced in the conflicts resolution, blocking the movement of all the pedestrians involved in a conflict with a certain probability. For these purposes, the parallel update strategy has been chosen for this model, configured with a friction parameter as introduced in Kirchner et al. [2003a].

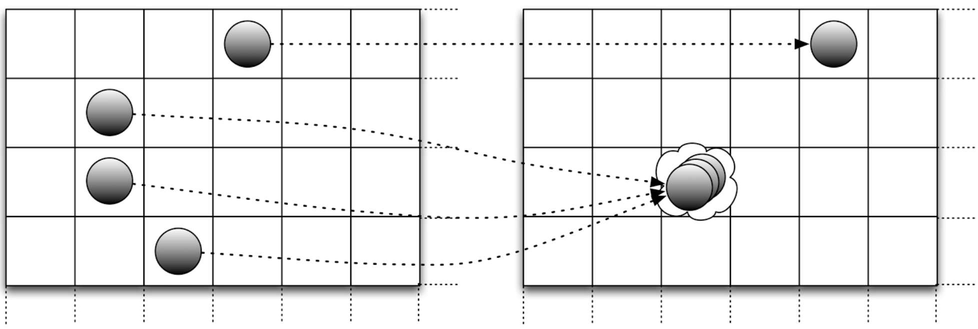

Figure 3.8: *The conflict detection activity: the intention of movement of agents are collected in a additional data structure that links the chosen destinations to the agents. Multiple choices of the same destination cell are saved in a dedicated list, in order to maintain the computational time of this task very limited.*

With this update strategy, the simulation life-cycle must consider that before carrying out the *movement* execution potential conflicts, essentially related to the simultaneous choice of two (or more) pedestrians to occupy the same cell, must be solved. The overall simulation step therefore follows a three step procedure:

- *update of choices* and *conflicts detection* for each pedestrian of the simulation. The conflict detection is performed with an additional data structure, illustrated in Figure 3.8, which optimizes the task;
- *conflicts resolution*, that is the resolution of the detected conflicts between pedestrian intentions;
- *pedestrians movement*, that is the update of pedestrians' positions exploiting the previous conflicts resolution, and *field update*, that is the computation of the new density field according to the new positions.

The resolution of conflicts employs an approach based on the notion of friction from Kirchner et al. [2003a], previously introduced. In order to understand the designed mechanism for the conflict resolution, two points must be firstly clarified. First of all, it must be noted that a conflict can involve two or more pedestrians: in case more than two pedestrians involved in a conflict for the same cell, the first step of the management strategy is to block all but two of them, chosen randomly, reducing the problem to the case of a simple conflict among two pedestrians. Secondly, as previously introduced in Section 3.1, this model is configured with a special rule that allows a temporary occupation of one cell by two pedestrians, to allow the management of very high densities. Hence the conflict resolution has to consider three possible outcomes: (i) none of the pedestrian involved in the conflict moves at the end of the step (friction);

(ii) one of the pedestrian moves (normal movement); (iii) two pedestrians moves (overlapping).

The management of a simple conflict is then regulated with another random number between 0 and 1, which is compared to two thresholds, $frict_l$ and $frict_h$, with $0 < frict_l < frict_h \leq 1$. The outcome will be that all pedestrians will stay blocked if the extracted number is lower than $frict_l$, only one moves (randomly chosen) when the extracted number is between $frict_l$ and $frict_h$, or two pedestrians move when the number is higher than $frict_h$ (in this case overlapping occurs). For our tests, the values of the thresholds make it relatively unlikely the resolution of a simple conflict with one pedestrian moving and the other one blocked, and much less likely their overlapping, but full details on the calibration parameters of this model will be provided in Chapter 4.

3.4 The Architecture of the Agent

With the aim of encompassing operational and tactical level behavior, a preliminary thought must be performed about the type of agents that will be implemented in this model. Books on artificial intelligence like the well-know text from Russell and Norvig [2003] – but also other important educational works on the field – list numerous agent types. For the purposes of this Thesis, it is important to differentiate:

- *Cognitive Agents*: agents that perform a significant reasoning on the information received by sensors, before sending the action to perform to its actuators;
- *Reactive Agents*: agents whose separation between the sensors and actuators is small and described by a simple reasoning, typically generated with a set of rules (as in the subsumption architecture from Brooks [1986]).

By considering the pedestrian behavior and especially regarding the three levels of behavior scheme, it comes out that the peculiarities of both agent types are needed to face the problem. Hence, a *hybrid* agent architecture has been designed, composed of a *body* that is dedicated to the purely reactive behavior at the operational level and a *tactical level component* where the plan computation and the route choice behavior is performed. The proposed architecture of the agent together with the representation of the problem is graphically explained in Figure 3.9.

A pedestrian of this multi-agent system is then formally defined by the couple $\langle body,\ tactical\ level\ component \rangle$. The body performs the perception on the physical layer of the environment using the floor fields and other information related to other agents, in case of groups, to reach the current destination of the agent. The tactical level component, by receiving the final destination as input, analyzes the cognitive map and compute the agent *plan*: a set of intermediate destinations and openings to reach, in order to arrive at the goal. The information that is passed between the two layers of

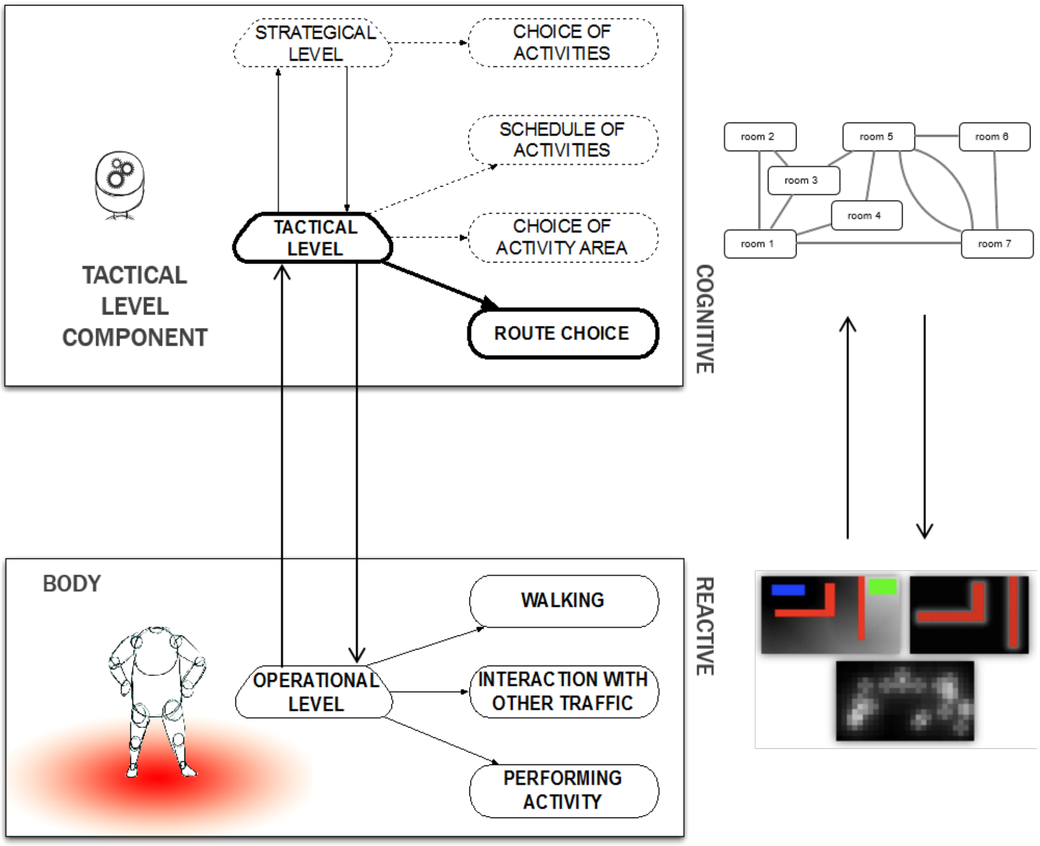

Figure 3.9: *A graphical representation of the proposed hybrid architecture of the agent. The tactical level component generates the set of destinations that the body will have to reach, under the influence of the floor fields.*

the architecture is nothing more than the pointer to the following path field to follow, once reached the minimum value of the current one. The two agent components will be analyzed in details with the following sections.

3.4.1 The Body of the Agent

The body of the agent is dedicated to the behavior of pedestrians at a local level, therefore the elements generating a significant influence on the walking path are considered in this component. The computational model underlying the body follows again the logic of the floor field model [Burstedde et al., 2001], with the definition of a probability function that indicates the choices of movement of the agents, but being innovative with the consideration of behavioral elements not comparing in that model.

The body of the hybrid agent architecture can be described as an utility-based agent with a state. Functions are defined for utility calculation and action choice, and rules are defined for state-change. Formally, the body of pedestrians is defined by the tuple $\langle Id, GroupId, State, Actions, Destination\rangle$, where:

1. $Id \in \mathbb{N}$ is the agent identification number;
2. $GroupId \in \mathbb{N}$ is the identification number of the group to which the pedestrian belong to; for pedestrians that are not member of any group this value is null.
3. $State$ that represents the state of the agent related to its position in the space and to its attitude with respect to the simulated scenario. It is defined as:

   $$State : \langle Position, PrevDirection\rangle$$

   where $Position$ indicates the coordinates (x, y) of the cell in which the agent is located, and $PrevDirection$ is the direction followed in the last movement;
4. $Actions$ is the set of possible actions that the agent can perform. Possible actions are movements in one of the eight neighbor cells (indicated as cardinal points), plus the action of remaining in the same cell (indicated by an 'X'). In this way, the *Moore* neighborhood structure is configured for the agent movement at each time-step:

   $$Actions = \{N, S, W, E, NE, SE, NW, SW, X\}$$

   Admissible actions $AdmAct$ ($\subseteq Actions$) are all the actions that move the pedestrian from cell c in cells that are free (or that make the agent maintain its position):

   $$AdmAct = \{a : a = X \vee (a \in Actions \ \wedge \ State(a(c)) = FREE)\}$$

   The effect of each action is, firstly, to move the pedestrian p in the direction indicated. This means that when an action a is chosen (for example, N), the new cell is calculated as follows:

   $$newCell = a(oldCell)$$
5. $Destination$ is the identifier of the current target of the agent, either intermediate target, opening object or final target. This parameter is important since it represents the point of contact with the *tactical level component* component of the hybrid agent. The id $Destination$ is then used to access to the current path field to follow:

   $$currentPathField = PathField(Destination)$$

All these elements take part in the mechanism that manages the movement of pedestrians: as previously introduced, they are utility-based agents. To every movement in the cell neighborhood a value of utility is associated, according to a set of factors that concur in the overall dynamics.

The set of actions going from the agent perception of the state of the environment to the choice of the action, defining the agent life-cycle for each step, is described by four steps:

1. the *perception* step provides to the agent all the information needed for evaluating and choosing its destination cell;

2. the *utility evaluation*, where the agent elaborates a desirability value for each of the admissible actions (movements), according to several factors;

3. the *choice of movement*, where the agent defines its intention of movement, by considering the evaluation performed at the previous step;

4. the *execution of movement*: since the current model is configured with the *parallel* update strategy this step is subjected to the outcome of possible conflicts, determined by the conflict solver.

With the perception phase, the agent will only extract values from the floor fields, in case it does not belong to a group (from now on called *individual agent*). Otherwise, it will perceive also the positions of the other group members within a configurable distance, for the calculation of the overall *cohesion* value, that will be explained in the following. The information achieved will be used for the utility calculation.

The action evaluation is actually the core element of the operational level model. Following the behavioral components generally considered in the literature, the evaluation is performed on the basis of the following elements:

- the desire to move towards a *goal*, a destination in the environment;
- the tendency to stay at a distance from the *obstacles* (e.g. walls, columns), that are perceived as repulsive;
- the desire to stay at a distance from other individuals, especially those that are not members of the same simple group, an effect of proxemics *separation*;
- a *direction inertia* factor, increasing the desirability of performing straight forms of movement;
- the penalization of those movements that cause an *overlapping* event, the temporary sharing of the same cell by two distinct pedestrians;
- two contributions related to the tendency to preserve *group cohesion*, respectively devoted to simple and structured groups.

All the above contributions, which will be more thoroughly described in the following part of this section, are considered by the overall utility function $U(c)$ of a destination cell c which corresponds to an action/direction for agent a, that takes the form of a weighted sum of components associated to the above factors:

$$U(c) = \frac{\kappa_g G(c) + \kappa_{ob} Ob(c) + \kappa_s S(c) + \kappa_d D(c) + \kappa_{ov} Ov(c) + \kappa_c C(c) + \kappa_i I(c)}{d}$$

where d is the distance of the new cell from the current position, that is 1 for cells in the Von Neumann neighborhood (vertically and horizontally neighbour cells) and $\sqrt{2}$ for diagonal cells: the factor is introduced to penalize the diagonal movements. Note that $\kappa_g, \kappa_{ob}, \kappa_s, \kappa_d, \kappa_{ov}, \kappa_c, \kappa_i \in \mathbb{R}$: the use of these parameters, in addition to allowing the calibration and the fine tuning of the model, also supports the possibility of describing and managing different types of pedestrian, or even different states of the same pedestrian in different moments of a single simulated scenario. Details about the calibration of these parameters, in order to fit empirical data from the literature, will be provided in Section 4.1.

Given the list of possible actions and associated utilities, an action is chosen with a probability proportional to its utility. In particular, the probability for an agent a of choosing an action associated to the movement towards a cell c is given by the exponential of the utility, normalized on all the possible actions the pedestrian can take in the current turn:

$$p(c) = N \cdot e^{U(c)}$$

where N is the normalization factor and c is the currently considered destination cell. Every element that contributes to the utility calculation will now be formally described. Since the groups compose an important and innovative element of this model, their functions will be explained afterwards.

Goal Attraction

Agents are driven towards their current target by using information from the relative path field, thus evaluating the distance between the possible movements and the destination. The function managing the goal attraction evaluates the reduction of distance moving from cell $Position$ in cell c, where $(x_p, y_p) = Position$ and (x_c, y_c) are the coordinates of c:

$$G(c) = \frac{PathF_{x,y} - PathF_{i,j}}{\sqrt{2}}$$

Given that the maximum distance between $Position$ and $c \in$ Moore neighborhood is $\sqrt{2}$, the following statement holds: $\forall c \in Cells, G(c) \in [-1, 1]$. In addition, since basically $\frac{PathF_{x,y} - PathF_{i,j}}{\sqrt{2}} = \frac{PathF_{x,y}}{\sqrt{2}} - \frac{PathF_{i,j}}{\sqrt{2}}$, an optimization has been achieved by modifying – before the beginning of the simulation – the path fields grids for all c of the grid as:

$$PathField(c) \leftarrow \frac{PathField(c)}{\sqrt{2}}$$

Obstacle Repulsion

The interaction between agents and obstacles and non-accessible areas in the environment has negative impact with the movement, because of the tendency of pedestrians to manage the available space without walking too close to obstacles and walls: for instance, considering the scenario of a corridor, pedestrians tend to stay in the center instead of being close to the walls. Information for the location and influence of obstacle are associated to the obstacle field introduced in Section 3.1.2. Considering a cell c with coordinates (x, y), the function is calculated as:

$$Ob(c) = -\frac{ObstacleField(x, y)}{r_{ob}}$$

where $\forall c \in Cells, Ob(c) \in [-1, 0]$. r_{ob} is the maximum distance for which an obstacle generates a repulsive effect. As stated in Section 3.1.2, this parameter has been set to 3 cells. As for the path field grids, the values of the obstacle field are modified with the static value r_{ob} in order to optimize the calculations during the simulation.

Proxemics Separation

All the interactions among pedestrians are subjected to the proxemics separation relationship, stating that all the persons tend to maintain a certain distance with respect to others and according to the local density calculated, stored and maintained into the grid of the density field. According to proxemics theory initially provided by Hall [1966], the persons tend to maintain a *public distance* with other unknown people. This distance is described to be between 3.0 m and 6.0 m. The main aim of this behavioral component is to reproduce these so-called *social distances*. Considering a cell c with coordinates (x, y):

$$S(c) = -\frac{ProxemicsField(x, y)}{Max(ProxemicsField)}$$

where $Max(ProxemicsField)$ is the maximum value of the field, according to the radius r used in its definition. By means of this value, the outputs of S function are in the range $[-1, 0]$.

Direction Inertia

The aim of this component is to reproduce the fact that pedestrians tend to maintain the direction during movement towards a destination. Unexpected changes of direction are

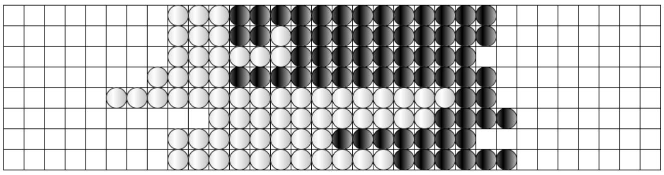

Figure 3.10: *A typical situation that can arise with bi-directional flow (here lighter pedestrians try to go to the right and vice-versa for the darker ones), even by employing mechanisms stimulating the well-known lane formation. To face this problem, this model allows a temporary double occupation of cells.*

usually avoided by pedestrians, while in a probabilistic model like this can be ordinary. For this purpose, a value is added in the case that cell c is located in the same direction with respect to the previous movement (except the case in which agent remained in the same cell, i.e. $PrevDirection = X$):

$$D(c) = \begin{cases} 1 & \textit{if } PrevDirection = Dir(c) \\ 0 & \textit{otherwise} \end{cases}$$

where $Dir(c)$ is the direction in which the agent must move to reach cell c from the current position.

Overlapping Extension

The discrete environment approach basically imply a well defined limit on the maximum pedestrian density that can be generated by the model, provided by the ratio $\frac{1}{CellSide^2}$. In the case of the model under discussion this would be $\frac{1}{0.16} = 6.25$ persons/m^2. Even if densities above this limit are not usually observed[2], on one hand, this limits the possibility to represent heavily crowded situations that are still possible. On the other hand, the restrictions on the space usage brought by the discrete environment can easily lead to a *freezing* of the simulation in case of scenarios with counter-flows, as illustrated in Figure 3.10.

For these reasons, the model has been enriched with a relaxation to the non-interpenetration principle, allowing the overlapping of two pedestrians in a single cell, as a means to overcome this limit in a controlled and systematic way. More in details, pedestrians are allowed to transiently overlap with a small probability: at each time step (a maximum of) two pedestrians are able to stay on each cell.

The set of admissible actions *AdmAct* – previously defined in a simplified way – is then modified allowing that also cells already occupied by another pedestrian are

[2] By looking at the set of fundamental diagrams shown in Figure 2.14(b) of Section 2.5, the only data-set which overcome this limit is the one of Helbing et al. [2007], achieved in a particularly overcrowded scenario, that is the Makkah pilgrimage.

admissible cells. Hence:

$$AdmAct = \{a : a \in Act \ \wedge \ (State(a(c)) = FREE \vee State(a(c)) = ONE\_PED)\}$$

With this extension, the aim is to model the fact that in some situations, especially in high densities, pedestrians rotate their body to pass in tight spaces. So, densities higher than the limit of $6.25\ m^{-2}$ are allowed, because of the maximum possible density is $12.5\ m^{-2}$, thought those parameters must be finely calibrated to prevent unreasonable (and not justified by empirical evidences) crowding conditions. To allow the calibration, overlapping negatively influences the calculation of utility function $U_a(c)$, assigning a penalty if the overlapping occurs:

$$Ov(c) = \begin{cases} -1 & \textit{if } State(c) = ONE\_PED \\ 0 & \textit{otherwise} \end{cases}$$

Because of overlapping event can happen just in particular situation of densities, a trade-off function on the basis of the density value in the scenario is defined, managing the calibration of overlapping event k_{ov} according to contextual factors (essentially the local density):

$$Balance_{ov}(c) = \begin{cases} k_{ov} & \textit{if } DensityField(c) \geq \delta_{high} \\ k_{ov} + \delta_{high} - DensityField(c) & \textit{if } \delta_{low} \leq DensityField(c) < \delta_{high} \\ 0 & \textit{otherwise} \end{cases}$$

where $DensityField(c)$ is the value of density field in the cell c (achieved with the density field explained in Section 3.1.4), δ_{high} and δ_{low} are the two density thresholds that regulate the activation of overlapping. Please note that a zero value for the κ_{ov} parameter does not mean that the overlapping comes without costs, on the contrary it means that the overlapping is *not* allowed. Therefore, the overall $Balance$ function gradually makes the overlapping phenomenon more likely with the growth of the local density.

Groups and Social Behavior

In this model two types of group have been considered: simple and structured. Simple or informal groups are generally made up of friends or family members and they are characterized by a high cohesion level, moving all together towards the same goal due to shared goals and to a continuous mechanism of adaptation of the chosen paths to try to preserve the possibility of performing non-verbal communication Costa [2010]. Structured groups, instead, are more complex entities, usually larger than simple groups (more than 4 individuals) and they can be considered as being composed of sub-groups that can be, in turn, either simple or structured. Structured groups are often artificially defined with the goal of organizing and managing the movement (or some kind of other operation) of a set of pedestrians.

Groups can be formally described as:

$$Group_j = \langle Id, [Group_1, \ldots, Group_m], [Ped_1, \ldots, Ped_n] \rangle$$

Structured groups include at least one subgroup, while simple groups only comprise individual pedestrians. In the following, the group an agent a *directly* belongs to will be referred as G_a, that is also the smallest group he belongs to; the *largest* group an agent a belongs to will instead be referred to as $\bar{G_a}$. It must be noted that $\bar{G_a} = G_a$ only when the agent a is member of a simple group that is not included in any structured group. Since a different behavior has been considered between the same members of a simple group and between members of two simple groups, belonging to the same structured group, two different components of the utility function has been designed.

Cohesion for Simple Groups

A positive contribution to the evaluation of the utility of a given cell is assigned whenever the movement towards that point of the environment is able to reduce the perceived distance from other members of a simple group. The overall reduction of distance is essentially an aggregation of the reduction of distance from all other members of the group; more formally the value of the C function for a given cell c, an agent a member of group G_a is defined as follows:

$$C(c) = \left[\left(\eta \cdot \sum_{a_i \in G_a} (DistFunction_{a,a_i}(c)) \right) \cdot 2 \right] - 1$$

where η is a normalization factor that, along with numerical values, allows to translate the cohesion value into the range $[-1, 1]$, and $DistFunction$ is a function that represents the gain of agent a with respect to agent a_i belonging to the same group G_a, moving into cell c. In the case of the evaluation of group cohesion, the perception of agents is expanded: every agent is able to perceive the members of the same group considering a distance parametric value g_d. $DistFunction$ is so defined as:

$$DistFunction_{a,a_i}(c) = \frac{distance(Position(a), Position(a_i)) - distance(c, Position(a_i))}{size(G_a) - 1}$$

representing the gain that agent a obtains moving in a particular cell c with respect to agent a_i.

Inter Group Cohesion

The role of this component of the utility associated to a movement is to increase the desirability of choices that reduce the distance from the members of the structured group the agent belongs to (if any). The form of the function is therefore relatively similar to the one associated to the cohesion of simple groups, with a significant difference: the larger a group is the more difficult is to perceive its "center" and also its direction. Moreover, ties between members of a large, possibly artificial group, are plausibly less influential than those binding members of a simple group. Therefore it has been decided to reduce the overall effect of cohesion for very large groups. The definition of a hierarchical structure of groups is also supported and this structure is exploited when computing the value for this contribution to the overall utility of a given movement.

Considering an agent a, it must be reminded that by $\bar{G}_a$ is denoted the largest group agent a belongs to; it could be a highly structured group including a subgroup, simple or structured, to which a directly belongs to, or it could even be equal to G_a, should a be member of a simple group not belonging to any structured group. Considering this notation, an $I(c)$ function for a given cell c, is defined as follows:

$$I(c) = \left[\left(\eta \cdot \sum_{a_i \in \bar{G}_a} (DistFunctionI\bar{G}_{a,a_i}(c)) \right) \cdot 2 \right] - 1$$

where function $DistFunctionI\bar{G}_{a,a_i}$ works on the tree-structure of the macro-group, identifying the proximity of two sub-groups G_a and G_{a_i} (i.e. the groups agents a and a_i directly belong to) in the tree of the group structure by means of the detection of the nearest common root of the two groups in $\bar{G}$.

More formally:

$$DistFunctionI\bar{G}_{a,a_i}(c) = \frac{1}{distance(c, Position(a_i))} \cdot \frac{1}{(Size(mcg(G_g, G_{a_i})) - 1)}$$

where mcg is the smallest sub-group of $\bar{G}_a$ including both G_a and G_{a_i}.

3.4.2 Adaptation Mechanism for Group Cohesion Preservation

While the above elements are sufficient to generate a simple pedestrian model that considers the presence of groups, even structured ones, the introduced mechanisms are not sufficient to preserve group cohesion, as discussed in a previous work adopting a very similar approach Bandini et al. [2011]. This is mainly due to the fact that in certain situations pedestrians adapt their behavior in a more significant way than what is supported by simple and relatively small modifications of the perceived utility of a certain movement. In certain situations pedestrians perform an adaptation that appears in a much more decisive way a *decision*: they can suddenly seem to temporarily loose interest in what was previously considered a destination to reach and they instead focus on moving closer to (or at least do not move farther from) members of their group, generally whenever they feel that the distance from them has become excessive. In the following a metric of group dispersion will be discussed, which has been adopted to quantify this perceived distance. Then it will be shown how this can be used to adapt the weights of the different components of the movement utility computation to preserve group cohesion.

Group Dispersion Metrics

Intuitively, the dispersion of a group can be seen as the degree of spatial distribution of their members. In the area of pedestrian modeling and simulation, the estimation of different metrics for group dispersion has been discussed in Bandini et al. [2011] in which different approaches are compared to evaluate the dispersion of groups through their movement in the environment. In particular, two different approaches are compared here: (i) dispersion as occupied area and (ii) dispersion as distance from the centroid of the group. This topic was also considered in the context of computer vision algorithms Schultz et al. [2010], in which however essentially only *line abreast* patterns were analyzed. Therefore the focus will be on the former approach.

Formally, the above introduced formulas of group dispersion for each approach are defined as follows:

$$Disp(Group) = \frac{Area(Group)}{Size(Group)} \quad \text{(Area method)}$$

$$Disp(Group) = \frac{\sum_{i=1}^{Size(Group)} distance(centroid, a_i)}{Size(Group)} \quad \text{(Centroid method)}$$

with $Area(Group)$ as the area occupied by the group, $Size(Group)$ as the number of its members, $centroid$ as its centroid. Results underline that the second approach suffers the effect of particular configurations in which the value of cohesion appears as low while a face validation of the situation indicates a good group cohesion. These wrong evaluations are detected in particular in medium and high-density situations in which groups tend to stretch themselves to walk through bottlenecks or narrow walkable areas. The centroid method identifies groups as highly disperse under these conditions, because some pedestrians can be far from the center of the group.

Differently, the first metric, that can appear as more simple, defines the dispersion of the group as the portion of space occupied by the group with respect to the size of the group. Figure 3.11 illustrates how this metric works: the first step works on all the vertices (i.e. the members of the group, see Fig. 3.11(a)), building a convex polygon with the minimum number of edges that contain all the vertices. The second step works on this output, calculating the area of the convex polygon (see Fig. 3.11(b)). The dispersion value is calculated as the relationship between the polygon area and the size of the group.

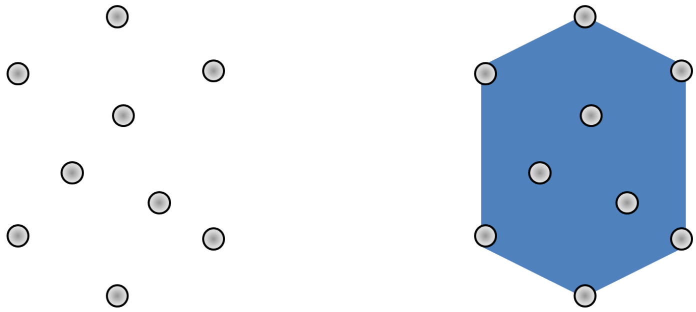

(a) (b)

Figure 3.11: *Graphical representation of a group composed of nine members and the area of the convex polygon that contains all the group members*

Trade-off Analysis

A trade-off process between the goal attraction value and the intra-inter cohesion value is required: in the situation in which the spatial dispersion value is low, the cohesion behavior has to count less than the goal attraction behavior. On the contrary, if the level of dispersion of group is high, the cohesion behavior is more important than the goal attraction behavior. A trade-off process between these two values is necessary, by means of a $Balance(k)$ function that can be used and expanded to face out this situation:

$$Balance(k) = \begin{cases} \frac{1}{3} \cdot k + (\frac{2}{3} \cdot k \cdot DispBalance) & \text{if } k = k_c \\ \frac{1}{3} \cdot k + (\frac{2}{3} \cdot k \cdot (1 - DispBalance)) & \text{if } k = k_g \vee k = k_i \\ k & \text{otherwise} \end{cases}$$

where k_i, k_g and k_c are the weighted parameters $U_a(c)$ and

$$DispBalance = tanh\left(\frac{Disp(Group)}{\delta}\right)$$

is another function that works on the value of group dispersion as the relationship between the area and the size of the group, applying on it the hyperbolic tangent. The value of δ is a constant that essentially represents a threshold above which the adaptation mechanism starts to become more influential; after a face validation phase, this value has been set to 2.5, allowing the output of $DispBalance$ function in the range $[0, 1]$ according to all elements in $U(c)$. The hyperbolic tangent approaches value 1 when $Disp(Group) \geq 6$ (values ≥ 6 indicate a high level of dispersion for small-medium size groups (1-4 members)).

A graphical representation of the trade-off mechanism is shown in Fig. 3.12: red and green boxes represent the progress of parameter k_c and parameter k_g (k_i is treated

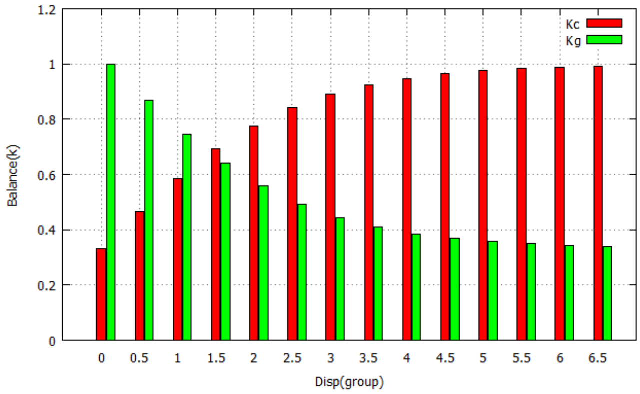

Figure 3.12: *Graphical representation of $Balance(k)$, for $k = 1$ and $\delta = 2.5$*

analogously), respectively. Note that the increasing of the dispersion value produces an increment of k_c value and a reduction of k_g parameter.

Furthermore, according to Xu and Duh [2010], the value of separation among group members has to be modified, on the basis of the assumption that pedestrians within a group allow to stay more close to each other with respect to strangers: more in detail, the value of separation in a group is equal to the half among strangers.

The S function must therefore be substituted by a S_a function, considering these social aspects. In particular, this function is defined as follows:

$$S_a(c) = -\frac{DensF_{i,j} - SepGroup_a(c)}{MaxDensity}$$

where $SepGroup_a(c)$ provides the value to discount to the separation repulsion on the basis of the group to which the agent a belongs to (the case in which agent does not belong to a group is also expressed):

$$SepGroup_a(c) = \begin{cases} \sum\limits_{a_i \in G - \{a\}} \dfrac{1}{distance(a_i, c)^2} \cdot 0.5 & \textit{if } a \in G \\ 0 & \textit{otherwise} \end{cases}$$

Details about the a preliminary validation performed on the adaptive model for the preservation of group cohesion will be proposed in Section 4.1.

3.4.3 Considering Slower Pedestrians: An Innovative Approach for the Management of Heterogeneous Speeds in Discrete Environments

In the literature – but up to now even in this model – discrete models generally assume only one speed profile for all the population and this is considered one of the main limitations of this approach: in order to consider an heterogeneous population, composed by persons with different necessities (e.g. elderly persons), but also particular areas of the environment that systematically modify the behavior, such as stairs, additional mechanisms must be considered. With the extension described in this section this limitation will be faced in an efficient and effective way, that is still able to reproduce the overall dynamics.

Firstly, an exploration of the relevant approaches to this problem is needed. Modeling different speed profiles in discrete models can be done in two main ways (the first one has been introduced in Kirchner et al. [2004])

1. By increasing pedestrian movement capabilities (i.e. they can move more than 1 cell per time step), according to their *desired speed*. In this way, given k the side of cells of the discrete grid, its possible to obtain speed profiles equal to $n \cdot k$ m/step, with $n \in \mathbb{N}$ equal to the maximum number of movements per step.

2. By modifying the current time scale, making it possible to cover the same distance in less time and achieving thus a higher maximum speed profile but at the same time allowing each pedestrian to yield their turn in a *stochastic* way according to an individual parameter, achieving thus a potentially lower speed profile.

Naturally, both methods can be more effective with a finer grained discretization, which supports a more precise representation of the environment and the micro-interactions between pedestrian Kirchner et al. [2004], but the simulation would be less efficient and behavioral rules more complicated. Computational costs increase proportionally to the ratio S_o/S_n, with S_o and S_n respectively equal to the old and new size of cells (e.g. if the size is halved, for performing the same space pedestrians will need a number of update cycles at least doubled).

The method supporting movements of more than a single cell can be effective, but it leads to complications and increased computational costs for the managing of micro-interactions and conflicts: in addition to already existing possible conflicts on the destination of two (or more) pedestrian movements, even potentially illegal crossing paths must be considered, effectively requiring the modeling of sub-turns. Therefore, it has been decided to retain a maximum velocity of one cell per turn, but shortening the turn duration and introducing a stochastic yielding for representing speed profiles lower than the maximum.

The computational model has therefore been modified in several parts. A new parameter $Speed_d$ is assigned in the $State$ of each pedestrian, describing its desired speed. For the overall scenario, a parameter $Speed_m$ is introduced for indicating the maximum speed allowed during the simulation (described by the assumed time scale). In order to obtain the desired speed of each pedestrian during the simulation, the pedestrian life-cycle is then *activated* according to the probability to move at a given step $\rho = \frac{Speed_d}{Speed_m}$.

By using this method, the speed profile of each pedestrian is modeled in a fully stochastic way and, given a sufficiently high number of steps, their effective speed will

Algorithm 2 Life-cycle update with heteregeneous speed

if $Random() \leq \alpha/\beta$ **then**
  if $updatePosition()$ == true **then**
    $\alpha \leftarrow \alpha - 1$
  else
    $\beta \leftarrow \beta + 1$
  end if
end if
$\beta \leftarrow \beta - 1$
if $\beta == 0$ **then**
  $(\alpha, \beta) = Frac(\rho)$
end if

be equal to the wanted one. But it must be noted that in a several cases the speed has to be rendered in a relatively small time and space window (think about speed decreasing on a relatively short section of *stairs*).

In order to overcome this issue, it was decided to consider ρ as an indicator to be used to decide if a pedestrian can move according to an *extraction without replacement* principle. For instance, given $Speed_d = 1.0m/s$ of an arbitrary pedestrian and $Speed_m = 1.6m/s$, ρ is associated to the fraction 5/8, that can be interpreted as an **urn** with 5 *move* and 3 *do not move* events. At each step, the pedestrian extracts one event from its urn and, depending on the result, it moves or stands still. The extraction is initialized anew when all the events are extracted. The mechanism can be formalized as follows:

- Let $Frac(r) : \mathbb{R} \rightarrow \mathbb{N}^2$ be a function which returns the minimal pair $(i, j) : \frac{i}{j} = r$.
- Let $Random$ be a pseudo-random number generator.
- Given ρ the probability to activate the life-cycle of an arbitrary pedestrian, according to its own desired speed and the maximum speed configured for the simulation scenario. Given (α, β) the result of $Frac(\rho)$, the update procedure for each pedestrian is described by the pseudo-code of Alg. 2. The method $updatePosition()$ describes the attempt of movement by the pedestrian: in case of failure (because of a conflict), the urn is not updated.

This basic mechanism allows the synchronization between the effective speed of an arbitrary pedestrian and its desired one every τ steps, with τ limited to $Speed_m \cdot 10^{\iota}$ step and ι is associated to the maximum number of decimal positions between $Speed_d$ and $Speed_m$. For instance, if the desired speed is fixed at $1.3m/s$ and the maximum one at $2.0m/s$, the resulting $Frac(\rho) = \frac{13}{20}$, therefore pedestrian's average velocity will match its desired speed every 20 steps.

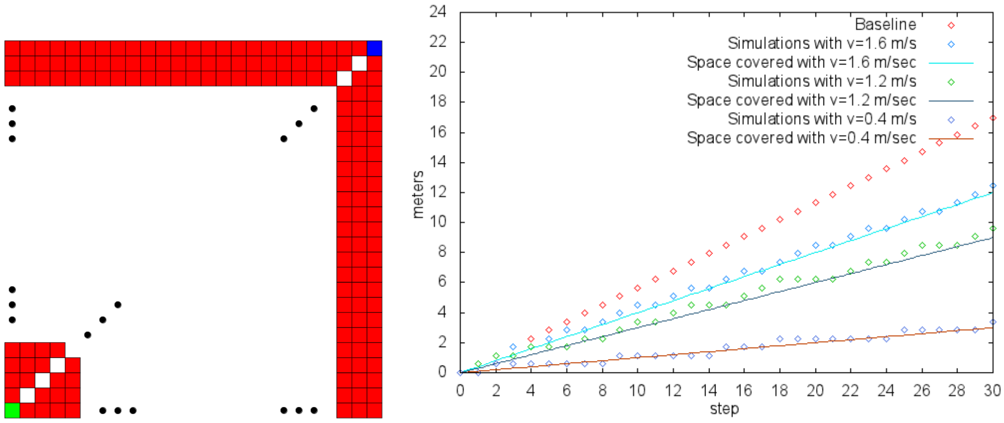

(a) (b)

Figure 3.13: *Space covered by the agent, per step, in a scenario where only diagonal movements are possible, shown on the left.*

As previously introduced, an effect of the discretization of the environment is the fact that diagonal movements generate a higher movement speed. In order to face this issue, this mechanism can be improved by considering these movements as a different kind of event during the extraction. With this strategy, each diagonal movement carried out by an agent decreases its probability to move in the next steps according to the ratio $\Delta = \frac{0.4*\sqrt{2}-0.4}{Speed_d*timeScale}$, where $timeScale = 0.4/Speed_m$ (considering the adopted scale of spatial discretization). This fraction represents the relationship between the additional covered space, due to the diagonal movement, and the desired speed of the agent expressed in step. In this way Δ represents the exact number of steps the agent will have to stand still to achieve a synchronization of desired and actual speed. In order to discount diagonal movements, therefore, a parameter $diagPenalty$ has been introduced in the agents' state, initially set to 0, which is increased by Δ each diagonal movement. Whenever $diagPenalty \geq 1$, the probability to move is decreased by adding in the urn of extraction one *do not move* event or, in reference to Alg. 2, by increasing of 1 unit the parameter β after $updatePosition()$ invocation, decreasing $diagPenalty$ by 1.

To test the reliability of this mechanism, an ad-hoc test scenario has been designed, shown in Figure 3.13(a). Only one agent is present in the environment in order to avoid the influence caused by conflicts. The scenario is designed to constrain the movement of the agent, which can only perform diagonal movements (either towards the destination or, less likely, backwards). Three desired speeds have been considered: 1.6, 1.2 and 0.4 m/sec. The turn duration is of 0.25 sec. The test results are shown in Figure 3.13(b). Baseline data represents the space covered by the agent with desired speed of 1.6 m/sec without using the proposed method for the penalization of diagonal movements: the additional space covered by means of diagonal movement causes the agent to achieve a speed of 2.26 m/sec. By applying the proposed method the error in the actual speed is significantly reduced: the mean absolute error in the distance covered at each step was about 0.25 m for desired speed of 1.6 m/sec, 0.35 m for desired speed of 1.2 m/sec and 0.18 m for 0.4 m/sec. Maximum errors have been, respectively, of 0.54 m, 0.83 m and 0.56 m for the lowest desired speed.

This method is now consistent for reproducing different speeds for pedestrians in a discrete environment also considering the Moore neighborhood structure. It must be noted, however, that if it is necessary to simulate very particular velocities (consider for instance a finer grained initialization of a population characterized by a normal distribution of speed profiles), $Frac(\rho)$ is such that a large number of turns is needed to empty the urn, that is, to achieve an average speed equal to the desired one. This means that locally in time the actual speed of a pedestrian could differ in a relatively significant way from this value. To improve the quality of simulations also regarding this effect an additional method has been designed, called the *sub-urn* method. During the life of each agent the fraction describing the probability is updated at each step and in several cases it will reach un-reduced forms, with $GCD(\alpha, \beta) > 1$. These situations can be exploited by splitting the urn into simpler sub-urns according to the GCD value. For example, given a case with $Frac(\rho) = \frac{5}{11}$, after one movement the urn will be associated to $\frac{4}{10}$; since $GCD(4, 10) = 2$ the urn can be split into 2 sub-urns containing 2 *move* and 3 *do not move* events that will be consumed before restarting from initial urn. The effect of this subdivision is to preserve a stochastic decision on the actual movement of the pedestrian but to avoid excessive local diversions from the desired speed.

To evaluate the improvements given by the sub-urn method another ad-hoc test scenario has been executed in a linear 1-dimensional environment which constrains the agent to perform only non-diagonal movements. Desired speed of the agent has been configured to 1.31 m/sec, which causes and initial urn of 160 events, where 131 of them are *moves* (i.e., the agent will assume exactly 1.31 m/sec every 160 steps). Figure 3.14 illustrates the aggregation of the results of 30 different runs of the simulation by using (darker dots) and not adopting (lighter dots) the proposed method. Results emphasize that the sub-urn method leads to a more accurate simulation of the desired speed: darker dots are in fact much closer to the line describing the distance covered with 1.31 m/sec in a continuous space. This result is also described by a lower mean and maximum absolute error: the proposed method produced a mean and maximum error of 0.23 m and 1.34 m against 0.56 m and 2.49 m for the baseline approach.

3.4.4 Modeling Classes of Pedestrians and Regions

Thanks to the above introduced mechanism for granting pedestrians the possibility to have a desired speed in their state definition it is now relatively straightforward to represent different classes of agents and a basic behavior for them in particular regions

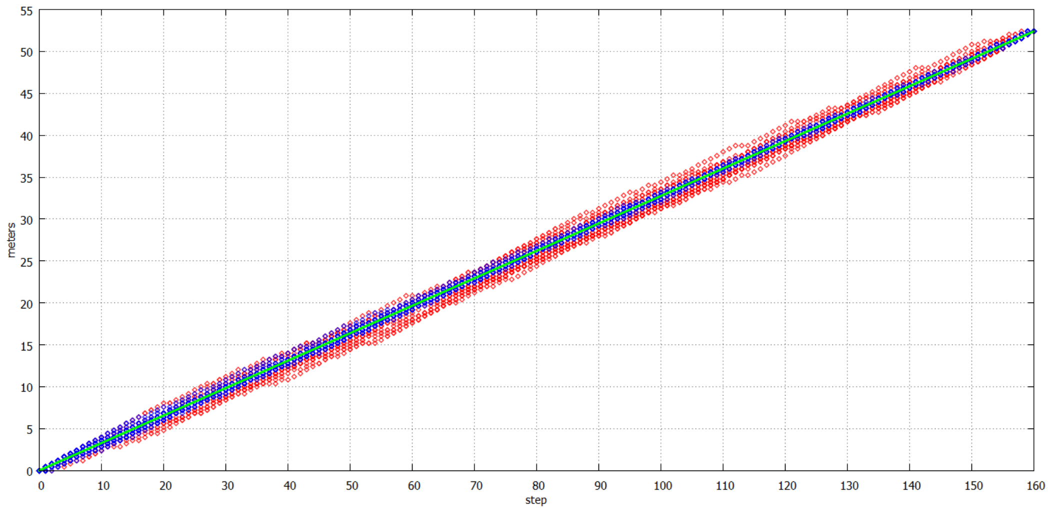

Figure 3.14: *Space covered by the agent in the second set of tests. Blue dots are obtained with the sub-urn method, while red ones without. The green line describes 1.31 m/sec.*

like stairs and ramps.

First of all, different classes of pedestrians can now be introduced in the model by means of their normal distribution of speeds, with average μ and standard deviation σ.

Secondly, to identify areas in which the velocity of pedestrians is altered, their type and associated speed modification is specified in the *region* marker. When the agents will perceive the entering in the related cells of these special regions, they will modify the desired speed according to the region specifications and to the class they belong to. The definition of different agent classes, in fact, allows also to consider types of pedestrians that have difficulties or are even not able to pass through several regions (e.g. persons with mobility impairments might not be able to walk along stairs). For this reason, each class of region is able to modify the agent speed in a different way according to the agent class.

The state of a pedestrian must be extended to include the area it is currently situated in. In this way, each pedestrian perceiving the presence of a marker in its position will: (i) update the region it is currently situated in; (ii) update the desired speed according to the constant associated to the marker class and referring to the pedestrian class it belongs to. By following this logic and to allow the definition of scenario similar to the real-world, the following types of regions have been considered and introduced in the model:

- *normal*
- *staircase*
- *ramp*

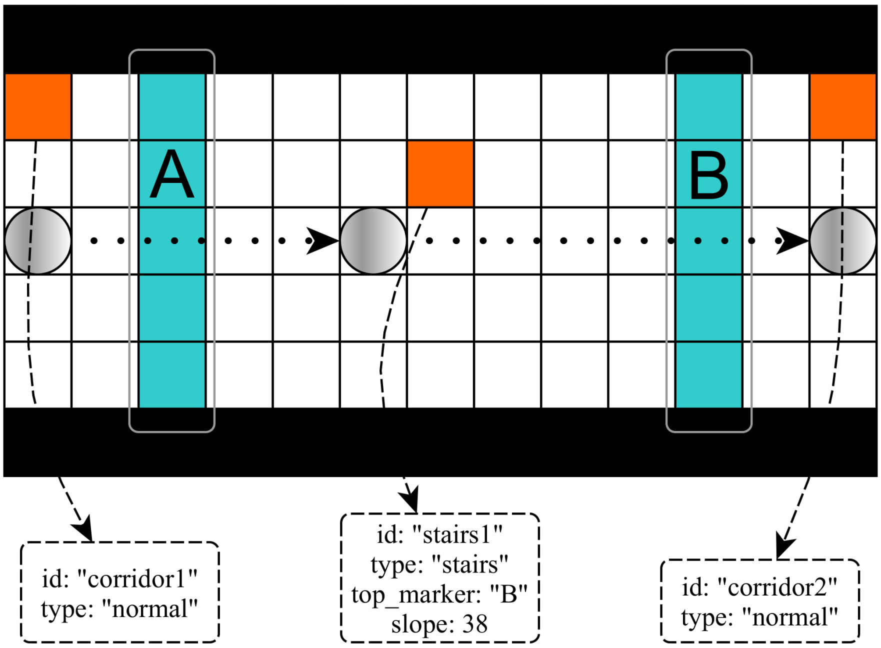

Figure 3.15: *A schema depicting an example representation of a staircase, that will change the speed of the pedestrian according to the parameter* slope.

- *escalator*
- *mobile ramp*

In particular, a normal staircase or ramp is configured firstly with the direction, achieved with the annotation of the top *opening* marker that delimits it. The *slope* parameter, then, will modify the agents' speeds depending on their desired speed. Differently, mobile ramps or escalators in the simulator will be configured with a parameter that will determine a fixed value of the agents speed: for simplicity, an additional walking along the escalator is not considered at the moment. In addition, these mobile ramps will not be able to be overtaken in counter-direction (this effect is reproduced with the tactical level, as will be explained in the following Section).

An example of this procedure and of a simple representation of a staircase is shown in Figure 3.15: in this case, a pedestrian is entering the staircase $stairs1$ from the left side (the lower one), delimited by the marker A, and exiting at the right side (the upper one), delimited by the marker B. When first crossing the marker A the pedestrian will update its state to remember the name and type of area it is currently situated in. Then, it will update its own speed by considering the *slope* of the stairs, taken from the region specifications, and its class. The pedestrian will maintain this speed until it crosses the marker B and enters to the next region. At this point, it will now record that it is not situated in area $stairs1$ anymore and it will update its desired speed according to the

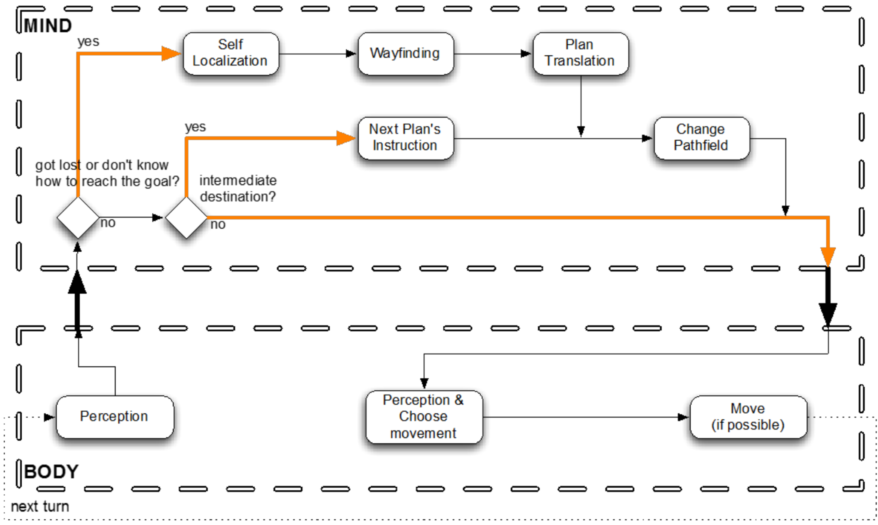

Figure 3.16: *The life-cycle of the agent.*

new specifications.

3.4.5 A Tactical Level Component for Dynamical Path Planning

Having explained how the physical movement in the simulated environment is performed by the agents, the tactical level component can be now discussed. This component is defined to allow the route choice activity of the agent, aiming to the composition of a set of intermediate targets that will be one by one passed to the body component. Following this aim, a basic life-cycle of the agent that allows a static planning of the route can be now introduced and it is shown in Figure 3.16.

The diagram shows the activities of the body and tactical level components at each time-step. The agents firstly perform the perception of the state of the environment at the body level. This information is then passed to the tactical level component component where the *plan building* (the top row of activities) or *plan management* (the second row) is performed, according to the current situation. The plan building is performed if the agent is a new-born or if, due to a high congestion situation, it entered in a new region without a particular intention: a sort of "failure" of the plan. This activity, as shown in the picture, is composed by the following activities:

- the *self localization* infers the position of the agent among the nodes of the cognitive map, by means of a checking of the floor fields values;
- the *wayfinding* is the core element of the route choice, composing the path through the cognitive map from the local position to the final destination. The position of the final destination is achieved with the cognitive map;

- the *plan translation*, finally, is simply the translation of the output of the previous operation to the list of path field indexes, mapped to the intermediate targets, which the agent will have to reach at the body level.

The plan management is more simple and describes the iteration of the list, activated when the agent reaches the position of one target.

The output of the tactical level component, described by the next target to follow, is then returned to the body. This will be activated for the evaluation and choice of the movement to perform – according to the utility function and the speed reproduction mechanism as explained in the previous Section – followed by the movement execution and update of the dynamic grids.

The flow of activities that compose the life of the agent and aims at solving the problem of representing the operational and tactical level of pedestrian behavior is now clear. The methodologies allowing the agent to calculate their route along the environment, on the other hand, is still completely unknown and will be clarified with the following.

The Wayfinding of Agents

First of all, it must be noted that the cognitive map is a graph with unitary edges and at this moment no information about the distances between the openings has been represented. On the other hand, a baseline approach for the route choice can be still provided with this state of the model.

Instead of calculating the physical shortest path through the environment, in fact, the agents are able to calculate the shortest path through the nodes of the cognitive map. This implies that they will consider the way describing the fewest number of regions. An example of this kind of reasoning is shown in the Figure 3.17. For the calculation, well-known algorithms from the literature can be used (such as the Dijkstra algorithm).

Despite the very basic approach, this algorithm can already appear quite cognitively logical, since in the normal everyday life everyone is usually considering a path which is not implying to pass through many rooms, preferring for example the usage of a corridor. But even with this consideration, the missing information of the distance between the opening markers becomes an issue in environment that describes multiple connections between the same couple of regions. For the algorithm of the cognitive map computation, this situation generates multiple edges between the two regions which are differently labeled (mapped to distinct path fields) but with the same associated weight. With the current strategy of the route choice, thus, there is no possibility to identify a proper one for the agent and so, in this case, a random choice would be performed. An example of the situation in exam is shown in the Figure 3.18. The usage of this basic approach would let the agents going out from room A and H to employ a random choice between the two doors of the rooms, generating not only longer distances for the individual pedestrians but also cross-flows and not realistic

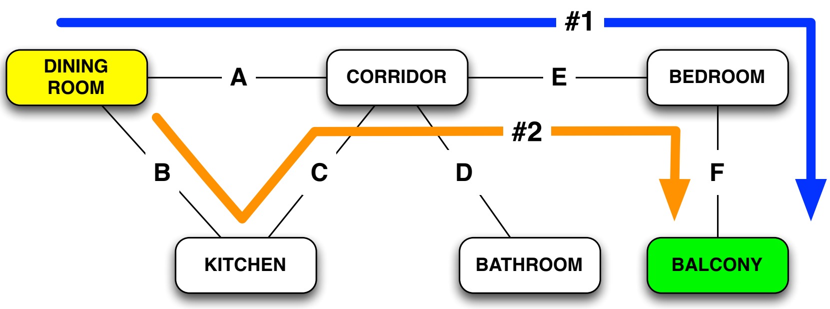

Figure 3.17: *The basic method for the route choice, producing the path with the minimum number of crossed nodes between the agent position (in yellow) and destination (in green). The route #1 will be the output, without considering the possibility offered by the route #2 in terms of distance.*

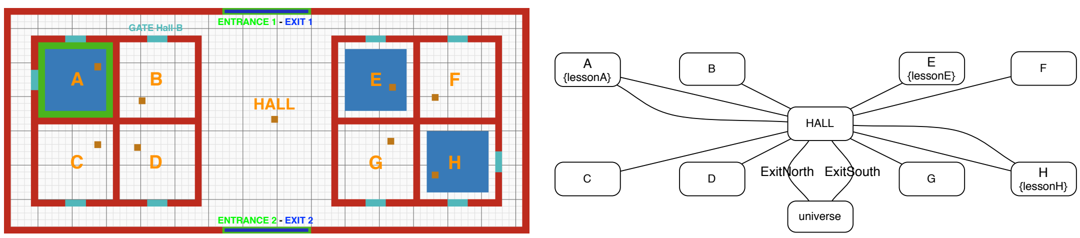

Figure 3.18: *From the left: the example scenario of the university buiding, also shown at the beginning of the Chapter and the respective cognitive map.*

congestions inside these areas.

The simplicity would be the only point in favor of this basic approach and, thus, a more detailed methodology moving towards the consideration of the physical distances must be introduced. With this purpose and without considering the introduction of additional data-structure, a slightly advanced procedure can be described by the enrichment of the cognitive map with information related to the reciprocal distances among the opening markers. The information can be added with a tabular representation in each node, with the number of rows and columns given by the number of openings accessible in the mapped region. Naturally, only half of the values of the table has to be calculated, since the distance must be symmetric.

On the other hand, for the presented model the symmetry between the distance values – which are provided by the path fields – cannot be ensured due to the discretization effects. In order to represent an effective distance metric, the following formulas are thus introduced. First of all, an opening marker ω must be associated to a unique position in the space, that is provided by:

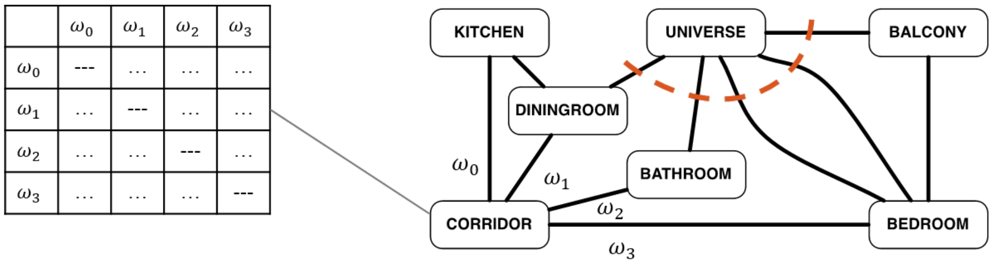

Figure 3.19: *The cognitive map with the integration of the distance between markers, inside each region. For simplicity the data are represented with a tabular version but, given the symmetry of the relation, more optimized data-structures can be easily defined (e.g. dictionary).*

$$Center(\omega) = \left(\left\lfloor \frac{\sum x_i}{|\omega|} \right\rfloor, \left\lfloor \frac{\sum y_i}{|\omega|} \right\rfloor \right), (x_i, y_i) \in \omega.$$

Given the center cell provided by this function, a function that returns the distance between ω_1 and ω_2 is then defined as the average between the path field values in the two center cells, i.e., the value of the floor field of ω_1 in $Center(\omega_2)$ and vice-versa. With the average, the function now respects the symmetry constraint that a distance metric must have.

At this point the integration of the information of the distance is straightforward. An example representation of the enriched cognitive map is presented in Figure 3.19. It is now possible to allow the agents to choose the shortest route and by considering the static settings. The additional usage of the information about the region classes will also let them choose the fastest route, considering their necessities and velocities.

Regarding the computational times, the usage of the Dijkstra algorithm – or alternatively the Floyd-Warshall – is not an issue as long as the route choice is performed statically, at the generation of the agents. On the other hand, the realization of a realistic behavior of the agents must imply a reconsideration and, eventually, a change of the current path due to *dynamical* feature arising in the simulation, such as congestion in front of exit. In order to allow the agents a dynamic calculation of their routes during the simulation, without providing at the same time an excessive load on the computational side, an additional data-structure has been introduced in the model. The structure represents a *decision tree* that is computed starting with the information of the cognitive map, where the traveling times related to paths towards a final destination are stored, limiting the number of computations at simulation time. The tree from now on will be called *Paths Tree* and is discussed in the following Section.

The Paths Tree

The *Paths Tree* is defined as a tree data-structure containing the set of plausible paths towards a destination, that will be mapped to its root. Before describing what is meant with the attribute plausible, that naturally can be seen as a fuzzy concept, a general definition of path must be provided.

A path is defined as a finite sequence of openings $X \rightarrow Y \rightarrow \ldots \rightarrow Z$ where the last element represents the final destination. It is easy to understand that not every sequence of openings represents a path that is walkable by an agent. First of all, in fact, a path must be a sequence of consecutive oriented openings regarding the physical space.

Definition 1 (Oriented opening)**.** Let $E = R_1, R_2$ be an opening linking the regions R_1 and R_2, (R_1, E, R_2) and (R_2, E, R_1) define the oriented representations of E.

An oriented opening will therefore describe a path from an arbitrary position of the first region towards the second one.

Definition 2 (Valid path)**.** let C a sequence of oriented openings $X \rightarrow \ldots \rightarrow Z$. C is a valid path if and only if:

- $|C| = 1$
- $|C| = 2$: by assuming $C = X \rightarrow Y$, the third element of the triple X must be equal to the first element of Y
- $|C| > 2$: each sub-sequence S of consecutive openings in C where $|S| = 2$ must be a valid path.

The last oriented opening in the path leads to the *universe* region.

Given a set of paths, the agent will consider only complete paths towards its goal, starting from the region where the agent is located.

Definition 3 (Start and Destination of a path)**.** Given p a path $(R_1, E, R_x) \rightarrow \ldots \rightarrow (R_y, O, \text{universe})$, the function $RS(p) = R_1$ will return the region R_1 where an agent can start the path p. $S(p) = E$ and $D(p) = O$ will respectively return the first opening (E) and the destination (O) of the path.

Definition 4. Let p a path, $T(p)$ is the function which return the expected travel time from the first opening to the destination.

$$T(p) = \sum_{i \in [1, |p|-1]} \frac{Dist(opening_i, opening_{i+1})}{speed} \tag{3.1}$$

Another basic rule is that a path must be loop-free: by assuming the aim to minimize the time to reach the destination, a plan passing through a certain opening more than once would be not plausible.

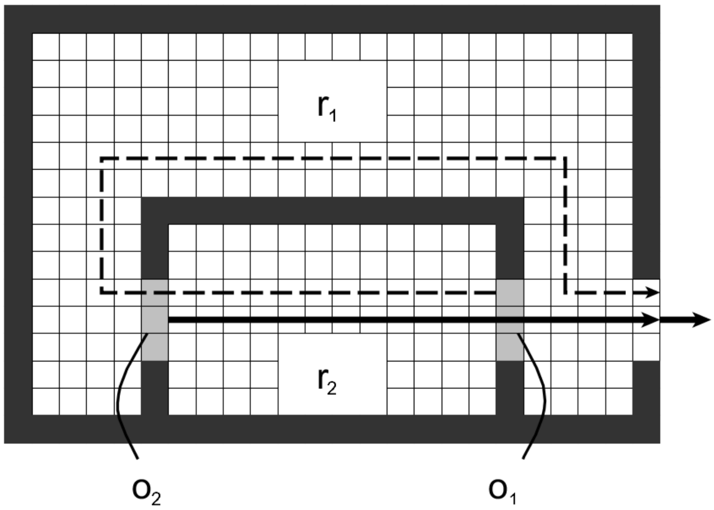

Figure 3.20: *A concave region can imply the plausibility of a path crossing it twice, but its identification is not elementary.*

Definition 5 (opening loop constraint)**.** A path $X \rightarrow \ldots \rightarrow Z$ must not contain duplicated openings.

This will not imply that an agent cannot go through a certain opening more than once during the simulation, but this will happen only with a change of the agent plan.

By assuming to have only convex regions in the simulated space, the set of plausible paths is easily achievable by extending 5 as to let a path not containing duplicated regions. However, since the definition of region describes also rooms, concave regions must be considered. Some paths may, thus, imply to pass through another region and then return to the first one to reduce the length of the path.

As shown in Figure 3.20, both paths starts from r_1, go through r_2, and then return to r_1. However, only the path represented by the continuous line is plausible, even if the constraint 5 is respected by both of them. Before the definition of the constraint that identifies the correct paths, the concept of *sub-path* has to be defined.

Definition 6 (Sub-path)**.** Let p be a path, a sub-path p' of p is a sub-sequence of oriented openings denoted as $p' \subset P$ which respects the order of appearance for the openings in p, but the orientation of openings in p' can differ from the orientation in p. p' must be a valid path.

The reason of the orientation change can be explained with the example in Fig. 3.21: given the path $p = (r_1, o_2, r_2) \rightarrow (r_2, o_1, r_1) \rightarrow universe$, the path $p' = (r_2, o_2, r_1) \rightarrow universe$ is a valid path and is considered as a sub-path of p, with a different orientation of o_2. In addition, given the path $p_1 = (r_2, o_2, r_1) \rightarrow universe$, the path

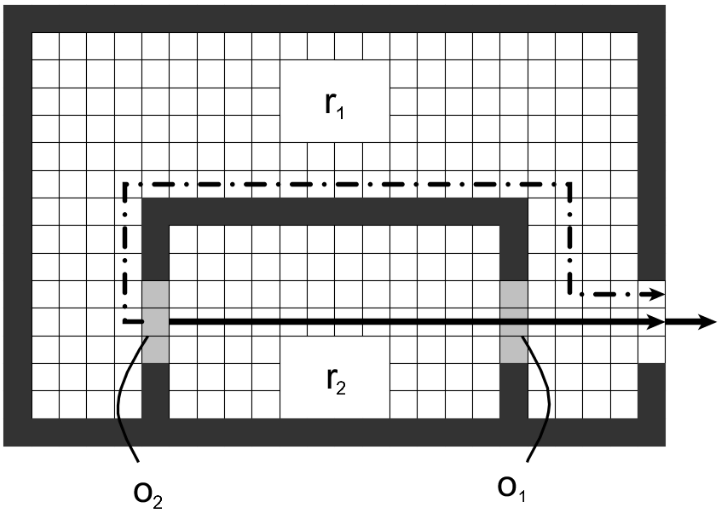

Figure 3.21: *The correct paths for this environment. Inside r_2 the choice between the two openings is also determined by the congestion.*

$p_2 = (r_1, o_2, r_2) \rightarrow (r_2, o_1, r_1) \rightarrow universe$ is as well a minimal path if and only if the travel time of p_2 is less than p_1. It is easy to understand that this situation can emerge only if r_1 is concave. Hence the starting region of the two paths is different, but the key element of the rule is the position of the opening o_2. If this rule is verified in the center position of the opening o_2, this path will be a considerable path by the agents surrounding o_2 in r_1.

In Figure 3.21 the correct paths for this example environment are shown. An agent located in r_2 can reach r_1 and then the destination D using both openings considering the congestions. An agent located in r_1 can go directly to the exit or chose the path $o_2 \rightarrow o_1 \rightarrow D$.

Definition 7 (Minimal path)**.** p is a minimal path if and only if it is a valid path and $\forall p' \subset p : S(p') = S(p) \wedge D(p') = D(p) \implies T(p') > T(p)$

The verification of this rule is a sufficient condition for the opening loop constraint 5 and it solves the problem on the region loop constraint independently from the configuration of the environment (i.e. convex or concave regions).

At this point the constraint that defines a minimal path has been provided. This can be used to build the complete set of minimal paths towards a destination before running the simulation. It must be noted that an arbitrary path represents a set of paths itself, since it can be undertaken at any region it crosses. Indeed every path p provides also information about the sub-paths achieved by cutting the head of p with an arbitrary number of elements. A minimal representation of the set is a tree-like structure that is now defined as:

Definition 8 (Paths tree)**.** Given a set of minimal paths towards a destination, the Paths-Tree is a tree where the root represents the final destination and a branch from every node to the root describes a minimal path, crossing a set of openings (other nodes) and regions (edges). Each node has an attribute describing the expected travel time to the destination.

An Algorithm to Compute the Paths Tree

Now that the concept of Paths Tree has been introduced with a formal definition, an algorithm for its computation will be provided. The proposed procedure builds the decision tree in a recursive way, starting from a path containing only the destination and iteratively adding nodes if and only if the generated path respects the definition of minimality.

Formally the Paths Tree is defined as $PT = (N, E)$ where N is the set of nodes and E the set of edges. Each node n is defined as a triple (id, o, τ) where:

- $id \in \mathbb{N}$ is the id of the node;
- $o \in \mathcal{O}$ is the name of the opening;
- $\tau \in \mathbb{R}^+$ is the expected travel time for the path described by the branch.

Each edge e is defined as a triple (p, c, r) where:

- $p \in \mathcal{O}$ is the id of the parent;
- $c \in \mathcal{O}$ is the id of the child;
- $r \in \mathcal{R}$ is the region connecting the child node to its parent.

To allow a fast access to the nodes describing a path that can be undertaken from a certain region, a structure called M has been added. This maps each r in the list of $p : (p, c, r) \in E$ (for every c).

Given a destination $D = (r_x, \text{universe})$, the paths tree computation is defined with the procedures described in the following.

Algorithm 3 Paths tree computation

1: add $(0, D, 0)$ to N
2: add 0 to $M[r_x]$
3: $\forall s \in \mathcal{O}$ ShortestPath[s] $\leftarrow \infty$
4: expand region($0, D, 0, R_x, ShortestPath$)

With the first line, the set N of nodes is initialized with the destination of all paths in the tree, marking it with the id 0 and expected travel time 0. In the third row the set of $ShortestPath$ is initialized. This will be used to track, for each branch, the expected travel time for the shortest sub-path, given a start opening s. $ExpandRegion$ is the core element of the algorithm, describing the recursive function which adds new nodes and verifies the condition of minimality. The procedure is described by the Algorithm 4.

Algorithm 4 ExpandRegion

Input: $(parentId,\ parentName,\ parentTime,\ RegionToExpand,\ ShortestPath)$

1: $expandList \leftarrow \emptyset$
2: $opList = Op(RegionToExpand) \setminus parentName$
3: **for** $o \in opList$ **do**
4:     $\tau = parentTime + \frac{D(o, parentName)}{speed}$
5:     **if** $CheckMin(ShortestPath, o, \tau)$ == True **then**
6:         add (id, o, τ) to N
7:         add $(parentId, id, r)$ to E
8:         $ShortestPath[o] \leftarrow \tau$
9:         $nextRegion = o \setminus r$
10:         add id to $M[nextRegion]$
11:         add $(id, o, \tau, nextRegion)$ to $expandList$
12:     **end if**
13: **end for**
14: **for** $el \in expandList$ **do**
15:     $ExpandRegion(el, ShortestPath)$
16: **end for**

In line 2 a list of openings candidates is computed, containing possible extensions of the path represented by $parentId$. Selecting all the openings present in this region (except for the one labeled as $parentName$) will ensure that all paths eventually created respect the validity constraint 2.

At this point, the minimality constraint 7 has to be verified for each candidate, by means of the function $CheckMin$ explained by the Algorithm 5. Since this test requires the expected travel time of the new path, this has to be computed before. A failure in this test means that the examined path – created by adding a child to the node $parentId$ – will not be minimal. Otherwise, the opening can be added and the extension procedure can recursively continue.

In line 6, id is a new and unique value to identify the node, which represents a path starting from the opening o and with expected travel time τ; line 7 is the creation of the edge from the parent to the new node. In line 8, $ShortestPath[o]$ is updated with the new discovered value τ. In line 9 the opening is examined as a couple of region, selecting the one not considered now. In fact, the element $nextRegion$ represents the region where is possible to undertake the new path. In line 10 the id of the starting opening is added to $M[nextRegion]$, i.e., the list of the paths which can be undertaken from $nextRegion$. In line 11 the node with his parameter is added to the list of the next expansions, which take place in line 13-14. This passage has to be done to ensure the correct update of $ShortestPath$.

Algorithm 5 CheckMin

Input: $(ShortestPath, o, \tau)$
1: **if** **then**$ShortestPath[o] > \tau$ **return** True
2: **else**
  return False
3: **end if**

To understand how the constraint of minimality is verified, two basical concepts of the procedure need to be clarified. Firstly, the tree describes a set of paths towards a unique destination, therefore given an arbitrary node n, the path described by the parent of n is a subpath with a different starting node and leading to the same destination. Furthermore, the expansion procedure implies that once reached a node of depth l, all the nodes of its path having depth $l - k$, $k > 0$ have been already expanded with all child nodes generating other minimal paths.

Note that the variable $ShortestPath$ is particularly important since, given p the current path in evaluation, it describes the minimum expected travel time to reach the destination (i.e. the root of the tree) from each opening already evaluated in previous expansions of the branch. Thus, if τ is less than $ShortestPath[o]$, the minimality constraint of the Definition 7 is respected.

To summarize the procedure and to improve the understanding of the reader, the computation of the paths tree for a simple environment is step-by-step illustrated in Figure 3.22. From (a) to (d), the procedure does the following passages:

- at the first passage (a), the root of the tree is generated and mapped to the final destination (FD) in the environment;
- the minimal paths at depth level 1 are added (b). Since there are no other paths at the moment, this passage is straightforward with the addition of the four openings reachable from the FD using r_1;
- the procedure is repeated for the nodes just added, verifying if the minimal paths can be expanded with additional nodes. In this case the openings o_1 and o_2 are not extended since, for both, a path starting from another node and passing through one of them (e.g. $o_3 \rightarrow o_2 \rightarrow Exit$) would imply a systematic increase of the traveling distance (compared with the paths described by the nodes at depth level 1), considered not rational for the agents modeled in this work;
- it is not the same case of o_3 and o_4. For the first one (c), the expansion generates the minimal paths $o_1 \rightarrow o_3 \rightarrow Exit$ and $o_2 \rightarrow o_3 \rightarrow Exit$. $o_4 \rightarrow o_3 \rightarrow Exit$ is not added since it implies a not justifiable usage of r_2 (it might be considerable in case of having congestion inside r_1 in the area between o_3 and o_4 but, for the behavior

considered in this model, this should not emerge and in any case this decision can be as well modeled with an additional opening in the interested area);

- the last passage illustrates the extension of the node o_4 with the generation of the path $o_2 \rightarrow o_4 \rightarrow Exit$.

Congestion Evaluation

The explained approach of the Paths Tree provides information on travel times implied by each path towards a destination. By only using this information, the choice of the agents will be still static, essentially describing the shortest path. To allow the dynamical evaluation of congestion in the surrounding of openings, an additional mechanism is now proposed.

The approach estimates, for each agent, the additional time deriving by passing through a jamming situation. This calculation considers two main aspects:

- the size of a congestion around an opening;
- the average speed of the agents inside the congested area.

Since the measurement of the average speed depends on the underlying model that describes the physical space and movement of the agents, we avoid to explain this component with full details, by only saying that the speed is estimated with an additional grid counting the *blocks* (i.e. when agents maintain positions at the end of the step) in the surrounding area of each opening. The average number of blocks defines the probability to move into the area per step, thus the speed of the agents inside. For the size of the area, the approach is to define a minimum radius of the area and (i) to increase it when the average speed becomes too low or (ii) to reduce it when it returns normal.

As illustrated in Figure 3.23, the presence of an obstacle in the room is well managed by using the floor field while defining the area for a given radius. If a sufficient number of agents try to pass through the same opening at the same time, a congestion will arise and this will impact on the average speed. Hence the area will increase its size. While this one increases the size, the estimated move probability gets higher again and this will stop the re-sizing at a certain point.

During this measurement the average speed value for each radius is stored. Values for sizes smaller than the size of the area will be used by the agents inside it, as it will be explained in the next section. Two functions are introduced for the calculation:

- $size(o)$: return the size of the congestion around the opening;
- $averageSpeed(o, s)$: return the average speed estimated in the area of size s around the opening o.

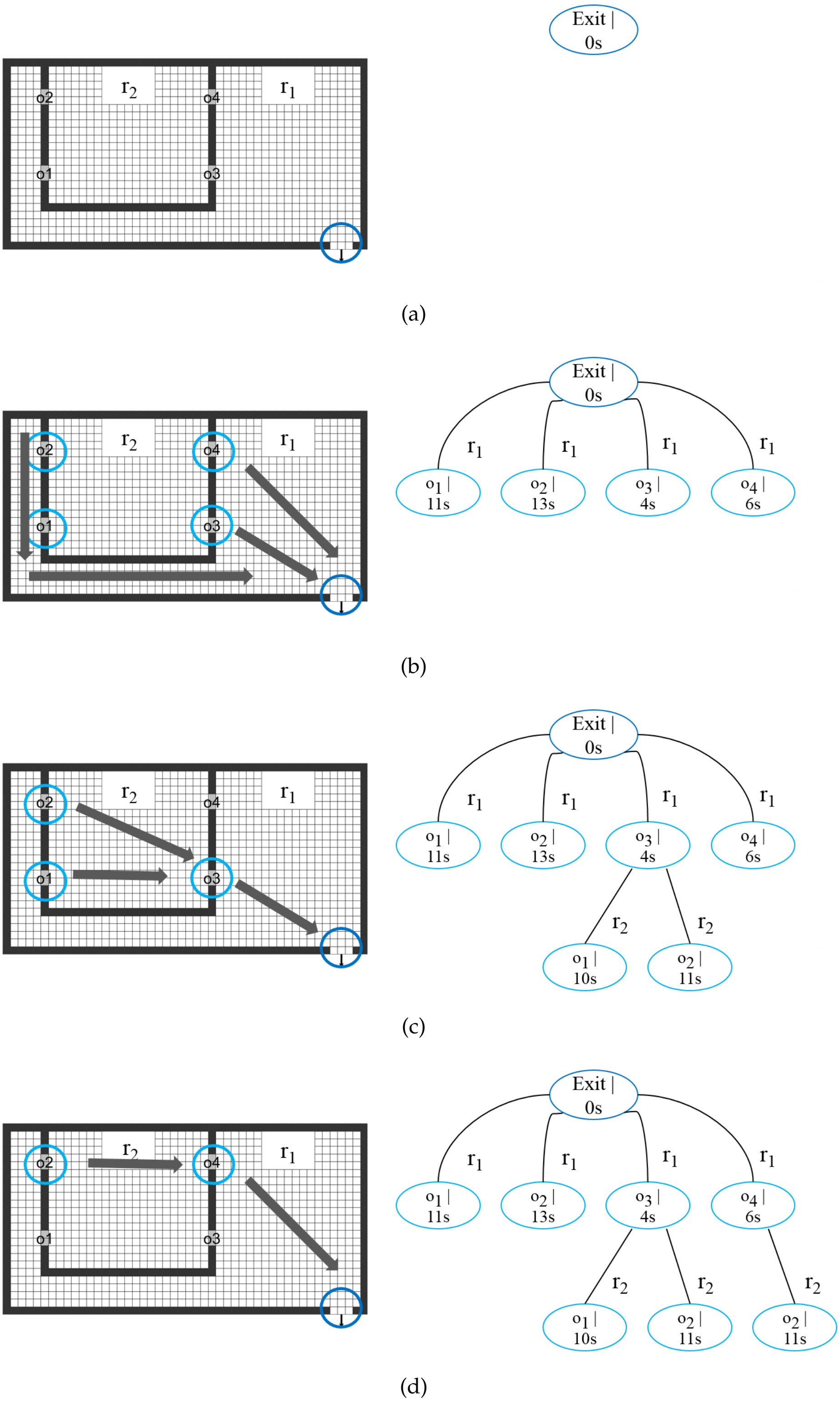

Figure 3.22: *Application of the Paths Tree computation algorithm in an example scenario.*

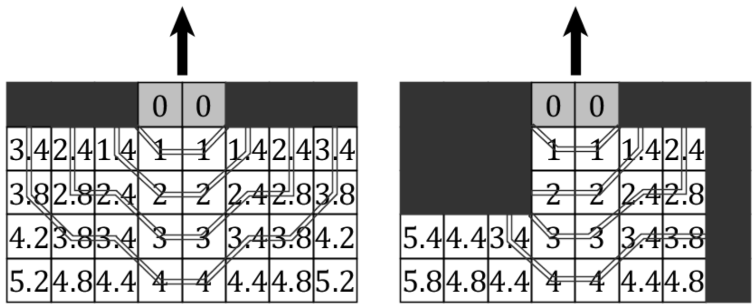

Figure 3.23: *Examples of surroundings of different sizes, for two configurations of the environment.*

Agents Dynamical Path Choice

At this point, the elements of information that the agents will use to make their decisions have been defined:

- the Paths Tree, computed before the simulation, will be used as a list of possible path choices;
- the position of the agent, which will be used to adjust the expected travel time considering the distance between the agent and the first opening of a path ($d(a, o)$);
- the information about congestion around each opening, computed during the simulation, will be used to estimate the delay introduced by each opening in the path.

The agent, which knows its position in the cognitive map (R_x), access the Paths Tree using an additional dictionary structure $M[R_x]$. This structure, given the input region R_x, returns a list of nodes representing the starting openings of each path. In this way, the agent will achieve the set of openings that it can directly access and then evaluate the total traveling time of the associated minimal paths. With this aim, it will firstly compute the expected traveling time to reach the first targets of the path, by considering its position. Then, it will add this value to the traveling time τ of the path, which is provided by the tree.

In order to minimize the traveling time, the agent will consider the eventual congestion in front of the openings that it is evaluating. In other words, it has to estimate the delay introduced by the crossing of an opening, by firstly achieving the size of the jammed area:

$$size_a(o) = \begin{cases} size(o) & \text{if } d(a, o) \geq r(o) \\ d(a, o) & \text{otherwise} \end{cases} \tag{3.2}$$

where $size_a(o)$ represents the estimate of the size of the area o by agent a, which is related to the actual size ($size(o)$) and the current position of the agent; more in detail, if its distance from the opening is smaller than the radius of the area (i.e. it is actually inside the area) it will not consider the whole size of the congestion but rather the remaining steps to the opening.

Up to now, the agent can suppose that for the length of the area it will travel at the average speed around the opening.

$$delay(o) = \begin{cases} \frac{size_a(o)}{averageSpeed(o)} - \frac{size_a(o)}{speed_a} & \text{otherwise} \\ 0, & \text{otherwise} \end{cases} \tag{3.3}$$

where $averageSpeed(o)$ is the average speed of agents in the surrounding of the opening o and $speed_a$ is the desired walking speed of agent a. If the agent is slower than the average speed around an opening, the additional delay is assumed to be 0.

At this point the agent can estimate the delay introduced by all openings.

$$pathDelay(p) = \sum_{o \in p} delay(o) \tag{3.4}$$

This is an example of omniscient agents, since they can always know the status of each opening. Of course, this is not realistic at all for the simulation of pedestrian motion, at least until it is not assumed to have particular displays and sensors providing the state of all doors in the environment. Hence another option is to assume that the agent is able to see only the state of the openings located in its region. In addition, the agent must be also able to remember the state of the opening when it left a region, otherwise the information used to estimate the traveling time at each time-step will not be consistent during the execution of the plan: if the agent forgets the congestion in the region just left, that led it to a plan re-computation, it will probably enter in that again! Thus, the traveling time associated to a path p is finally calculated as:

$$Time(p) = \left[\tau_p + \frac{d(a, S(p))}{speed_a} + pathDelay_a(p)\right] \cdot \xi_a \tag{3.5}$$

Where:

- τ_p : the expected travel time of the path p;
- $\frac{d(a,S(p)}{speed_a}$: the expected time to reach $S(p)$ from the position of the agent;
- $pathDelay_a(p)$: the estimation of the delay introduced by each opening in the path, based on the information and the memory of the agent a (which may or may not be updated for each opening). The information will be related only to the openings accessible from its region;
- ξ_a : a random perturbation, whose range can vary among the agents.

For the time being, no function acting on the memory of the agent has been considered. This means that the values which have been stored by an arbitrary agent, once left a region, remain the same until its plan is changed to one that implies again to pass through that region. Hence, the dynamism of the route calculation is restricted to the region where the pedestrian is located: it is not able to perceive the change of times related to any previously perceived congestion, so in a sense it assumes that the jamming situations are not changing with the simulation time.

The introduction of such function might bring significant changes in the simulation results but, on the other hand, no evidence on this very detailed behavioral component can be found in the literature, so in this manuscript this element has not been considered for further analysis. Furthermore, an alternative approach that allows a complete understanding of the traveling times is proposed in Chapter 5.

It should now be clear how the evaluation of each path is performed by the hybrid agents, which will estimate the traveling times and choose the best for them. It must be now explained *when* the agents will perform the re-computation. Another time, a simple strategy would be to allow the re-consideration of the traveling times at every time-step of the simulation but this, in addition to be computationally heavy, would be again not realistic. On the other hand, as stated in the Section 2.5 of the state of the art Chapter, there are no observation that led to knowledge on this particular topic, therefore every proposed strategy must be considered as an exploratory work.

The proposal of this model aimed at configuring a plausible and calibrable method for the tactical level activation, based on a more cognitive perception of the congestion in the environment. In particular, the agent will re-consider their path when the size of the congestion in front of the next opening is above a given threshold ϕ_{jam}, changing it in case of a better alternative. In case no better alternative is found, the agent will preserve this decision until it will have passed through the congestion, saving the computational times.

Hence the final life-cycle of the agent, considering its behavior at operational level and the dynamical route choice, is shown in Figure 3.24.

Different Paths Trees for Different Agent Classes

The previous model is general for each class of agents defined by the speed parameter. To represent different classes of agents, a function $Speed(agentClass, regionClass, direction)$ is defined. This will return the speed of the agent class inside the region of type $regionClass$, given the direction. It is essentially a generalization of the value $speed_a$ used in Equation 3.4.5.

For the experiments presented in the next Chapter of this Thesis, three classes of agents have been identified:

- *normal*: it is a normal agent, with no particular preferences;

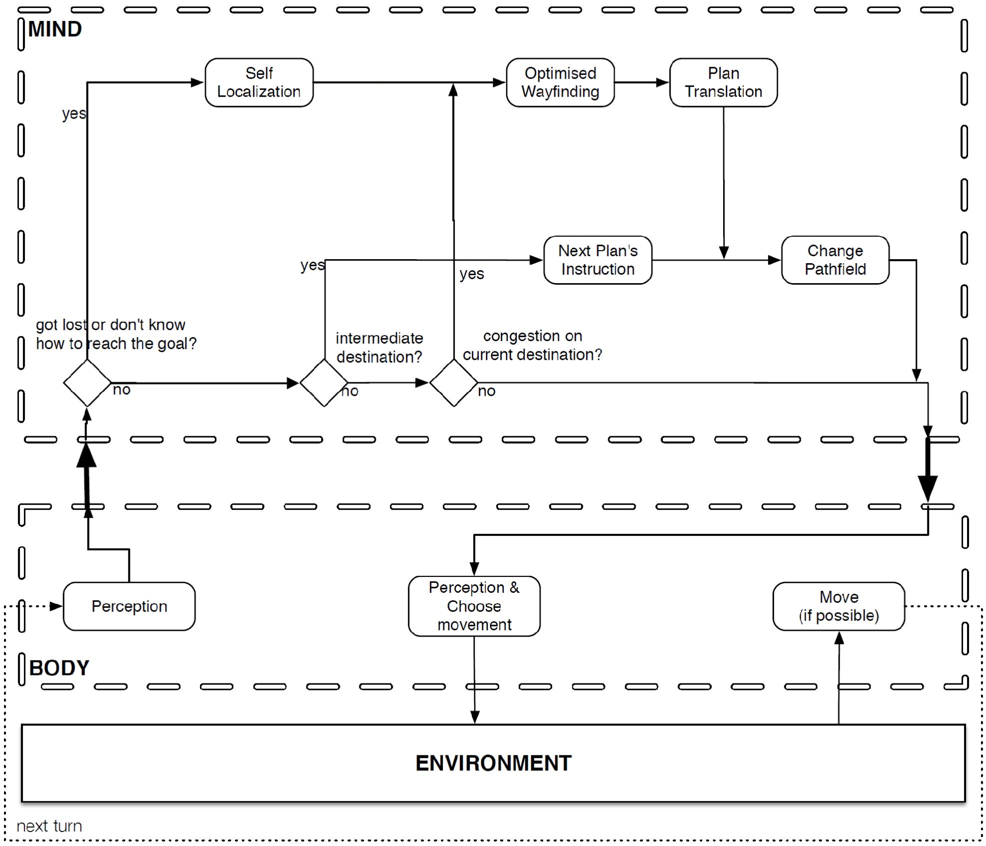

Figure 3.24: *The final life-cycle of the agent: the core component of the dynamical route choice procedure is the wayfinding, which is now performed with the Paths Tree. The last decision node linking at it manages the activation of the procedure, with respect to the perceived congestion.*

- *special*: it is a special agent, with a low base speed and which is slowed even more on stairs and ramps;
- *selective*: it is a selective agent, which deliberately avoid stairs and escalator.

Given the function $Speed$, a paths tree for each class of agent is generated, by adapting the speed parameter in the Function 3.1, given the room and the direction if needed. In order to represent the selective agent, it is sufficient to let the function $Speed$ return 0 for the region the agent wants to avoid. In this way, the expected travel time of the path will be infinite and this will not be added to the tree, leading the agents to never choose it. This approach can also be used to block the creation of paths that do not respect the eventual *direction* constraint of certain regions: more in details, the function $Speed$ will return 0 also for the region of type *escalator* if the direction of the expansion does not match its direction.

4

Validation And Experiments

This Chapter will propose a large number of test scenarios, with the aim to understand and evaluate the proposed model mechanisms and algorithms. Following the logic explained in the state of the art Chapter with the discussion on the validation problem, the physical properties of the model will be firstly analyzed by means of the fundamental diagram[1]. Then, the results of a particular *in-vivo* observation – carried out with the purpose of understanding the behavior of pedestrians in groups – will be compared with the simulations for an evaluation of the cohesion mechanism. Finally, more qualitative experiments will be proposed for the evaluation of the algorithms managing the tactical level and route choice of the pedestrians.

4.1 Properties of the Operational Level and Validation

Summarizing what has been explained with the model discussion in the previous Chapter, the operational level component of the agent can be imagined as its *body*, where the locomotion of the pedestrian is realized. This component describes thus the physical engine of the simulator and the validation must firstly pass through the analysis of the motion properties, by checking whether the model is able to respect the relation between density and flow. With this aim, a set of experiments in elementary portions of the environments (i.e. corridors) with uni-directional and bi-directional flow have been configured and the resulting fundamental diagram data will be discussed in the next Section. After this quantitative validation of the overall operational level model, additional tests with more focus on the two main contributions of this Thesis at this level, which are the methodology for the heterogeneous speeds of agents and the mechanism for the group cohesion, will be proposed and analyzed.

For the experiments described in this Section, the calibration parameters of the model have been assigned as shown in the Table 4.1.

[1] The data-sets of the literature, used for the evaluation, have been downloaded from http://www.asim.uni-wuppertal.de/datenbank/data-from-literature/fundamental-diagrams.html

Parameter	*Value*
density radius r	3 cells
time-step duration	0.25 s
cell side length $cell_side$	0.4 m
desired speed of agents (if not further specified)	1.4 $\frac{\mathrm{m}}{\mathrm{s}}$
maximum speed of agents	1.6 $\frac{\mathrm{m}}{\mathrm{s}}$
utility parameter κ_g	6.0
utility parameter κ_{ob}	4.0
utility parameter κ_s	28.0
utility parameter κ_d	2.0
utility parameter κ_{ov}	6.5
utility parameter κ_c	6.0
utility parameter κ_i (used only for inducing lane formation)	6.0
conflict management parameter $frict_l$	0.8
conflict management parameter $frict_h$	0.96
stairs *slope* parameter (if not further specified)	2.2

Table 4.1: *Assignment of the calibration parameters regarding the operational level model.*

4.1.1 Fundamental Diagram for uni-directional and bi-directional Flow

The fundamental diagram is the main instrument to have a quantitative evaluation and to understand the reliability of the simulation model. With the aim to analyze the flow-density relation generated by the model in case of uni-directional and bi-directional flow, a corridor setting of 3.2×10 m^2 have been modeled. The environment configuration is illustrated in Figure 4.1. A set of simulations with a growing number of pedestrians, fixing the overall density of the scenario, have been configured. The probabilistic nature of the model can also lead to a significant variability of the results, therefore for each level of density many iterations have been carried out. The duration of each iteration has been fixed to around 2400 steps = 10 minutes. After the initialization of all the agents needed, at each iteration the traveling times of pedestrians are collected. This statistic describes the time passed from the agents generation to the step when they reached the end of the corridor. In this way the average speed of the agent a along the corridor and associated to the density ρ is calculated as:

$$\nu_a(\rho) = \frac{CorridorLength}{TravelingTime_a}$$

By means of the velocity, the pedestrian flow is then calculated as $J(\rho) = \nu \cdot \rho$.

To have a sufficiently large amount of data even for the single iteration, each pedestrian is re-initialized at the opposite side of the corridor once arrived. This maintains the system and the density in a stable state. The desired speed of all the

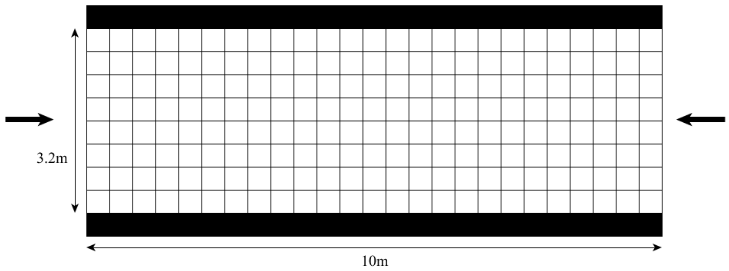

Figure 4.1: *The corridors used for the fundamental diagram tests.*

pedestrians have been set to 1.4 m/s, while the duration of the time-step ensure a maximum walking speed of 1.6 m/s.

The results of the simulations for the case of uni-directional flow are shown in Figure 4.2 in the form density-velocity (a) and density-flow (b). For this evaluation, the empirical data from the work of Mori and Tsukaguchi [1987], Helbing et al. [2007] and Hankin and Wright [1958] have been used, all of them describing uni-directional motion of pedestrians. Despite these data-sets have been achieved in very different situations and places, they have been used together since they describe a similar trend. Overall the model preserves the properties of the floor field model and the results are relatively in tune with the empirical data from the literature. At densities between 1.5 and 4 persons/m^2 the simulations generate slightly higher velocities than empirical observations, and this leads to a translation of the critical density value towards the right, approximately to 3 persons/m^2. Below 4 pedestrians/m^2 the range provided by the literature data-sets is again respected.

For the case of bi-directional flow, the results are shown in Figure 4.4. The set of simulations have been configured with the same corridor, with the difference that the population for each level of density is equally split among the two entrances. To allow a stable and reliable average of the results, 10 iterations for each level of density explored have been performed, each one with a duration of 2000 steps. To stimulate the formation of lanes, the agents belonging to each flow are attracted each other with the mechanism used for the inter-group cohesion, explained in Section 3.4.1. This mechanism, in fact, is suitable for the generation of a light attraction that can lead to both stable or dynamical lanes, as shown in the screen-shots of the Figure 4.3. By looking at the resulting fundamental diagram, in this case the average velocities and flows respect the range provided by the empirical results, which are taken from Older [1968], and also with design manuals [Weidmann, 1993]. A critical point of this result can be given by the variability of the results, that visibly appears to be quite high. On the other hand, the higher values of velocities and flows are probably achieved at the beginning of the simulation, where the simulation has not reached yet a completely stable state.

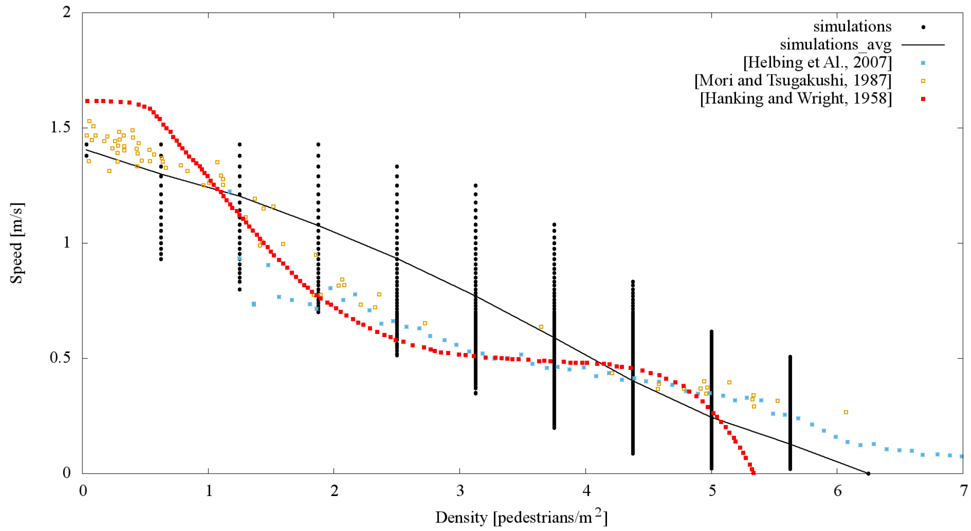

(a) density-speed

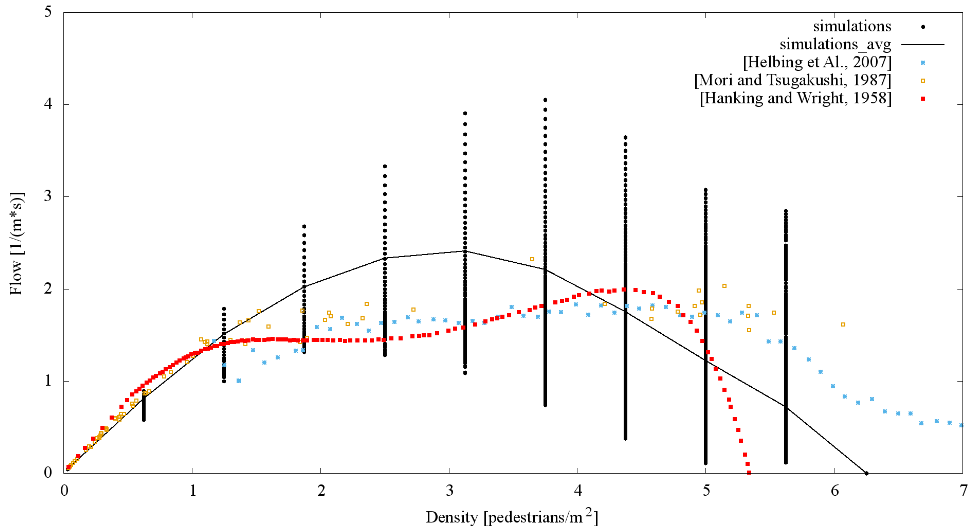

(b) density-flow

Figure 4.2: *Comparison with the fundamental diagrams from simulations and data-sets from the literature.*

The combined results suggest that a more careful calibration of the parameters involved in the rendering of social repulsion but not related to the counter-flow caused conflicts could improve the achieved results in the uni-directional flow.

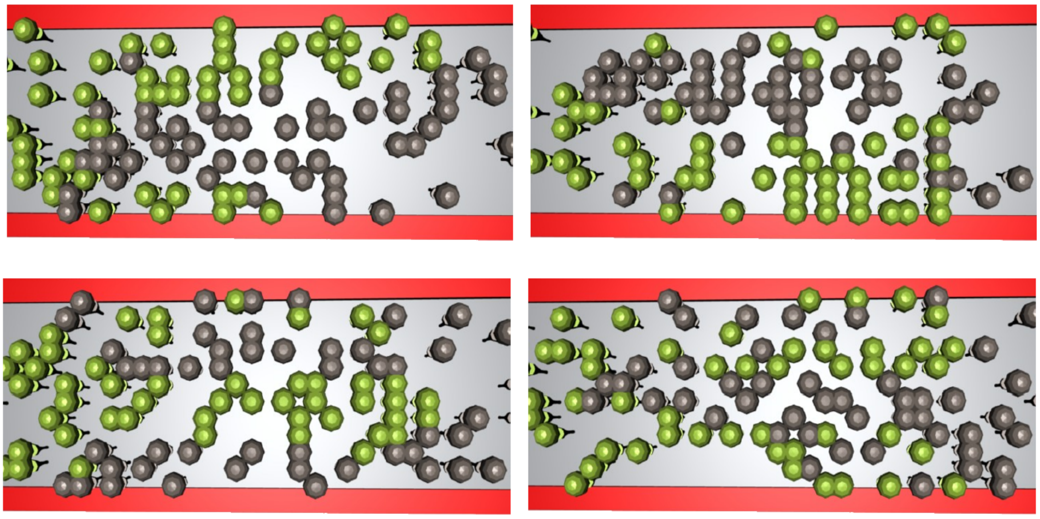

Figure 4.3: *Example of emergence of the lane formation effect with the simulation of bi-directional flow. In these simulations both large and stable lanes (on the top) and more dynamic ones (on the bottom) have been arisen.*

4.1.2 Evaluating the Effects of a Rotation of the Environment

In the vein of the work by Koyama et al. [2013], it has been considered the performance of the heterogeneous speed management mechanism in situations characterized by frequent diagonal movements by the pedestrians. In particular, the flow generated in a long corridor with 0 (Figure 4.5 (a)) and 45 of rotation (Figure 4.5 (b)), both in uni-directional and bi-directional pedestrian flows. In this case, the aim is not actually to discuss the similarity between the achieved fundamental diagrams and the ones described in the literature, but instead to compare the results achieved with the normal and the rotated corridor. Hence, the empirical data-sets shown before are omitted in this diagrams. Figure 4.6 (a) compares the unidirectional flows of pedestrians in two simulated corridors: although the points of the two data sets are quite close, there is a sensible difference among the flows generated between 1.8 and 3.5 persons/m^2. There are two main reasons that lead to this effect: on one hand, the rotated corridor has a slightly higher width than in the normal case (3.44 instead of 3.2 m). On the other hand, a significant influence is brought by the more probable diagonal orientation of the agents in the movement, that decreases the probability of having conflicts for the same movement choice. Nonetheless, the critical density is reached slightly before with the rotated corridor and the results become much closer around 3 persons/m^2, having again the same trend from about 3.5 persons/m^2.

Figure 4.6 (b) describes instead the bidirectional flows in the same corridor, comparing again the normal and rotated scenario. In this case, the differences between the

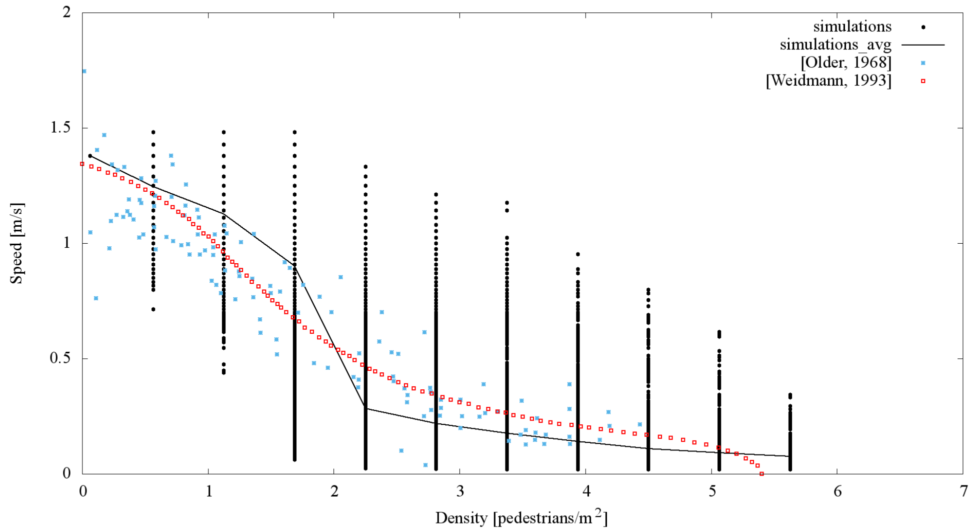

(a) density-velocity

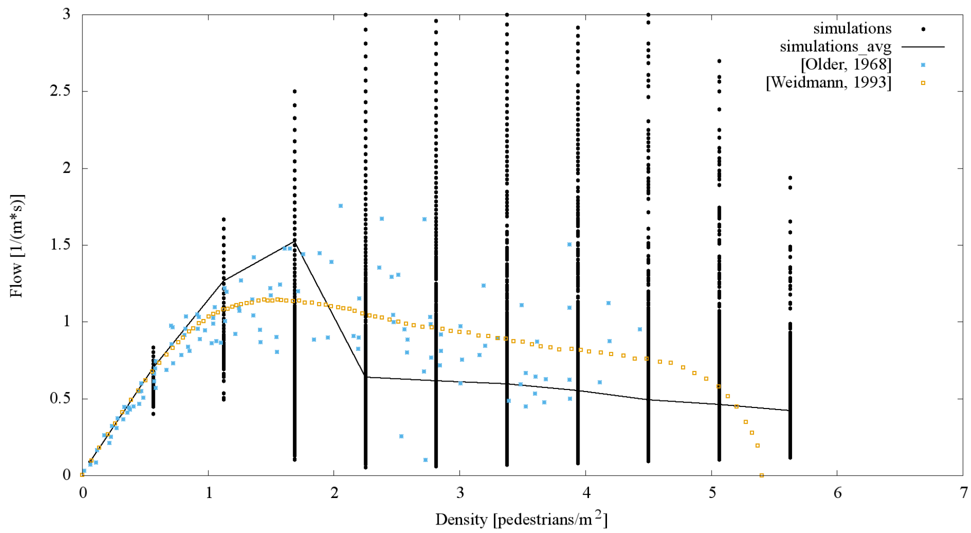

(b) density-flow

Figure 4.4: *Fundamental diagrams achieved with the simulation of bi-directional flow in the corridor. The empirical data-sets are taken from Older [1968] and Weidmann [1993].*

two situations are quite smaller and less systematic: the critical density in the rotated corridor seems to be in the same range of the normal scenario. The lower probability to have a conflict in the rotated scenario makes also in this case the simulated flow slightly higher than in the normal case, but the additional conflicts generated by the

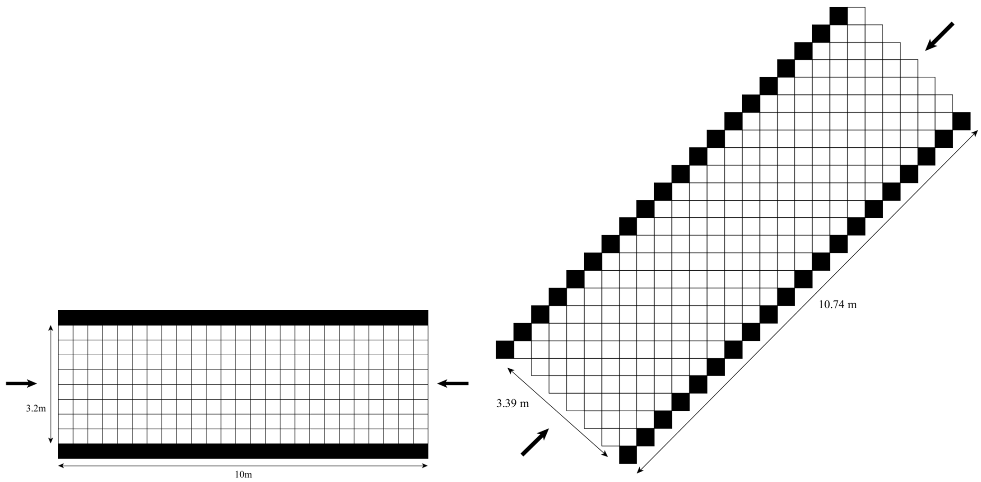

(a) Standard corridor (b) 45 rotated corridor

Figure 4.5: *The corridors used for the environment rotation experiments.*

bi-directional flow sensibly mitigate this effect. In the end, there is still a significant difference in the same range of densities achieved with the uni-directional experiment (from 2 to 3.5 persons/m^2), but the comparison is overall acceptable. This experimental rotation of 45 degrees represents, in fact, the worst case for the environment discretization applied in this model. With a baseline definition of the model, without employing the mechanisms introduced for the management of different speeds of agents, these discretization effects would lead to a much higher difference among the results of the two simulated scenarios and this would definitely impact on the applicability of the model for the simulation of real-world scenarios.

Another experimental scenario is instead aimed at understanding if the approach introduced for the management of heterogeneous velocities causes problems in the reproduction of patterns of space utilization that are observable in reality, especially in environments including a corner. The T-junction scenario is characterized by two branches of a corridor that meet and form a unique stream (as described in an experimental observation described by Zhang et al. [2012] and in a simulation study described by Vizzari et al. [2013]). In this kind of situation it is not unusual to reach high local densities due to preferences in pedestrian trajectories, especially where the incoming flows meet to turn and merge in the outgoing corridor. The results of this scenario is not represented by fundamental diagram data, but rather by an indication on how the pedestrians used the available space by moving in the environment throughout the simulation. The *cumulative mean density* (CMD) statistics has been used, associating to every position of the environment the average density perceived by pedestrians that passed through that point. It is quite straightforward to compute this value in

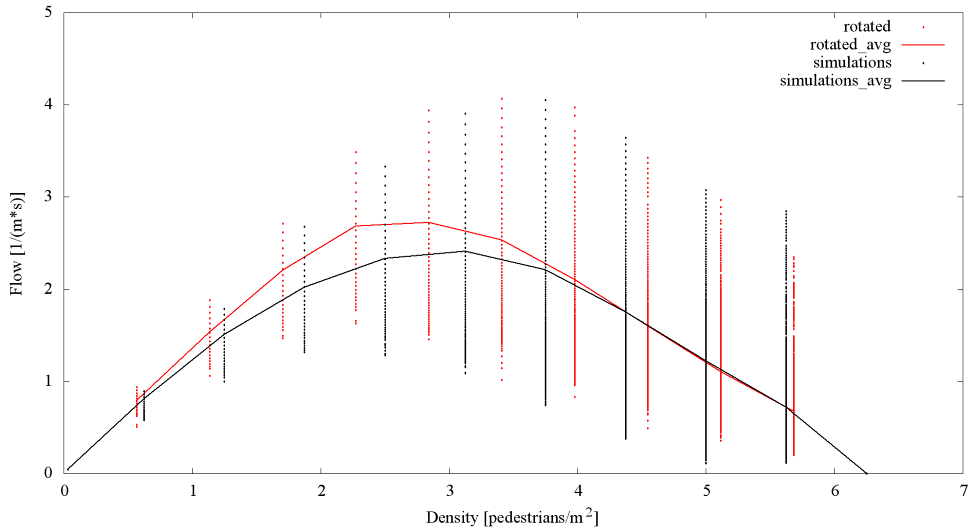

(a) Uni-directional corridor

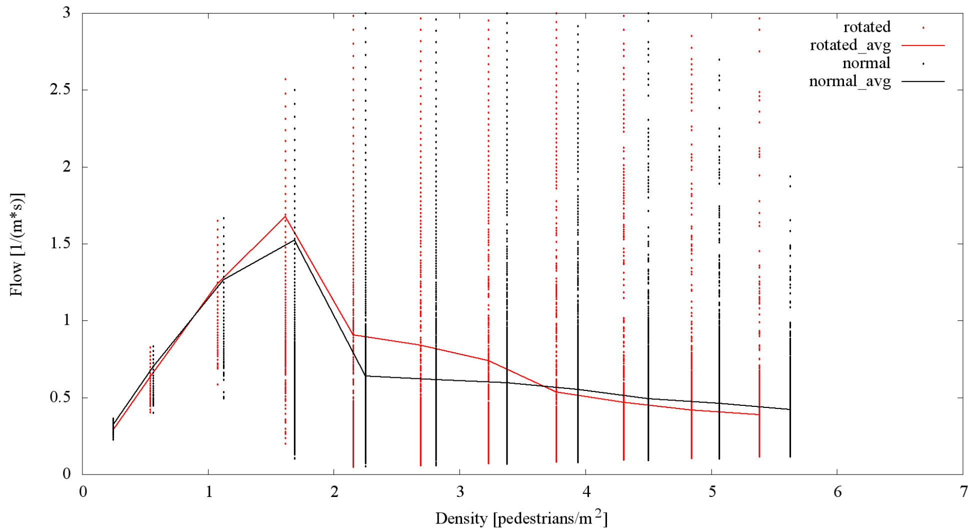

(b) Bi-directional corridor

Figure 4.6: *Achieved fundamental diagrams comparing the flow generated with the two corridors, in case of uni-directional and bi-directional flow.*

a discrete approach like the one described in this work. Results shown in Figure 4.7, analyzing situations of medium density, show qualitative phenomena (areas of low or high utilization) that are in tune with available empirical data on this kind of scenario: in particular, there is an area of low density forming a sort of arch near the merge

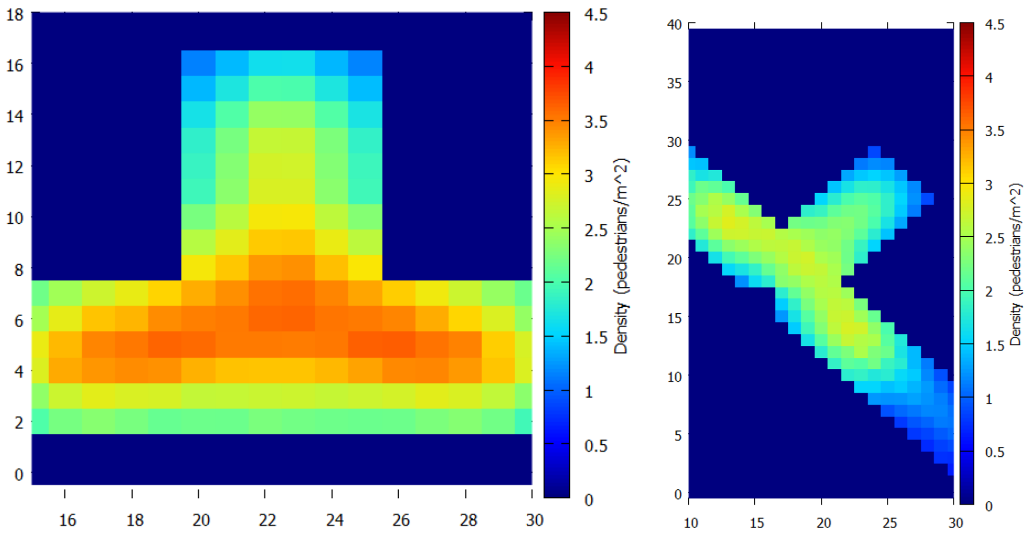

(a) (b)

Figure 4.7: *Comparison of density diagrams for the T-junction scenario in the case of* 0 *and* 45 *rotation.*

between the two branches, that pedestrians likely avoid to choose the inner side of the corner, while just above this area the density is higher. Moreover, after the bend and after the merging of the flows, the density lowers. These results are in tune with empirical evidences from Zhang et al. [2012] and, once again, they are quite similar even if the scenario is rotated 45: the measured levels of density are slightly lower in the rotated scenario, which seems compatible with the unidirectional corridor results. In fact, at this level of density, pedestrians are probably slightly slower in the diagonal situation which causes a lower congestion in the cells just before and in the middle of the merge area.

To verify the physical properties of the model in case of stairs, whose mechanisms have been described in Section 3.4.4 of the previous Chapter, a scenario with a linear staircase (i.e. containing one region of type *staircase*) has been tested with a unidirectional flow. As with the corridor scenario, the size of the staircase has been set to 3.2×10 m. In this case no rotation has been applied. By looking at the results, shown in Figure 4.8, the walking speed of pedestrians at low densities are in compliance to the expected one of $0.6m/s$ [Burghardt et al., 2013]. An interesting particular is that in this case the density starts to significantly influence the speed around 3 persons/m^2, where the state transition is visible. Before that point the effects of densities are smoothed by the low velocities. It is possible to conclude that the introduced mechanism is effectively able to reproduce heterogeneous walking speeds.

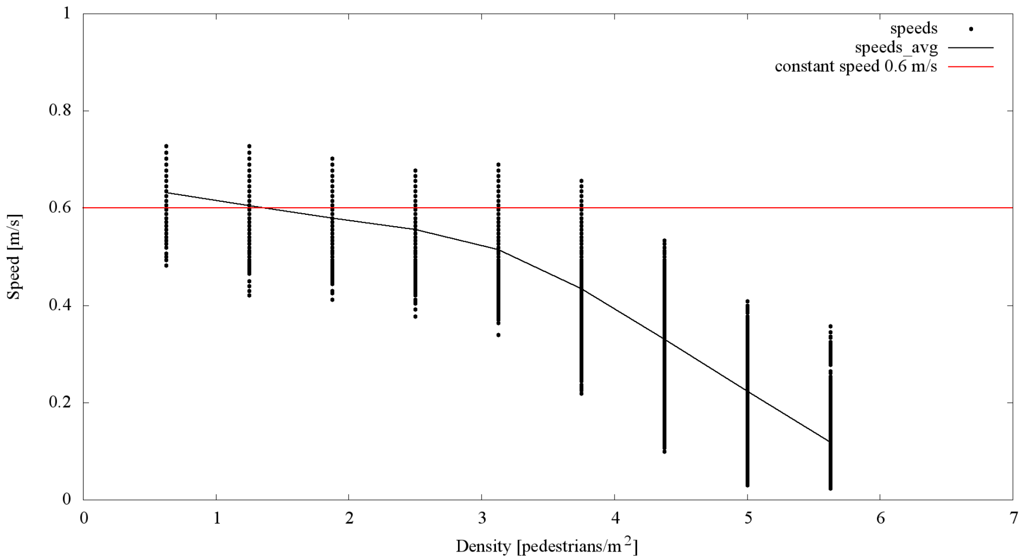

Figure 4.8: *Fundamental diagram achieved with the staircase scenario.*

4.1.3 Evaluation of the Cohesion Mechanism for Pedestrian Groups

The data that can be gathered with the simulations covers a wide array of observable measurements. By means of this set of experiments, the main purpose is the validation of reproduced behavior of the agents inside groups, evaluating therefore the plausibility of the cohesion mechanism encompassed by the model.

The simulation scenario modeled with these tests represents a portion of the Vittorio Emanuele II Gallery of Milan, where an observation in the field has been performed in 2012. As already introduced, that observation had the particular aim to provide additional understanding of the groups behavior in walking. The full description of the observation and its results will not be described in this Section, that is dedicated to the simulation validation. To give completeness to this Thesis, on the other hand, these details will be as well provided in the Appendix A. With the following, the simulation results and their comparison with the observed data will be presented.

The observed scenario, the portion recorded with the footage and the methodology applied for the data collection, are shown in Figure 4.9. The simulated scenario has been configured with similar size of the portion considered for the observation, representing a large corridor with 12.8×12.8 m^2. Individual pedestrians and groups of different sizes have been introduced at the two extremes of the corridor and directed to the opposite side, configuring the observed bi-directional flow with respect to the frequency observed.

The first analysis performed represents an indicator of the average dispersion of

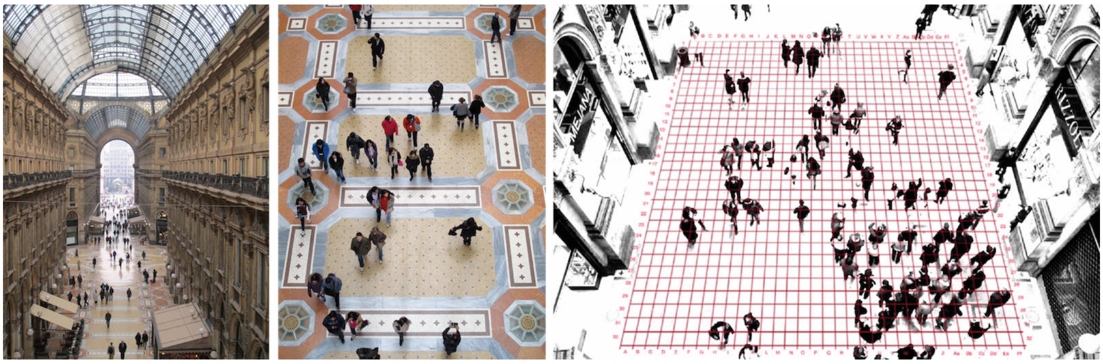

Figure 4.9: *From the left: an overview of the Vittorio Emanuele II gallery, the streaming of passerby within the walkway and a snapshot of the recorded video images with the superimposed grid for the data analysis. A completely similar grid will be used for the simulation scenario, with pedestrian flows directed either to north or south sides.*

LOS	Size	Av. Dispersion	Observed
A	2	0.336 (± 0.157)	
	3	0.479 (± 0.153)	
	4	0.575 (± 0.146)	
B	2	0.351 (± 0.174)	0.35 (± 0.14)
	3	0.505 (± 0.194)	0.53 (± 0.17)
	4	0.609 (± 0.210)	0.67 (± 0.12)

Table 4.2: *Average groups dispersion achieved by the simulations (standard deviation inside breaks).*

different types of group during the simulation. Several methods have been proposed in the literature to describe the dispersion, since it is an fuzzy concept that can be formalized in different ways [Bandini et al., 2011]. The results shown in Table4.2 have been achieved by using the centroid method. This method has been already explained in the previous Chapter, but it is reported in the following to improve the readability:

$$Disp(Group) = \sum_{a \in Group} \frac{distance(centroid(Group), a)}{Size(Group)}$$

$$Centroid(Group) = \sum_{a \in Group} \frac{(x_a, y_a)}{Size(Group)}$$

The metric describes the dispersion as the average distance assumed by members of the group from its center of gravity, which is the vector calculated as the average position of all the group members.

LOS	Size	Av. Speed	Observed
A	1	1.19	
	2	1.115	
	3	1.119	
	4	1.11	
B	1	1.172	1.22
	2	1.107	0.92
	3	1.105	0.73
	4	1.099	0.65

Table 4.3: *Average speeds of groups.*

LOS	Size	Av. Distance	Observed
A	1	13.767 (± 0.57)	
	2	13.922 (± 0.621)	
	3	13.980 (± 0.624)	
	4	14.052 (± 0.653)	
B	1	13.857 (± 0.577)	13.96 (± 1.11)
	2	13.99 (± 0.628)	13.39 (± 0.38)
	3	14.049 (± 0.654)	13.34 (± 0.27)
	4	14.087 (± 0.653)	13.16 (± 0.46)

Table 4.4: *Average traveled distance of groups.*

The results show that the cohesion mechanism is quite effective: the dispersion of groups in the two settings (LOS A and B) is similar and the increase of density have led to a very light increase of the average and standard deviation. The most important consideration, however, is the fact that these data are consistent with the empirically observed values (which refer to the B LOS conditions).

Table 4.3 shows instead the average speed characterizing the movement of the different types of pedestrians (individuals or members of a certain type of group), calculated using the length of the actual trajectory and the time needed to move from the start area to any cell of the destination area of the corridor. In this case the model has only been able to reproduce results similar to the empirically observed data only for individuals and it only showed a slight decrease in the velocity of group members. On the other hand, it must be noted that all the agents have been configured with the same desired speed of $1.3\ m/s$, that is based on empirically observed velocity for pedestrians traveling for business purpose [Schultz et al., 2010]. The same observation reports that pedestrians moving for leisure generally have a lower average walking speed. Therefore, our conjecture is that the much lower walking speed of groups might be due not only to the fact that members try to preserve the possibility to establish verbal and non-verbal communication, but also to a change in the reason and motivation for moving in the environment. Further analyses on this issue are object of future studies.

Finally, Table 4.4 analyses average travel distances covered by pedestrians in the simulations. This measure is obviously strictly related to the previous one, being actually used in the computation of the walking speed. As a consequence, even if simulated trajectories are very close to the measured ones also in this case the model was not able to differentiate paths covered by individuals and group ones (in some cases the traveled distance of individuals was actually lower, unlike in the observed data). In addition to the above considerations on motivations of the movement, that can also have an influence in the frequency of direction changes, it is wanted to emphasize that a discrete model has intrinsic limits in the faithful reproduction of trajectories (that are inherently jagged and not as smooth as the real ones), so it could be difficult improving this kind of result adopting a discrete model.

4.2 Tests on Tactical Level

The experiments explained in this Section aim at analyzing and evaluating the model component for the route choice management. Firstly, a purely qualitative experiment showing the expressiveness of the model will be proposed, describing a simple scenario with a choice between a staircase or a ramp. The experiment will illustrate three different types of agents, with different strategies for the route choice. Then, a more complex scenario will be shown, describing an evacuation from an imaginary environment.

The only parameter concerning the tactical level model is ϕ_{jam}, which describes the threshold radius of the congested area surrounding the intermediate target: while the congestion size is bigger than this parameter, the agents perceiving it are considering alternative routes to reach the final target. For these simulations it has been assigned to 7 cells $=$ 2.8 m.

4.2.1 Modeling Different Classes of Agents and Environments

With this simple experiment the aim is to show the behavior of various classes of simulated pedestrians, which have been explained in the Section 3.4.5. The scenario represents an elementary environment that could describe an entrance to a building, comprising one stair and one ramp that can be used by people with mobility impairment. This structure is illustrated in Figure 4.10(a). A flow of about 1000 persons populates the scenario, with an arrival rate of about 1.5 persons/second and divided into the three classes with a distribution of 60% normal, 20% special and 20% region selective. Figure 4.10 (c) and (d) show two frames of the simulation where the agents of the three classes have been visualized with different colors, respectively red, green and blue. This approach automatically lets the *region selective* agents (blue colored) choose the ramp instead of the stairs.

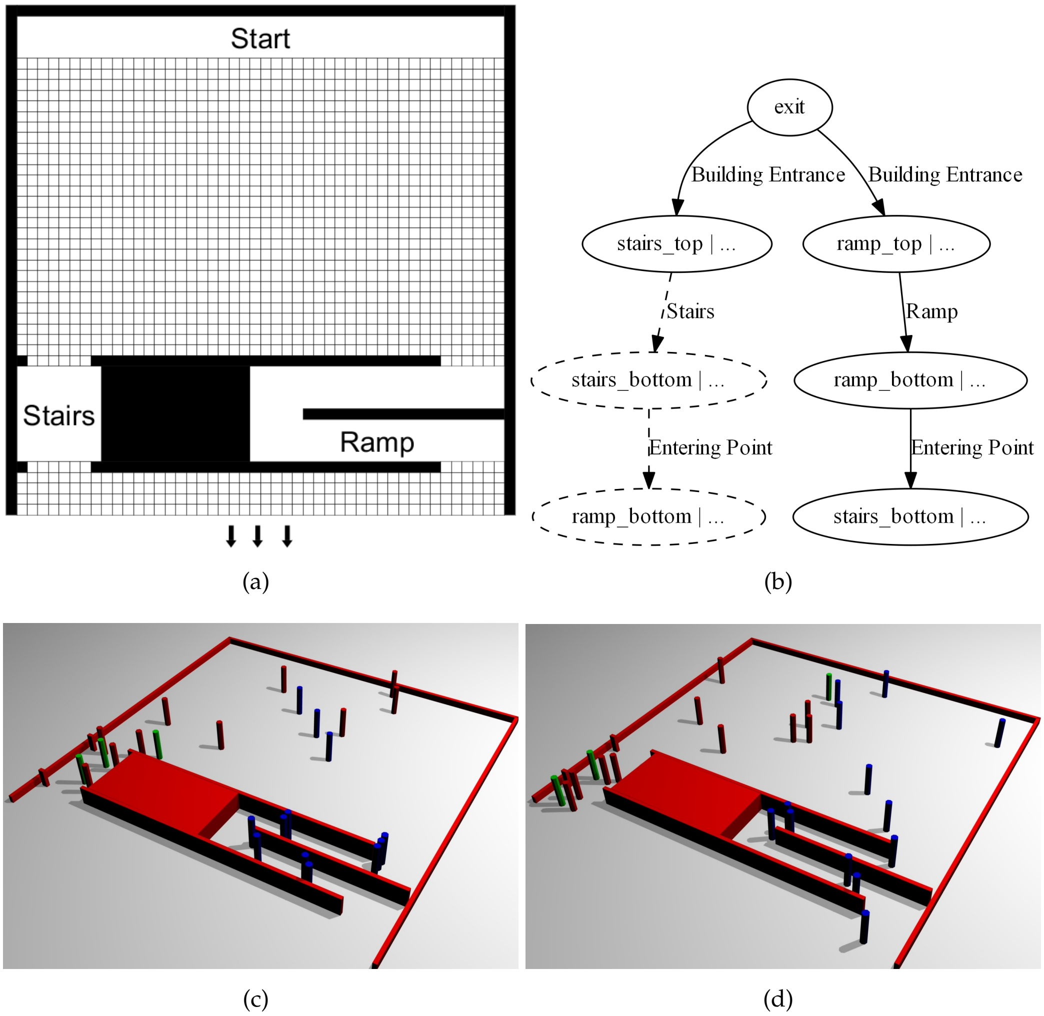

Figure 4.10: *The qualitative test scenario (a), representing an entrance to a building with a small stair and a ramp for people with mobility impairments. In (b) a "merge" between the paths tree dedicated to* normal *agents and for the* region selective *agents is shown. The dashed branch, passing through the stairs region, appears only in the normal agents tree. This approach automatically lets the* region selective *agent (blue colored) choose the ramp instead of the stairs (c – d).*

By looking at the two pictures, the different behavior of agents belonging to the diverse classes is clearly understandable: while the stairs are component of the tactical plan of the largest part of the *normal* and *special* agents, none of the *region selective* pedestrians employed them. This choice has been a-priori constrained with the paths tree computed for this agent class, shown in Figure 4.10 (b), where the branch describing the stairs path (the dashed one in the figure) has not been added due to the "infinite" time that it would imply (unless helped, a pedestrian with specific mobility impairments would simply be unable to climb a stair). On the other hand, the longer distance implied by the usage of the ramp causes agents belonging to the other classes to generally avoid it in favor of the stairs.

Due to the low densities arisen in the scene, this first test scenario does not show any sign of the adaptive agent behavior at tactical level. The following one, instead, will focus on this point to show the potential of the proposed approach and the possibility to tune its mechanisms to vary the *sensitivity* of the agent dynamical path re-calculation. This parameter influences the frequency of re-computation of the path to be followed due to changes in the perceived level of congestion in the next opening: a high level of sensitivity will lead to more frequent re-computation, potentially detecting more quickly the opportunity to change a sub-optimal plan but also potentially leading to higher computational costs and even excessive oscillations in agents' decisions.

4.2.2 Simulation of an Evacuation Scenario

The experimental scenario here proposed represents an evacuation in a hypothetical scenario, simulated with a consistent incoming flow of people. A graphical representation of the environment and flow configuration is depicted in Fig. 4.11(a): it is a sample situation in which two flows of pedestrians enter an area with six exits, distributed among 3 equal rooms, at a rate of 10 pedestrians per second. Only agents of the *normal* class will be used. An important peculiarity is the slightly asymmetrical configuration of the environment, that causes shorter distances towards the three southern exits. This is reflected by the illustrated paths tree in Figure 4.11 (b) where, to give an example, the paths starting from $o4$ and $o5$ and leading out through $o2$ take a little more time than the ones going out by using $o7$. As it will be shown, this slight asymmetry would significantly affect the results of the simulations, but the discussion will start by characterizing the effect of the adaptive mechanism for path selection at tactical level, compared to a baseline shorter distance choice strategy.

In particular, the results of this comparison concern the evolution of the number of pedestrians contemporary present in the scenario at each time-step, shown in Figure 4.12 (a), and the evolution of travel time for pedestrians going out from the simulation environment at a given time, shown in Figure 4.12 (b). In both diagrams the results of two different scenarios are shown, aiming to verify the difference between:

- a baseline scenario where the agents are configured to only choose the *shortest path* towards the exit, thus without activating the adaptive algorithm for the route choice;
- a scenario where the dynamic route choice is activated.

The first diagram highlights the fact that when pedestrian agents only choose their paths according to the covered distance, they employ a variable time to vacate the area, growing along the time of the simulation and with the number of agents inside. This is due to the fact that they do not exploit the trajectories that are sub-optimal from the point of view of the distance to be covered, but which become appealing by considering the traveling time with the emerged congestion. Analogously, the evolution of the traveling time during the simulation shows that, in this situation, congestion has a much lower impact on adaptive agents with an awareness of the spatial representation of the environment, as long as the environment offers alternatives that are not subject to congestion as well. More in details, by looking at the traveling times of Figure 4.12 (b), it is possible to understand that, with the adaptive route choice of agents, the environment is able to sustain the incoming flow of pedestrians: the average traveling time remains stable once reached a “plateau”. Another interesting aspect of the Figure is that several *dot clouds* with a linear shape are recognizable and they identify the time of the simulation when the agents have modified their route.

The above mentioned diagrams are surely important in quantitatively estimating the overall impact of this adaptive choice strategy, and they can represent a first way of validating it should actual data about the evacuation of a building presenting suitable characteristics were available. However, these metrics are too aggregated to actually illustrate the actual spatial utilization of the environment by the pedestrians. Cumulative mean density maps were also acquired to describe in a qualitative and quantitative way the behavior of adaptive agents and they are shown in Figure 4.13. In this case, these heat maps have been collected for a time window of 50 steps.

In particular, the diagrams show results of two simulations in which two different adaptive tactical level choice strategies have been adopted. First of all, it must be noted that all exits are used, although with a different frequency, whereas the static shortest path route choice would have selected just four exits. Moreover, northern and southern exits are generally chosen almost equally by the agents, despite the slight difference in the actual distance, due to the above introduce asymmetry. This is due to the fact that a random error of $\pm 10\%$ has been added to the overall calculation of the traveling time $Time(p)$ in order to consider the fact that pedestrians do not have an *exact* estimation of distances and delays caused by perceived congestion, in a more commonsense spatial reasoning framework Bandini et al. [2007]. The different adopted strategies consider a different triggering condition for the re-computation of the travel times: agents, in fact, must reconsider their choices in the light of the perceived contextual conditions. For instance, an agent chooses an exit in the middle room because the closest one is congested only to realise, later on, that also the chosen one is crowded.

As it has been explained in Section 3.4.5, the route choice of the agent is activated when this perceive the congestion. This mechanism is regulated with the parameter ϕ_{jam}: if the perceived congestion in front of the next target of plan does not exceed this threshold, the agent will continue with the planned course of actions. The first row of Figure 4.13 shows the evolution of the system with a relatively low threshold, and

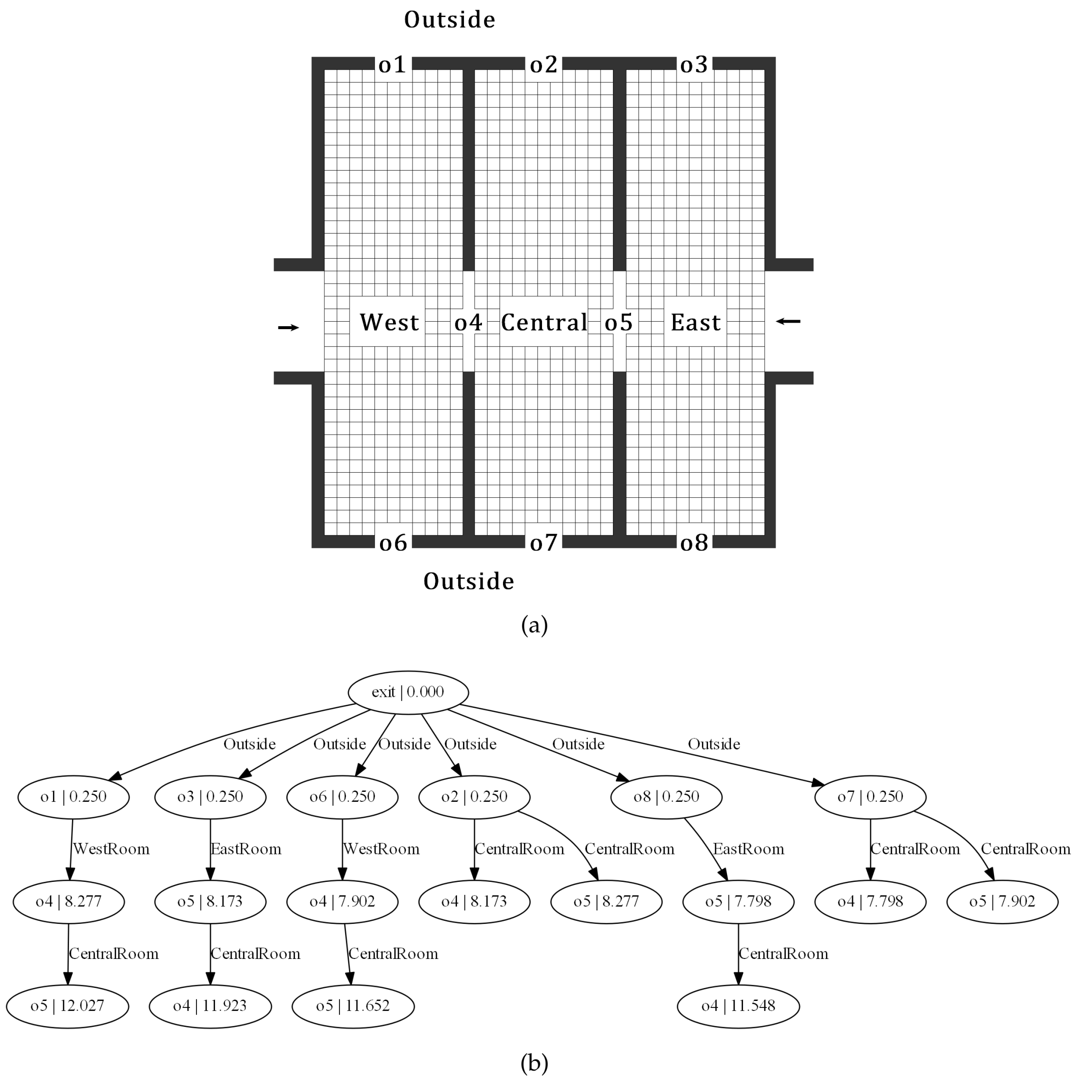

Figure 4.11: *The environment (a) and respective paths tree (b) used for the second experiment. The traveling times written in the paths tree nodes refer only to the normal agent class.*

therefore a high sensitivity to congestion. Alternatively a lower sensitivity to congestion has been configured to achieve the results respectively in the top and bottom rows. The differences are relatively small, and they do not lead to significant changes in the average travel time, but here is possible to understand that route adaptation is enacted a little later in case of low sensitivity to congestion, leading to a slightly higher congestion in the adopted exits.

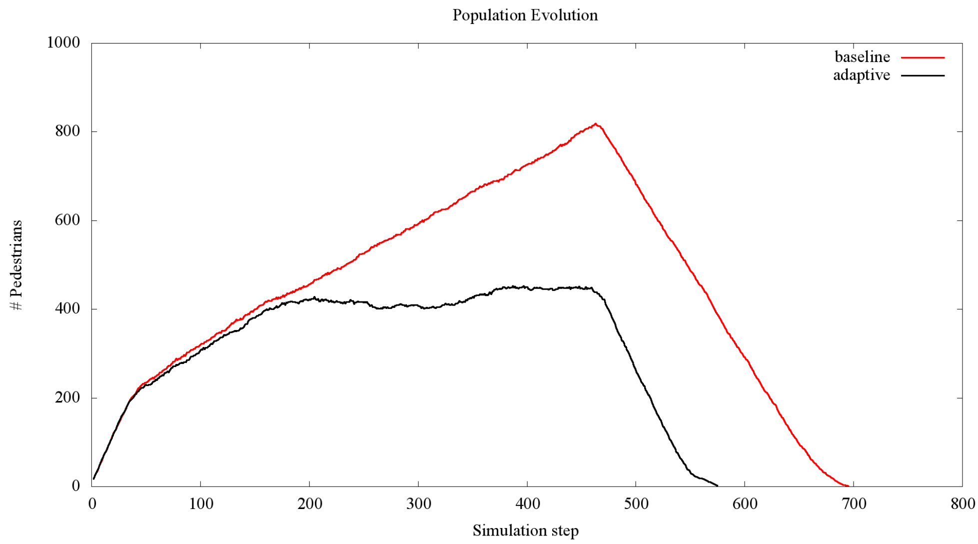

(a)

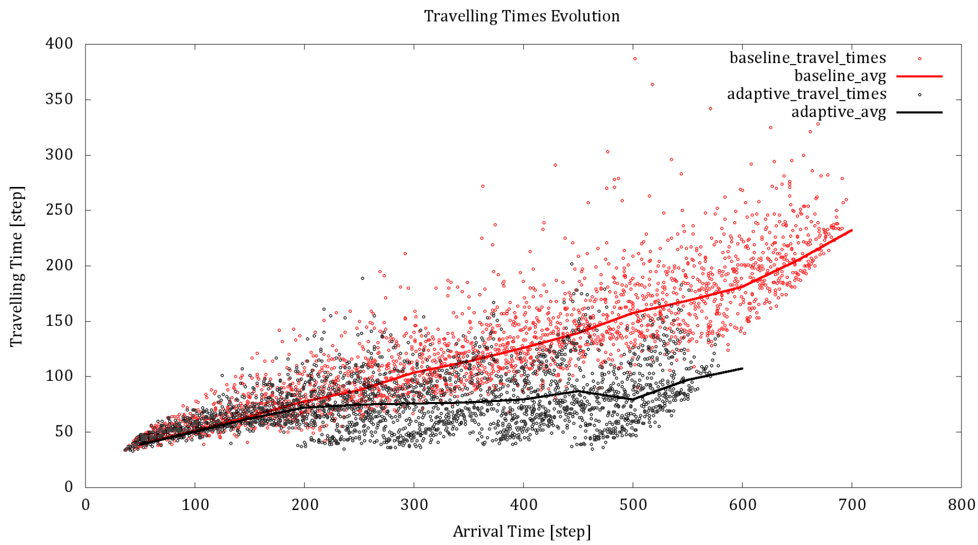

(b)

Figure 4.12: *A diagram showing the evolution of the number of pedestrians still in the scenario in time (a) and a graph showing the evolution of travel time for pedestrians entering the simulation environment at a given time (b).*

4.3 A Preliminar Analyis of the Computational Times

Before closing the Chapter, an idea of the overall trend of the computational times during the simulations must still be provided and, following this purpose, two additional

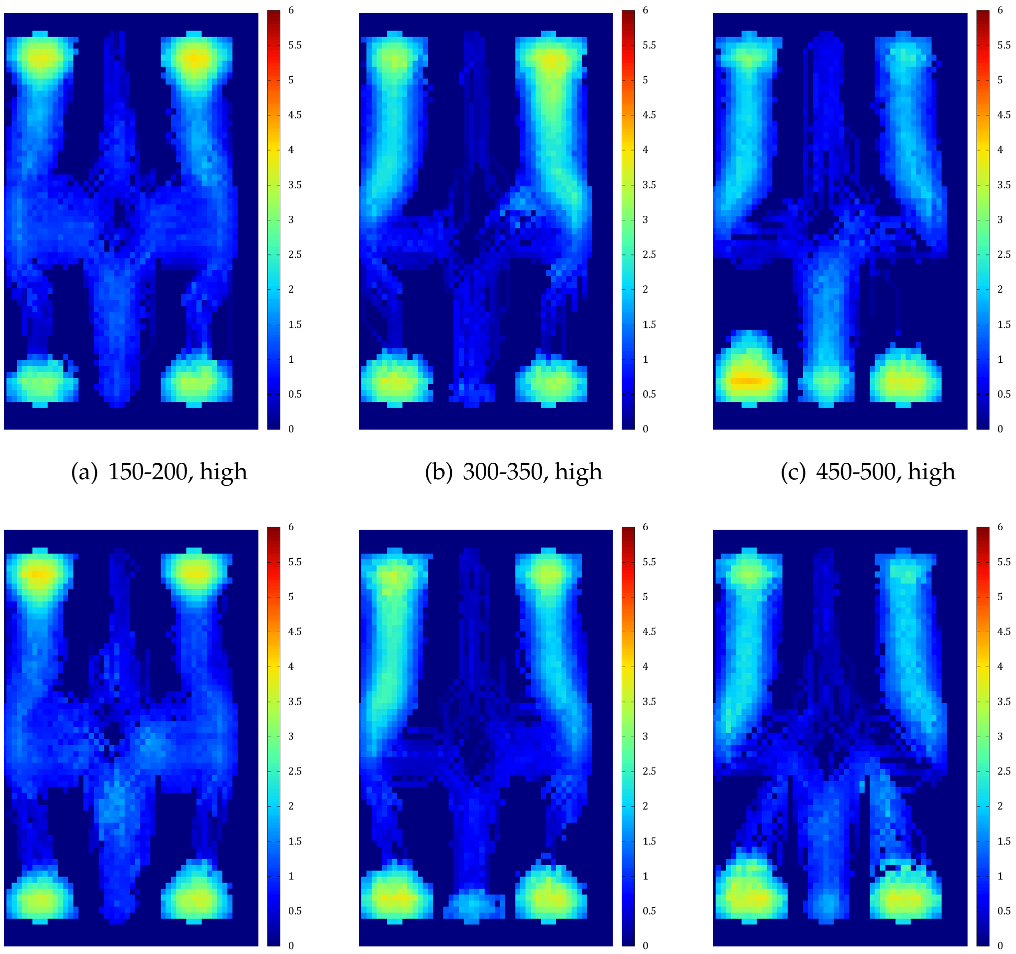

(a) 150-200, high (b) 300-350, high (c) 450-500, high

(d) 150-200, low (e) 300-350, low (f) 450-500, low

Figure 4.13: *The test scenario respectively with a high and low sensitivity of the agents for the plan re-computation. A few, but important, differences can be identified and explain the impact of the low sensitivity on the congestion areas: in this case the route adaptation is performed a bit after, leading to higher congestion in the employed exits.*

simulations scenario have been designed. Both benchmarks have been run in a laptop pc with CPU Intel(R) i7 2.3 Ghz, 16 GB RAM and operative system windows 8.1-x64.

The first scenario aims at evaluating the computational cost of only the operational level component of the model, by modeling a scenario that can host a large population of agents without the generation of congestion or other effects that can affect the normal execution: in case of congestion, in fact, the agents would evaluate less possibilities of movement, since the available space would be constrained, therefore also the com-

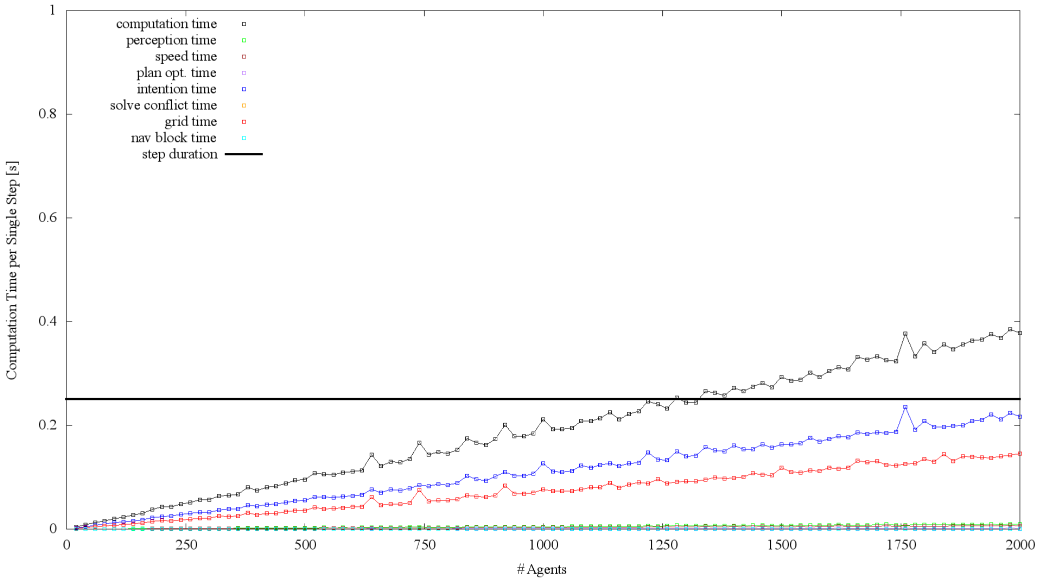

Figure 4.14: *Times for the computation of a single step achieved with the simulation of the operational level.*

putational times would be affected. After these considerations, a very large corridor environment of dimensions 200×200 m^2 has been designed. A single simulation hosting a uni-directional flow with an increasing number of agents has been run and at each time-step the computation time of each task has been collected. The results are shown in Figure 4.14. It must be noted that these results have been achieved without a parallel implementation of the software and, in addition, the provided implementation is not particularly optimized: the *Python* programming language has been used and it has not given a particular attention to the optimization of the data-structures.

An appreciable thing, on the other hand, is that the computational times are growing linearly with the number of simulated agents. By looking at the image, it is clearly understandable that the main activities of the operational level are the computation of the agent intention, comprising the utility evaluation, and the update of the dynamic grids (the floor fields) that costs almost half of the computation of the main activity. This leads the simulation to be faster than real time until about 1200 agents, when the turn duration of 0.25 seconds is reached by the total computation time. Since the discrete nature of the model and the parallel update strategy leads to a high suitability for an implementation using multiple processes and parallelization, this results can be significantly improved.

To preliminary quantify the entity of the tactical level, a slightly different scenario has been designed. The dimensions are the same of the corridor scenario, to again host a large amount of agents, but the settings is now composed of three large rooms

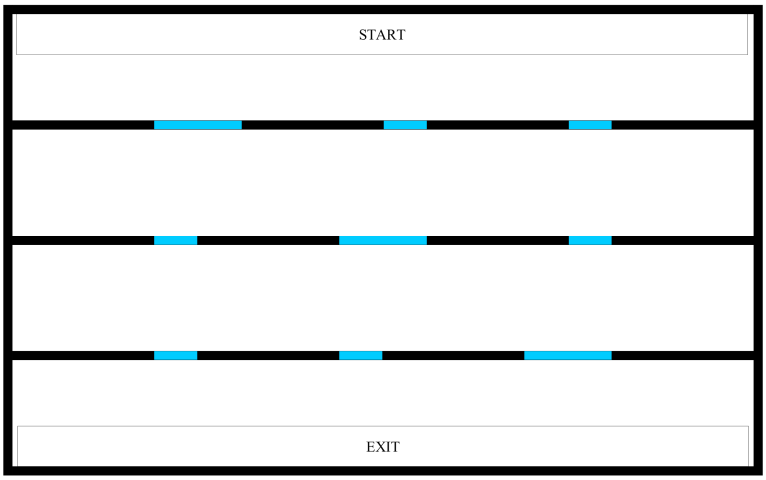

(a)

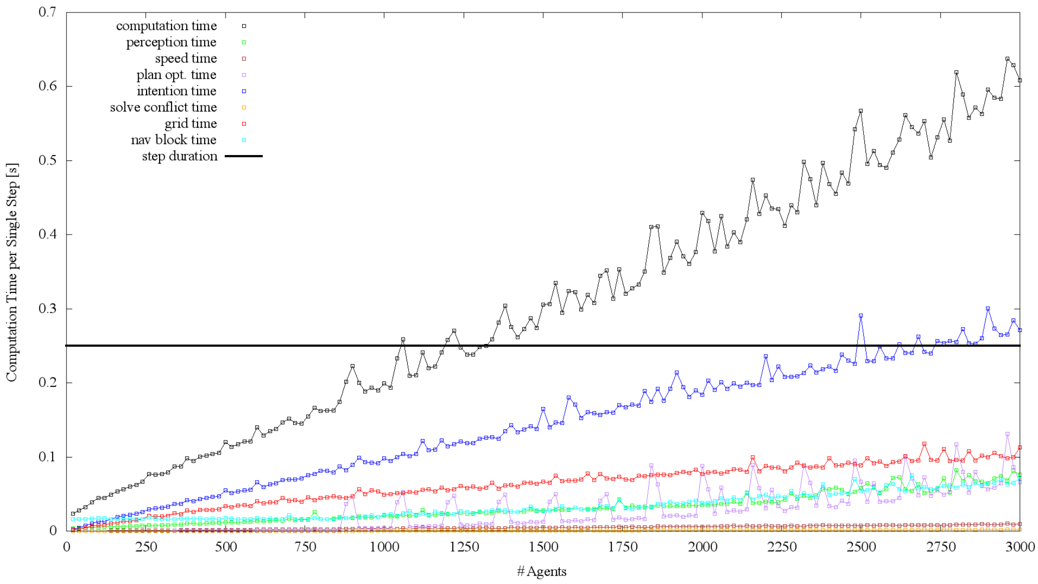

(b)

Figure 4.15: *The benchmark scenario (a) used for the analysis of the computational times of the tactical level and the respective results (b).*

connected one by one by three doors of different sizes: a large one of 5 m and two small ones of 2 m. The environment configuration is shown in Figure 4.15(a). Figure 4.15(b) shows the results of the computational times analysis. It is possible to notice that the trend is again linear and the results are overall very close to the ones previously achieved with the operational level: the computation of the agent intention is still the main component of the step computation. The tactical level affects the time by means of three main activities, which are the perception of the congestion in the chosen path, the eventual route re-computation and the calculation of the block probabilities for the estimation of the congestion time. The plan re-computation (the purple line in the Figure) is the most significant one, since it “bounces” from having the lowest value between the three activities to a much higher one sometimes also overcoming the floor field update of the operational level. In the end the trend of these activities is as well linear and their duration has remained almost not significant until 1000 agents for this simulation.

5

Coupling Mesoscopic and Microscopic Simulations: A Multiscale Model for Detailed Simulations of Urban Areas

The microscopic model presented in Chapter 3 provides a detailed behavioral model that is suitable for the simulation of purely pedestrian environment, allowing the consideration of an heterogeneous population, composed also of pedestrian groups, and with pedestrians able to adapt their decisions along the evolving of the simulation. On the other hand, as it has been shown in Section 4.3, this approach is relatively not able to scale with computational times over the number of agents and this restrict its possibilities of application in very large scenarios such as metropolitan areas. It must be noted that this problem is not only suffered by the previously proposed model, but it represents a general limit of the microscopic modeling.

During the PhD period and in particular with an internship abroad at the Forschunszentrum Jülich in Germany, an alternative investigated approach has focused on the possibilities to realize a multi-scale simulation model, with the integration of the mesoscopic and microscopic modeling approach. The overall aim has been to overcome the issues related to the computational times and to allow the simulation of large metropolitan areas with different level of details and also with different modes of transportation. On one hand, the simulation system should provide the possibility to introduce more details in some parts of the scenario, with the modeling of bi-dimensional environments. On the other hand, the mesoscopic approach would be used to design and simulate the metropolitan traffic network, with the usage of a queue model that is particularly suitable for these purposes.

The simulation of a so large area leads to a significant work to the user side and thus a brief consideration on the overall aims of this approach must be done. While the microscopic model mainly offers a simulation software which, given the input configuration of the pedestrian flows in the environment, leads to the recognition of possible critical zones. These can be later solved by testing eventual alternative solutions, aimed at modifying the directions of the flows or even the environment itself.

By considering a metropolitan area, this kind of work-flow is less plausible since it

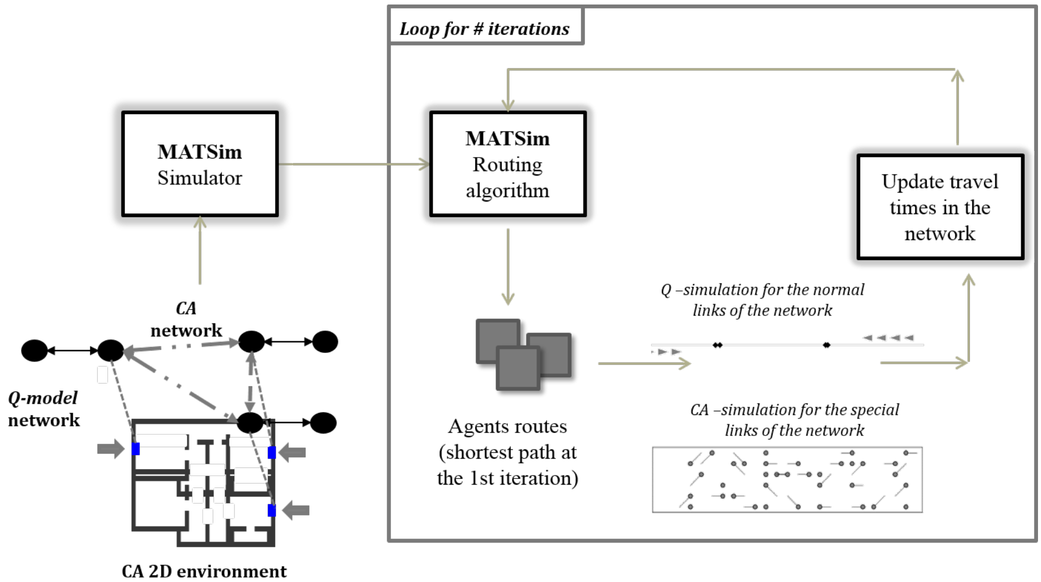

Figure 5.1: *The proposed approach for the multi-scale simulation system, employing mesoscopic simulations with MATSim and microscopic simulations with the discrete model proposed in this Chapter.*

could lead to an incredibly long job, given the explosion of situations and possibilities provided by the dimensions of the considered scenario. The overall aim of this simulation approach, therefore, is slightly different and aims to automatically find solutions – configurations of pedestrian and traffic flows – to optimize the traveling times, with the identification of equilibrium and optimum states. This will be performed with the iterative equilibrium search algorithm of the open-source mesoscopic simulation system MATSim, which will be integrated with the innovative and optimized microscopic model that will be presented in this Chapter. The contribution of the work here presented, in fact, is not located at the mesoscopic modeling approach, since state of the art methodologies will be directly used with the integration of MATSim. They are instead linked to the overall approach for the multi-scale simulation, offering a final product that allows an automatic optimization of the flows in relatively short times and considering road networks as well as bi-dimensional pedestrian environments.

The overall idea behind the integration is summarized in Figure 5.1. The bi-dimensional pedestrian environments are linked to the network of the mesoscopic model by means of their graph representation, representing the links among the intermediate and final targets of the scenario weighted with their traveling times. The simulation system MATSim then initializes the plans of the agents, configuring their routes. At each iteration, the simulation of both queue model and pedestrian model are executed in a synchronous way and without a dynamical adaptation of the routes.

After the simulation iteration, the routes of each agent are re-considered and eventually re-calculated by means of their experienced traveling times. It must be noted that the number of iterations for the convergence towards an equilibrium or an optimum state cannot be known a-priori and depends on the configuration of the simulation scenario. This provides high motivations for the design of a particularly optimized model that allows as well reliable simulations of pedestrian flows in bi-dimensional environments. The overall approach will be now described, starting from the discussion of the innovative discrete model and its physical properties, then explaining the algorithm for the iterative search of equilibrium states and finally providing the first results achieved with the simulation of pedestrian environments.

5.1 An Optimized Model for Fast Pedestrian Simulations

Given the aims explained in the introduction part, the model presented in this Chapter is a bi-dimensional Cellular Automaton with a square-cells grid representation of the space. The environment structure is similar to the one of the microscopic model discussed in Chapter 3, but will be as well briefly discussed in order to improve the readability. If the reader is familiar with the concepts introduced in the Sections describing the environment, he/she can skip the next Section, which will partially repeat them.

The Cellular Automaton rules are based on the idea explained by Flötteröd and Lämmel [2015] and defines an innovative extension in order to allow the simulation of bi-dimensional environments. Decisions at tactical level will be managed on the base of multiple destinations, introduced in the environment by the user, and with the iterative approach previously introduced and that will be argued in Section 5.2.

This Section breaks down as the following: Section 5.1.1 introduces the mechanisms of the environment that allow the pedestrians to move towards a destination, while Sec. 5.1.3 describes the rules that generate the dynamics of the system. Properties of the model are discussed in Sec. 5.1.4.

5.1.1 Environment Representation and Floor Fields

The environment is modeled by a grid of square cells, whose $0.4 \times 0.4\ m^2$ size describes the average space occupation of a person [Weidmann, 1993] and reproduces a maximum pedestrian density of 6.25 persons/m^2, that covers the values usually observable in the real world. A cell of the environment can be of type *walkable* or of type *obstacle*, meaning that it will never be occupied by any pedestrians during the simulation. It must be noted that the granularity of this grid can be too coarse to represent small objects like small columns or street lamps, but this work focuses to more macroscopic scenarios, avoiding this level of detail for the moment[1].

[1]In addition, this problem could be managed by using adaptive grid sizes and micro-stepping.

The movement of the simulated pedestrians is influenced by the location of their destinations. Path creation is handled on the tactical level, which is discussed in Section 4. It includes, for example, the avoidance of congested corridors if better, possibly longer, alternatives exit. On the operational level paths are decomposed into intermediate targets that are processed one after another. Here, intermediate targets mark the extremes of a particular region of the environment (e.g. a room or a corridor), with a complete analogous approach to the previous microscopic model, while final goals are the open edges of the environment, i.e., the entrances/exits of the CA space (an example is illustrated in Figure 5.2). Since the concept of region is fuzzy and the de-composition of the environment is a subjective task that can be tackled with different methods, the configuration of their position in the simulation scenario is not automatic and is left to the user.

Pedestrians are directed towards each target – either intermediate or final – by specific gradients spread on overlaid grids, which are the static floor fields. A relevant aspect is the way in which gradients are diffused from the targets. Different spreading methods can lead to different space utilizations of the simulated pedestrians. The work of Kretz et al. [2010] gives an overview about the most common methods. As also for the microscopic model, the *Chessboard* metric with the $\sqrt{2}$ variant over corners has been used in this model, since provides better results than the other presented metrics.

An important aspect of the floor field diffusion algorithm is the stopping criterion. If no stopping criterion is defined the method spreads the floor field to all cells of the environment. In this work, the diffusion is stopped at obstacles and intermediate targets. The main reason to stop at intermediate targets, is to allow a complete representation of all possible paths, as it has been already discussed in Section 3.1 and it is again reported in Figure 5.2. In general, it allows to map the environment onto a network, where nodes represent targets and links describe the presence of a direct connection between two targets (i.e. there are no other intermediate targets to cross in between). This makes path computation simple and reduces the computational costs, because floor fields are only computed where needed. Moreover, it would allow to parallelize the floor field computation in a simple way. The resulting network will be mapped to the MATSim network, as previously introduced, and will be thus used on the tactical level for the route computation at each iteration. Details on this aspect are discussed in Section 5.2.

5.1.2 Method for the Local Density estimation

The estimation of *local densities* is very important for this model, allowing it to reproduce empirically derived fundamental diagrams as well as disaggregated dynamic situations, by means of a simple set of rules managing the pedestrian motion. These rules depend also on the local pedestrian density, therefore a valid density estimation approach is needed.

Several methods have been defined in the literature to accomplish this task (see Stef-

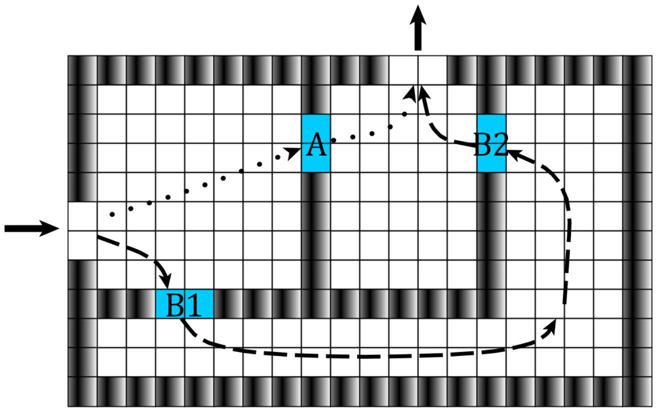

Figure 5.2: *Example of a scenario with different paths leading to the exit. The need to stop the floor field diffusion of the intermediate target $B2$ in the cell of A is evident: by diffusing it over the whole space, pedestrians travelling from $B1$ to $B2$ would travel as well through A cells.*

fen and Seyfried [2010]) and the resulting most versatile is the so-called *Voronoi* method. The positive peculiarity of the method is that it provides a stable and continuous value of the local density in every point of the scene, without the need of any calibration parameter. On the other hand, its computational complexity is relevant and in case of discrete models its improvements in the precision are limited. The computational cost of this model has been kept low by means of a more simple and efficient method for a discrete calculation of the local density, computing the *number density* of pedestrians. This quantity describes the overall density of people in the surrounding of each cell, within a constant distance. The method is the same as the one explained in Chapter 3 and it is briefly summarized in the following.

The estimation is performed with an additional grid working as a dynamic floor field, changing its values over time. The simple idea is to spread the presence of each pedestrian in the nearby space, i.e., in all cells belonging to a fixed radius d of distance. This parameter defines the local aspect of the density calculation and is the only parameter of the method. The local density ρ of a cell c is calculated as:

$$\rho = \frac{n}{A(c)} \tag{5.1}$$

where n representing the number of persons within the distance d from the cell c and $A(c)$ is the area of the set of cells (i) belonging to the same neighborhood and (ii) which are not containing obstacles. The second point is particularly important, since it means that the presence of obstacles restricts the local area where the calculation is performed. The main purpose is that the calculation must give an idea of the available

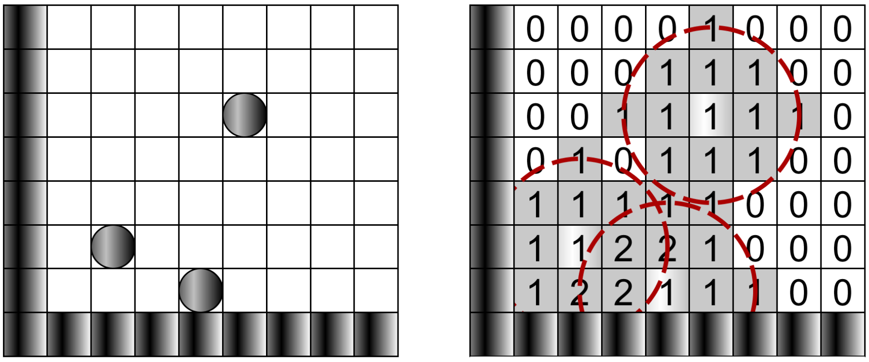

Figure 5.3: *The density field working principle: at the beginning of the time-step, pedestrians signal their presence by adding 1 in the nearby cells (here the radius is 2 cells).*

space for the pedestrians.

The update phase of the density grid is illustrated in Figure 5.3: at the beginning of each simulation step, the presence of pedestrians is spread to the surrounding cells, which are not containing obstacles, within radius d. In this way each cell of the grid contains the n value. The area $A(c)$ must be calculated for every cell of the environment at the beginning of the simulation, but in any case the total cost of the computation grows linearly with the number of pedestrians (see Section 5.3.4 for a analysis of the computational times).

5.1.3 Rules of the Dynamics: Definition and Implementation for 2-dimensional Environments

The proposed CA model offers a computationally efficient calculation of the pedestrian dynamics in bi-dimensional environments. Table 5.1 gives a parameter overview. The models extends the ideas and rules of Flötteröd and Lämmel [2015], who discussed a theoretical model on one-dimensional pedestrian flows. In the theoretical model the movement is controlled by three rules:

- **Movement rule**: a pedestrian cannot change her position before τ_m seconds,
- **Jam rule**: if a cell is occupied at time t by the pedestrian p, every pedestrian $\overline{p} \neq p$ cannot occupy that cell before time $t + \tau_j$,
- **Counter-flow rule**: if two pedestrian in two consecutive cell at time t are in a head-on conflict, then they will swap their position ("squeeze past" each other) at time $t + \tau_m + \tau_s$.

The movement rule defines the free-flow cell travel time, as well as the time-step duration of the discrete model. In this way, the equal maximum speed for all

Parameter	*Value*
density spreading parameter d	2
time-step duration tau_m	0.3s
conflict delay coefficient β	0.39s
conflict delay exponent γ	1.43
normalization factor η	1
sensitivity parameter κ_F	6
cell side length $cell_side$	0.4m

Table 5.1: *Assignment of the parameters of the new CA model.*

pedestrians is given by the ratio $cell_side/\tau_m$. In the present work τ_m is assumed to be 0.3 s, in order to have a pedestrian speed of about 1.3 m/s. Other approaches allow for individual maximal speeds, as the one discussed in Section 3.4.3. These approaches allow to overcome artifacts resulting from the space discretization, as well as from the diagonal movements that here imply an increase of the pedestrian speed by $\sqrt{2}$. This contribution focuses on the reproduction of fundamental properties in particular for higher densities. Therefore, individual maximal speeds are out of scope, but will be part of future directions.

Flötteröd and Lämmel [2015] discuss the following continuity constraint, without it the model would behave discontinuously when going from arbitrary small but strictly positive counter-flow to a uni-directional flow:

$$\tau_j = \tau_m + \tau_s \tag{5.2}$$

Furthermore, they made the jam and counter-flow parameters density dependent and used a least squares estimator to fit the model against empirical data. The density dependence is defined by the following equation:

$$\tau_s = \beta \left(\frac{cellSide \cdot \rho}{m^{-1}} \right)^{\gamma} \tag{5.3}$$

where $cell\_side$ is the width of the pedestrian, ρ is the local density for the pedestrian under consideration, and (β, γ) are parameters.

This contribution extends the work of Flötteröd and Lämmel [2015] and the related computer implementation to two-dimensional environments. In a one-dimensional environment the movement is constrained to streams of pedestrians, while in a two-dimensional environment pedestrians can move freely in multiple directions. There are various options how the direction choices can be modeled.

In this work, pedestrians choose their movement directions by a simple probability function, similar to the one of the floor field model by Burstedde et al. [2001]. The

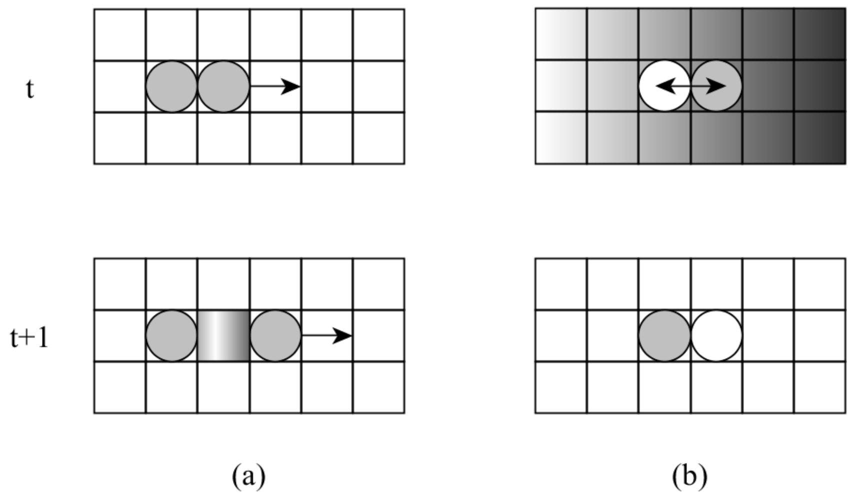

Figure 5.4: *The jam (a) and counter-flow (b) rules. In (a), the cell that became empty remains blocked. In (b) two counter-flow pedestrians (the light pedestrian follows the dark color and vice-versa) swap their positions.*

movement capabilities of pedestrians are restricted to the Moore neighborhood, allowing them to also perform diagonal movements. The probability for a pedestrian at location xy to move to the cell with coordinates ij is:

$$P_{ij} = \eta \, \varepsilon_{ij} \, e^{\kappa_F (F_{xy} - F_{ij})} (1 - \Omega_{ij}) \tag{5.4}$$

where η is a normalization factor; ε_{ij} describes the impenetrability of obstacles (i.e.: it is 0 if there is an obstacle in ij, 1 otherwise); F_{xy} and F_{ij} are the values of the static floor field respectively in the position of the pedestrian and the evaluated position; Ω_{ij} forbids movements in cells already occupied by other pedestrians, basically returning 1 if ij is not free or 0 otherwise; κ_F is a calibration parameter.

The *update strategy* is parallel, meaning that not all the intentions of movement lead to a position change at the end of the step. Conflicts arising for choices of the same destinations are dealt with by a randomly extracting a winner, leading the other involved pedestrians to yield and choose a new move at the next simulation time-step.

The adaptation and implementation of the jam and counter-flow rules are graphically explained in Figure 5.4.

The first mechanism implements the jam rule by extending the presence of pedestrians for τ_j time to their previously occupied cells. The procedure works as follows: each pedestrian that moves at time t leaves a tag ω_t on its previous position. This tag will act as an obstacle for every person until time $t + \tau_j$. In this way, every person will cause a delay only to the persons behind. The leaders of a line, thus, will not be affected by the

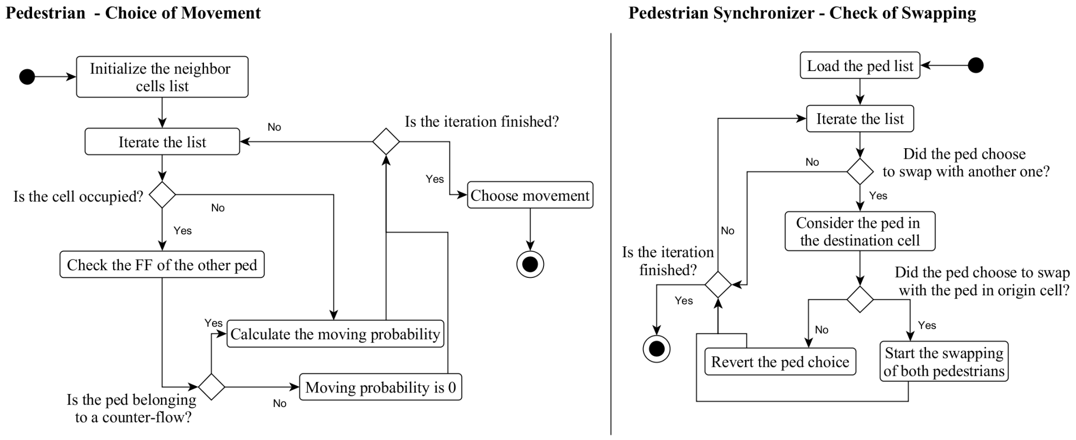

Figure 5.5: *Activity diagram illustrating the algorithm for the swapping rule of the CA. Pedestrians check the direction of the others in front by the floor field (FF) and are allowed to choose movements in positions occupied by counterflow pedestrians. At the end of the step, the Pedestrian Synchronizer swaps only those pedestrians, where movement choices match.*

eventual congestion behind them and, albeit density perception is isotropic, the overall be-havior is anisotropic, as observed in real-life. Since the time is discrete, a naïve implementation of this mechanism would require τ_j to be a multiple of the time-step duration τ_m. Nonetheless, a usage of $\tau_j \in \mathbb{R}$ is allowed and has been implemented by introducing a stochastic management of this variable. The tag ω_t will stay in the cell for at least $\left\lfloor \frac{\tau_j}{\tau_m} \right\rfloor$ simulation time-steps, while the decimal part of the fraction will define the probability that the trace will stay for one additional time-step longer. This aspect is important since the parameter vary with the local density ρ, according to the continuity constraint 5.2 and the density dependent conflict delay 5.3.

The counter-flow rule implies that two pedestrians which chose to swap their position, due to opposite movement directions, will do so after $\tau_m + \tau_s$ seconds. The question of having $\tau_s \in \mathbb{R}$ is again valid as discussed above and the same method is used.

A deeper clarification needs to be provided about the definition and recognition of counter-flow during the simulation: when the position swapping becomes available for the two pedestrians, and how it is performed (see, Figure 5.4 (b) for a illustration). The swapping, in fact, is a coordinated action, which needs to be synchronized. To allow this, the algorithm graphically explained in Figure 5.5 has been introduced, designing the following *hand-shaking* protocol:

1. pedestrian A choose to move to the cell where pedestrian B resides;

2. pedestrian B choose to move to the cell of pedestrian A;

3. pedestrian A and B swap positions and start waiting $\tau_m + \tau_s$ seconds before they choose the next movement.

This sequence of events describes, of course, only the successful option: if one of the two pedestrians does not choose to swap, the other one would stay where she is and choose a new move in the next simulation time-step. In any case, the hand-shaking protocol starts with the assumption that at least one of the two pedestrians chooses to move to the position of the other. The probability function 5.4 would not allow this kind of selection due to Ω_{ij}. To solve this issue Ω_{ij} needs to return 0 not only for empty cells but also for those that are occupied counter-flow pedestrians. Counter-flow pedestrians can be identified by comparing values of the individual perceived floor fields. Let assume pedestrian A and B are at locations ij and xy respectively, with each cell belonging to the Moore neighborhood of the other. Pedestrian A will identify B as a counter-flow pedestrian, and vice-versa, if and only if both values $F_{ij} - F_{xy}$, by considering the static floor field felt by B, and $F_{xy} - F_{ij}$, by considering the static floor field of A, are positive, i.e., they effectively belong to two opposite flows.

5.1.4 Model Properties & Validation

To validate the CA on the operational level a uni-directional and a bi-directional experiment have been performed. The settings mimic those of the laboratory experiments of Zhang et al. [2011] and Zhang et al. [2012]. Thus, a straightforward comparison of the simulation re-sults with the empirical observations is possible. The comparison is limited to the unidirectional and bidirectional FD. In the experiments, the pedestrian walk through a channel. For the unidirectional case the inflow into the channel is controlled by an entrance bottleneck, while the outflow is limited by an exit bottleneck of variable width. For the bi-directional case entrance bottlenecks just in front of the channel control the inflows. The outflow is unbounded, which means pedestrians can leave the channel unhindered either to the right or to the left, circumventing the entrance bottlenecks. In the bi-directional case the flows are balanced (i.e. inflow and consequently directional densities are similar). To cover the whole range of densities a number of simulations with variable population sizes have been setup.

To determine the flow generated by the CA, the travel time from the beginning to the end of the corridor has been recorded for every pedestrian, converting it to the specific flow according to:

$$J(\rho) = \rho \cdot \nu$$

where $\nu = corridor_length/travel_time$ describes the average speed of the simulated pedestrians and ρ the average density inside the channel. For every setting the simulation has been run long enough with a sufficient number of pedestrians to reach a stationary state (i.e. until flow and density remains constant). For both, uni-directional

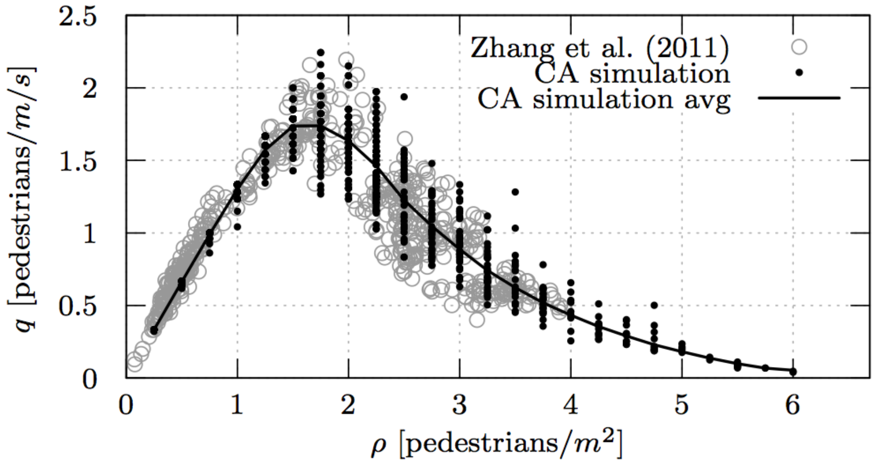

(a)

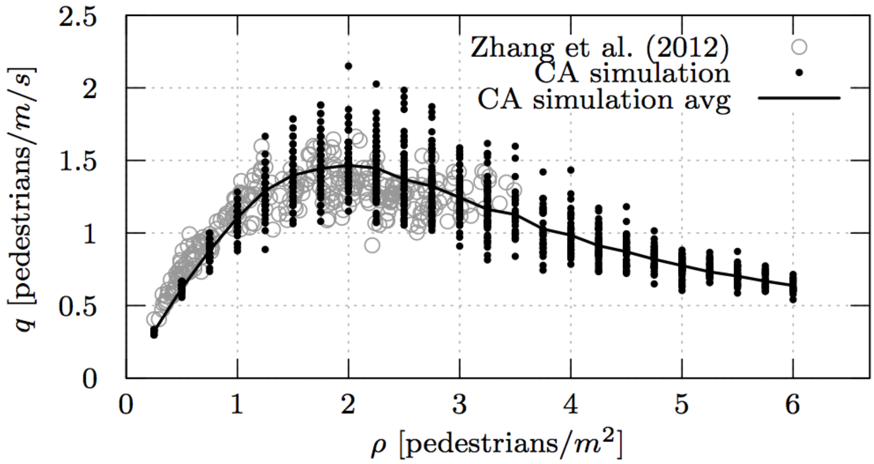

(b)

Figure 5.6: *Fundamental diagrams for uni-directional (a) and bi-directional (b) flows. Black dots are measurements from the simulations, while gray circles are the empirical data from Zhang et al. [2011, 2012]. Average flow per simulated density is indicated by the solid curve.*

and bi-directional case, the simulation based fundamental diagram is created from measurements that are collected during stationary states.

A comparison of simulation based FDs with those of the laboratory experiments is given in Figure 5.6 (a) and (b).

Simulation based results show an almost perfect agreement with the available empirical data. Nevertheless, the simulation extrapolates to densities for which no empirical data exits.

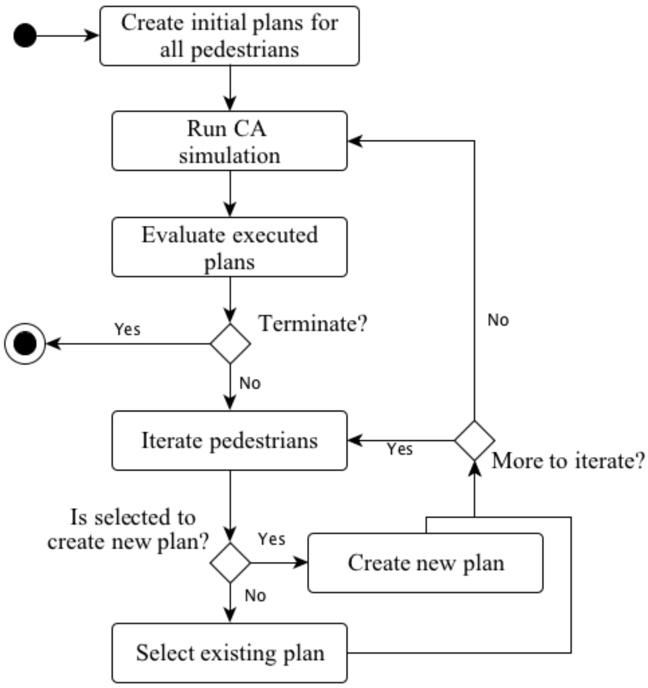

Figure 5.7: *Illustration of the route assignment search strategy.*

The plot for the bi-directional case in Figure 5.6 (a) demonstrates that the model is able to sustain stable flows over the whole density range and thus overcome the unrealistic rapid state transition from free flow to total jam as observed, e.g., in the work of Fukui and Ishibashi [1999]. Another observation is that for high densities, beyond capacity, the bi-directional flow exceeds the uni-directional flow. This is in line with findings that have been widely reported in empirical studies (see, e.g., Kretz et al. [2006], Zhang et al. [2012], Liu et al. [2014]).

5.2 Iterative Route Assignment Strategy

This Section discusses the route assignment on the strategic and tactical level. Raney and Nagel [2004] propose an iterative approach, where vehicular route assignments move towards a Nash equilibrium (NE). Oncoming vehicles move in opposite lanes and thus do not interact. In contrast, this contribution deals with a CA simulation for omnidirectional pedestrian flows. This opens, besides the question of general applicability, also some computational issues.

The general approach is depicted in Figure 5.7. At startup the simulation framework creates initial plans. In the underlying work, plans are limited to routes with specific departure times[2]. The initial plans are executed in the CA simulation and subsequently evaluated. After the plans evaluation it must be decided whether to continue or to terminate. If the simulation framework runs on, the pedestrians will revise their travel plans, before the cycle starts again. In the following, Section 5.2.1 discusses plans creation, Section 5.2.2 plans selection, and Section 5.2.3 the termination criterion.

5.2.1 Plans Creation

As discussed previously, the simulation environment is mapped onto a set of nodes (targets) that are connected by unidirectional links. Routes (i.e. lists of targets) for the initial plans are computed by the A^* shortest path algorithm. Link weights correspond to free speed travel times. The free speed travel time T_a^{free} for link a of length l_a is defined as:

$$T_a^{free} = \frac{l_a \cdot \tau_m}{cell\_size} \tag{5.5}$$

The actual length of a link is not obvious, since a link represents a rather abstract relation from one target (origin) to the next target (destination). A reasonable behavioral assumption is that, in the absence of others, real people choose the shortest connection between two targets. The length of the shortest connection from an origin to a destination has implicitly already been computed by the floor field generation (see Section 3.4.5 where a distance metric using floor fields is defined). The value of the floor field for a given cell corresponds to the shortest distance between this cell and the origin from where the floor field has been spread. In this way the link length is determined at the beginning of the simulation.

When pedestrians travel from one target to the next one, they experience individual travel costs. Travel costs are averaged over time slices k and stored in hash tables for later use as discussed in Lämmel et al. [2010]. An obvious travel cost component is travel time.

Pedestrians, who are selected to create a new plan, compute new routes based on the averaged time-dependent travel costs from the previous CA simulation run.

Let $T_a(k)$ denote the averaged time-dependent link travel time of link a and time slice k. If time is the only travel costs component, then the overall route assignment moves towards an NE.

Another component is the time-dependent delay that individual pedestrians impose to others because of their route choice. Following the nomenclature used in economics, the time-dependent delays imposed to others are external costs, while the time dependent travel-times are internal costs. Let $E_a(k)$ denote the time-dependent external costs that a pedestrian imposes to the others if it enters link a during time slice k. The sum of internal and external costs yield the marginal social costs:

[2] In general, plans can cover complex activity chains, e.g., of travel related daily routines. This is, however, beyond the scope of this contribution.

$$M_a(k) = T_a(k) + E_a(k) \tag{5.6}$$

If new routes are computed based on the marginal social costs the overall route assignment moves towards the system optimum (SO). Unlike internal costs (travel times), external costs are not directly observable, but they can be derived from the observed flow dynamics of the CA simulation. Lämmel and Flötteröd [2009] give a continuous formulation of the external costs for a queue simulation model. They derive the following approximation from the continuous formulation:

$$e(t_0) = t^e - (t_0 + T^{free}) \tag{5.7}$$

where $e(t_0)$ are the individual external costs for a traveler who entered a congested link at time t_0 and t^e is the time when the congestion dissolves. In the following a simpler implementation in the CA simulation context is discussed.

External costs occur only on delayed links. These are links where obstruction occurs. The current implementation estimates the external costs for all links isolated and thus neglects spillback. Furthermore, it is assumed that the flow on the isolated links is stationary for the whole period where delays occur. Assume the pedestrian under consideration enters link a at time t and leaves it again at time t'. The pedestrian traversed link a during a period of delays if and only if $t' - tT_a^{free}$. In this case, the pedestrian impose external costs to the system. Under the stationarity assumption the outflow q_a of link a stays constant for the whole period. Thus, the amount of delay the pedestrian imposes to each subsequently following pedestrian is $1/q_a$. The number of delayed pedestrians is equal to $q_a \cdot (t^e - t')$. This yields for its individual external costs:

$$e(t) = q_a \cdot (t^e - t') \cdot \frac{1}{q_a} = t^e - t' \tag{5.8}$$

The individual external costs are in the same way aggregated and stored in hash tables as the travel times. NE routing and SO routing are applied under the assumption travel costs remain the same from one CA simulation run to the next. However, running the CA simulation with changed route assignments might also change the travel costs. A best practice to deal with this issue is to select only a fraction of 10% of all pedestrians for new plans creation. Those pedestrians who do not create new plans select a previously executed one from its memory.

5.2.2 Plans Selection

The plans selection procedure is similar to the Metropolis sampling approach [Metropolis et al., 1953]. In order to apply this approach, plans need to be scored. The score of a plan is the negative value of its experienced travel costs (travel times for NE and marginal social costs for SO). Let s_c be the score of the currently executed plane and s_r

is the score of a randomly selected plan from memory. The probability to switch from the current plan to the randomly selected one is:

$$p_{switch} = \min\left(1, \kappa \cdot e^{\lambda \cdot (s_r - s_c)/2}\right) \tag{5.9}$$

The parameter κ reflects the probability to switch when both plans have the same score and λ is a sensitivity parameter. In this work these parameters are set to $(\kappa, \lambda) = (0.01, 1)$.

5.2.3 Plans Termination

Obviously, the simulation framework should terminate once the desired route assignments haven been reach (i.e. either NE or SO). This opens two questions: (i) how to detect whether NE or SO have been reached and (ii) does the system converge after all?

The first question can be answered by performing a simple test. An intrinsic property of an NE is that nobody can find a faster route by unilateral re-routing. Furthermore, the SO corresponds to an NE with respect to the marginal costs instead of travel times [Beckmann et al., 1956]. Thus, SO and NE can be verified by the same test. An according test would have to iterate over all pedestrians to create new plans. If the new plans are exactly the same as the old ones the system would have reached a fixed point and thus depending on the cost function an NE or the SO. This leads to the question regarding convergence and uniqueness.

Because of the stochasticity of the system a fixed point might never be reached and convergence and uniqueness remains unclear. Instead, the termination criterion is decided heuristically by looking at the changes in average travel times over iteration cycles. Once those changes remain small, the system is in a relaxed state and the simulation framework terminates. From experience it is usually enough to run 100 iterations to reach a relaxed state as also shown in the next Section.

5.3 Results on Experimental Scenarios

The overall performance of the proposed simulation framework is demonstrated by a number of simulations. Firstly, tests of the simulation approach on well-known transportation paradoxes will be presented. Then the investigation will continue with laboratory experiments. Finally, a simulation on a large scenario will show the overall functioning of the iterative model and after that a discussion on the computational cost will finish the Chapter.

5.3.1 Paradoxes in Transportation Networks

The transportation paradox by Braess [1968] is illustrated in Figure 5.8(a). After an initial long channel, the network presents a choice between two paths: a long one (c)

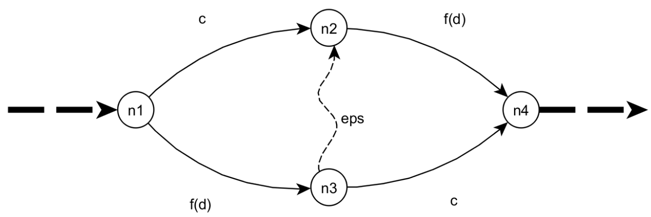

(a)

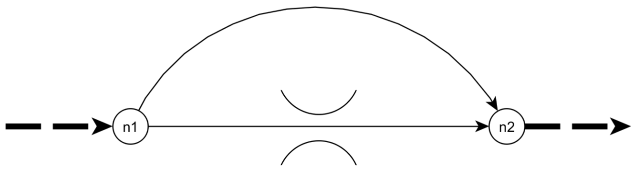

(b)

Figure 5.8: *Graph representations of the network explained by Braess [1968] (a) and Daganzo [1998] (b). Labels of edges represent their cost.*

with a constant travel time and a shorter one (f(d)) whose travel time is affected by the number of travelers. Connecting the two nodes at the center, as illustrated by the dashed link, will influence the path choice of the travelers, leading to a decrease of the network performances. The paradox asserts that an improvement to the structure of the network can lead to a worsening of the outgoing flow under Nash conditions but does not so for the SO. To simulate the situation defined by the paradox, the pedestrian environment has been configured as in Figure 5.9 (a). The two narrow corridors (top left and bottom right) represent the capacity restricted short links of the Braess paradox. The high capacity links are modeled as wide zigzag corridors (bottom left and top right). The central corridor implements the special link in the Braess paradox (dashed link in Figure 5.8(a)). In the absence of the special link, the pedestrians will utilize the upper and the lower path equally. However, once the special link is there, at least a fraction of pedestrians will walk from the top left narrow corridor via the special link to the bottom right narrow corridor. Once this happens, the path via the wide bottom left corridor to the narrow bottom right corridor becomes slower than the analog path along the top. Thus, more and more pedestrians will switch to the top left narrow corridor, leading to a complete disuse of the bottom right wide corridor. Effectively, the capacity of the network will be reduced to that of one single narrow corridor.

A crowd of 2000 pedestrians that walks from the left en-trance to the right exit of the environment has been setup. Figure 5.10 (a) shows the results for the NE approach. In case the special link is not present (i.e. the central corridor is blocked by obstacles), the average travel time stabilizes at about 13 minutes. Once the central

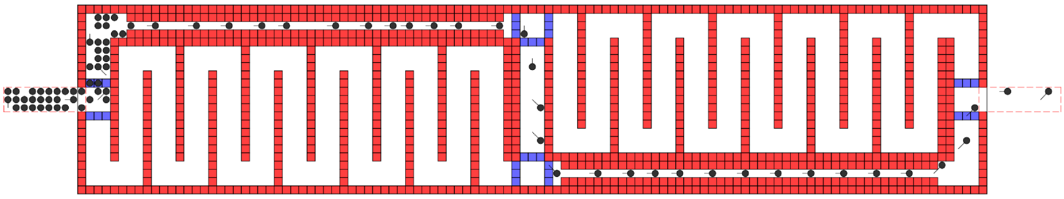

(a)

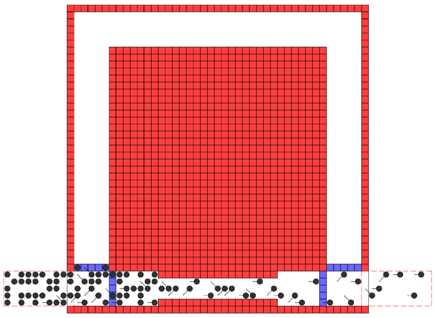

(b)

Figure 5.9: *(a) Implementation of the Braess (the corridor at the center is the additional link) and (b) Daganzo (with bottleneck width of 1.2 m) experiments. The environment borders and blue objects represent the nodes of the underlying network.*

corridor becomes available the average travel time decreases to 22 minutes. Thus, the NE route assignment behaves exactly as Braess asserts. Since the SO is a state with minimum average travel time, the presents of the special link must have no negative impact. This is shown in Figure 5.11 (a), where the average travel time is about 13 minutes in both cases, the SO approach works as expected.

Daganzo [1998] discusses a generalization of the Braess paradox, exempli-fying another situation where a structural improvement to the network reduces the outflow for NE. The described network is reported in Figure 5.8(b), characterized by a choice between a short link, containing a bottleneck, and a longer but wider one. If the examined network is improved by increasing the width of the bottleneck – until the travel time of the short link is smaller than the other one, even in the congested case – the Nash equilibrium will imply disuse of the long link, negatively impacting on the outgoing flow from the network.

To represent this example, the environment for the CA has been designed as in Figure 5.9 (b). Three sets of experiments have been tested, describing different bottleneck widths inside the short link, with a crowd size and arrival frequency similar to the configuration of the Braess experiments. NE results are shown in Figure 5.10 (b), explaining the key-point of the paradox: once reached a condition of equilibrium, the average travel time related to the scenario with the narrowest bottleneck is lower

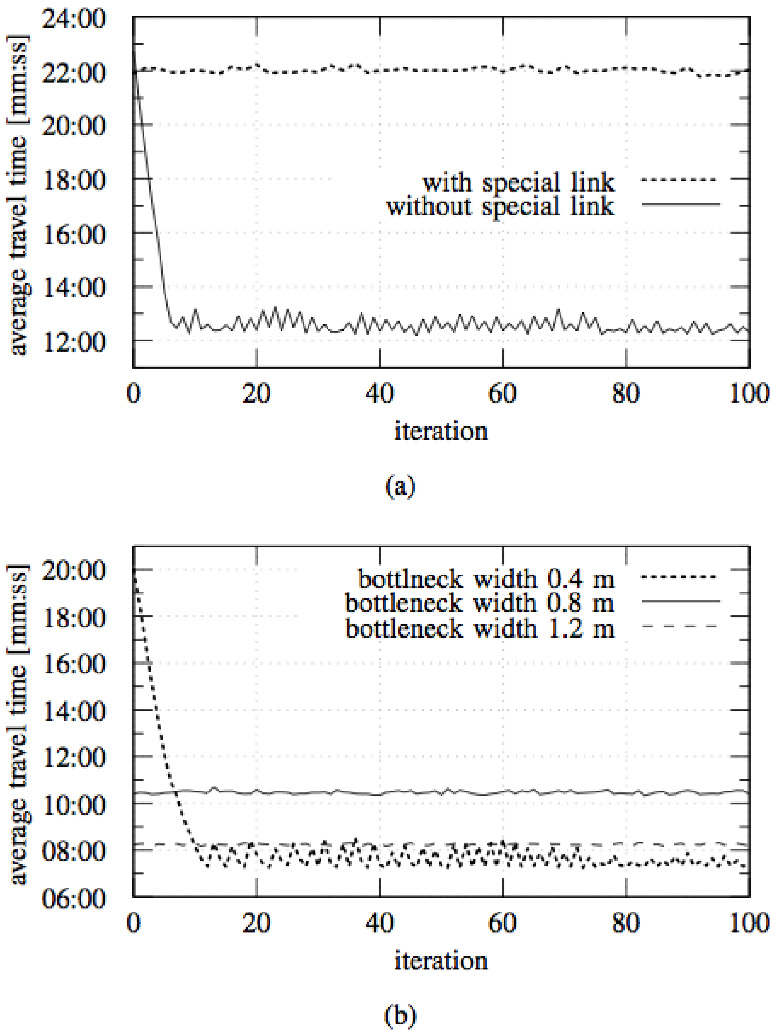

Figure 5.10: *Average travel times of agents within the simulations of the Braess (a) and Daganzo (b) paradox scenarios.*

or equal to the other ones. Similar to the Braess example, those paradoxes are not observed in the SO case, as depicted in Figure 5.11 (b).

These observations imply an interesting application of the Nash equilibrium and system optimum approach. It is generally accepted that travelers try to minimize their individual travel time during their daily commutes. Thus, transport systems are rather in a state of an NE than in the state of the SO. However, as it has been shown in the experiments, there might be situations where the SO solution coincides with an NE in a slightly different network. Moreover, the SO also tells how the network has to be changed in order to force the NE towards the SO. An approach to realize this could

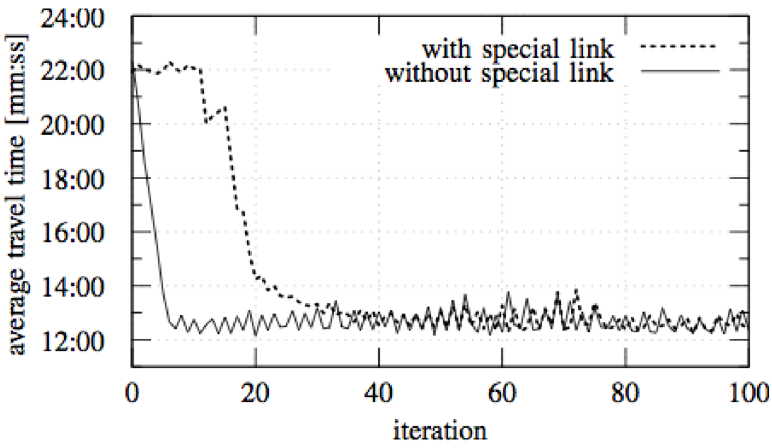

(a)

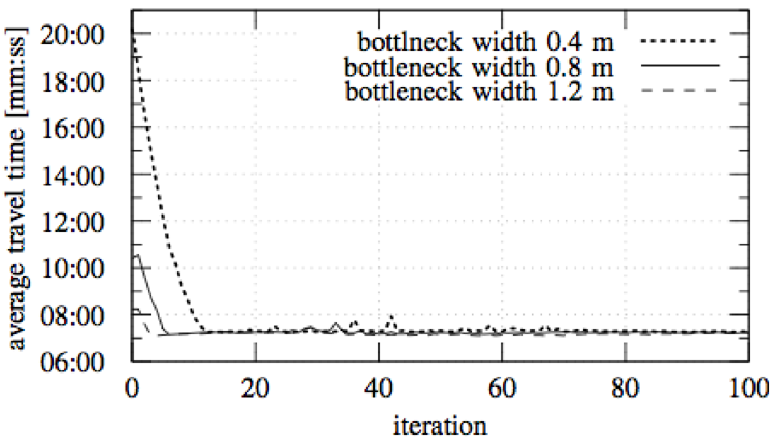

(b)

Figure 5.11: *Iterative system optimum search for the scenario of the Braess (a) and Daganzo (b) paradox.*

make use of the observed flows in the SO and use these values as the maximum allowed flow for the NE (e.g. by introducing artificial bottlenecks). This approach has indeed limitations as it makes the assumption of static flows[3]. Still, it works for both paradoxes discussed in this section. In the Braess example no pedestrian takes the special link in the SO case. This implies when blocking the special link the NE coincides with the system optimum (cf. Figures 5.10 (a) and 5.11 (a)), which is exactly what is stated in Braess [1968].

[3]The static flow assumption can be softened to a piecewise static flow assumption by introducing dynamic bottlenecks that can be adapted over time.

For the Daganzo experiments it is observed that in the SO case the flow on the restricted short link never exceeds the flow that can be handled by a bottleneck of 0.4 m width. Thus, restricting the flow to this value the NE also moves towards the SO. This has indeed been shown in Figure 5.10 (b). The ratio between the average travel time of an NE and the SO is also known as the *price of anarchy*. It gives an indicator about how much gain is possible by changing the layout of the network or the behavior of the travelers (see, e.g., Roughgarden [2005] for a detailed discussion on this matter).

5.3.2 Effects of Bi-directional Flows on the System

This section demonstrates how accurate the proposed CA model reproduces pedestrian dynamics observed under laboratory conditions. The proposed model is tested on two data sets gathered at Technical University Berlin in Germany. The first dataset describes a bi-directional flow experiment, where two groups of pedestrians move past each other with an inter-section angle of 180 degree. The groups consist of 47 and 51 volunteers respectively. Details about the experiments and the data set are discussed in Plaue et al. [2011].

Plaue et al. [2012] report a dataset of a crossing experiment, where two groups of pedestrians cross at an intersection angle of 90 degrees. The groups consist of 78 and 143 volunteering university students respectively.

The general layout is the same for both experiments. The CA grid layout used for the simulations is depicted in Figure 5.12. Solid arrows indicate the movement direction for the 90-degree intersection experiment and the solid left-to-right arrows and the dashed arrows indicate the movement directions for the 180-degree intersection experiment.

One way to appraise the feasibility of the proposed simulation model is comparing time series for speed and density (density over time and speed over time) resulted from the simulation with those observed in the laboratory experiments. To do so, it is necessary to apply the same method to collect the data for both the simulation and the experiments. The data from the laboratory experiments is provided as person individual. Similar trajectory files have been created from the CA simulation results. Densities and speeds are measured in a 7-by-7 cells area (2.8 m x 2.8 m) as indicated by the dashed red square in Figure 5.12, using a method based on Voronoi diagrams following Steffen and Seyfried [2010]. The CA simulation resolves conflicts in a probabilistic way, thus speeds, flows and travel times are stochastic and depend on the initial random seed. To appraise this effect each simulation run has been repeated 1000 times with different ran-dom seeds and both the time series of average density (speed) and the corresponding standard deviation is reported in the following plots. Figure 5.13 refers to the 180-degree intersection experiment. It compares the time series of average density (a) and average speed (b). There is a good general agreement between the simulation and the experiments. The standard deviation *sd* is small, indicating that the dynamics produced by the CA simulation is independent of the random seed.

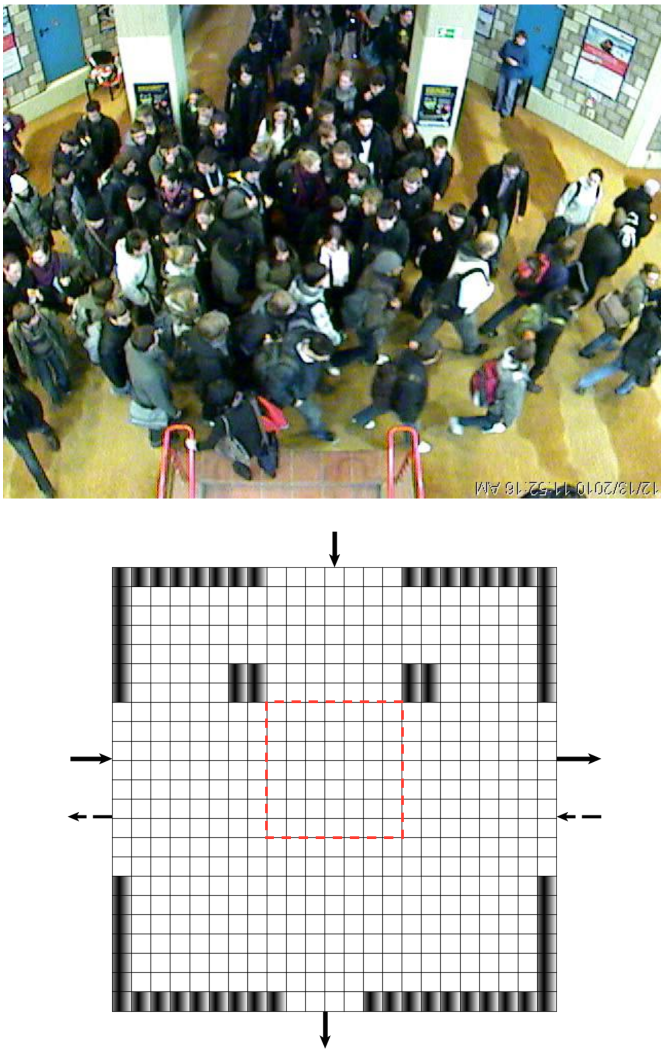

Figure 5.12: *A frame taken from the footage of the experiments performed by Plaue et al. [2012] and the CA environment layout for both 90- and 180-degree intersection experiments.*

Towards the end (after 27 sec), there is a deviation in the observed speed. While the simulated speed keeps constant, the observed speed drops down. One explanation for this deviation is that in the laboratory experiments the last pedestrians walking through the scene display a lag of motivation and are walking much slower than actually possible[4]. The proposed CA does not model different kinds of motivation but instead always assumes that pedestrians are determined to walk to the desired

[4]This lag of motivation is clearly visibly in the video recordings of the experiment. The recordings are available at http://www.math.tu-berlin.de/projekte/smdpc/

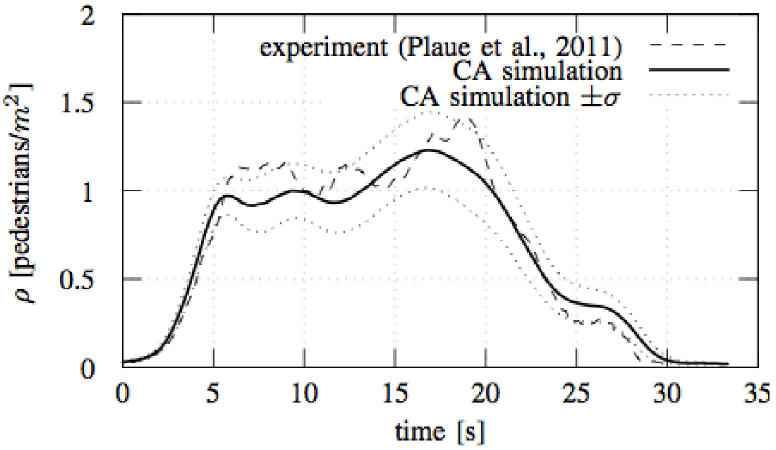

(a)

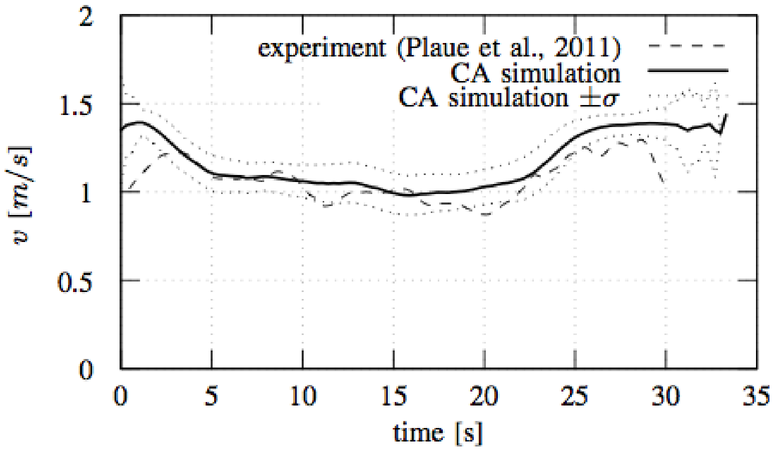

(b)

Figure 5.13: *Time series of density and speed of 180-degree intersection experiment compared with CA simulation.*

(intermediate) target. The modeling of different motivations is indeed an open topic, to the authors best knowledge there exists no simulation approach that can model those concepts adequately. The plots for the 90-degree experiment with similar results are reported in Figure 5.14. The deviation in speed towards the end (after 40 sec) is even stronger compared to the 180-degree experiment. While the density in the laboratory experiment approaches zero, the speed drops well below 1 m/s. As for the 180-degree intersection experiment, video recordings indicate a lag of motivation for the last pedestrians walking through the scene. Overall it is shown that the proposed CA reproduces the complex dynamics observed in laboratory experiments reasonably well at least for

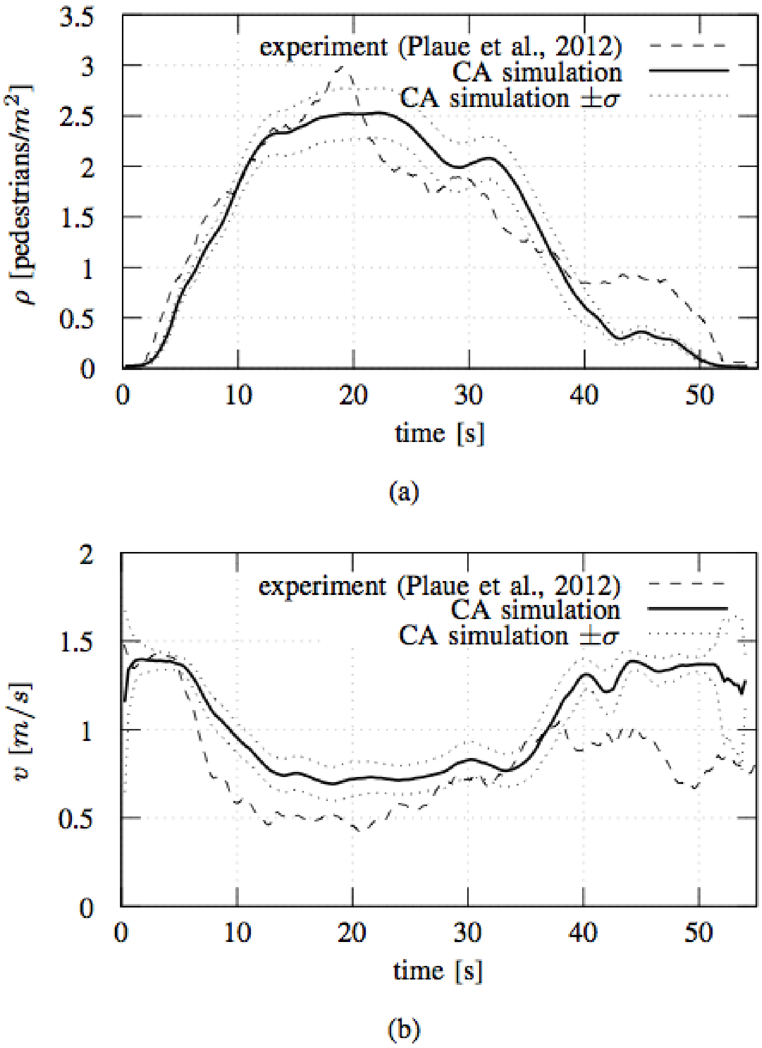

Figure 5.14: *Time series of density and speed of 90-degree intersection experiment compared with CA simulation.*

situations where the pedestrians are determined to reach their desired destination and do not linger. Principally, it would be possible to modify the parameters of the CA to display a kind of "linger" behavior, however, it is still unclear how to quantify it.

5.3.3 Simulation of a Large Scenario

In the following the results of two large scenario simulations are discussed. The evacuation scenario explained by Hoogendoorn et al. [2013] has been chosen as an illustrative example. It describes an area of $50 \times 50m^2$, divided into 5 vertical sections

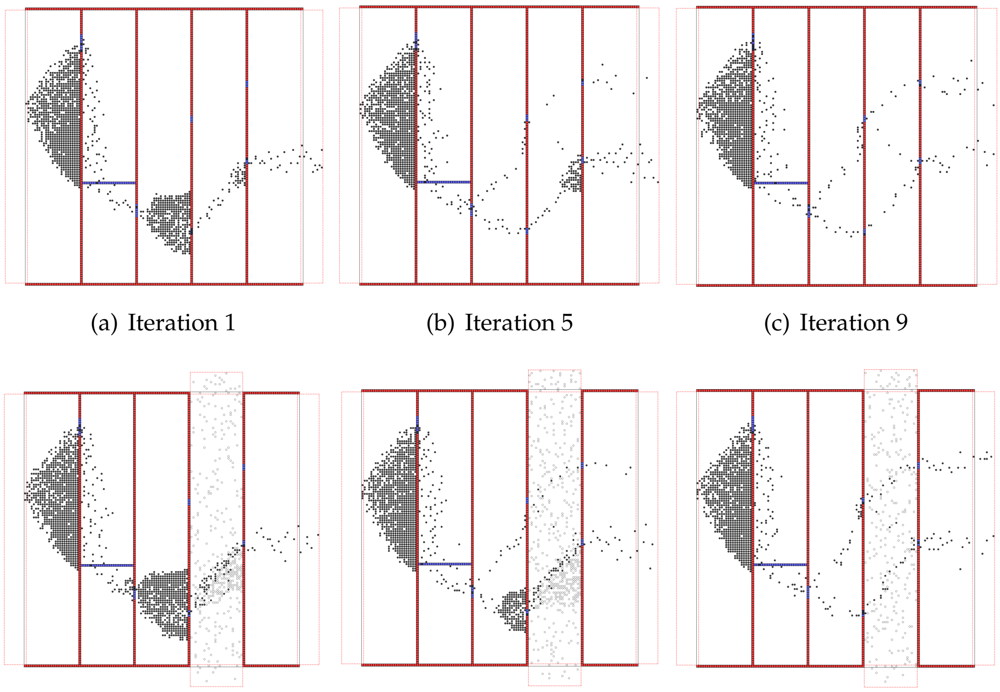

(a) Iteration 1 (b) Iteration 5 (c) Iteration 9

(d) Iteration 1 (e) Iteration 5 (f) Iteration 9

Figure 5.15: *Simulation of the large scenario: the top row refers to the base setting, while the bottom one shows the dynamics with the introduction of counter-flow. All screenshots are taken at the same simulation time, around 5:30min.*

of equal size. From left to right, the first 3 sections are linked by 1 opening of 2.4 m, while the last 2 sections are linked by 2 openings of 1.2 m. The setting is depicted in Figure 5.15.

Two different scenarios have been simulated. In the first experiment (see, top row Figure 5.15) a unidirectional flow, similar to the example of Hoogendoorn et al. [2013], moves through the environment from left to right. A crowd of 2000 pedestrians enters at a rate of 50 persons/s. In the second experiment an additional flow crosses the fourth section from south to north, as shown in the bottom row of Figure 5.15. The additional crossing-flow enters the environment at a rate of 10 persons/s. Both scenarios have been simulated for 9 iterations with the NE route assignment approach. In iteration 1 all pedestrians follow the shortest path. This leads to congestion in front of the bottom bottleneck of the middle section. Over the iterations this congestion dissolves. Comparing the two scenarios, the effect of the counter-flow is clearly visible. In particular in the first iteration conflicts resulting from the crossing flow cause spill-back from the fourth to the middle section. In iteration 5, congestion has almost dissolved in the unidirectional flow experiment, while in the crossing flow experiment congestion only dissolves in iteration 9. For unidirectional experiment, the qualitative results in terms of route choice are similar to those of Hoogendoorn et al. [2013]. The crossing flow experiment is an interesting extension, demonstrating the effect of conflicts arising from crossing flows.

5.3.4 Computational Times Analysis

A computing time analysis for the crossing flow experiment, discussed in the previous section, is shown in Figure 5.16 (a). It is shown that route computation never takes more than 1 s. Another interesting aspect is that the computing time for the CA simulation drops over the iterations. A reason for that is as pedestrians find better routes the overall congestion drops and thus the pedestrians reach their destinations earlier (i.e. the number of computation steps drops).

A second computing time analysis investigates the speedup of the CA simulation (i.e. the ratio of real time and computing time). Therefore, a simulation scenario consisting of a huge corridor of 80×640 m (200×1600 cells) that is crossed by a total population of 50,000 pedestrians has been setup. The maximum number of pedestrians that are simultaneously inside the corridor was about 25,000. Results of the speedup analysis are given in Figure 5.16 (b). It is clearly shown that the CA simulation can simulate situations with up to 13,000 pedestrians in real-time. Moreover, the computing time increases only linear with the number of simulated pedestrians.

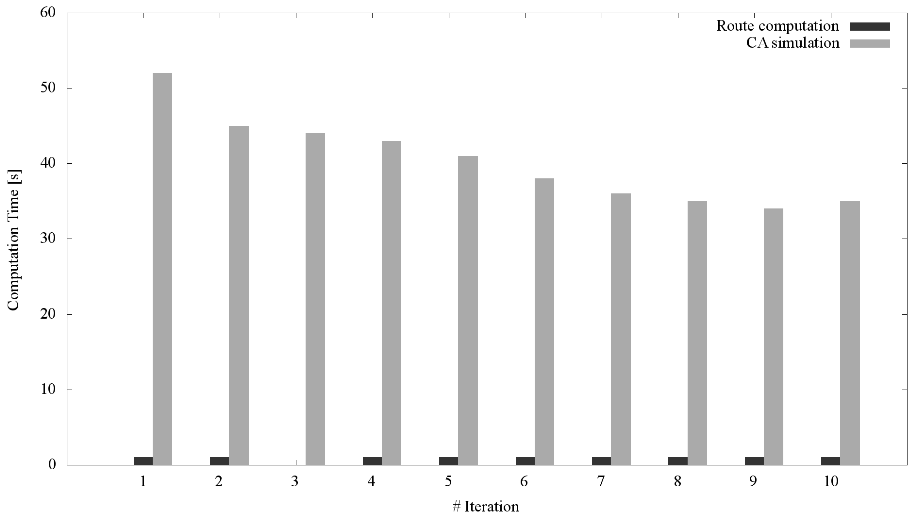

(a)

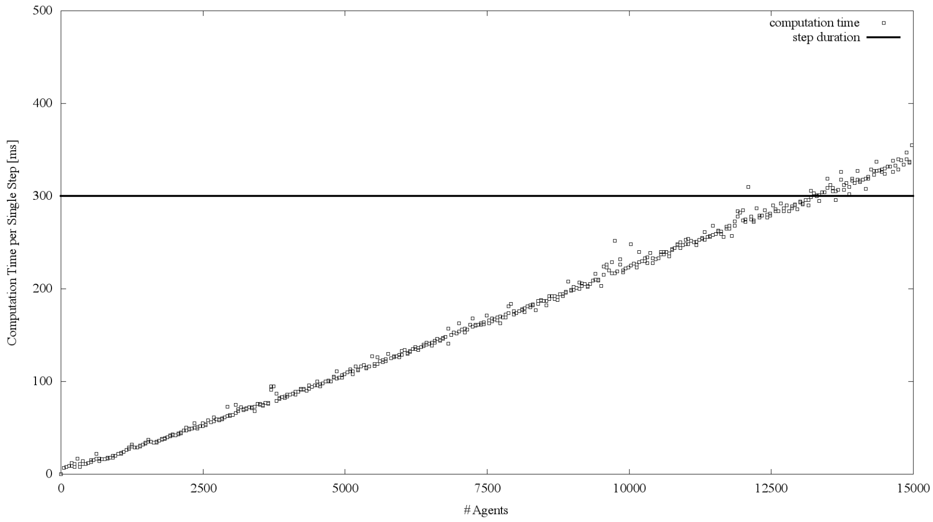

(b)

Figure 5.16: *Computing time analysis: (a) computing time of route computation and CA simulation over iteration number, achieved with the simulation of the large scenario; (b) computational times per single time-step over the number of agents.*

6 Conclusions and Future Research Directions

As a conclusion of this Thesis, a summary of the provided contributions at different levels is provided.

Regarding the microscopic modeling approach, a hybrid agent architecture has been proposed, aiming to simulate the operational and tactical levels of pedestrian behavior in discrete 2-dimensional environment. At the operational level, the model reproduces multi-directional flows of pedestrians with the possibility to consider persons in groups and also different velocities.

The cohesion mechanism for the management of the group behavior is *adaptive*, in a way that allows temporarily fragmentation of the group, which is always re-composed after the obstacle or counter-flow has been overcome. This is achieved by monitoring the *dispersion* of the group, which balances the probability to move towards the current target and, instead, moving towards other group members.

The reproduction of different velocities is allowed by means of an additional stochastic mechanisms, which dynamically manages the probability to perform the movement at each step by the pedestrians. The probability is calculated on the basis of the *desired speed* of the pedestrian, which can be fixed in $\mathbb{R}$. This makes the model suitable for the consideration of stairs and other particular components of the environment, but also other types of pedestrians, as children and elderly, which typically present a different walking speed.

The tests on the validation of the microscopic model, based on the fundamental diagram and shown in Section 4.1, illustrated an overall accordance between the data-sets provided in the literature and the simulation results. In particular, the simulation model shows more errors in the case of uni-directional flows, between densities of 2 to 3.5 persons/m^2. Regarding the simulation of the bi-directional flows the average results fit the empirical data-sets very well, despite a high variability of the simulated data which are mainly due to the probabilistic nature of the model. The mechanisms proposed for the velocity management have been also tested in a stair scenario, and have also contributed for the improvement of simulation results in case of a rotation of the environment.

At the tactical level of behavior, an approach to deal with adaptive route choice of pedestrians has been proposed. The model allows the dynamic choice of the route considering the aim of the agents to minimize their traveling time towards the destination, by taking into account the configuration of the environment and the potential congestion in the surrounding of a passage. The proposed approach allows, on one hand, to represents systematical differences for the route choice of pedestrians belonging to different classes, considering their capabilities to pass through the individual environment components. On the other hand, the simulation of such adaptive behavior is suitable for scenarios describing evacuation, where the targets of pedestrians is well defined and the assumption of a systematic minimization of the traveling times from the pedestrians is overall realistic.

Finally, an exercise of integrated multi-scale modeling has been performed. This integrated micro-mesoscopic model is an alternative approach to modeling and investigating operational and tactical level decision models. An additional microscopic model that considers less behavioral details, with simpler rules for the management of the operational level, has been proposed. This model misses the level of details of the pedestrian behavior provided with the previous one. The reason behind the definition of this additional model can be mainly find in the efficiency element: as discussed in Section 5.3.4 this model is able to execute faster than real-time simulations until about 13000 thousands of agents, without the usage of any parallel implementation. In addition, the simplicity of the rules is balanced with the possibility of fully calibrate the simulated results on the basis of the fundamental diagram data-sets. This has been shown in Section 5.6. The effectiveness and efficiency of this model to simulate the pedestrian flows in bi-dimensional environments is suitable for an integration with the mesoscopic simulation system MATSim, which constitutes the main aim of this contribution, going towards the realization of a multi-scale simulator for the simulation of vehicular and pedestrian traffic at a urban scale.

To provide a conclusive discussion, the approaches provided for the fully microscopic model and the one proposed for the multi-scale simulation system does not only differ on the rules for the reproduction of the physical movement. The discussed iterative algorithm is, in fact, an alternative way to manage decisions at the tactical level. By looking at the two approaches, the adaptive model proposed in Chapter 3 considers the adaptability of the route only at a local level, since the agents are not allowed to perceive the delays due to congestion in other regions of the environment. The iterative algorithm, instead, uses the complete travel experiences to let the agents recompute their route for the following iteration, having thus a more global perspective. The former approach has more demanding requirements to practically inform and define the model, but provides theoretically results from the first run and it allows a very detailed level of customization. The latter approach, instead, does not have such a demanding requirement for preliminary information about the simulated reality, but it requires a number of iterations to explore the complexity and reach a plausible equilibrium.

For both modeling approaches, the validation of generated dynamics is still an open challenge in the general case: in specific situations, e.g. evacuations, the validation is achievable, but in more general and complex scenarios the necessary data is still largely unavailable.

Future works are mainly targeted at actually performing a validation of the model in more general and realistic scenarios. Moreover, the multi-scale modeling approach is promising and it will be further developed and investigated in more complex real-world scenario.

A

An In-vivo Observation to Understand the Behavior of Pedestrian Groups

This Appendix comprises several empirical studies aimed at investigating pedestrian crowd dynamics in the natural context by using on-field observation. In particular the survey was aimed at studying the impact of grouping and proxemics behavior on the whole crowd pedestrian dynamics. Data analyses were focused on: (i) *level of density and service*, (ii) *presence of groups* within the pedestrian flows, (iii) *trajectories and walking speed* of both singles and group members. Furthermore the *spatial dispersion* of group members while walking was measured in order to propose an innovative empirical contribution for a detailed description of group proxemics dynamics while walking.

The survey was performed the last 24^{th} of November 2012 from about 2:50 pm to 4:10 pm. It consisted in the observation of the bidirectional pedestrian flows within the Vittorio Emanuele II gallery, a popular commercial-touristic walkway situated in the Milan city center (Italy). The gallery was chosen as a crowded urban scenario, given the large amount of people that pass through it during the weekend for shopping, entertainment and visiting touristic-historical attractions in the center of Milan.

The team performing the observation was composed of four people. Several preliminary inspections were performed to check the topographical features of the walkway. The balcony of the gallery, that surrounds the inside volume of the architecture from about ten meters in height, was chosen as location thanks to possibility to (i) position the equipment for the video recording from a quasi-zenithal point of view and (ii) to avoid as much as possible to influence the behavior of observed subjects, thanks to a railing of the balcony partly hiding the observation equipment. The equipment consisted of two professional full HD video cameras with tripods. The existing legislation about privacy was consulted and complied in order to exceed ethical issues about the privacy of the people recorded within the pedestrian flows.

Two independent coders performed a manual data analyses, in order to reduce errors by crosschecking their results. A square portion of the walkway was considered for data analysis: 12.8 meters wide and 12.8 meters long (163.84 square meters). In order to perform data analyses, the inner space of the selected area was discretized in

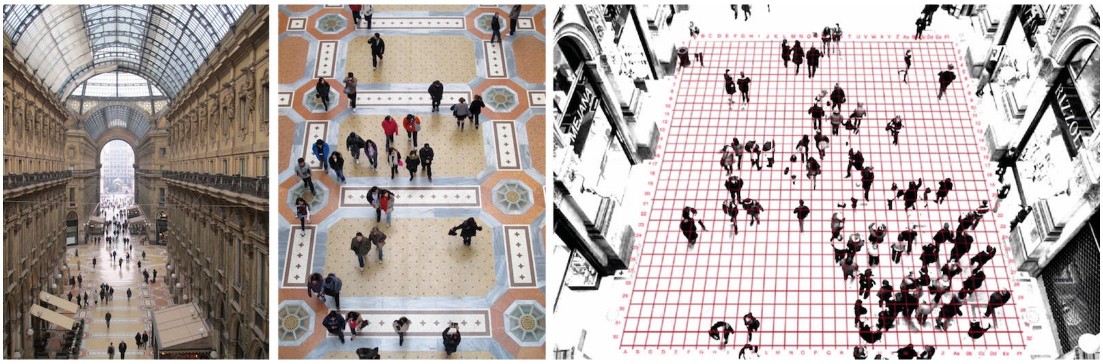

Figure A.1: *From the left: an overview of the Vittorio Emanuele II gallery, the streaming of passerby within the walkway and a snapshot of the recorded video images with the superimposed grid for data analysis*

cells by superimposing a grid[1] on the video (see Figure A.1); the grid was composed of 1024 squares 0.4 meters wide and 0.4 meters long. The video and the annotation data will soon be made available only for research purposes through the web.

A.1 Level of Density and Service

The bidirectional pedestrian flows (from North to South and vice-versa) were manually counted minute by minute: 7773 people passed through the selected portion of the Vittorio Emanuele II Gallery from 2:50 pm to 4:08 pm. The average level of density within the selected area (defined as the quantitative relationship between a physical area and the number of people who occupy it) was detected considering 78 snapshots of video footages, randomly selected with a time interval of one minute. The observed average level of density was low (0.22 people/squared meter). Despite it was not possible to analyze continuous situations of high density, several situation of irregular and local distribution of high density were detected within the observed scenario.

According to the Highway Capacity Manual by Milazzo II et al. [1999], the level of density in motion situation was more properly estimated taking into account the bidirectional walkway level of service criteria: counting the number of people walking through a certain unit of space (meter) in a certain unit of time (minute). The average level of flow rate within the observed walkway scenario belongs to a *B* level (7.78 pedestrians/min/m) that is associated with an irregular flow in low-medium density

[1]The grid was designed using *Photoshop CS5* (according to the perspective of the video images). An alphanumeric code was added on the sides of the grid. Finally, the grid with a transparent background was superimposed to a black-white version of the video images by means of *iMovie*. To perform counting activities, the video was reproduced by using *VLC* player thanks to its possibility to playback the images in slow motion and/or frame by frame and to use an extension time format that included hundredths of a second.

condition.

A.2 Flow Composition

The second stage of data analysis was focused on the detection of groups within the pedestrian flows, the number of group members and the group proxemics spatial arrangement while walking. The identification of groups in the streaming of passerby was assessed on the basis of verbal and nonverbal communication among members: visual contact, body orientation, gesticulation and spatial cohesion among members. To more thoroughly evaluate all these indicators the coder was actually encouraged to rewind the video and take the necessary time to tell situations of simple local (in time an space) similar movements, due to the contextual situation, by different pedestrians from actual group situations. The whole video was sampled considering one minute every five: a subset of 15 minutes was extracted and 1645 pedestrians were counted (21.16% of the total bidirectional flows). Concerning the flow composition, 15.81% of the pedestrians arrived alone, while the 84.19% arrived in groups: 43.65% of groups were couples, 17.14% triples and 23.40% larger groups (composed of four or five members). Large structured groups, such as touristic committees, that were present in the observed situation, were analysed considering sub-groups.

A.3 Trajectories and Walking Speed

The walking speed of both singles and group members was measured considering the path and the time to reach the ending point of their movement in the monitored area (corresponding to the center of the cell of the last row of the grid) from the starting point (corresponding to the center cell of the first row of the grid). Only the time distribution related to the *B* level of service was considered (as mentioned, the 59% of the whole video footages), in order to focus on pedestrian dynamics in situation of irregular flow. A sample of 122 people was randomly extracted: 30 singles, 15 couples, 10 triples and 8 groups of four members. The estimated age of pedestrians was approximately between 15 and 70; groups with accompanied children were not taken into account for data analyses. About gender, the sample was composed of 63 males (56% of the total) and 59 females (44% of the total). Differences in age and gender were not considered in this study. The selected pedestrians were chosen among those not stopping at shops' windows or entering shops, to actually focus on movement dynamics and not on the choice of activities (like in the vein of Dijkstra et al. [2011]).

The alphanumeric grid was used to track the trajectories of both single and group members within the walkway and to measure the length of their path[2] (considering

[2]To measure the walking path and speed we considered each pedestrian as a point without mass in a two-dimensional plane. By using the alphanumeric grid, we considered the cell occupied by the feet of each pedestrian as its own actual position. The starting and final steps were measured from the half of the

the features of the cells: 0.4 m wide, 0.4 m long).

A first analysis was devoted to the identification of the length of the average walking path of singles (M=13.96 m, $\pm$1.11), couples (M=13.39 m, $\pm$ 0.38), triples (M=13.34 m, $\pm$ 0.27) and groups of four members (M=13.16 m, $\pm$ 0.46). Then, the two tailed t-test analyses were used to identify differences in path among pedestrian. Results showed a significant difference in path length between: singles and couples (p value$<$0.05), singles and triples (p value $<$ 0.05), singles and groups of four members (p value $<$ 0.05). No significant differences were detected between path length of couples and triples (p value $>$ 0.05), triples and groups of four members (p value $>$ 0.05), couples and groups of four members (p value $>$ 0.05). The results showed that the path of singles is 4,48% longer than the average path of group members (including couples, triples and groups of four members).

The walking speed of both singles and group members was detected considering the path of each pedestrian within the flows and the time to reach the ending point from their starting point. A first analysis was devoted to the identification of the average walking speed of singles (M=1.22 m/s, $\pm$ 1.16), couples (M=0.92 m/s, $\pm$ 0.18), triples (M=0.73 m/s, $\pm$ 0.10) and groups of four members (M=0.65 m/s, $\pm$ 0.04). Then, the two tailed t-test analyses were used to identify differences in walking speed among pedestrian. Results showed a significant difference in walking speed between: singles and couples (p value $<$ 0.01), singles and triples (p value $<$ 0.01), singles and groups of four members (p value $<$ 0.01), couples and triples (p value $<$ 0.01), triples and groups of four members (p value $<$ 0.05). In conclusion, the results showed that the average walking speed of group members (including couples, triples and groups of four members) is 37.21% lower than the walking speed of singles.

The correlated results about pedestrian path and speed showed that in situation of irregular flow singles tend to cross the space with more frequent changes of direction in order to maintain their velocity, avoiding perceived obstacles like slower pedestrians or groups. On the contrary, groups tend to have a more stable overall behavior, adjusting their spatial arrangement and speed to face the contextual conditions of irregular flow: this is probably due to (i) the difficulty in coordinating an overall change of direction and (ii) the tendency to preserve the possibility of maintaining cohesion and communication among members.

A.4 Group Proxemics Dispersion

In order to improve the understanding of pedestrian proxemics behavior the last part of the study is focused on the dynamic spatial dispersion of group members while walking. The dispersion among group members was measured as the summation of

cell, consequently 0.2 m is the corresponding length of the each related path; any diagonal step cell by cell was measured as the diagonal between the two cells (0.56 m); any straight step was measured as the segment between the center of two cells (0.4 m).

the distances between each pedestrian and the centroid (the geometrical center of the group) all normalized by the cardinality of the group. The centroid was obtained as the arithmetic mean of all spatial positions of the group members, considering the alphanumeric grid. In order to find the spatial positions, the trajectories of the group members belonging to the previous described sample (15 couples, 10 triples and 8 groups of four members) were further analyzed. In particular, the positions of the group members were detected analysing the recorded video images every 40 frames (the time interval between two frames corresponds to about 1.79 seconds, according to the quality and definition of the video images) starting from the co-presence of the all members on the alphanumeric grid. This kind of sampling permitted to consider 10 snapshots for each groups.

A first analysis was devoted to the identification of the average proxemics dispersion of couples (M=0.35 m, $\pm$ 0.14), triples (M=0.53 m, $\pm$ 0.17) and groups of four members (M=0.67 m, $\pm$ 0.12). Then, the two tailed t-test analyses were used to identify differences in proxemics dispersion among couples, triples and groups of four members. Results showed a significant difference in spatial dispersion between: couples and triples (p value < 0.05), couples and groups of four members (p value < 0.01). No significant differences between triples and groups of four members (p value > 0.05). In conclusion, the results showed that the average spatial dispersion of triples and groups of four members while walking is 40.97% higher than the dispersion of couples.

Starting from the achieved results about group proxemics dispersion, we finally focused on a quantitative and detailed description of group spatial layout while walking. The relative positions of each group member with respect to the centroid and the movement direction were detected by means of a sample of 10 snapshots for each groups (15 couples, 10 triple and 8 groups of four members) and then further analyzed in order to identify the most frequent group proxemics spatial configurations, taking into account the degree of alignment of each pedestrian (see Figure A.2). Result showed that couple members tend to walk side by side, aligned to the each other with a distance of 0.4 m (36% of the sample) or 0.8 m (24% of the sample), forming a line perpendicular to the walking direction (line abreast pattern); triples tend to walk with a line abreast layout (13% of the sample), with the members spaced of 0.60 m. Regarding groups of four members it was not possible to detect a typical spatial pattern: the reciprocal positions of group members appeared much more dispersed than in the case of smaller groups, probably due to the continuous arrangements in spatial positioning while walking.

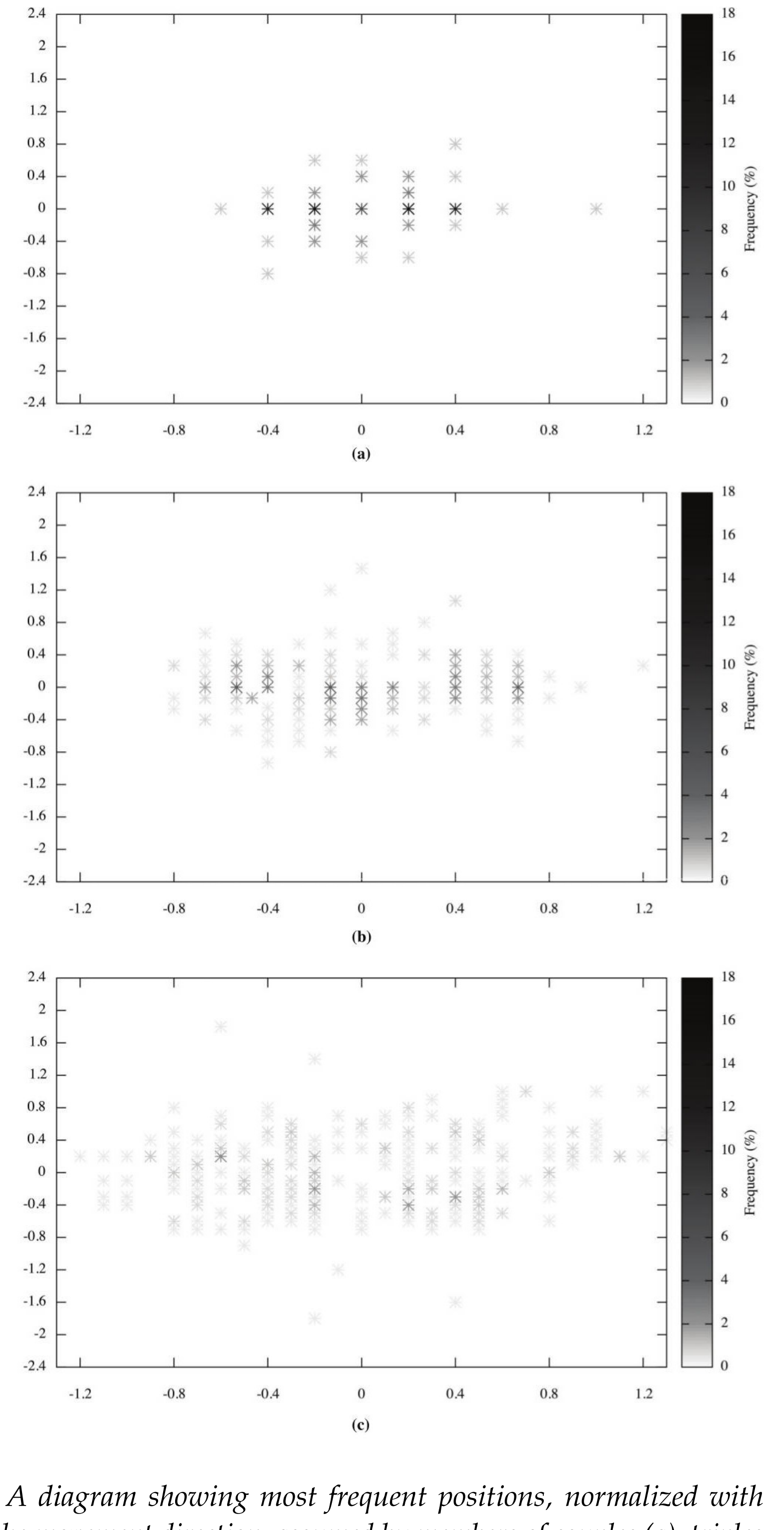

Figure A.2: *A diagram showing most frequent positions, normalized with respect to the centroid and the movement direction, assumed by members of couples (a), triples (b) and groups of four members (c).*

Bibliography

World Population Ageing: 1950-2050. Technical report, United Nations, Dep. of Economic and Social Affairs - Population Division, 2002.

Global Age-Friendly cities: A Guide, 2007.

World Urbanisation Prospect - The 2011 Revision, 2011.

L. a.M. Galea and D. Kimura. Sex differences in route-learning. *Personality and Individual Differences*, 14(1):53–65, 1993.

C. Appert-Rolland, J. Cividini, and H. J. Hilhorst. Frozen shuffle update for an asymmetric exclusion process on a ring. *Journal of Statistical Mechanics: Theory and Experiment*, 2011(7):P07009, 2011. ISSN 1742-5468. doi: 10.1088/1742-5468/2011/07/P07009.

A. F. Aveni. The Not-So-Lonely Crowd: Friendship Groups in Collective Behavior. *Sociometry*, 40(1):96, 1977. ISSN 00380431. doi: 10.2307/3033551. URL http://www.jstor.org/stable/3033551?origin=crossref.

S. Bandini, A. Mosca, and M. Palmonari. Common-sense spatial reasoning for information correlation in pervasive computing. *Applied Artificial Intelligence*, 21(4-5):405–425, 2007. ISSN 08839514. doi: 10.1080/08839510701252676. URL 10.1080/08839510701252676$\delimiter"026E30F$nhttp://search.ebscohost.com/login.aspx?direct=true{&}db=bth{&}AN=25059082{&}site=ehost-live.

S. Bandini, F. Rubagotti, G. Vizzari, and K. Shimura. An Agent Model of Pedestrian and Group Dynamics: Experiments on Group Cohesion. In R. Pirrone and F. Sorbello, editors, *AI*IA*, volume 6934 of *Lecture Notes in Computer Science*, pages 104–116. Springer, 2011. ISBN 978-3-642-23953-3.

S. Bandini, A. Gorrini, and G. Vizzari. Towards an integrated approach to crowd analysis and crowd synthesis: A case study and first results. *Pattern Recognition Letters*, 44: 16–29, 2014. ISSN 01678655. doi: 10.1016/j.patrec.2013.10.003. URL http://www.sciencedirect.com/science/article/pii/S0167865513003760.

S. Bandini, L. Crociani, and G. Vizzari. Pedestrian Simulation: Considering Elderlies in the Models and in the Simulation Results. In B. Andò, P. Siciliano, V. Marletta, and A. Monteriù, editors, *Ambient Assisted Living*, volume 11 of *Biosystems & Biorobotics*, pages 11–21. Springer International Publishing, 2015. ISBN 978-3-319-18373-2. doi: 10.1007/978-3-319-18374-9{_}2. URL http://dx.doi.org/10.1007/978-3-319-18374-9{_}2.

M. R. Baroni. *Psicologia ambientale*. Il Mulino, Bologna, 1998.

M. Beckmann, C. B. McGuire, and C. B. Winsten. *Studies in the Economics of Transportation*. Yale University Press, 1956.

V. Blue and J. Adler. Emergent Fundamental Pedestrian Flows from Cellular Automata Microsimulation, 1998.

V. Blue and J. Adler. Modeling Four-Directional Pedestrian Flows. *Transportation Research Record: Journal of the Transportation Research Board*, 1710(-1):20–27, jan 2000. doi: 10.3141/1710-03. URL http://dx.doi.org/10.3141/1710-03.

V. J. Blue and J. L. Adler. Cellular Automata Microsimulation of Bi-Directional Pedestrian Flows. *Transportation Research Record*, 1678:135–141, 1999.

V. J. Blue and J. L. Adler. Cellular automata microsimulation for modeling bi-directional pedestrian walkways. *Transportation Research Part B: Methodological*, 35(3):293–312, 2001. ISSN 01912615. doi: 10.1016/S0191-2615(99)00052-1.

M. Boltes and A. Seyfried. Collecting pedestrian trajectories. *Neurocomputing*, 100: 127–133, jan 2013. ISSN 09252312. doi: 10.1016/j.neucom.2012.01.036. URL http://www.sciencedirect.com/science/article/pii/S0925231212003189.

M. Boltes, J. Zhang, A. Seyfried, and B. Steffen. T-junction: Experiments, trajectory collection, and analysis. In *Computer Vision Workshops (ICCV Workshops), 2011 IEEE International Conference on*, pages 158–165, nov 2011. doi: 10.1109/ICCVW.2011.6130238.

J. Borenstein and Y. Koren. Real-time obstacle avoidance for fast mobile robots. *Systems, Man and Cybernetics, IEEE Transactions on*, 19(5):1179–1187, 1989.

D. Braess. {Ü}ber ein {P}aradoxon aus der {V}erkehrsplanung. *Unternehmensforschung*, 12:258–268, 1968.

D. Braess, A. Nagurney, and T. Wakolbinger. On a Paradox of Traffic Planning. *Transportation Science*, 2005. URL http://pubsonline.informs.org/doi/abs/10.1287/trsc.1050.0127.

R. Brooks. A robust layered control system for a mobile robot. *IEEE Journal on Robotics and Automation*, 2(1):14–23, 1986. doi: 10.1109/JRA.1986.1087032.

S. Burghardt, A. Seyfried, and W. Klingsch. Performance of stairs – Fundamental diagram and topographical measurements. *Transportation Research Part C: Emerging Technologies*, 2013. ISSN 0968-090X. doi: http://dx.doi.org/10.1016/j.trc.2013.05.002.

C. Burstedde, K. Klauck, A. Schadschneider, and J. Zittartz. Simulation of pedestrian dynamics using a two-dimensional cellular automaton. *Physica A: Statistical Mechanics and its Applications*, 295(3 - 4):507–525, 2001. ISSN 0378-4371.

doi: 10.1016/S0378-4371(01)00141-8. URL http://www.sciencedirect.com/science/article/pii/S0378437101001418.

U. Chattaraj, A. Seyfried, and P. Chakroborty. Comparison of Pedestrian Fundamental Diagram Across Cultures. *Advances in Complex Systems*, 12(3):393–405, 2009. doi: 10.1142/S0219525909002209. URL http://arxiv.org/abs/0903.0149.

M. Chraibi, A. Seyfried, and A. Schadschneider. Generalized centrifugal-force model for pedestrian dynamics. *Phys. Rev. E*, 82(4):46111, 2010. doi: 10.1103/PhysRevE.82.046111. URL http://link.aps.org/doi/10.1103/PhysRevE.82.046111.

M. Costa. Interpersonal Distances in Group Walking. *Journal of Nonverbal Behavior*, 34(1):15–26, 2010. ISSN 0191-5886. URL http://dx.doi.org/10.1007/s10919-009-0077-y.

C. F. Daganzo. Queue Spillovers in Transportation Networks with a Route Choice. *Transportation Science*, 32(1):3–11, 1998. ISSN 0041-1655. doi: 10.1287/trsc.32.1.3. URL http://pubsonline.informs.org/doi/abs/10.1287/trsc.32.1.3.

J. Dijkstra, J. Jessurun, H. Timmermans, and B. de Vries. A Framework for Processing Agent-Based Pedestrian Activity Simulations in Shopping Environments. *Cybernetics and Systems*, 42:526–545, 2011. ISSN 0196-9722. doi: 10.1080/01969722.2011.610705. URL http://www.tandfonline.com/doi/abs/10.1080/01969722.2011.610705.

D. C. Duives, W. Daamen, and S. P. Hoogendoorn. State-of-the-art crowd motion simulation models, 2013. ISSN 0968090X.

T. Emonet, C. M. Macal, M. J. North, C. E. Wickersham, and P. Cluzel. AgentCell: a digital single-cell assay for bacterial chemotaxis. *Bioinformatics*, 21(11):2714–2721, 2005.

G. Flötteröd and G. Lämmel. Bidirectional pedestrian fundamental diagram. *Transportation research part B: methodological*, 71:194–212, 2015.

E. Forcael, V. González, F. Orozco, S. Vargas, A. Pantoja, and P. Moscoso. Ant Colony Optimization Model for Tsunamis Evacuation Routes. *Computer-Aided Civil and Infrastructure Engineering*, 29(10):723–737, nov 2014. ISSN 10939687. doi: 10.1111/mice.12113. URL http://onlinelibrary.wiley.com/doi/10.1111/mice.12113/full.

J. J. Fruin. *Pedestrian Planning and Design*. new York, metropolitan association of urban designers and environmental, 1971.

M. Fukui and Y. Ishibashi. Self-organized phase transitions in cellular automaton models for pedestrians. *Journal of the Physical Society of Japan*, 68(8):2861–2863, 1999. ISSN 00319015. doi: 10.1143/JPSJ.68.2861.

C. Gawron. An Iterative Algorithm to Determine the Dynamic User Equilibrium in a Traffic Simulation Model. *International Journal of Modern Physics C*, 09(03):393–407, 1998. doi: 10.1142/S0129183198000303. URL http://www.worldscientific.com/doi/abs/10.1142/S0129183198000303.

I. G. Georgoudas, G. C. Sirakoulis, and I. T. Andreadis. An Anticipative Crowd Management System Preventing Clogging in Exits During Pedestrian Evacuation Processes, 2010. ISSN 19328184.

R. Geraerts. Planning short paths with clearance using explicit corridors. In *2010 IEEE International Conference on Robotics and Automation*, pages 1997–2004. IEEE, may 2010. ISBN 978-1-4244-5038-1. doi: 10.1109/ROBOT.2010.5509263. URL http://ieeexplore.ieee.org/lpdocs/epic03/wrapper.htm?arnumber=5509263.

R. Geraerts and M. Overmars. The Corridor Map Method: A General Framework for Real-Time High-Quality Path Planning, 2007. ISSN 1546-4261. URL http://dspace.library.uu.nl/handle/1874/31848.

P. Gipps. A behavioural car-following model for computer simulation, 1981. ISSN 01912615.

A. Goni-Moreno and M. Amos. DiSCUS: A Simulation Platform for Conjugation Computing. 2014.

E. T. Hall. *The hidden dimension*. Doubleday New York Ed., 1966.

B. D. Hankin and R. A. Wright. Passenger Flow in Subways. *OR*, 9(2):pp. 81–88, 1958. ISSN 14732858. URL http://www.jstor.org/stable/3006732.

D. Helbing. A fluid dynamic model for the movement of pedestrians. *Complex Systems*, 6:391–415, 1992. ISSN 08912513. doi: citeulike-article-id:3945298.

D. Helbing and P. Molnar. Social force model for pedestrian dynamics. *Physical review E*, 1995.

D. Helbing, A. Johansson, and H. Z. Al-Abideen. Dynamics of crowd disasters: An empirical study. *Phys. Rev. E*, 75(4):46109, apr 2007. doi: 10.1103/PhysRevE.75.046109. URL http://link.aps.org/doi/10.1103/PhysRevE.75.046109.

L. F. Henderson. The Statistics of Crowd Fluids. *Nature*, 229(5284):381–383, feb 1971. URL http://dx.doi.org/10.1038/229381a0.

S. Hoogendoorn, W. Daamen, D. Duives, and F. Van Wageningen-Kessels. Optimal crowd evacuation, nov 2013. URL http://resolver.tudelft.nl/uuid:baf5791e-174a-4969-a6be-6515cbb59876.

S. P. Hoogendoorn and P. H. L. Bovy. Pedestrian route-choice and activity scheduling theory and models. *Transportation Research Part B: Methodological*, 38(2):169–190, 2004. ISSN 01912615. doi: 10.1016/S0191-2615(03)00007-9.

R. L. Hughes. A continuum theory for the flow of pedestrians. *Transportation Research Part B: Methodological*, 36(6):507–535, 2002. ISSN 01912615. doi: 10.1016/S0191-2615(01)00015-7.

Y. Q. Jiang, P. Zhang, S. C. Wong, and R. X. Liu. A higher-order macroscopic model for pedestrian flows. *Physica A: Statistical Mechanics and its Applications*, 389(21):4623–4635, 2010. ISSN 03784371. doi: 10.1016/j.physa.2010.05.003.

O. Khatib. Real-time obstacle avoidance for manipulators and mobile robots. *The international journal of robotics research*, 5(1):90–98, 1986.

A. Kirchner, A. Namazi, K. Nishinari, and A. Schadschneider. Role of Conflicts in the Floor Field Cellular Automaton Model for Pedestrian Dynamics. In *2nd International Conference on Pedestrian and Evacuation Dynamics*, 2003a.

A. Kirchner, K. Nishinari, and A. Schadschneider. Friction effects and clogging in a cellular automaton model for pedestrian dynamics. *Phys. Rev. E*, 67(5):56122, 2003b. doi: 10.1103/PhysRevE.67.056122. URL http://link.aps.org/doi/10.1103/PhysRevE.67.056122.

A. Kirchner, H. Klüpfel, K. Nishinari, A. Schadschneider, and M. Schreckenberg. Discretization effects and the influence of walking speed in cellular automata models for pedestrian dynamics. *Journal of Statistical Mechanics: Theory and Experiment*, 2004 (10):P10011, 2004. URL http://stacks.iop.org/1742-5468/2004/i=10/a=P10011.

H. Klüpfel. *A Cellular Automaton Model for Crowd Movement and Egress Simulation*. PhD thesis, University Duisburg-Essen, 2003.

Y. Koren and J. Borenstein. Potential field methods and their inherent limitations for mobile robot navigation. In *Robotics and Automation, 1991. Proceedings., 1991 IEEE International Conference on*, pages 1398–1404. IEEE, 1991.

S. Koyama, N. Shinozaki, and S. Morishita. Pedestrian flow modeling using cellular automata based on the Japanese public guideline and application to evacuation simulation. *Journal of Cellular Automata*, 8(5-6):361–382, 2013. URL http://www.scopus.com/inward/record.url?eid=2-s2.0-84894099308{&}partnerID=40{&}md5=0462d5f79facf99c408b81f6aa37c6a3.

T. Kretz, A. Grünebohm, M. Kaufman, F. Mazur, and M. Schreckenberg. Experimental study of pedestrian counterflow in a corridor. *Journal of Statistical Mechanics:*

Theory and Experiment, 2006(10):P10001, 2006. URL http://stacks.iop.org/1742-5468/2006/i=10/a=P10001.

T. Kretz, C. Bönisch, and P. Vortisch. Comparison of Various Methods for the Calculation of the Distance Potential Field. In W. W. F. Klingsch, C. Rogsch, A. Schadschneider, and M. Schreckenberg, editors, *Pedestrian and Evacuation Dynamics 2008*, pages 335–346. Springer Berlin Heidelberg, 2010. ISBN 978-3-642-04503-5. doi: 10.1007/978-3-642-04504-2{_}29. URL http://dx.doi.org/10.1007/978-3-642-04504-2{_}29.

T. Kretz, K. Lehmann, I. Hofsäß, and A. Leonhardt. Dynamic Assignment in Microsimulations of Pedestrians. *Annual Meeting of the Transportation Research Board, 14-0941 (2014)*, pages 14–0941, jan 2014. URL http://arxiv.org/abs/1401.1308.

G. Lämmel and G. Flötteröd. Towards system optimum: Finding optimal routing strategies in time-tependent networks for large-scale evacuation problems. In B. Mertsching, M. Hund, and Z. Aziz, editors, *KI 2009: Advances in Artificial Intelligence*, volume 5803 of *LNCS (LNAI)*, pages 532–539. Springer, Berlin Heidelberg, 2009. doi: 10.1007/978-3-642-04617-9{_}67.

G. Lämmel, H. Klüpfel, and K. Nagel. The MATSim network flow model for traffic simulation adapted to large-scale emergency egress and an application to the evacuation of the Indonesian City of Padang in case of a tsunami warning, pedestrian behavior. *Pedestrian behavior: Models, Data Collection and Applications*, pages 245—-265, 2009.

G. Lämmel, D. Grether, and K. Nagel. The representation and implementation of time-dependent inundation in large-scale microscopic evacuation simulations. *Transportation Research Part C: Emerging Technologies*, 18(1):84–98, 2010.

L. Leal-Taixé, G. Pons-moll, and B. Rosenhahn. Everybody needs somebody: Modeling social and grouping behavior on a linear programming multiple people tracker. In *2011 IEEE International Conference on Computer Vision Workshops (ICCV Workshops)*, pages 120–127, 2011. ISBN 978-1-4673-0063-6. doi: 10.1109/ICCVW.2011.6130233. URL http://ieeexplore.ieee.org/articleDetails.jsp?arnumber=6130233.

M. J. Lighthill and G. B. Whitham. On Kinematic Waves. I. Flood Movement in Long Rivers. *Proceedings of the Royal Society A: Mathematical, Physical and Engineering Sciences*, 229(1178):281–316, 1955. ISSN 1364-5021. doi: 10.1098/rspa.1955.0088.

X. Liu, W. Song, and J. Zhang. Extraction and quantitative analysis of microscopic evacuation characteristics based on digital image processing. *Physica A: Statistical Mechanics and its Applications*, 388(13):2717–2726, jul 2009. ISSN 03784371. doi: 10.1016/j.physa.2009.03.017. URL http://www.sciencedirect.com/science/article/pii/S0378437109002131.

X.-d. Liu, W.-g. Song, and W. Lv. Empirical Data for Pedestrian Counterflow through Bottlenecks in the Channel. *Transportation Research Procedia*, 2:34–42, 2014. ISSN 23521465. doi: 10.1016/j.trpro.2014.09.006. URL http://www.sciencedirect.com/science/article/pii/S2352146514000428.

N. Metropolis, A. Rosembluth, M. Rosembluth, and A. Teller. Equation of State Calculations by Fast Computing Machines. *Journal of Chemical Physics*, 21:1087–1092, 1953.

J. A. Michon. A Critical View of Driver Behavior Models: What Do We Know, What Should We Do? In L. and Evans and R. C. Schwing, editors, *Human Behavior and Traffic Safety*, pages 485–524. Springer US, 1985. ISBN 978-1-4612-9280-7. doi: 10.1007/978-1-4613-2173-6{_}19. URL http://dx.doi.org/10.1007/978-1-4613-2173-6{_}19.

J. S. Milazzo II, N. M. Rouphail, J. E. Hummer, and D. P. Allen. Quality of service for interrupted-flow pedestrian facilities in Highway Capacity Manual 2000. *Transportation Research Record: Journal of the Transportation Research Board*, 1678(1):25–31, 1999.

M. Mori and H. Tsukaguchi. A new method for evaluation of level of service in pedestrian facilities. *Transportation Research Part A*, 21(3):223–234, 1987.

N. Moussa. Simon-Gutowitz bidirectional traffic model revisited. *Physics Letters, Section A: General, Atomic and Solid State Physics*, 372(45):6701–6704, 2008. ISSN 03759601. doi: 10.1016/j.physleta.2008.08.081.

M. Moussaïd, N. Perozo, S. Garnier, D. Helbing, and G. Theraulaz. The walking behaviour of pedestrian social groups and its impact on crowd dynamics. *PloS one*, 5(4): e10047, 2010. URL http://www.pubmedcentral.nih.gov/articlerender.fcgi?artid=2850937{&}tool=pmcentrez{&}rendertype=abstract.

K. Nagel and M. Schreckenberg. A cellular automaton model for freeway traffic. *Journal de Physique I*, 2(12):2221–2229, dec 1992. ISSN 1155-4304. doi: 10.1051/jp1:1992277. URL http://www.edpsciences.org/10.1051/jp1:1992277.

K. Nagel, D. E. Wolf, P. Wagner, and P. Simon. Two-lane traffic rules for cellular automata: A systematic approach. *Physical Review E*, 58(2):1425, 1998.

L. Navarro, F. Flacher, and V. Corruble. Dynamic Level of Detail for Large Scale Agent-Based Urban Simulation. *AAMAS '11: The 10th International Conference on Autonomous Agents and Multiagent Systems*, 2:701–708, 2011.

L. Navarro, V. Corruble, F. Flacher, and J.-D. Zucker. A flexible approach to multi-level agent-based simulation with the mesoscopic representation. In *Proceedings of the*

Twelfth International Conference on Autonomous Agents and Multiagent Systems, pages 159–166, 2013. ISBN 978-1-4503-1993-5.

L. Navarro, F. Flacher, and C. Meyer. SE-Star: A Large-Scale Human Behavior Simulation for Planning, Decision-Making and Training. In *Proceedings of the 2015 International Conference on Autonomous Agents and Multiagent Systems*, pages 1939–1940. International Foundation for Autonomous Agents and Multiagent Systems, 2015.

S. J. Older. Movement of Pedestrians on Footways in Shopping Streets. *Traffic Engineering and Control*, 1968.

S. Paris and S. Donikian. Activity-Driven Populace: A Cognitive Approach to Crowd Simulation. *IEEE Computer Graphics and Applications*, 2009.

S. Paris, S. Donikian, and N. Bonvalet. Environmental abstraction and path planning techniques for realistic crowd simulation. *Computer Animation and Virtual Worlds*, 17(3-4):325–335, 2006. ISSN 1546-4261. doi: 10.1002/cav.136. URL http://doi.wiley.com/10.1002/cav.136.

M. Plaue, M. Chen, G. Bärwolff, and H. Schwandt. Trajectory extraction and density analysis of intersecting pedestrian flows from video recordings. *Lecture Notes in Computer Science (including subseries Lecture Notes in Artificial Intelligence and Lecture Notes in Bioinformatics)*, 6952 LNCS:285–296, 2011. ISSN 03029743. doi: 10.1007/978-3-642-24393-6{_}24.

M. Plaue, M. Chen, G. Bärwolff, and H. Schwandt. Multi-view extraction of dynamic pedestrian density fields. *Photogrammetrie-Fernerkundung-Geoinformation*, 2012(5): 547–555, 2012.

V. M. Predtechenskii and A. I. Milinski. *Planning for foot traffic flow in buildings*. 1978.

F. Qiu and X. Hu. Modeling group structures in pedestrian crowd simulation. *Simulation Modelling Practice and Theory*, 18(2):190–205, 2010. ISSN 1569190X. doi: 10.1016/j.simpat.2009.10.005.

B. Raney and K. Nagel. Iterative Route Planning for Large-Scale Modular Transportation Simulations. *Future Generation Computer Systems*, 20(7):1101–1118, 2004.

M. Rickert, K. Nagel, M. Schreckenberg, and A. Latour. Two lane traffic simulations using cellular automata. *Physica A: Statistical Mechanics and its Applications*, 231(4): 534–550, 1996.

T. Roughgarden. *Selfish Routing and the Price of Anarchy*. MIT Press, 2005. ISBN 0262182432.

S. J. Russell and P. Norvig. *Artificial Intelligence: A Modern Approach*. Pearson Education, 2 edition, 2003. ISBN 0137903952.

S. Sarmady, F. Haron, and A. Z. H. Talib. Modeling groups of pedestrians in least effort crowd movements using cellular automata. In *Proceedings - 2009 3rd Asia International Conference on Modelling and Simulation, AMS 2009*, pages 520–525, 2009. doi: 10.1109/AMS.2009.16.

A. Schadschneider, W. Klingsch, H. Klüpfel, T. Kretz, C. Rogsch, and A. Seyfried. Evacuation Dynamics: Empirical Results, Modeling and Applications. In R. A. Meyers, editor, *Encyclopedia of Complexity and Systems Science*, pages 3142–3176. Springer, 2009. ISBN 978-0-387-75888-6.

M. Schultz, C. Schulz, and H. Fricke. Passenger Dynamics at Airport Terminal Environment. In W. W. F. Klingsch, C. Rogsch, A. Schadschneider, and M. Schreckenberg, editors, *Pedestrian and Evacuation Dynamics 2008*, pages 381–396. Springer Berlin Heidelberg, 2010. ISBN 978-3-642-04503-5. doi: 10.1007/978-3-642-04504-2{_}33.

M. Seitz, G. Köster, and A. Pfaffinger. Pedestrian group behavior in a cellular automaton. In *Pedestrian and Evacuation Dynamics 2012*, pages 807–814. Springer, 2014.

G. Shafabakhsh, R. Mirzanamadi, and M. Mohammadi. Micro simulation of the elderly population's effect on Iran's pedestrian's walking flow. *PROMET - Traffic & Transportation*, 25(4):331–342, 2013.

W. Shao and D. Terzopoulos. Autonomous pedestrians. *Graphical Models*, 69(5-6): 246–274, 2007.

K. Shimura, K. Ohtsuka, G. Vizzari, K. Nishinari, and S. Bandini. Mobility analysis of the aged pedestrians by experiment and simulation. *Pattern Recognition Letters*, 44: 58–63, 2014. ISSN 01678655. doi: 10.1016/j.patrec.2013.10.027.

P. Simon and H. Gutowitz. Cellular automaton model for bidirectional traffic, 1998. ISSN 1063-651X.

F. Solera, S. Calderara, and R. Cucchiara. Structured learning for detection of social groups in crowd. In *Advanced Video and Signal Based Surveillance (AVSS), 2013 10th IEEE International Conference on*, pages 7–12, 2013. doi: 10.1109/AVSS.2013.6636608.

B. Steffen and A. Seyfried. Methods for measuring pedestrian density, flow, speed and direction with minimal scatter. *Physica A: Statistical Mechanics and its Applications*, 389(9):1902–1910, may 2010. ISSN 03784371. doi: 10.1016/j.physa.2009.12.015. URL http://www.sciencedirect.com/science/article/pii/S0378437109010115.

H. a. Taylor and B. Tversky. Descriptions and depictions of environments. *Memory & cognition*, 20(5):483–496, 1992.

S. Timpf, G. Volta, D. Pollock, and M. Egenhofer. A conceptual model of wayfinding using multiple levels of abstraction. In *Theories and Methods of Spatio-Temporal Reasoning in Geographic Space*, volume 639, pages 348–367. 1992. ISBN 978-3-540-55966-5. doi: 10.1007/3-540-55966-3{_}21. URL http://dx.doi.org/10.1007/3-540-55966-3{_}21.

M. Twarogowska, P. Goatin, and R. Duvigneau. Macroscopic modeling and simulations of room evacuation. *Applied Mathematical Modelling*, 2014. ISSN 0307904X. doi: 10.1016/j.apm.2014.03.027. URL http://www.sciencedirect.com/science/article/pii/S0307904X14001309.

G. Vizzari, L. Manenti, and L. Crociani. Adaptive Pedestrian Behaviour for the Preservation of Group Cohesion. *Complex Adaptive Systems Modeling*, 1(7), 2013.

I. von Sivers and G. Köster. Dynamic Stride Length Adaptation According to Utility And Personal Space. page 30, jan 2014. URL http://arxiv.org/abs/1401.7838.

A. U. K. Wagoum, M. Chraibi, J. Mehlich, A. Seyfried, and A. Schadschneider. Efficient and validated simulation of crowds for an evacuation assistant. *Journal of Visualization and Computer Animation*, 23(1):3–15, 2012a.

A. U. K. Wagoum, A. Seyfried, and S. Holl. Modelling dynamic route choice of pedestrians to assess the criticality of building evacuation. *Advances in Complex Systems*, 15(07):15, 2012b.

D. C. Walker, J. Southgate, G. Hill, M. Holcombe, D. R. Hose, S. M. Wood, S. Mac Neil, and R. H. Smallwood. The epitheliome: agent-based modelling of the social behaviour of cells. *Biosystems*, 76(1):89–100, 2004.

J. Was, R. Lubaś, and W. Myśliwiec. Proxemics in discrete simulation of evacuation. In *Cellular Automata*, pages 768–775. Springer, 2012.

U. Weidmann. Transporttechnik der Fussgänger - Transporttechnische Eigenschaftendes Fussgängerverkehrs (Literaturstudie). Literature Research 90, Institut füer Verkehrsplanung, Transporttechnik, Strassen- und Eisenbahnbau IVT an der ETH Zürich, 1993.

A. Willis, N. Gjersoe, C. Havard, J. Kerridge, and R. Kukla. Human movement behaviour in urban spaces: implications for the design and modelling of effective pedestrian environments. *Environment and Planning B: Planning and Design*, 31(6): 805–828, 2004. ISSN 0265-8135. doi: 10.1068/b3060. URL http://www.envplan.com/abstract.cgi?id=b3060.

S. Xu and H. B.-l. Duh. A Simulation of Bonding Effects and Their Impacts on Pedestrian Dynamics. *IEEE Transactions on Intelligent Transportation Systems*, 11(1):153–161, 2010. ISSN 1524-9050. doi: 10.1109/TITS.2009.2036152.

D. Yanagisawa, A. Kimura, A. Tomoeda, R. Nishi, Y. Suma, K. Ohtsuka, and K. Nishinari. Introduction of frictional and turning function for pedestrian outflow with an obstacle. *Phys. Rev. E*, 80(3):36110, 2009. doi: 10.1103/PhysRevE.80.036110. URL http://link.aps.org/doi/10.1103/PhysRevE.80.036110.

W. Yu, R. Chen, L. Dong, and S. Dai. Centrifugal force model for pedestrian dynamics, 2005. ISSN 1539-3755.

J. Zhang, W. Klingsch, T. Rupprecht, A. Schadschneider, and A. Seyfried. Empirical study of turning and merging of pedestrian streams in T-junction. *ArXiv e-prints*, page 8, 2011.

J. Zhang, W. Klingsch, A. Schadschneider, and A. Seyfried. Ordering in bidirectional pedestrian flows and its influence on the fundamental diagram. *Journal of Statistical Mechanics: Theory and Experiment*, (02):9, 2012. ISSN 1742-5468. doi: 10.1088/1742-5468/2012/02/P02002. URL http://arxiv.org/abs/1107.5246.